Order Number 9035319

Electrochemical phase diagrams for aqueous redox systems

Zappia, Michael Joseph, Ph.D.

Case Western Reserve University, 1990

U·M·I
300 N. Zeeb Rd.
Ann Arbor, MI 48106

ELECTROCHEMICAL PHASE DIAGRAMS FOR AQUEOUS REDOX SYSTEMS

by

MICHAEL JOSEPH ZAPPIA

Submitted in partial fulfillment of the requirements
for the Degree of Doctor of Philosophy

Thesis Advisor: Professor John C. Angus

Department of Chemical Engineering
CASE WESTERN RESERVE UNIVERSITY

May, 1990

CASE WESTERN RESERVE UNIVERSITY

GRADUATE STUDIES

We hereby approve the thesis of

Michael Joseph Zappia

candidate for the Ph.D.

degree.*

Signed:

(Chairman)

Date DECEMBER 11, 1989

*We also certify that written approval has been obtained for any proprietary material contained therein.

ELECTROCHEMICAL PHASE DIAGRAMS FOR AQUEOUS REDOX SYSTEMS

Abstract

by

MICHAEL JOSEPH ZAPPIA

An entirely new type of electrochemical phase diagram, the electron number diagram, has been discovered. The theoretical foundation for the electron number diagram and its relationship to conventional potential–pH diagrams have been developed. Electron number diagrams are obtained by a thermodynamic transformation in which potential is replaced by a measure of the number of electrons. The chemical potential of electrons and the number of electrons are conjugate thermodynamic variables. The areas in which electron number diagrams provide information complementary to and in addition to that from conventional potential–pH diagrams have been identified.

Experimental electron number diagrams have been constructed for the aqueous sulfur system. Two–dimensional sections of the three–dimensional electron number diagram at both constant pH and constant electron number have been determined and compared with the sections computed from theory. Agreement between the computed and measured diagrams has been found.

A rigorous thermodynamic theory for complex aqueous redox systems has been developed and used for interpretation of the various types of electrochemical phase diagrams. The dimensionality of potential–pH and electron number diagrams has been related to the Gibbs phase rule analysis of aqueous redox systems.

An efficient computational method, based on the theoretical analysis of complex aqueous redox systems, has been developed. The equations describing the equilibrium composition are obtained from a minimum set of formation reactions. The formation reactions use a set of reactants (components) whose chemical potentials are chosen to be the independent variables in the computation. This procedure permits the sequential rather than simultaneous solution of the equation set in the case of ideal solutions. Efficient stability criteria, obtained from theory, were used to determine the stability of solid phases. The algorithm was implemented on IBM PCs and compatible computers.

Electron number, potential–pH and chemical potential diagrams have been computed for a variety of complex aqueous systems, including the following systems containing two active redox elements: the aqueous Cd–Te system; the aqueous Ga–As system; and the aqueous U–C system.

ACKNOWLEDGEMENTS

I would like to thank my advisor, Professor John C. Angus for his guidance, encouragement and technical assistance over the years.

The substantial experimental work of Ms. Rebecca Yung on the sulfur system is gratefully acknowledged.

The programming efforts of Ms. Bei Lu in the area of potential–pH diagrams were also greatly appreciated.

I would like to thank Professors Landau, Matisoff and Payer for serving on my defense committee, Ming–Chang Yang for providing EDS analysis and Terry Stover for performing total sulfur analysis. I would also like to express my appreciation for the contributions (technical and otherwise) of the graduate students, staff and faculty of the Chemical Engineering Department. Karen Henck and Kathy Lipnis, in particular, have been extremely helpful.

Completion of this degree would not have been possible without the unwavering support of my family, especially my wife Barb, my parents and my brother Mark.

I would like to express my gratitude to DuPont for fellowship support. This work was supported in part by Martin Marietta Energy Systems (Oak Ridge) under contract to the Department of Energy and by the US Army Research Office. The continuing support and encouragement of Dr. Jon Bullock (Martin Marietta) and Dr. Robert Reeber (US Army Research Office) is gratefully acknowledged.

TABLE OF CONTENTS

ABSTRACT ii

ACKNOWLEDGEMENTS iv

LIST OF FIGURES x

LIST OF TABLES xvi

CHAPTER 1 INTRODUCTION 1

CHAPTER 2 THERMODYNAMIC FUNDAMENTALS 3

2.1 Chemical Reaction Equilibria 3

2.1.1 Selection of Components 4
2.1.2 The Basic Equilibrium Criterion 6
2.1.3 Aqueous Systems Containing One Active Redox Element 6
2.1.4 Virtual Species 7

2.2 Phase Rule Analysis 9

2.3 Summary of Working Equations 10

2.3.1 Aqueous Systems Containing Two Redox Elements . . . 11
2.3.2 Aqueous Systems Containing One Redox Element . . . 13

2.3.2.1 Equilibrium Between a Single Solid Phase and the Aqueous Phase 17
2.3.2.2 Equilibrium Between Two Solid Phases and the Aqueous Phase 17
2.3.2.3 Equilibrium Between Three Solid Phases and the Aqueous Phase 19

2.3.3 The Calculation of Concentrations and Activities . 20

2.4 Phase Stability 22

2.4.1 Aqueous Systems Containing One Redox Element . . . 22
2.4.2 Aqueous Systems Containing Two Redox Elements . . . 24

CHAPTER 3 POTENTIAL–PH DIAGRAMS FOR AQUEOUS SYSTEMS CONTAINING ONE REDOX ELEMENT 25

3.1 The Structure of Potential–pH Diagrams 25

3.2 Applications of Potential–pH Diagrams 33

3.3 Experimental Potential–pH Diagrams 37

3.4 Related Diagrams 38

CHAPTER 4 THE CALCULATION OF POTENTIAL–PH DIAGRAMS FOR AQUEOUS SYSTEMS CONTAINING ONE REDOX ELEMENT. 40

4.1 Previous Methods of Calculation 40

4.1.1 Point–by–Point Methods 41
4.1.2 Convex Polygon Methods 41

4.2 New Method of Calculation 42

4.2.1 Basis of New Computational Method 42
4.2.2 Assumptions 42
4.2.3 Conventions for Nomenclature 43
4.2.4 Algorithm for the Construction of Pourbaix Diagrams 43
4.2.5 Algorithm for Construction of Predominance Diagrams 45
4.2.6 Examples of Pourbaix and Predominance Diagrams . . 46

4.3 Discussion 53

4.3.1 Limitations of Calculated Potential–pH Diagrams . . 53
4.3.2 Advantages of the New Method 53
4.3.3 Specification of Components and Their Activities . 56
4.3.4 Specification of a Second Redox Element 56
4.3.5 Gaseous Species Containing the Active Redox Element 57

CHAPTER 5 ELECTRON NUMBER DIAGRAMS FOR AQUEOUS SYSTEMS CONTAINING ONE REDOX ELEMENT. . . 59

5.1 Introduction 59

5.1.1 Problems with Potential–pH Diagrams 59
5.1.2 Basic Concept of Electron Number Diagrams 60

5.2 Electron Numbers 60

5.2.1 Choice of System 60
5.2.2 Practical Measure of Electron Concentration 61
5.2.3 Elementary Calculations Using Electron Numbers . . 64

5.3 Examples of Electron Number Diagrams 66

5.3.1 Computations 66
5.3.2 Plotting Electron Number Diagrams 66
5.3.3 Examples of $-\log_{10}[M]_{aq}$ versus $\bar{z}$ Diagrams 86

5.3.4 Constant Potential Lines 93
5.3.5 Lines of Constant Gas Pressure 95
5.3.6 Examples of $-\log_{10}[M]_{aq}$ versus pH Diagrams 95
5.3.7 Examples of $\bar{z}$ versus pH Diagrams 96

5.4 Use of Electron Number Diagrams 97

5.4.1 Material Balances on Electron Number Diagrams . . . 97
5.4.2 Electron Balances on Electron Number Diagrams . . . 98
5.4.3 Concentration or Dilution Trajectories at Constant $\bar{z}$ 100
5.4.4 Concentration or Dilution Trajectories at Constant E 100
5.4.5 Precipitation of Solid Phases 101
5.4.6 Mixing Processes 102
5.4.7 Precipitation of Solids at Constant $\bar{z}$ and Variable pH 104

5.5 Discussion 105

5.5.1 Relationship Between E and $\bar{z}$ 105
5.5.2 Relationship Between Electron Number Diagrams and Prior Diagrams 106
5.5.3 Phase Behavior 107
5.5.4 Solubility Curves 108
5.5.5 Unusual Features on the Diagrams 109
5.5.6 Experimental Diagrams 110
5.5.7 Computed Diagrams 111
5.5.8 Systems with Two Active Elements 111
5.5.9 Activity Coefficients 112
5.5.10 Comparison of Electron Number Diagrams and Potential–pH Diagrams 113

5.6 Conclusions 114

CHAPTER 6 EXPERIMENTAL ELECTRON NUMBER DIAGRAMS FOR THE AQUEOUS SULFUR SYSTEM 116

6.1 Equipment and Procedure 116

6.1.1 Indirect Determination Experiments 119
6.1.2 Direct Determination Experiments 120

6.2 Experimental Results 120

6.3 Discussion 135

6.3.1 Duration of Experimental Runs 148
6.3.2 Effect of Thiosulfate Ion 149
6.3.3 Experimental Error 150

6.3.3.1 Indirect Determination Experiments 153
6.3.3.2 Direct Determination Experiments 153

6.3.4 Comparison of Experimental Results with Theoretical Predictions 154

6.4 Utility of Experimental Electron Number Diagrams 159

CHAPTER 7 ELECTROCHEMICAL PHASE DIAGRAMS FOR SYSTEMS CONTAINING TWO REDOX ELEMENTS . . 160

7.1 Importance of Diagrams Containing Two Redox Elements . . 160

7.2 Previous Computational Methods 160

7.3 Method of Calculation 167

7.4 Examples of Diagrams for Systems Containing Two Redox Elements 171

7.5 Extension to Systems of Arbitrary Complexity 178

CHAPTER 8 CONCLUSIONS AND RECOMMENDATIONS 189

8.1 Conclusions 189

8.2 Recommendations 190

LIST OF SYMBOLS 192

REFERENCES 196

APPENDIX A DERIVATION OF THE GENERAL EQUATION FOR ACTIVITY IN AQUEOUS SYSTEMS CONTAINING TWO REDOX ELEMENTS 200

APPENDIX B LIMITING SLOPES OF SOLUBILITY CURVES ON ELECTRON NUMBER DIAGRAMS IN SYSTEMS CONTAINING ONE ACTIVE REDOX ELEMENT . . . 206

APPENDIX C QUANTITIVE ANALYSIS OF TOTAL SULFUR 210

C.1 Conversion of All Sulfur to Sulfate 210

C.2 Precipitation of Barium Sulfate 211

C.3 Determination of the Weight of Barium Sulfate 213

APPENDIX D CALCULATION OF POINTS ON EXPERIMENTAL ELECTRON NUMBER DIAGRAMS FROM EXPERIMENTAL DATA 214

D.1 Direct Determination Data 215

D.2 Indirect Determination Data 218

D.3 Error Analysis of Indirect Determination Experiments . . 220

APPENDIX E CALCULATION OF CONTOURS OF CONSTANT CONCENTRATION ON THE SOLID–AQUEOUS EQUILIBRIUM SURFACE IN SYSTEMS CONTAINING TWO ACTIVE REDOX ELEMENTS 224

LIST OF FIGURES

Figure		page
3–1	Potential–pH diagram for the aqueous copper system	26
3–2	Three–dimensional potential/pH/$-\log_{10}a_{Cu}$ diagram for the aqueous copper system	29
3–3	Three–dimensional potential/pH/$-\log_{10}a_{S}$ diagram for the aqueous sulfur system	31
3–4	Potential–pH diagram for the aqueous Cu–Cl^- system for $a_{Cl^-} = 0.1$	34
4–1	Pourbaix diagram for the aqueous U system	47
4–2	Predominance diagram for the aqueous U system	49
4–3	Pourbaix diagram for the aqueous U–F^-–$CO_2(g)$ system at $a_{F^-} = 0.0001$ and $a_{CO_2(g)} = 0.00033$	50
4–4	Predominance diagram for the aqueous U–F^-–$CO_2(g)$ system at $a_{F^-} = 0.0001$ and $a_{CO_2(g)} = 0.00033$	51
5–1	Three–dimensional electron number diagram for the aqueous copper system	71
5–2	Three–dimensional electron number diagram for the aqueous sulfur system	72
5–3	Electron number diagram for the aqueous copper system at pH = 0	73

5–4 Electron number diagram for the aqueous copper system at pH = 6 74

5–5 Electron number diagram for the aqueous copper system at pH = 8.81 75

5–6 Electron number diagram for the aqueous copper system at pH = 10 76

5–7 Electron number diagram for the aqueous copper system at pH = 14 77

5–8 Electron number diagram for the aqueous Cu–Cl^- system at pH = 6 and $[Cl^-]$ = 0.01m 78

5–9 Electron number diagram for the aqueous Cu–Cl^- system at pH = 6 and $[Cl^-]$ = 1.0m 79

5–10 Electron number diagram for the aqueous sulfur system at pH = 4 80

5–11 Electron number diagram for the aqueous sulfur system at pH = 7 81

5–12a Electron number diagram for the aqueous sulfur system at pH = 8. (Bisulfate and sulfate ions are not included in the calculation.) 82

5–12b Electron number diagram for the aqueous sulfur system at pH = 8. (Bisulfate and sulfate ions are included in the calculation.) 83

5–13 Electron number diagram for the aqueous chromium system at pH = 4 84

5–14 Electron number diagram for the aqueous uranium system at pH = 4 85

5–15 $-\log_{10}[S]_{aq}$ vs. pH diagram for the aqueous sulfur system at $\bar{z}_{aq} = -1$ 87

5–16 The effect of activity coefficients on calculated sulfur solubility as a function of pH 88

5–17 $\bar{z}$ vs. pH diagram for the aqueous copper system at $-\log_{10}[Cu]_{aq} = 8$ 89

5–18 $\bar{z}$ vs. pH diagram for the aqueous copper system at $-\log_{10}[Cu]_{aq} = 2$ 90

6–1 The experimental apparatus 117

6–2 Results of indirect determination experiments for the aqueous sulfur system at pH = 2.8 ± 0.3 123

6–3 Potential measurements for the aqueous sulfur system at pH = 2.8 ± 0.3 125

6–4 Potential measurements for the aqueous sulfur system at pH = 5.3 ± 0.2 126

6–5 Results of direct determination experiments for the aqueous sulfur system at pH = 2.8 132

6–6 Results of direct determination experiments for the aqueous sulfur system at pH = 4.7 ± 0.5 133

6–7 The change in pH versus time for Run 2, an indirect determination experiment 134

6–8 The change in pH versus time for Run 136, a direct determination experiment 137

6–9 Results of direct determination experiments for the aqueous sulfur system at $\bar{z} = -1.85$ 139

6–10 Results of direct determination experiments for the aqueous sulfur system at $\bar{z} = -1.5$ 140

6–11 Results of direct determination experiments for the aqueous sulfur system at $\bar{z} = -1.0$ 141

6–12 Results of direct determination experiments for the aqueous sulfur system at $\bar{z} = 0.0$ 142

6–13 Results of direct determination experiments for the aqueous sulfur system at $\bar{z} = 1.0$ 143

6–14 Results of direct determination experiments for the aqueous sulfur system at $\bar{z} = 1.5$ 144

6–15 Results of direct determination experiments for the aqueous sulfur system at $\bar{z} = 1.86$ 145

6–16 Results of direct determination experiments for the aqueous sulfur system at $\bar{z} = 2.0$ 146

6–17 Results of direct determination experiments for the aqueous sulfur system at $\bar{z} = 2.25$ 147

6–18 Results of indirect determination experiments for the aqueous sulfur system at pH = 2.8 ± 0.3, with estimated experimental uncertainties 152

6–19 Direct determination experimental data for the aqueous sulfur system at pH = 4.7 ± 0.5, corrected for pH 157

7–1 Prism in chemical potential space, formed by the minimum and maximum values of $(\mu_M - \mu_M^\circ)/RT$, $(\mu_N - \mu_N^\circ)/RT$ and E . . . 166

7–2 Equilibrium diagram for the aqueous U–C system at pH = 4 in chemical potential space 167

7–3 Equilibrium diagram for the aqueous U–C system at pH = 4 in $-\log_{10}[U]_{aq}/-\log_{10}[C]_{aq}/E$ space 172

7–4 Equilibrium diagram for the aqueous U–C–F^- system at pH = 4 and $a_{F^-} = 0.1$ in chemical potential space 173

7–5 Equilibrium diagram for the aqueous U–C–F^- system at pH = 4 and $a_{F^-} = 0.1$ in $-\log_{10}[U]_{aq}/-\log_{10}[C]_{aq}/E$ space 174

7–6 Equilibrium diagram for the aqueous U–C–F^- system at pH = 4 and $a_{F^-} = 1$ in chemical potential space 175

7–7 Equilibrium diagram for the aqueous U–C–F^- system at pH = 4 and $a_{F^-} = 1$ in $-\log_{10}[U]_{aq}/-\log_{10}[C]_{aq}/E$ space 176

7–8 Equilibrium diagram for the aqueous Ga–As system at pH = 13 in chemical potential space 177

7–9 Equilibrium diagram for the aqueous Ga–As system at pH = 13 in $-\log_{10}[Ga]_{aq}/-\log_{10}[As]_{aq}/E$ space 179

7–10 Equilibrium diagram for the aqueous Cd–Te system at pH = 2.5 in chemical potential space 181

7–11 Equilibrium diagram for the aqueous Cd–Te system at pH = 2.5 in $-\log_{10}[Cd]_{aq}/-\log_{10}[Te]_{aq}/E$ space 182

7–12 Equilibrium diagram for the aqueous Cd–Te system at pH = 10 in chemical potential space 183

7–13 Equilibrium diagram for the aqueous Cd–Te system at pH = 10 in $-\log_{10}[Cd]_{aq}/-\log_{10}[Te]_{aq}/E$ space 184

7–14 Equilibrium diagram for the aqueous Cd–Te system at pH = 10 in $-\log_{10}[Cd]_{aq}/-\log_{10}[Te]_{aq}/\overline{z}$ space 186

LIST OF TABLES

Table		page
2–1	Examples of Formation Reaction Coefficients and Thermodynamic Data for an Aqueous U–C–F^- System at 25°C	5
2–2	Examples of Formation Reaction Coefficients and Thermodynamic Data for an Aqueous Cu–Cl^- System at 25°C	8
3–1	Aqueous Cu System: Species Included in Calculations	27
3–2	Aqueous S System: Species Included in Calculations	32
3–3	Aqueous Cu–Cl^- System: Species Included in Calculations	35
4–1	Aqueous U System: Species Included in Calculations	48
4–2	Aqueous U–F^-–CO_2 System: Species Included in Calculations	52
5–1	Species Used to Calculate the Electron Number Diagrams in Figures 5–3 Through 5–13	67
6–1	Results of Indirect Determination Experiments for the Aqueous Sulfur System	121
6–2	Results of Additional Indirect Determination Experiments for the Aqueous Sulfur System	124
6–3	Results of Direct Determination Experiments for the Aqueous Sulfur System	127

6–4 Summary of Long Term Indirect Experiments 136

6–5 Results of Direct Determination Experiments Using Sulfite and Thiosulfate at pH = 2.8 and z = 0.00 138

6–6 Correction of Direct Experimental Data at pH = 4.7 . . . 158

7–1 Aqueous U–C System: Species Included in Calculations 168

7–2 Aqueous Ga–As System: Species Included in Calculations 180

7–3 Aqueous Cd–Te System: Species Included in Calculations 185

CHAPTER 1

INTRODUCTION

A phase diagram is a useful means of summarizing a large amount of thermodynamic information in a convenient, compact form. This thermodynamic information can be used to understand the behavior of complex systems, to plan experiments and to interpret experimental data. Although kinetic information is necessary to determine the rates at which chemical reactions occur in a system, a thermodynamic analysis can provide insight into the energetically allowed possibilities.

Various types of phase diagrams have been developed for electrochemical systems. Potential–pH diagrams, which display the stability of chemical species on a field of potential vs. pH, have been applied to corrosion studies, hydrometallurgy, geologic sudies and electrodeposition. In these and other applications, potential–pH diagrams have been successfully used in the prediction of behavior, the determination of conditions for experimental studies and the interpretation of experimental results.

Several factors have limited the usefulness of potential–pH diagrams. Inconsistencies in the methods used to compute and present potential–pH diagrams have caused great confusion in their interpretation. Furthermore, the link between the phase behavior of electrochemical systems and these diagrams has not always been clear. Additionally, potential–pH diagrams are inconvenient or inappropriate in some applications because potential is not a conserved quantity. Improvements in these areas would increase the utility of

electrochemical phase diagrams as tools for the study of aqueous redox systems.

The purpose of this work is to improve the understanding of electrochemical phase diagrams for aqueous redox systems by developing: (1) a thermodynamic framework for the study of aqueous redox systems; (2) new electrochemical phase diagrams; and (3) efficient methods of computing electrochemical phase diagrams.

These goals will be addressed in the following specific manner. The necessary thermodynamic structure of aqueous redox systems will be introduced and developed (Chapter 2). This structure will be applied to potential–pH diagrams (Chapter 3) and their computation (Chapter 4). The electron number diagram, an entirely new type of electrochemical phase diagram, will then be introduced (Chapter 5). Experimental electron number diagrams for the aqueous sulfur system will be shown (Chapter 6). Methods of calculating electrochemical phase diagrams will be extended to systems containing two redox elements, and these methods will then be used to construct electrochemical phase diagrams for various systems containing two redox elements (Chapter 7). Finally, conclusions will be drawn and recommendations for further work will be listed (Chapter 8).

CHAPTER 2

THERMODYNAMIC FUNDAMENTALS

In this chapter, thermodynamic analysis of aqueous systems containing two active redox elements and two additional components (complexing agents) is given. The analysis can easily be generalized to systems containing arbitrary numbers of active redox elements and additional components. This is discussed in Chapter 7.5.

Detailed analysis is also presented for aqueous systems containing one active redox element. Systems containing a single active redox element are of great interest and have been studied widely. Furthermore, general algebraic solutions can be written for the equations necessary for the generation of electrochemical phase diagrams for systems containing a single active redox element.

2.1 Chemical Reaction Equilibria

In the thermodynamic analysis of an aqueous redox system, a set of independent chemical reactions must be chosen. In choosing this set, it is important that no assumptions are made about major or dominant species. It is also desirable to have a reaction set that allows species to be added or deleted without altering the structure of the solution.

For an aqueous redox system containing two active redox elements, M and N, as well as additional components, X and Y, a formation equation of the following form can be written for each species S_k:

$$\left[\frac{\alpha_{M,k}}{\alpha_{M,k} + \alpha_{N,k}}\right] M + \left[\frac{\alpha_{N,k}}{\alpha_{M,k} + \alpha_{N,k}}\right] N$$

$$= \left[\frac{1}{\alpha_{M,k} + \alpha_{N,k}}\right] S_k + h_k H^+ + w_k H_2O + x_k X + y_k Y + z_k e^- \qquad (2.1\text{–}1)$$

where $\alpha_{M,k}$ is the number of atoms of element M per molecule of species S_k and $\alpha_{N,k}$ is the number of atoms of element N per molecule of species S_k. Note that the formation equation, in this normalized form, is written for a total of one mole of the two active redox elements. In a system containing n species which contain one or both of the active redox elements, n–2 independent formation equations of this type can be written.

For example, consider an aqueous system containing the two active redox elements, uranium and carbon. The standard formation reaction for $UO_2(CO_3)_2^{2-}$ is written as:

$$\frac{1}{3} U + \frac{2}{3} C = \frac{1}{3} UO_2(CO_3)_2^{2-} + \frac{16}{3} H^+ - \frac{8}{3} H_2O + \frac{14}{3} e^- \qquad (2.1\text{–}2)$$

where $S_k = UO_2(CO_3)_2^{2-}$, M = U, N = C, $\alpha_{U,k} = 1$, $\alpha_{C,k} = 2$, $h_k = 16 / 3$, $w_k = -8 / 3$, $z_k = 14 / 3$, $x_k = 0$ and $y_k = 0$.

Table 2–1 gives additional examples of the formation reaction coefficients for species in an aqueous system containing the two active elements, U and C, in addition to F^-, which is treated as electrochemically inactive in this case.

2.1.1 Selection of Components

In the set of formation equations (Equation 2.1–1), H_2O, H^+, e^- and the active redox elements M and N are chosen as components. This set of independent formation equations has been chosen because it provides a particularly convenient form for the solution of equilibrium equations and for the determination of phase stability for aqueous redox systems.

Table 2–1

Examples of Formation Reaction Coefficients and Thermodynamic Data for an Aqueous U–C–F^- System at 25°C

Solid Species:

S_k	$\alpha_{U,k}$	$\alpha_{C,k}$	h_k	w_k	z_k	x_k	$\Delta_f G^\circ_k$	ΔG°_k
UO_2CO_3	1	1	5	$\frac{-5}{2}$	5	0	–1563.1	–188.7
UC	1	1	0	0	0	0	–99.2	–49.6
U_2C_3	2	3	0	0	0	0	–187.4	–37.48
UO_2F_2	1	0	4	–2	6	–2	–1551.8	–520.0
C	0	1	0	0	0	0	0	0

Dissolved Species:

S_k	$\alpha_{U,k}$	$\alpha_{C,k}$	h_k	w_k	z_k	x_k	$\Delta_f G^\circ_k$	ΔG°_k
$UO_2(CO_3)_2^{2-}$	1	2	$\frac{16}{3}$	$\frac{-8}{3}$	$\frac{14}{3}$	0	–2105.4	–69.5
UO_2^{2+}	1	0	4	–2	6	0	–953.5	–479.2
UF_3^+	1	0	0	0	4	–3	–1485.3	–648.9
H_2CO_3	0	1	4	–3	4	0	–623.08	88.31

Notes: Coefficients correspond to the formation reaction in Equation 2.1–1, with M = U, N = C and X = F^-. $\Delta_f G^\circ_k$ is given in units of kJ per mole of S_k. ΔG°_k was calculated using Equation 2.3–1 and is given in units of kJ per mole of total U + C in S_k. The following standard free energy values were also used: $\Delta_f G^\circ_{H_2O}$ = –237.129 kJ/mol; $\Delta_f G^\circ_{F^-}$ = –278.79 kJ/mol.

Additional components X and Y can also be used to allow consideration of systems containing complexing agents and reactive gases, e.g., F^- and $CO_2(g)$. The choice of components can be somewhat arbitrary. When possible, the choice should be based on the physical situation being considered. For example, in a system containing carbonates, four different species could be used as a component: $CO_2(g)$, H_2CO_3, HCO_3^- or $CO_3^=$. If $CO_2(g)$ pressure were fixed, then $CO_2(g)$ would be the logical choice for a component.

2.1.2 The Basic Equilibrium Criterion

The basic equilibrium criterion for the reaction in Equation 2.1–1 is given by

$$\left[\frac{\alpha_{M,k}}{\alpha_{M,k} + \alpha_{N,k}}\right]\mu_M + \left[\frac{\alpha_{N,k}}{\alpha_{M,k} + \alpha_{N,k}}\right]\mu_N = \left[\frac{1}{\alpha_{M,k} + \alpha_{N,k}}\right]\mu_k + h_k\mu_{H^+} + w_k\mu_{H_2O} + x_k\mu_X + y_k\mu_Y + z_k\mu_{e^-} \quad (2.1\text{–}3)$$

For example, the equilibrium criterion for the formation reaction in Equation 2.1–2 is:

$$\frac{1}{3}\mu_U + \frac{2}{3}\mu_C = \frac{1}{3}\mu_{UO_2(CO_3)_2^{2-}} + \frac{16}{3}\mu_{H^+} - \frac{8}{3}\mu_{H_2O} + \frac{14}{3}\mu_{e^-} \quad (2.1\text{–}4)$$

2.1.3 Aqueous Systems Containing One Active Redox Element

For a system containing one active redox element, M, and two additional component species, X and Y, Equation 2.1–1 simplifies to

$$M = S_k / \alpha_{M,k} + h_kH^+ + w_kH_2O + x_kX + y_kY + z_ke^- \quad (2.1\text{–}5)$$

where $\alpha_{M,k}$ is the number of atoms of element M per molecule of species S_k. For a system in which n species contain redox element M, n–1 independent formation equations of this type can be written.

For example, the standard formation reaction for $CuCl_3^{2-}$ in an aqueous copper system containing an additional component Cl^- is

$$Cu = CuCl_3^{2-} + e^- - 3\,Cl^- \qquad (2.1\text{–}6)$$

where M = Cu, $S_k = CuCl_3^{2-}$, $X = Cl^-$, $\alpha_{M,k} = 1$, $h_k = 0$, $w_k = 0$, $z_k = 1$, $x_k = -3$ and $y_k = 0$.

Table 2–2 gives additional examples of the formation reaction coefficients for species in an aqueous Cu–Cl^- system.

The equilibrium criterion for the formation reaction in Equation 2.1–6 is

$$\mu_{Cu} = \mu_{CuCl_3^{2-}} + \mu_{e^-} - 3\mu_{Cl^-} \qquad (2.1\text{–}7)$$

In the notation for systems containing one redox element, the following definition is sometimes used

$$\nu_{M,k} \equiv 1 / \alpha_{M,k} \qquad (2.1\text{–}8)$$

As a further example, the formation reaction for $S_2O_3^{2-}$ in an aqueous sulfur system is

$$S = \tfrac{1}{2} S_2O_3^{2-} + 3H^+ - \tfrac{3}{2} H_2O + 2e^- \qquad (2.1\text{–}9)$$

where $S_k = S_2O_3^{2-}$, M = S, $\alpha_{S,k} = 2$, $\nu_{S,k} = 1 / 2$, $h_k = 3$, $w_k = -3 / 2$, $z_k = 2$, $x_k = 0$ and $y_k = 0$.

2.1.4 Virtual Species

It is not necessary that the component species used in the formation reactions in Equations 2.1–1 and 2.1–5 actually exist as independent entities in solution. Virtual species, which are not physically present in the system, can be used in thermodynamic analysis of the system because their chemical potentials can be well defined. For example, even when redox element M is not present in its elemental form in the system, its chemical potential is well defined. Free

Table 2–2

Examples of Formation Reaction Coefficients and Thermodynamic Data for an Aqueous Cu–Cl^- System at 25°C

Solid Species:

S_k	$\alpha_{Cu,k}$	h_k	w_k	z_k	x_k	$\Delta_f G_k^\circ$	E_k° (V)
Cu	1	0	0	0	0	0	0
Cu_2O	2	1	$\frac{-1}{2}$	1	0	–146	0.472
CuO	1	2	–1	2	0	–129.7	0.557
CuCl	1	0	0	1	–1	–119.86	0.118
$CuCl_2 \cdot 3Cu(OH)_2$	4	$\frac{3}{2}$	$\frac{-3}{2}$	2	$\frac{-1}{2}$	–1339.5	0.448

Dissolved Species:

S_k	$\alpha_{Cu,k}$	h_k	w_k	z_k	x_k	$\Delta_f G_k^\circ$	E_k° (V)
Cu^+	1	0	0	1	0	49.98	0.518
Cu^{2+}	1	0	0	2	0	65.49	0.339
$CuCl^+$	1	0	0	2	–1	–68.2	0.327
$CuCl_3^{2-}$	1	0	0	1	–3	–376	0.183
CuO_2^{2-}	1	4	–2	2	0	–183.6	1.506

Notes: Coefficients correspond to the formation reaction in Equation 2.1–5, with M = Cu and X = Cl^-. $\Delta_f G_k^\circ$ is in units of kJ per mole of S_k. E_k° was calculated using Equations 2.3–12 and 2.3–1. The following standard free energy values were also used: $\Delta_f G^\circ_{H_2O} = -237.129$ kJ/mol; $\Delta_f G^\circ_{Cl^-} = -131.228$ kJ/mol.

electrons do not exist in measurable quantities in solution, but their chemical potential is well defined and measurable. The use of virtual species in the computation of chemical equilibrium has previously been discussed for gas phase systems (White,1967) and for aqueous redox systems (Angus and Angus,1985).

2.2 Phase Rule Analysis

The phase rule for chemically reacting systems is given by

$$f = s - r - P + 2 \qquad (2.2\text{–}1)$$

where f is the number of degrees of freedom, s is the total number of species (real and virtual), r is the number of independent reactions that can be written among the species and P is the number of phases present.

Consider an aqueous system of two redox elements, M and N, two additional components, X and Y, and n species that contain M or N or both M and N. To write formation equations for the system, five components in addition to M and N are needed: H_2O, H^+, e^-, X and Y. Substitution into Equation 2.2–1 gives

$$f = (n + 5) - (n - 2) - P + 2 \qquad (2.2\text{–}2)$$

$$f = 9 - P \qquad (2.2\text{–}3)$$

If temperature and pressure are fixed, Equation 2.2–3 becomes

$$f = 7 - P \qquad (2.2\text{–}4)$$

For an aqueous redox system containing a single redox element M, two additional component species X and Y and n species that contain element M, the same five component species in addition to M are necessary to write the formation reactions. There are now, however, only n–1 independent reactions. Equation 2.2–1 yields

$$f = (n + 5) - (n - 1) - P + 2 \tag{2.2–5}$$

$$f = 8 - P \tag{2.2–6}$$

At fixed temperature and pressure, Equation 2.2–6 becomes

$$f = 6 - P \tag{2.2–7}$$

In this phase rule analysis, species such as OH^- have not been listed. Inclusion of an additional species, OH^-, would necessitate the inclusion of an additional independent reaction (e.g., $H^+ + OH^- = H_2O$), thereby leaving the number of degrees of freedom unchanged. Similarly, listing an electroneutrality condition among the system equations would require consideration of an inert counter ion, again leaving the phase rule analysis unchanged.

Examination of Equations 2.2–4 and 2.2–7 shows that, at constant temperature and pressure, the general form of the phase rule becomes

$$f = t - P \tag{2.2–8}$$

where t is the total number of components necessary to describe the stoichiometry of the reacting system.

Equation 2.2–8 gives the number of chemical potentials that may be specified independently. The maximum number of dimensions, D, needed to represent the equilibrium of the system graphically can be determined by setting the number of phases to its minimum value (P = 1) in Equation 2.2–8:

$$D = t - 1 \tag{2.2–9}$$

2.3 Summary of Working Equations

In this section, working equations for the calculation of electrochemical phase diagrams for aqueous redox systems are introduced. Appendix A shows the derivation of the general activity equation for aqueous systems containing two

redox elements; many of the following equations are simplifications or special cases of equations from Appendix A. Further discussion of the equations, especially for aqueous systems containing one redox element, is available elsewhere (Angus and Angus, 1985; Angus, Lu and Zappia, 1987).

2.3.1 Aqueous Systems Containing Two Redox Elements

Free energy information for each species is necessary for the determination of the equilibrium composition of an aqueous redox system. For each species S_k that contains one or both of the two active redox elements M and N, standard free energy data is used to compute ΔG_k°, the standard free energy change for the formation reaction given in Equation 2.1–1 (the formation of S_k from M, N, H_2O, H^+, e^-, X and Y).

$$\Delta G_k^\circ = \left[\frac{1}{\alpha_{M,k} + \alpha_{N,k}}\right]\Delta_f G_k^\circ + h_k \Delta_f G_{H^+}^\circ + w_k \Delta_f G_{H_2O}^\circ + x_k \Delta_f G_X^\circ + y_k \Delta_f G_Y^\circ - \left[\frac{\alpha_{M,k}}{\alpha_{M,k} + \alpha_{N,k}}\right]\Delta_f G_M^\circ - \left[\frac{\alpha_{N,k}}{\alpha_{M,k} + \alpha_{N,k}}\right]\Delta_f G_N^\circ \quad (2.3\text{–}1)$$

where $\Delta_f G_k^\circ$ is the standard free energy of formation of species S_k from the elements.

For $S_k = UO_2(CO_3)_2^{2-}$, ΔG_k° is given by

$$\Delta G_k^\circ = \tfrac{1}{3}(-2105.4) + \tfrac{16}{3}(0) - \tfrac{8}{3}(-237.129) + 0 + 0 - \tfrac{1}{3}(0) - \tfrac{2}{3}(0)$$
$$= -69.5 \text{ kJ} \quad (2.3\text{–}2)$$

Notice that Equation 2.3–2 is written for a total of one mole of the two active redox elements, U and C.

Table 2–1 gives additional examples of thermodynamic data (Wagman, et al., 1982; Langmuir, 1978) and ΔG_k° values for species in an aqueous U–C–F^- system.

The general equation for activity of a species S_k in a system containing two redox elements, M and N, is

$$a_k = \exp\left[(\alpha_{M,k} + \alpha_{N,k})\left[\left[\frac{\alpha_{M,k}}{\alpha_{M,k} + \alpha_{N,k}}\right]\frac{(\mu_M - \mu_M^\circ)}{RT} + \left[\frac{\alpha_{N,k}}{\alpha_{M,k} + \alpha_{N,k}}\right]\frac{(\mu_N - \mu_N^\circ)}{RT} + h_k(\ln 10)pH - w_k \ln a_{H_2O} - x_k \ln a_X - y_k \ln a_Y + z_k\left[\frac{F}{RT}\right]E - \frac{\Delta G_k^\circ}{RT}\right]\right] \quad (2.3\text{–}3)$$

For $S_k = UO_2(CO_3)_2^{2-}$, Equation 2.3–3 gives

$$a_k = \exp\left[\frac{(\mu_U - \mu_U^\circ)}{RT} + (2)\frac{(\mu_C - \mu_C^\circ)}{RT} + (16)(\ln 10)pH + (8)\ln a_{H_2O} + (14)\left[\frac{F}{RT}\right]E + \frac{(208.5\ \text{kJ/mol})}{RT}\right] \quad (2.3\text{–}4)$$

Equation 2.3–3 can be rearranged to give:

$$\left[\frac{\alpha_{M,k}}{\alpha_{M,k} + \alpha_{N,k}}\right]\frac{(\mu_M - \mu_M^\circ)}{RT} + \left[\frac{\alpha_{N,k}}{\alpha_{M,k} + \alpha_{N,k}}\right]\frac{(\mu_N - \mu_N^\circ)}{RT} - z_k\frac{(\mu_{e^-})}{RT} = -h_k(\ln 10)pH + w_k \ln a_{H_2O} + x_k \ln a_X + y_k \ln a_Y + \frac{\Delta G_k^\circ}{RT} + \left[\frac{1}{\alpha_{M,k} + \alpha_{N,k}}\right]\ln a_k \quad (2.3\text{–}5)$$

For a pure solid, S_s, $a_s = 1$. For example, for pure solid UO_2CO_3, Equation 2.3–5 gives

$$(0.5)\frac{(\mu_M - \mu_M^\circ)}{RT} + (0.5)\frac{(\mu_N - \mu_N^\circ)}{RT} - (5)\frac{(\mu_{e^-})}{RT} = -(5)(\ln 10)pH - (2.5)\ln a_{H_2O} + \frac{(-188.7\ \text{kJ/mol})}{RT} + 0 \quad (2.3\text{–}6)$$

The following equation for the free energy of the formation reaction of

species S_k from the components is useful in the determination of phase stability in aqueous systems containing two redox elements.

$$\frac{\Delta G_k}{RT} = -h_k(\ln 10)pH + w_k \ln a_{H_2O} + x_k \ln a_X + y_k \ln a_Y + \frac{\Delta G_k^\circ}{RT} + \left[\frac{1}{\alpha_{M,k} + \alpha_{N,k}}\right] \ln a_k - \left[\frac{\alpha_{M,k}}{\alpha_{M,k} + \alpha_{N,k}}\right]\frac{(\mu_M - \mu_M^\circ)}{RT} - \left[\frac{\alpha_{N,k}}{\alpha_{M,k} + \alpha_{N,k}}\right]\frac{(\mu_N - \mu_N^\circ)}{RT} - z_k\left[\frac{F}{RT}\right]E \qquad (2.3\text{–}7)$$

The use of Equation 2.3–7 will be described in Chapter 2.4.2.

In the following example, Equation 2.3–7 is written for pure solid UO_2CO_3.

$$\frac{\Delta G_k}{RT} = -(5)(\ln 10)pH - (2.5)\ln a_{H_2O} + \frac{(-188.7 \text{ kJ/mol})}{RT} + 0 - (0.5)\frac{(\mu_M - \mu_M^\circ)}{RT} - (0.5)\frac{(\mu_N - \mu_N^\circ)}{RT} - (5)\frac{FE}{RT} \qquad (2.3\text{–}8)$$

2.3.2 Aqueous Systems Containing One Redox Element

The equation for the activity of species S_k containing one active redox element M can be obtained from Equation 2.3–3 by setting $\alpha_{N,k}$ equal to zero:

$$a_k = \exp\left[(\alpha_{M,k})\left[\frac{(\mu_M - \mu_M^\circ)}{RT} + h_k(\ln 10)pH - w_k \ln a_{H_2O} - x_k \ln a_X - y_k \ln a_Y + z_k\left[\frac{FE}{RT}\right] - \frac{\Delta G_k^\circ}{RT}\right]\right] \qquad (2.3\text{–}9)$$

where ΔG_k° is given by Equation 2.3–1.

For example, ΔG_k° can be calculated for $S_k = Cu^{2+}$ with Equation 2.3–1 and the thermodynamic information (Wagman, et al., 1982) in Table 2–2.

$$\Delta G_k^\circ = (1)(65.49) + 0 + 0 + 0 + 0 - 0 - 0 = 65.49 \text{ kJ/mol} \qquad (2.3\text{–}10)$$

With the value of ΔG_f° from Equation 2.3–10, an expression for the activity of

Cu^{2+} can be written. For $S_k = Cu^{2+}$, Equation 2.3–9 gives

$$a_k = \exp\left[\frac{(\mu_{Cu} - \mu^\circ_{Cu})}{RT} + (2)\left[\frac{FE}{RT}\right] - \frac{(65.49\ \text{kJ/mol})}{RT}\right] \qquad (2.3\text{–}11)$$

E°_k, the standard electrode potential for the formation of S_k by the reaction in Equation 2.1–5, is defined as

$$E^\circ_k \equiv \frac{\Delta G^\circ_k}{z_k F} \qquad \text{for } z_k \neq 0 \qquad (2.3\text{–}12)$$

The conventions involving the sign of E°_k can be confusing. Although half–cell reactions are written as reductions by IUPAC convention, the formation reaction as written in Equation 2.1–5 is an oxidation when $z_k > 0$. (The decision to write Equation 2.1–5 in this form will be discussed in Chapter 5.) However, examination of Equations 2.1–5, 2.3–1 and 2.3–12 shows that E°_k, as defined above, is positive when the standard free energy change of the reaction in Equation 2.1–5, *written as a reduction*, is negative. Thus, the sign of E°_k is consistent with IUPAC conventions. Consequently, E°_k values computed with Equations 2.3–1 and 2.3–12 are consistent with listings of standard reduction potentials.

For example, for $S_k = Cu^{2+}$, Equation 2.3–12 gives

$$E^\circ_k = \frac{(65{,}490)}{(2)(96487)} = 0.339\ \text{V} \qquad (2.3\text{–}13)$$

This value of E°_k for the reaction involving Cu and Cu^{2+} agrees with listed standard electrode potential values (Bard and Faulkner, 1980; Stumm and Morgan, 1981).

Table 2–2 lists E°_k values for additional species in an aqueous Cu–Cl^- system.

Equations 2.3–9 and 2.3–12 can be combined to give a convenient expression

for the activity of a species S_k:

$$a_k = \exp\left[(\alpha_{M,k})\left[\frac{(\mu_M - \mu_M^\circ)}{RT} + h_k(\ln 10)pH - w_k \ln a_{H_2O} - x_k \ln a_X - y_k \ln a_Y + z_k\left[\frac{F}{RT}\right](E - E_k^\circ)\right]\right] \quad (2.3\text{–}14)$$

For example, for $S_k = CuCl_3^{2-}$ Equation 2.3–14 gives

$$a_k = \exp\left[\frac{(\mu_M - \mu_M^\circ)}{RT} + (3)\ln a_{Cl^-} - \left[\frac{F}{RT}\right](E - 0.183\ V)\right] \quad (2.3\text{–}15)$$

From Equation 2.3–14, an expression for the ratio of the activities of two species, S_i and S_j, can be obtained:

$$\frac{a_i}{a_j} = \exp\left[(\alpha_{M,i} - \alpha_{M,j})\frac{(\mu_M - \mu_M^\circ)}{RT} + (\alpha_{M,i}h_i - \alpha_{M,j}h_j)(\ln 10)pH - (\alpha_{M,i}w_i - \alpha_{M,j}w_j)\ln a_{H_2O} - (\alpha_{M,i}x_i - \alpha_{M,j}x_j)\ln a_X - (\alpha_{M,i}y_i - \alpha_{M,j}y_j)\ln a_Y + (\alpha_{M,i}z_i - \alpha_{M,j}z_j)\left[\frac{F}{RT}\right](E) - (\alpha_{M,i}z_iE_i^\circ - \alpha_{M,j}z_jE_j^\circ)\left[\frac{F}{RT}\right]\right] \quad (2.3\text{–}16)$$

Equation 2.3–16 can be used to determine the relationship between the activities of Cu^{2+} (S_i) and Cu^+ (S_j):

$$\frac{a_{Cu^{2+}}}{a_{Cu^+}} = \exp\left[\left[\frac{F}{RT}\right](E) - \left[(2)(0.339) - (1)(0.518)\right]\left[\frac{F}{RT}\right]\right]$$

$$= \exp\left[\left[\frac{F}{RT}\right](E - 0.160\ V)\right] \quad (2.3\text{–}17)$$

Equation 2.3–17 can be rearranged to give

$$E = 0.160\ V + \ln(10)\frac{RT}{F}\log_{10}\left[\frac{a_{Cu^{2+}}}{a_{Cu^+}}\right] \quad (2.3\text{–}18)$$

Equation 2.3–18 is simply the Nernst equation for the Cu^{2+}/Cu^+ couple. Thus, the well known Nernst equation is contained within the general formalism used here.

Combining Equations 2.1–8 and 2.3–14 and rearranging gives

$$a_k^{\nu_{M,k}} = \exp\left[\frac{(\mu_M - \mu_M^\circ)}{RT} + h_k(\ln 10)pH - w_k \ln a_{H_2O} - x_k \ln a_X - y_k \ln a_Y + z_k\left[\frac{F}{RT}\right](E - E_k^\circ)\right] \quad (2.3\text{–}19)$$

Equation 2.3–19 can be summed over all dissolved species. Solving for the chemical potential of the redox element M gives

$$\left[\frac{(\mu_M - \mu_M^\circ)}{RT}\right]_{aq} = -\ln \Sigma \exp\left[h_d(\ln 10)pH - w_d \ln a_{H_2O} - x_d \ln a_X - y_d \ln a_Y + z_d\left[\frac{F}{RT}\right](E - E_k^\circ)\right] + \ln\left(\Sigma a_d^{\nu_{M,d}}\right) \quad (2.3\text{–}20a)$$

where the sums are taken over all dissolved species. Equation 2.3–20a clearly shows that the chemical potential of the redox element M is well defined even if element M does not exist in elemental form in the system.

For example, for an aqueous Cu system containing two dissolved species, $CuCl^+$ and CuO_2^{2-}, Equation 2.3–20a gives

$$\left[\frac{(\mu_{Cu} - \mu_{Cu}^\circ)}{RT}\right]_{aq} = -\ln\left[\exp\left[\ln a_{Cl^-} + \left[\frac{2F}{RT}\right](E - 0.326\ V)\right] + \exp\left[(4)(\ln 10)pH + 2\ln a_{H_2O} + \left[\frac{2F}{RT}\right](E - 1.506\ V)\right]\right] + \ln\left(a_{CuCl^+} + a_{CuO_2^{2-}}\right) \quad (2.3\text{–}20b)$$

Since all of the terms on the right hand side of Equation 2.3–20b can be measured or are known constants, the left hand side can be unambiguously determined.

Equation 2.3–19 can also be rearranged to give the following expression for the chemical potential of redox element M in species S_k:

$$\left[\frac{(\mu_M - \mu_M^\circ)}{RT}\right]_k = -h_k(\ln 10)pH + w_k \ln a_{H_2O} + x_k \ln a_X + y_k \ln a_Y - z_k\left[\frac{F}{RT}\right](E - E_k^\circ) + \nu_{M,k} \ln a_k \quad (2.3\text{–}21)$$

2.3.2.1 Equilibrium Between a Single Solid Phase and the Aqueous Phase

Consider the case of a pure solid phase S_s that contains redox element M. Setting a_s to 1 in Equation 2.3–21 gives

$$\left[\frac{(\mu_M - \mu_M^\circ)}{RT}\right]_s = -h_s(\ln 10)pH + w_s \ln a_{H_2O} + x_s \ln a_X + y_s \ln a_Y - z_s\left[\frac{F}{RT}\right](E - E_s^\circ) \quad (2.3\text{–}22)$$

For example, when $S_s = CuO$, Equation 2.3–22 yields

$$\left[\frac{(\mu_{Cu} - \mu_{Cu}^\circ)}{RT}\right]_s = -(2)(\ln 10)pH - \ln a_{H_2O} - \left[\frac{2F}{RT}\right](E - 0.557\ V) \quad (2.3\text{–}23)$$

The value of the chemical potential of M from Equation 2.3–22 can then be substituted back into Equation 2.3–19 to give an expression for the activity of a dissolved species S_d in equilibrium with solid S_s:

$$a_d^{\nu_{M,d}} = \exp\left[(h_d - h_s)(\ln 10)pH - (w_d - w_s)\ln a_{H_2O} - (x_d - x_s)\ln a_X - (y_d - y_s)\ln a_Y + \frac{F}{RT}\left[z_d(E - E_d^\circ) - z_s(E - E_s^\circ)\right]\right] \quad (2.3\text{–}24)$$

For example, the activity of Cu^+ (S_d) in equilibrium with solid CuO (S_s) is given by

$$a_d = \exp\left[(-2)(\ln 10)pH - \ln a_{H_2O} + \frac{F}{RT}\left[(E - 0.518\ V) - 2(E - 0.557\ V)\right]\right]$$

$$= \exp\left[(-2)(\ln 10)pH - \ln a_{H_2O} + \frac{F}{RT}(-E + 0.596\ V)\right] \quad (2.3\text{–}25)$$

2.3.2.2 Equilibrium Between Two Solid Phases and the Aqueous Phase

Next, consider the equilibrium between two solid species, S_u and S_v, and the aqueous phase. Equation 2.3–22 can be written for each solid. At equilibrium, the chemical potential of the redox element M is equal in the two

solids, so the two right hand sides can be equated. The resulting equation is solved for E.

$$E = \left[\frac{z_u E^\circ_u - z_v E^\circ_v}{z_u - z_v}\right] + \frac{RT\ /\ F}{z_u - z_v}\left[(w_u - w_v)\ln a_{H_2O} + (x_u - x_v)\ln a_X + (y_u - y_v)\ln a_Y - (h_u - h_v)(\ln 10)pH\right] \quad (2.3\text{–}26)$$

Using Equation 2.3–26, the equilibrium relationship between two solids can be determined. In the following example, $S_u = Cu_2O$ and $S_v = CuO$:

$$E = \left[\frac{(1)(0.472) - (2)(0.557)}{(1 - 2)}\right] + \frac{RT/F}{(1 - 2)}\left[(0.5)\ln a_{H_2O} - (1 - 2)(\ln 10)pH\right]$$
$$= 0.642\ V - \ln(10)\left[\frac{RT}{F}\right]pH - \left[\frac{RT}{2F}\right]\ln a_{H_2O} \quad (2.3\text{–}27)$$

Substitution of Equation 2.3–26 into Equation 2.3–24 to eliminate E results in an expression for the activity of any dissolved species S_d in equilibrium with two solids S_u and S_v.

$$a_d^{\nu M,d} = \exp\left[\frac{1}{z_v - z_u}\left[(\ln 10)(pH)\left[z_v(h_d - h_u) + z_u(h_v - h_d) + z_d(h_u - h_v)\right] + \left[z_v(x_u - x_d) + z_u(x_d - x_v) + z_d(x_v - x_u)\right]\ln a_X + \left[z_v(y_u - y_d) + z_u(y_d - y_v) + z_d(y_v - y_u)\right]\ln a_Y + \frac{F}{RT}\left[z_v E^\circ_v(z_d - z_u) + z_u E^\circ_u(z_v - z_d) + z_d E^\circ_d(z_u - z_v)\right]\right]\right] \quad (2.3\text{–}28)$$

In Equation 2.3–28, the terms associated with $\ln a_{H_2O}$ have been dropped. In the calculations, the $\ln a_{H_2O}$ term was typically neglected; this will be discussed further later.

In the following example, Equation 2.3–28 is used to obtain the relationship between pH and the activity of Cu^{2+} (S_d) in equilibrium with CuO (S_u) and Cu_2O (S_v):

$$a_d = \exp\left[\frac{1}{(1-2)}\left[(\ln 10)(pH)\left[(1)(0-2)+(2)(1-0)+(2)(2-1)\right]\right.\right.$$
$$\left.\left.+\frac{F}{RT}\left[(1)(0.472)(2-2)+(2)(0.557)(1-2)+(2)(0.339)(2-1)\right]\right]\right]$$
$$= \exp\left[(-2)(\ln 10)pH + 17.0\right] \qquad (2.3\text{–}29)$$

2.3.2.3 Equilibrium Between Three Solid Phases and the Aqueous Phase

The equilibrium between three solids and the aqueous phase has also been considered. Equation 2.3–22 can be written for three solid species S_t, S_u and S_v. For equilibrium among these three solid species:

$$\left[\frac{(\mu_M - \mu_M^\circ)}{RT}\right]_t = \left[\frac{(\mu_M - \mu_M^\circ)}{RT}\right]_u = \left[\frac{(\mu_M - \mu_M^\circ)}{RT}\right]_v \qquad (2.3\text{–}30)$$

Equations 2.3–30 can be solved for E and pH.

$$E = \left[z_u E_u^\circ(h_v - h_t) + z_v E_v^\circ(h_t - h_u) + z_t E_t^\circ(h_u - h_v) + \left[x_u(h_v - h_t)\right.\right.$$
$$\left.+ x_v(h_t - h_u) + x_t(h_u - h_v)\right](RT/F)\ln a_X + \left[y_u(h_v - h_t)\right.$$
$$\left.\left.+ y_v(h_t - h_u) + y_t(h_u - h_v)\right](RT/F)\ln a_Y\right](A^{-1}) \qquad (2.3\text{–}31)$$

$$pH = -\left[\left[z_u E_u^\circ(z_v - z_t) + z_v E_v^\circ(z_t - z_u) + z_t E_t^\circ(z_u - z_v)\right](F/RT) + \left[x_u(z_v - z_t)\right.\right.$$
$$\left.+ x_v(z_t - z_u) + x_t(z_u - z_v)\right]\ln a_X + \left[y_u(z_v - z_t)\right.$$
$$\left.\left.+ y_v(z_t - z_u) + y_t(z_u - z_v)\right]\ln a_Y\right](\ln 10)^{-1}(A^{-1}) \qquad (2.3\text{–}32)$$

where

$$A \equiv z_u(h_v - h_t) + z_v(h_t - h_u) + z_t(h_u - h_v) \qquad (2.3\text{–}33)$$

For example, in an aqueous Cu–Cl^- system with $a_{Cl^-} = 0.1$, three solids (Cu = S_t; CuCl = S_u and Cu_2O = S_v) are in equilibrium at

$$E = \Big[(1)(0.118)(1-0) + (1)(0.472)(0-0) + (0)(0)(0-1) + \Big[(-1)(1-0) + (0)(0-0) + (0)(0-1)\Big]\frac{(8.3143)(298.15)}{(96,487)}\ln(0.1)\Big](1) = 0.177\ \text{V} \quad (2.3\text{–}34)$$

$$pH = -\Big[\Big[(1)(0.118)(1-0) + (1)(0.472)(0-1) + (0)(0)(1-1)\Big]\frac{(96,487)}{(8.3143)(298.15)} + \Big[(-1)(1-0) + (0)(0-1) + (0)(1-1)\Big]\ln(0.1)\Big](0.4343)(1) = 4.98 \quad (2.3\text{–}35)$$

where

$$A = (1)(1-0) + (1)(0-0) + (0)(0-1) = 1 \quad (2.3\text{–}36)$$

Equations 2.3–31, 2.3–32 and 2.3–33 could, if desired, be used in Equations 2.3–9 and 2.3–22 to compute the activity of any dissolved species in equilibrium with the three solid phases.

2.3.3 The Calculation of Concentrations and Activities

The activity, a_M^*, of an active redox element M is defined as

$$a_M^* \equiv \sum_d \alpha_{M,d} a_d \quad (2.3\text{–}37)$$

where the sum is taken over all dissolved species. Equation 2.3–3 can be substituted into Equation 2.3–37 to give:

$$a_M^* = \sum_d \alpha_{M,d} \exp\Bigg[(\alpha_{M,d}+\alpha_{N,d})\Bigg[\Bigg[\frac{\alpha_{M,d}}{\alpha_{M,d}+\alpha_{N,d}}\Bigg]\frac{(\mu_M - \mu_M^\circ)}{RT} + \Bigg[\frac{\alpha_{N,d}}{\alpha_{M,d}+\alpha_{N,d}}\Bigg]\frac{(\mu_N - \mu_N^\circ)}{RT} + h_d(\ln 10)pH - w_d \ln a_{H_2O} - x_d \ln a_X - y_d \ln a_Y + z_d\Big[\frac{F}{RT}\Big]E - \frac{\Delta G_d^\circ}{RT}\Bigg]\Bigg] \quad (2.3\text{–}38)$$

Notice that Equation 2.3–38 allows the calculation of a_M^* in a system that contains active redox elements M and N.

Another definition of activity is used exclusively in aqueous systems containing a single active redox element M. This activity, denoted a_M, is defined as

$$a_M \equiv \sum_d a_d^{\nu_{M,d}} \tag{2.3–39}$$

Comparison of Equations 2.3–37 and 2.3–39 shows that $a_M^* = a_M$ if $\alpha_{M,d} = 1$ for all dissolved species S_d in a system. (Recall that $\nu_{M,d} \equiv 1/\alpha_{M,d}$.)

The substitution of Equation 2.3–19 into Equation 2.3–39 yields

$$a_M = \sum_d \exp\left[\frac{(\mu_M - \mu_M^\circ)}{RT} + h_d(\ln 10)pH - w_d \ln a_{H_2O} - x_d \ln a_X - y_d \ln a_Y + z_d\left[\frac{F}{RT}\right](E - E_d^\circ)\right] \tag{2.3–40}$$

where the sum is taken over all dissolved species.

The concentration, $[S_d]$, of a dissolved species S_d is related to the activity of S_d by

$$[S_d] = \frac{a_d}{\gamma_d} \tag{2.3–41}$$

where γ_d is the activity coefficient of dissolved species S_d. Using Equation 2.3–41, an equation for $[M]_{aq}$, the total dissolved concentration of active redox element M, can be written

$$[M]_{aq} = \sum_d \alpha_{M,d} \frac{a_d}{\gamma_d} \tag{2.3–42}$$

Equation 2.3–3 can be substituted into 2.3–42 to give

$$\sum_d \frac{\alpha_{M,d}}{\gamma_d} \exp\left[(\alpha_{M,d}+\alpha_{N,d})\left[\left[\frac{\alpha_{M,d}}{\alpha_{M,d}+\alpha_{N,d}}\right]\frac{(\mu_M - \mu_M^\circ)}{RT}\right.\right.$$
$$+\left[\frac{\alpha_{N,d}}{\alpha_{M,d}+\alpha_{N,d}}\right]\frac{(\mu_N - \mu_N^\circ)}{RT} + h_d(\ln 10)pH$$
$$\left.\left. - w_d \ln a_{H_2O} - x_d \ln a_X - y_d \ln a_Y + z_d\left[\frac{F}{RT}\right]E - \frac{\Delta G_d^\circ}{RT}\right]\right]$$
$$= [M]_{aq} \qquad (2.3\text{–}43)$$

where the sum is taken over all dissolved species. Notice that this equation can be used in a system containing two active redox elements. Also, if the assumption is made that $\gamma_d = 1$ for all dissolved species S_d, then $a_M^* = [M]_{aq}$.

Although $[M]_{aq}$, a_M^* and a_M can be equal in the special cases described above (all $\gamma_d = 1$, all $\alpha_{M,d} = 1$), these three measures of the overall concentration or activity of the active redox element M in the aqueous phase generally differ.

For example, consider an aqueous sulfur system containing the following three species: $S_4O_6^{2-}$ ($\alpha_{S,S_4O_6^{2-}} = 4$), S_2^{2-} ($\alpha_{S,S_2^{2-}} = 2$) and HSO_3^- ($\alpha_{S,HSO_3^-} = 1$). According to Equation 3–37, a_S^* for this system is:

$$a_S^* = 4a_{S_4O_6^{2-}} + 2a_{S_2^{2-}} + a_{HSO_3^-} \qquad (2.3\text{–}44)$$

From Equation 3–39, a_S for the same system is:

$$a_S = (a_{S_4O_6^{2-}})^{0.25} + (a_{S_2^{2-}})^{0.5} + a_{HSO_3^-} \qquad (2.3\text{–}45)$$

From Equation 2.3–42, $[S]_{aq}$ is

$$[S]_{aq} = 4\frac{a_{S_4O_6^{2-}}}{\gamma_{S_4O_6^{2-}}} + 2\frac{a_{S_2^{2-}}}{\gamma_{S_2^{2-}}} + \frac{a_{HSO_3^-}}{\gamma_{HSO_3^-}} \qquad (2.3\text{–}46)$$

2.4 Phase Stability

2.4.1 Aqueous Systems Containing One Redox Element

Consider an aqueous system containing one redox element, M, and two solid

species, S_u and S_v. From Equation 2.1–3, an equilibrium relationship with the components M, H^+, H_2O, X and Y can be written for each solid.

$$\mu_{M,u} = \nu_{M,u}\mu_u + h_u\mu_{H^+} + w_u\mu_{H_2O} + x_u\mu_X + y_u\mu_Y + z_u\mu_{e^-} \quad (2.4\text{–}1)$$

$$\mu_{M,v} = \nu_{M,v}\mu_v + h_v\mu_{H^+} + w_v\mu_{H_2O} + x_v\mu_X + y_v\mu_Y + z_v\mu_{e^-} \quad (2.4\text{–}2)$$

where $\mu_{M,u}$ and $\mu_{M,v}$ are the chemical potentials of M in solids S_u and S_v respectively, and the coefficients $\nu_{M,u}$ and $\nu_{M,v}$ are simply equal to $1/\alpha_{M,u}$ and $1/\alpha_{M,v}$ respectively.

To determine the relative stability of the solids S_u and S_v when the chemical potentials of the component species other than M are fixed, Equation 2.1–5 can be written for each solid. The equations can then be combined, eliminating M, to give:

$$\nu_{M,u}S_u + h_uH^+ + w_uH_2O + x_uX + y_uY + z_ue^- = \nu_{M,v}S_v + h_vH^+ + w_vH_2O + x_vX + y_vY + z_ve^- \quad (2.4\text{–}3)$$

The free energy change for this reaction is given by

$$\Delta G = \nu_{M,v}\mu_v - \nu_{M,u}\mu_u + (h_v - h_u)\mu_{H^+} + (w_v - w_u)\mu_{H_2O} + (x_v - x_u)\mu_X + (y_v - y_u)\mu_Y + (z_v - z_u)\mu_{e^-} \quad (2.4\text{–}4)$$

However, comparison of Equations 2.4–1, 2.4–2 and 2.4–4 yields

$$\Delta G = \mu_{M,v} - \mu_{M,u} \quad (2.4\text{–}5)$$

Equation 2.4–5 shows that the free energy change for the phase transition from S_u to S_v is simply equal to the difference in the chemical potential of the redox element M within the solid phases. When S_u and S_v are in equilibrium, $\mu_{M,v} = \mu_{M,u}$ and $\Delta G = 0$. Equation 2.3–21 permits the direct computation of the chemical potential of redox element M in solid species S_s. Therefore, in aqueous systems containing one redox element, Equation 2.4–5 provides a very simple test for the stability of solid phases.

2.4.2 Aqueous Systems Containing Two Redox Elements

Phase stability in systems containing two redox elements M and N can be evaluated using Equation 2.3–7. If values of the chemical potentials of all components are known, then, for a solid S_k, the free energy of the formation reaction given by Equation 2.1–1 can be computed. A positive value of ΔG_k indicates that solid S_k is thermodynamically unstable. A negative value indicates that solid S_k will tend to form, but that the solid is not currently in equilibrium with the components. When $\Delta G_k = 0$, solid S_k is in equilibrium with the system. For a given set of chemical potentials of the components of a system, a solid S_k is stable and in equilibrium with the system if $\Delta G_k = 0$ and $\Delta G_{i \neq k} \geq 0$, where $\Delta G_{i \neq k}$ are the free energies of the formation reactions for all solids except S_k.

CHAPTER 3

POTENTIAL – PH DIAGRAMS FOR AQUEOUS SYSTEMS CONTAINING ONE REDOX ELEMENT

The best known electrochemical phase diagrams are potential–pH diagrams, also known as Pourbaix diagrams. Developed by Marcel Pourbaix (1945), these diagrams are usually constructed from tabulated thermodynamic data. They display the stability of chemical species at equilibrium on a field of potential versus pH. Potential–pH diagrams have been widely used in a variety of areas, including corrosion studies, geochemistry and hydrometallurgy.

3.1 The Structure of Potential–pH Diagrams

Potential–pH diagrams are constructed in a three–dimensional chemical potential space. The three axes used are practical measures of the chemical potentials of components of the system. Electrochemical potential, E, is a measure of μ_{e^-}, pH is a measure of μ_{H^+} and $-\log_{10} a_M$ is a measure of μ_M, where M is the active redox element.

The utility of potential–pH diagrams is related to their unique structure. A potential–pH diagram for the aqueous Cu system is shown in Figure 3–1. The species used in the calculation of this diagram are listed in Table 3–1. This system can be represented with four components: Cu, H_2O, H^+ and e^-. The dimensionality of the system, calculated using Equation 2.2–9, is three. Each dotted line in Figure 3–1 is a contour, along which the value of $-\log_{10} a_{Cu}$ is fixed at the indicated value. The three–dimensional nature of the diagram is apparent

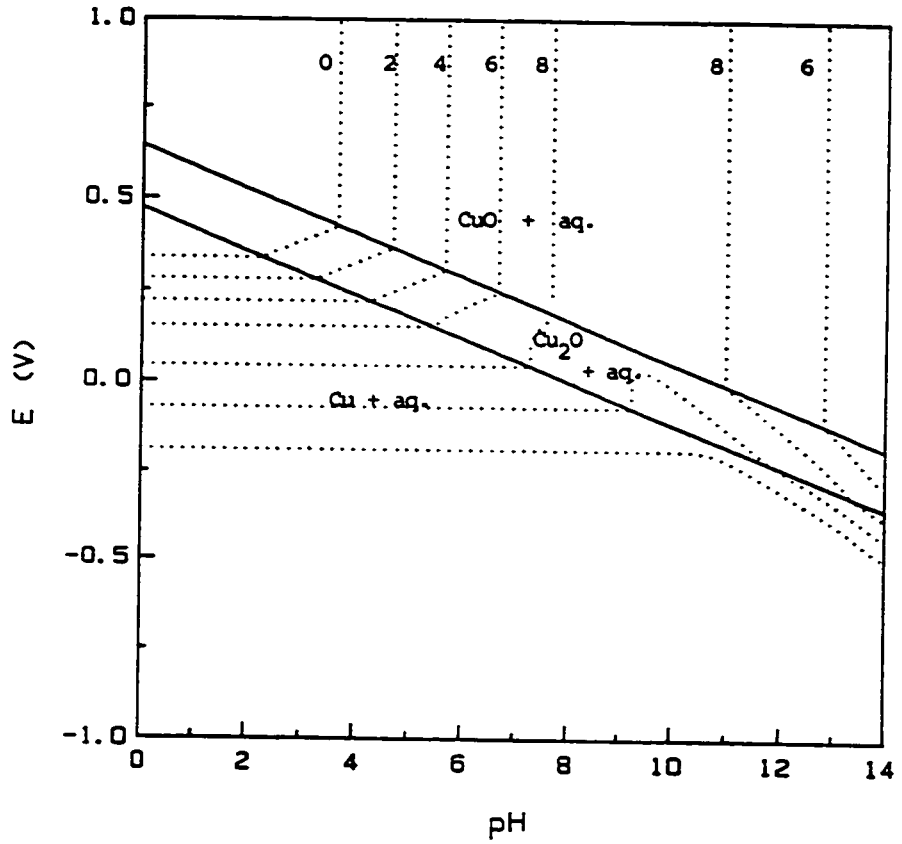

Figure 3–1 Potential–pH diagram for the aqueous copper system. The dotted lines are contours of constant $-\log_{10}{}^{a}Cu$. Contours are shown for the following values of $-\log_{10}{}^{a}Cu$: 0, 2, 4, 6, 8, 10, 12.

Table 3–1

Aqueous Cu System: Species Included in Calculations

Solid Species	Dissolved Species
Cu	Cu^{+}
Cu_2O	Cu^{2+}
CuO	CuO_2^{2-}
$Cu(OH)_2$	$HCuO_2^{-}$

in Figure 3–2, in which Figure 3–1 is replotted in the three–dimensional space defined by E, pH and $-\log_{10}a_{Cu}$.

Figure 3–2 shows that the potential–pH diagram for the aqueous copper system is a surface which divides space into two regions. In the region behind the surface, at lower $-\log_{10}a_{Cu}$, the system can not exist in equilibrium, as solubility limits would be exceeded. In the region in front of the surface, i.e., at higher $-\log_{10}a_{Cu}$, a single aqueous phase is stable. According to Equation 2.2–8, the number of degrees of freedom in this system in the presence of a single phase is three. Figure 3–2 shows that three intensive variables must be fixed to locate a point in the single–phase region.

On the surface, a solid phase containing Cu is in equilibrium with an aqueous phase that contains dissolved copper species. The equilibrium surface consists of the separate surfaces associated with each of the different stable solids. The equilibrium surface in Figure 3–2 consists of three sections, each characterized by the coexistence of the aqueous phase and a different stable solid. These stable solids are CuO at high potentials, Cu_2O at moderate potentials, and elemental Cu at low potentials. On the surface, the number of degrees of freedom is two; i.e., fixing two intensive variables specifies a point on the surface.

Intersections of the surfaces associated with two individual solids are three–phase lines, along which two solids are in equilibrium with the aqueous phase. The number of degrees of freedom in the system in the presence two solid phases and the aqueous phase is one. Thus, along either of the two three–phase lines in Figure 3–2, specification of pH, for example, fixes both the potential and $-\log_{10}a_{Cu}$.

Four–phase points occur at the intersections of three three–phase lines. At

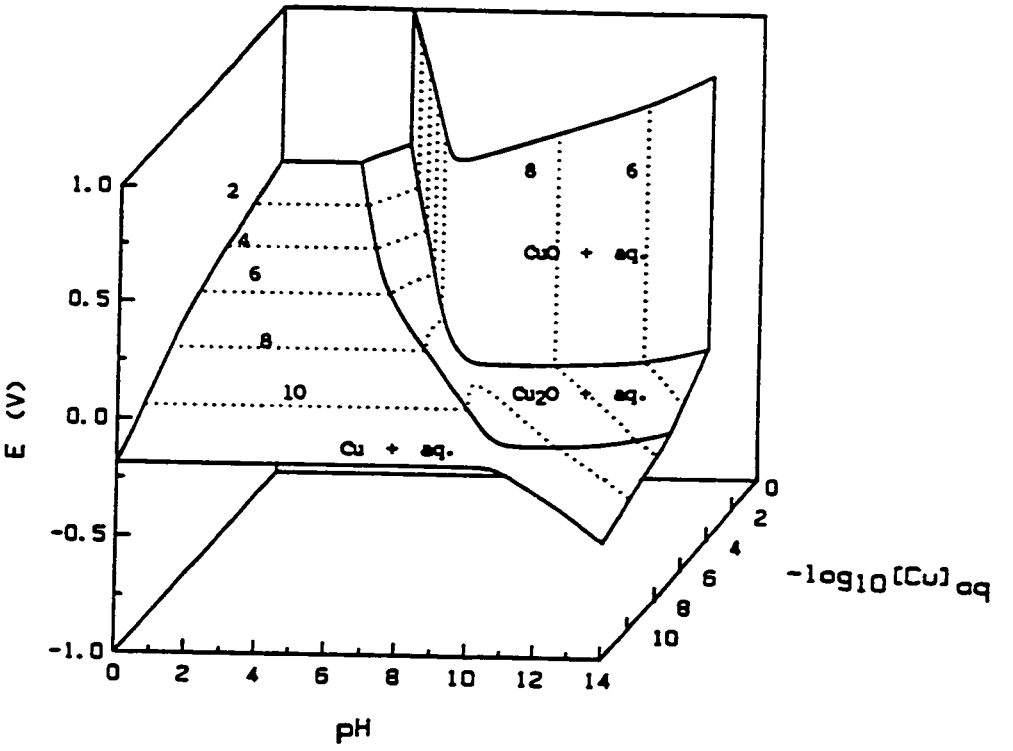

Figure 3–2 Three–dimensional potential/pH/$-\log_{10}{}^{a}_{Cu}$ diagram for the aqueous copper system. The same figure is projected onto the E–pH plane in Figure 3–1.

a four–phase point, three solids coexist in equilibrium with the aqueous phase. Phase rule analysis shows that the simultaneous stability of four phases in an aqueous system containing one active redox element represents an invariant point. No four–phase points appear in Figure 3–2. In fact, it will be shown that such points can not occur in aqueous systems that can be specified using only the following components: the active redox element M, H^+, H_2O and e^-.

On the equilibrium surface, specification of pH and potential fixes $-\log_{10}{}^{a}Cu$; i.e., $-\log_{10}{}^{a}Cu$ is a single–valued function of potential and pH. Thus, when the three–dimensional equilibrium surface is projected onto the E–pH plane, lines of $-\log_{10}{}^{a}Cu$ do not cross. Consequently, these three–dimensional diagrams can be conveniently displayed in a two–dimensional form; in fact, this is the usual convention.

Figure 3–3 shows the three–dimensional potential–pH diagram for the aqueous sulfur system. This diagram was calculated using the species listed in Table 3–2. Inside the surface, i.e., at lower values of $-\log_{10}{}^{a}S$, the system can not exist in equilibrium. Outside the surface, a single aqueous phase exists. On the surface, solid elemental sulfur exists in equilibrium with an aqueous phase containing dissolved sulfur species. Only one solid species was considered in this case, so no more than two phases exist at any point in Figure 3–3.

Consider the slope of the three–phase lines on potential–pH diagrams for aqueous systems that can be specified with the components M (the active redox element), H^+, H_2O and e^-. In these systems, for any solid species S_s, it can easily be shown that

$$h_s = z_s \qquad (3.2\text{–}1)$$

where h_s and z_s are coefficients in the formation reaction given in Equation 2.1–5.

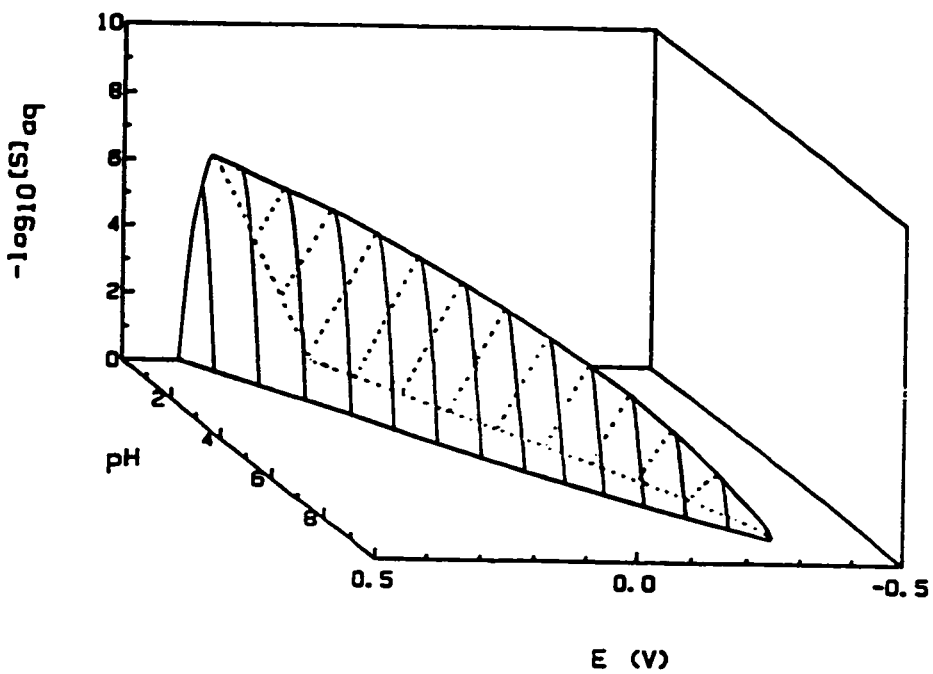

Figure 3–3 Three–dimensional potential/pH/$-\log_{10}a_S$ diagram for the aqueous sulfur system. Constant potential lines are drawn on the the two–phase equilibrium surface.

Table 3–2

Aqueous S System: Species Included in Calculations

Solid Species	Dissolved Species
S	S^{2-}
	HS^-
	H_2S
	$S_2O_3^{2-}$
	$HS_2O_3^-$
	$H_2S_2O_3$
	SO_3^{2-}
	HSO_3^-
	H_2SO_3
	S_2^{2-}
	S_3^{2-}
	S_4^{2-}
	S_5^{2-}
	$S_2O_4^{2-}$
	$HS_2O_4^-$
	$H_2S_2O_4$
	$S_4O_6^{2-}$
	$S_5O_6^{2-}$
	$S_3O_6^{2-}$

The relationship between E and pH along a three–phase line is given by Equation 2.3–26. If the ln a_{H_2O} term is neglected (This will be discussed in Chapter 4.), then Equation 2.3–26 reduces to

$$E = \left[\frac{z_u E^\circ_u - z_v E^\circ_v}{z_u - z_v}\right] - (RT/F)(\ln 10)pH \qquad (3.1\text{–}2)$$

Thus, the slopes of all three–phase lines in these systems are identical. Since four–phase points occur at the intersections of three–phase lines and these three–phase lines are all parallel, four–phase points can not occur in these systems.

In aqueous systems containing one active redox and another component (in addition to H^+, H_2O and e^-), four–phase points can appear. For example, the potential–pH diagram for the aqueous Cu–Cl^- system at $a_{Cl^-} = 1$, shown in Figure 3–4, shows three stable four–phase points. At a point near pH = 5.0 and E = 0.3 V, Cu_2O, CuCl, $CuCl_2 \cdot 3Cu(OH)_2$ and the aqueous phase are all stable. Figure 3–4 was constructed using the the species listed in Table 3–3.

3.2 Applications of Potential–pH Diagrams

The use of potential–pH diagrams has been particularly widespread in corrosion studies. Potential–pH diagrams can be used to predict the conditions, in terms of potential and pH, under which: (1) a metal is thermodynamically stable in its elemental form; (2) a protective solid is expected to form; and (3) metal dissolution is expected. Applications of potential–pH diagrams to corrosion prediction have been discussed previously (Pourbaix, 1966; Silverman, 1982).

Potential–pH diagrams have also been used in the analysis of experimental corrosion data. For a variety of alloys in high salinity geothermal brines,

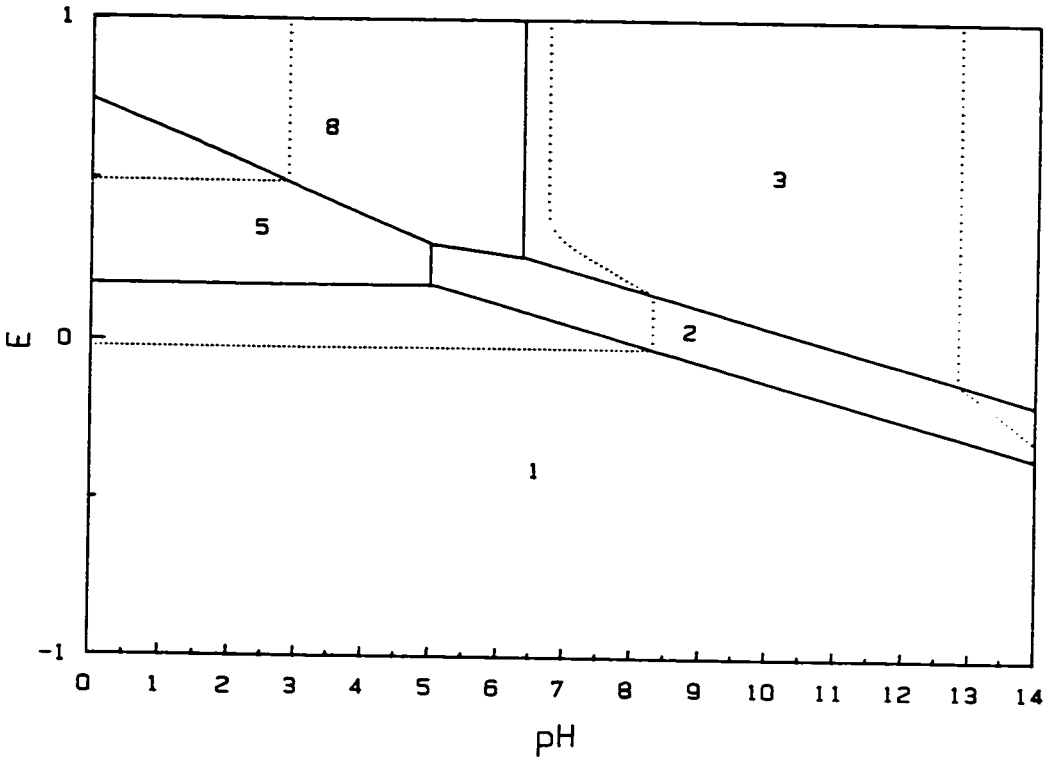

Species Codes

1 Cu
2 Cu2O
3 CuO
5 CuCl
8 CuCl2. 3Cu(OH)2

Figure 3–4 Potential–pH diagram for the aqueous Cu–Cl^- system for $a_{Cl^-} = 0.1$. Note the three four–phase points. Contours of constant a_{Cu} shown for the following values of $-\log_{10} a_{Cu}$: 0, 6.

Table 3–3

Aqueous $Cu–Cl^-$ System: Species Included in Calculations

In addition to the species listed in Table 3–1, the following species were included in calculations for the aqueous $Cu–Cl^-$ system :

Solid Species	Dissolved Species
$CuCl$	$CuCl^+$
$CuCl_2$	$CuCl_2$
$CuCl_2 \cdot 2H_2O$	$CuCl_2^-$
$CuCl_2 \cdot 3Cu(OH)_2$	$CuCl_3^{2-}$

potential–pH diagrams for the key metals in the alloys (Fe, Ni, Cr, Ti) were used to analyze corrosion behavior and interpret experimental results (Macdonald, Syrett and Wing, 1979). In a study of the stress corrosion cracking, a potential–pH diagram for Cr with Fe was used with experimental results to hypothesize a possible protective mechanism (Cubicciotti and Ljungberg, 1985).

In some cases, experiments have been designed specifically for comparison with potential–pH diagrams. In an x–ray photoelectron spectroscopy study of aluminum corrosion/passivation in dilute sulfate solutions under various conditions, the stable solid, according to thermodynamic predictions, did not typically form initially (Davis, Moshier, Ahearn, Hough and Cote, 1987). These results were taken as an indication that kinetic factors were significant in the early stages of film formation. In a study of the crevice corrosion of iron in chromate/chloride solutions, the equilibrium conditions within the crevice and experimental results were found to be consistent with the aqueous Fe potential–pH diagram (McCafferty, 1989).

Over ranges of variables where experimental data are not well established, potential–pH diagrams can be used to predict behavior. For example, potential–pH diagrams for the aqueous Ti, Mo, Pt and Cr systems have been calculated, using estimated free energy values, for temperatures up to 300°C (Lee, 1981; Radhakrishnamurty and Adaikkalam, 1982).

In the study of mineral stability and solubility in geologic applications, potential–pH diagrams have been used to provide equilibrium models with which experimental data can be compared. In comparison to applications in other fields, geologic potential–pH diagrams frequently consider more components simultaneously and thus require more constraints (Garrels, 1982). Potential–pH

diagrams were used in the application of uranium mineral equilibria to sedimentary ore deposits (Langmuir, 1978). Among geologists, an alternate form of potential–pH diagram, the pϵ–pH diagram, is sometimes used (Stumm and Morgan, 1970; 1981). The potential E is related to pϵ by the following equation:

$$p\epsilon = \frac{F}{2.3RT} E \qquad (3.2\text{–}1)$$

Potential–pH diagrams have also been developed to predict the long–term durability of nuclear waste glasses in geologic environments (Jantzen, 1989).

Potential–pH diagrams have also been used in the analysis of hydrometallurgical processes. The use of these diagrams in the determination of thermodynamically feasible decomposition schemes has been demonstrated in detail for the sulfide minerals of Cu, Pb, Zn, Ni and Mo (Peters, 1976).

In electrodeposition, potential–pH diagrams have been used chiefly in the identification and prediction of possible anode and cathode reactions (Kruger, 1982).

3.3 Experimental Potential–pH Diagrams

Experimental potential–pH diagrams have also been generated. Experimental diagrams can incorporate kinetic, as well as thermodynamic information. Also, in complicated alloy systems, potentiodynamic polarization curves were used to determine experimental potential–pH diagrams for aqueous Ni and aqueous steel systems (Lennon and Robinson, 1986). In a study of occluded cell corrosion, potentikinetic polarization curves and zero–current potential–time curves were used to construct experimental potential–pH diagrams for 18–10 austenitic stainless steel (Jingyi, Pourbaix, Chunchun and Youping, 1989).

3.4 Related Diagrams

In addition to potential–pH diagrams, numerous other thermodynamic stability diagrams have been developed; several of these are described below. These other diagrams use practical measures of the chemical potentials of system components as axes. Some diagrams use temperature, which can be viewed as a measure of the thermal potential of a system, as an axis.

In stability diagrams used in the study of hot corrosion, the logarithms of gas pressures, which are measures of the chemical potentials of the gases, are often used as axes. For example, the stability of nickel has been plotted on a field of $\log_{10}p_{SO_2}$ versus $\log_{10}p_{O_2}$ (Barry and Dinsdale, 1987). In investigations of hot corrosion beneath fused salt films, diagrams involving $\log_{10}p_{O_2}$, $-\log_{10}a_{Na_2O}$ and $\log_{10}p_{SO_3}$ were used to interpret oxide solublity data in fused Na_2SO_4 (Rapp, 1986, 1987).

Partial pressure diagrams, using quantities such as $\log_{10}p_{O_2}$, $\log_{10}p_{S_2}$ and $\log_{10}p_{CO_2}$ for axes, have also been used to show mineral stabilities in geologic contexts. Diagrams using ion activities, products of ion activities or ratios of ion activities to label the axes have also been used to show phase stabilities in complex mineral systems (Garrels and Christ, 1966; Woods and Garrels, 1986). Composition diagrams relating mineral stabilities to the activities of dissolved species in complex systems, as well as diagrams in which the chemical potentials of components are used as axes, were developed mainly by Korzhinskii (1959).

Diagrams of RT ln p_{O_2} versus T (Pourbaix–Ellingham diagrams) have been used in metallurgical applications, including carbothermic reduction processes (Downing, 1982). Diagrams of RT ln p_{O_2} versus 1/T and E versus T have also been constructed for a variety of systems (Pourbaix, Yang, Zhang and Zhang,

1986).

Alternative forms for potential–pH diagrams have also been developed for for aqueous systems at 25°C. For example, in a study of the aqueous Cu–NH_3, Ni–NH_3 and Co–NH_3 systems, activity–activity diagrams were generated using a variety of pairs of variables (Osseo–Asare and Fuerstenau, 1978). The fields on which these stability diagrams were plotted included $-\log_{10}p_{O_2}$ versus pH, $-\log_{10}p_{H_2}$ versus pH, $-\log_{10}[NH_3 + NH_4^+]$ versus pH, $-\log_{10}[M]_{aq}$ versus pH and $-\log_{10}[M]_{aq}$ versus $-\log_{10}[NH_3 + NH_4^+]$.

CHAPTER 4

THE CALCULATION OF POTENTIAL–PH DIAGRAMS FOR AQUEOUS SYSTEMS CONTAINING ONE REDOX ELEMENT

4.1 Previous Methods of Calculation

Pourbaix's method for constructing potential–pH diagrams begins with the listing of all possible reactions between pairs of species in the system, including reactions between two solids, reactions between two dissolved species and reactions between a solid species and a dissolved species. For each reaction, an equation relating E, pH and the activities of the two species can be written. The activities of solid species are set to unity. An activity, often 10^{-6}, is assigned to the dissolved species when reactions between dissolved species and solid phases are considered. With these assumptions, the equation for each reaction is reduced to a straight line on the E–pH plane. These lines can be drawn for each reaction. Stability conditions are then used to eliminate lines and segments of lines for species that are not stable.

Pourbaix's method was conceived as a means of producing potential–pH diagrams by hand. Despite the simple nature of this method, the construction of diagrams by hand is a tedious, repetitive task. As a result, the use of computers to calculate potential–pH diagrams has become popular (Froning, Shanley and Verink, 1976; Pelton and Bale, 1977; Rosof, 1977; Barry, 1980; Chen and Aral, 1982; Imai, Osato and Nakauchi, 1987; El–Raghy and El–Dermerdash, 1988). Computer methods for the generation of potential–pH diagrams have been reviewed (Linkson, Phillips and Rowles, 1979). Previous computer methods can

be grouped into two general categories: point–by–point methods and convex polygon methods.

4.1.1 Point–by–Point Methods

Point–by–point methods establish the stability fields of species by calculation of the equilibrium composition at a large number of closely spaced points on potential–pH plane. The activities of solid phases are set to unity. The activities of the dissolved species are set to a predetermined value when reactions between solid species and dissolved species are considered. At each individual point, equilibrium calculations can then be performed to determine the most stable species. The resolution with which the boundaries of the stability fields are determined depends on the number of points considered. One major disadvantage of this method is its inefficiency; calculations must be performed at an inordinate number of points to obtain reasonable resolution.

4.1.2 Convex Polygon Methods

It has been shown that convex polygon theory, from operations research, can be applied to the calculation of potential–pH diagrams (Froning, Shanley and Verink, 1976). The first step is to formulate the set of linear equations in potential and pH that describe each possible reaction in the aqueous redox system. Mathematical techniques developed in operations research are then used to determine convex polygonal areas of predominance from the set of reaction equilibrium equations.

4.2 New Method of Calculation

4.2.1 Basis of the New Computational Method

In the new method, the equilibrium problem is formulated by writing formation reactions from a set of component species chosen for computational simplicity. A set of the minimum number of equations is solved only at those points where multi–phase equilibria can occur. The diagram is then constructed by joining the stable, multi–phase points. The new computational method, based on the thermodynamic structure of aqueous redox systems, provides a very efficient method of solving complex equilibrium problems.

4.2.2 Assumptions

Pure solid phases have been assumed; the activities of all stable solid species are thus set to unity.

The term $\ln a_{H_2O}$ appears in the general equilibrium equations for activity. The assumption has been made that a_{H_2O} is sufficiently close to one that the term $\ln a_{H_2O}$ is small and can thus be neglected. Note that neglecting this term is equivalent to assuming $a_{H_2O} = 1$. This assumption is expected to be reasonable, especially in dilute solutions. The error introduced by neglecting this term is also expected to be small in comparison to error resulting from uncertainties in the free energy data. Furthermore, this assumption, which is almost always made in calculations of potential–pH diagrams, greatly simplifies the equilibrium calculations. Actually, the activity of water is related to the activities of the species in solution by the Gibbs–Duhem equation. In very careful calculations and in concentrated solutions, the activity of water would have to be taken into account.

4.2.3 Conventions for Nomenclature

In the absence of standard nomenclature, the following conventions have been adopted for this work. Potential–pH diagrams showing the stability of solid phases, with contours at constant values of total dissolved activity of the active redox element, will be designated Pourbaix diagrams. Potential–pH diagrams that show the regions of dominance of dissolved species will be called predominance diagrams.

4.2.4 Algorithm for the Construction of Pourbaix Diagrams

Before thermodynamic calculations for an aqueous redox system can be performed, the following data must be provided for each species in the system: the name of the species; the coefficients from Equation 2.1.5; the free energy of formation of the species; and the phase of the species.

Pourbaix diagrams are calculated using the equations given in Chapter 2.3. First, stable four–phase points are determined by considering all possible sets of three solids in the system. Using Equations 2.3–31, 2.3–32 and 2.3–33, the E and pH for the equilibrium of three particular solids (S_t, S_u, S_v) with the aqueous phase are calculated. These values, E' and pH', are used in Equation 2.3–22 to calculate the chemical potential $(\mu_M - \mu_M^\circ)_{t,u,v}/RT$ of the active redox element M in the solids S_t, S_u, S_v. If $(\mu_M - \mu_M^\circ)_{t,u,v}/RT < (\mu_M - \mu_M^\circ)_k/RT$ for all other solid species S_k in the system, then by the stability criterion in Equation 2.4–5, these three solids, S_t, S_u, S_v, and the aqueous phase comprise a stable four–phase point at E' and pH'.

The number of possible sets of three solids, n_3, in a system containing n_s solids is:

$$n_3 = \frac{n_s!}{(n_s - 3)!\ 3!} \qquad (4.2\text{–}1)$$

After all stable four–phase points are determined, stable three–phase points on the E and pH boundaries are determined. First, each possible pair of solids (S_u, S_v) is tested for stability at the lower limit of pH. This is done by fixing the pH at its lower limit and solving Equation 2.3–26 for E. The coordinates (pH_{low}, E") are then used in Equation 2.3–22 to calculate the chemical potential $(\mu_M - \mu_M^\circ)_{u,v}/RT$ of the active redox element M in the solids S_u and S_v. If $(\mu_M - \mu_M^\circ)_{u,v}/RT < (\mu_M - \mu_M^\circ)_k/RT$ for all other solid species S_k in the system, then, by the stability criterion in Equation 2.4–5, (pH_{low}, E") is a stable three–phase boundary point. This procedure is repeated along each of the other three boundaries: pH_{high}, E_{low} and E_{high}.

Once all stable four–phase points and three–phase boundary points have been determined, lines are drawn to connect the points. Two four–phase points are connected if the have two solids in common. Each stable four–phase point within the pH and E limits of the diagram must be connected to three other points, which may be either four–phase points or three–phase boundary points. The potential–pH relationship along the line connecting two stable points is given by Equation 2.3–26 written for the appropriate pair of solids.

In addition to the network of three–phase lines, contours of constant activity, a_M, of the active redox element M can be projected onto the potential–pH plane. The activity a_M can be calculated using Equation 2.3–40. For given value of a_M, the contours are calculated using an iterative routine that begins at points on the three–phase lines and potential and pH boundaries where a_M is equal to the specified value.

4.2.5 Algorithm for Construction of Predominance Diagrams

The network of lines that divide the potential–pH field into areas of dominance of individual dissolved species containing active redox element M is determined by the criterion

$$a_b^{\nu_{M,b}} = a_c^{\nu_{M,c}} \tag{4.2–2}$$

where S_b and S_c are dissolved species.

Substitution of Equation 2.3–19 into Equation 4.2–2 gives the following relationship between E and pH for any arbitrary pair of dissolved species S_b and S_c:

$$E = \left[\frac{z_b E_b^\circ - z_c E_c^\circ}{z_b - z_c}\right] + \frac{RT/F}{z_b - z_c}\Big[(w_b - w_c)\ln a_{H_2O} + (x_b - x_c)\ln a_X + (y_b - y_c)\ln a_Y - (h_b - h_c)(\ln 10)pH\Big] \tag{4.2–3}$$

Note that Equation 4.2–3 is independent of the concentration of active element M.

Except for interpretation of the subscripts, Equation 4.2–3 is identical to Equation 2.3–26, which gives the equilibrium relationship between E and pH for two solids containing one active redox element. Therefore, Equations 2.3–31, 2.3–32 and 2.3–33 can be used to determine the points where three dissolved species have identical values of $a_b^{\nu_{M,b}}$.

The procedure for constructing predominance diagrams is almost identical to that for constructing the network of three–phase lines on Pourbaix diagrams. The difference is the criterion used to determine whether or not a three–species point should be discarded. For predominance diagrams, a three–species point, i.e., where $a_b^{\nu_{M,b}} = a_c^{\nu_{M,c}} = a_d^{\nu_{M,d}}$, is kept only if $a_b^{\nu_{M,b}}$ is greater than $a_k^{\nu_{M,k}}$ for all other dissolved species S_k.

After the three–species points and two–species boundary points are determined, the three–species points with two dissolved species in common are connected by straight lines. The potential–pH relationship along such a line is given Equation 4.2–3, written for the appropriate pair of dissolved species, S_b and S_c.

4.2.6 Examples of Pourbaix and Predominance Diagrams

Pourbaix and predominance diagrams have been computed on IBM–PC, IBM–PC/AT and compatible computers using software written in BASIC (Angus, Lu and Zappia, 1986; Angus, Zappia and Lu, 1990). All diagrams shown have been calculated for 25°C and a total pressure of 1 bar. Free energy data used here have been taken primarily from the NBS listing (Wagman, et al., 1982). Free energy data for species not found in the NBS listing were obtained from other sources (Langmuir, 1978; Barner and Scheuerman, 1978).

Figure 4–1 shows a Pourbaix diagram for the aqueous U system; the species included in the calculation are listed in Table 4–1. A predominance diagram for the same system is shown in Figure 4–2. Figure 4–3 shows the Pourbaix diagram for the aqueous U–F^-–CO_2 system, for $a_{F^-} = 10^{-4}$ and $a_{CO_2} = 3.3 \times 10^{-4}$; Figure 4–4 shows the predominance diagram for the same system. The species used to calculate Figures 4–3 and 4–4 are listed in Table 4–2.

Comparison of Figures 4–1 and 4–3 shows that the addition of F^- and CO_2 has little effect on the aqueous U system at high pH. However, at low pH, the addition of F^- and CO_2 not only leads to the formation of several fluoride–containing solids, but it also causes a significant decrease in uranium solubility in the range of approximately –1.5 V to 0.5 V. Comparison of Figures

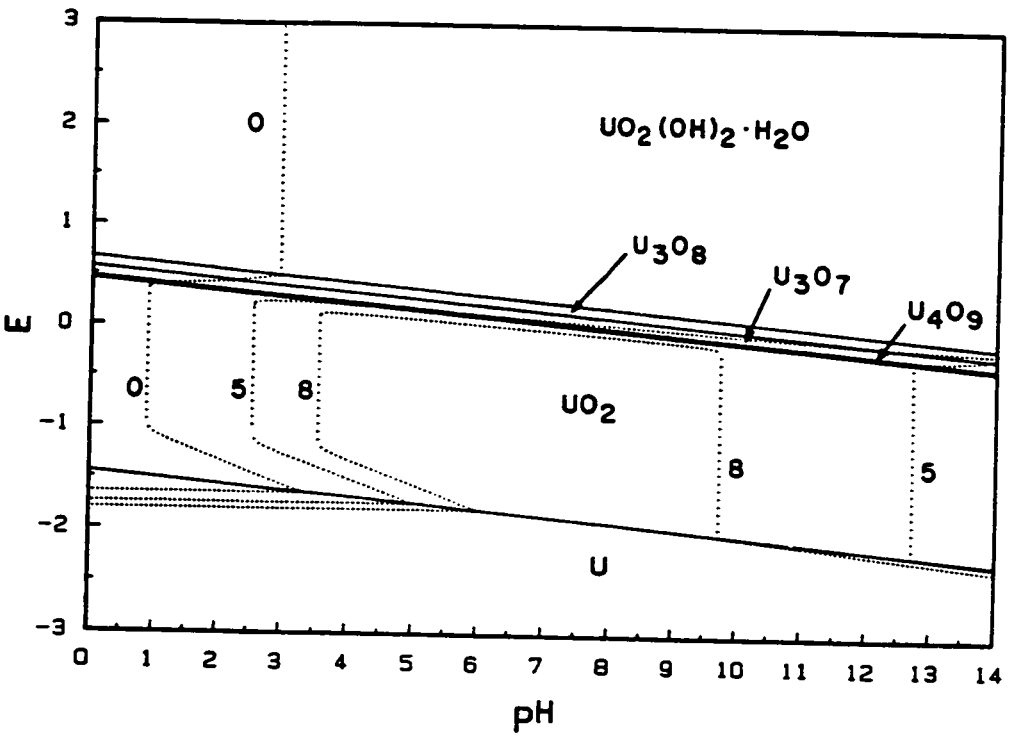

Figure 4–1 Pourbaix diagram for the aqueous U system. Contours of constant a_U are shown for the following values of $-\log_{10}a_U$: 0, 5, 8.

Table 4–1

Aqueous U System: Species Included in Calculations

Solid Species	Dissolved Species
U	U^{3+}
UO_2	U^{4+}
U_4O_9	UOH^{3+}
U_3O_7	UO_2^{+}
U_3O_8	UO_2^{2+}
UO_3(gamma)	$UO_2(OH)_2$
UO_3(alpha)	$U(OH)_2^{2+}$
UO_3(beta)	$U(OH)_3^{+}$
$UO_3 \cdot H_2O$	$U(OH)_4$
$UO_3 \cdot 2H_2O$	$U(OH)_5^{-}$
$UO_2(OH)_2$	$U_6(OH)_{15}^{9+}$
$UO_2(OH)_2 \cdot H_2O$	UO_2OH^{+}
	$(UO_2)_2(OH)_2^{2+}$
	$(UO_2)_3(OH)_5^{+}$

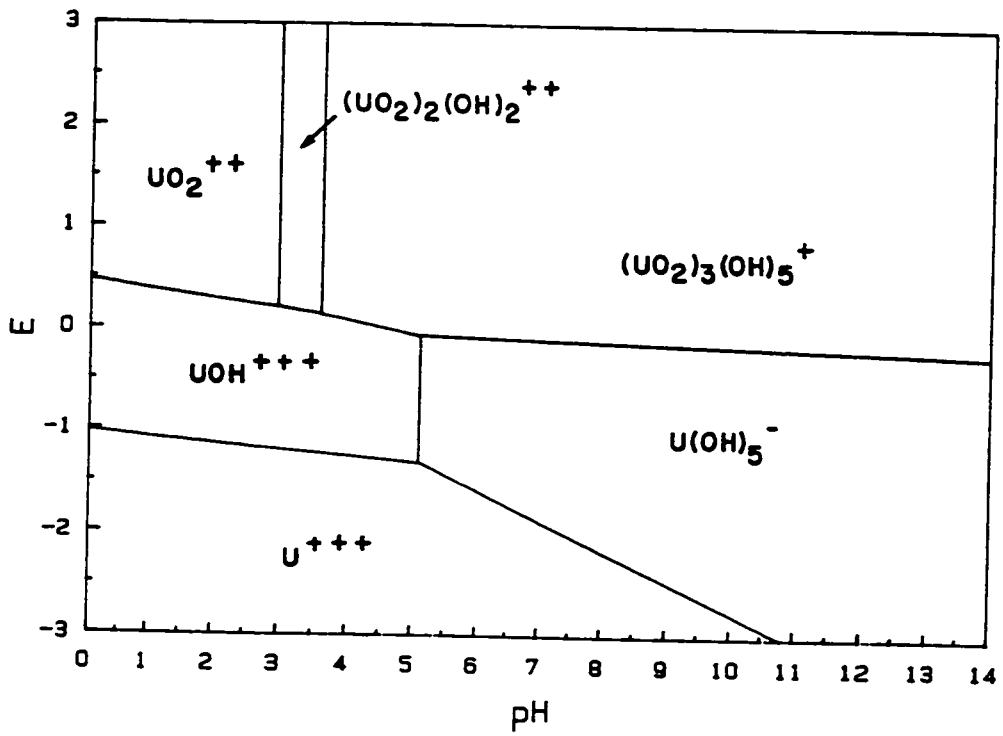

Figure 4–2 **Predominance diagram for the aqueous U system.**

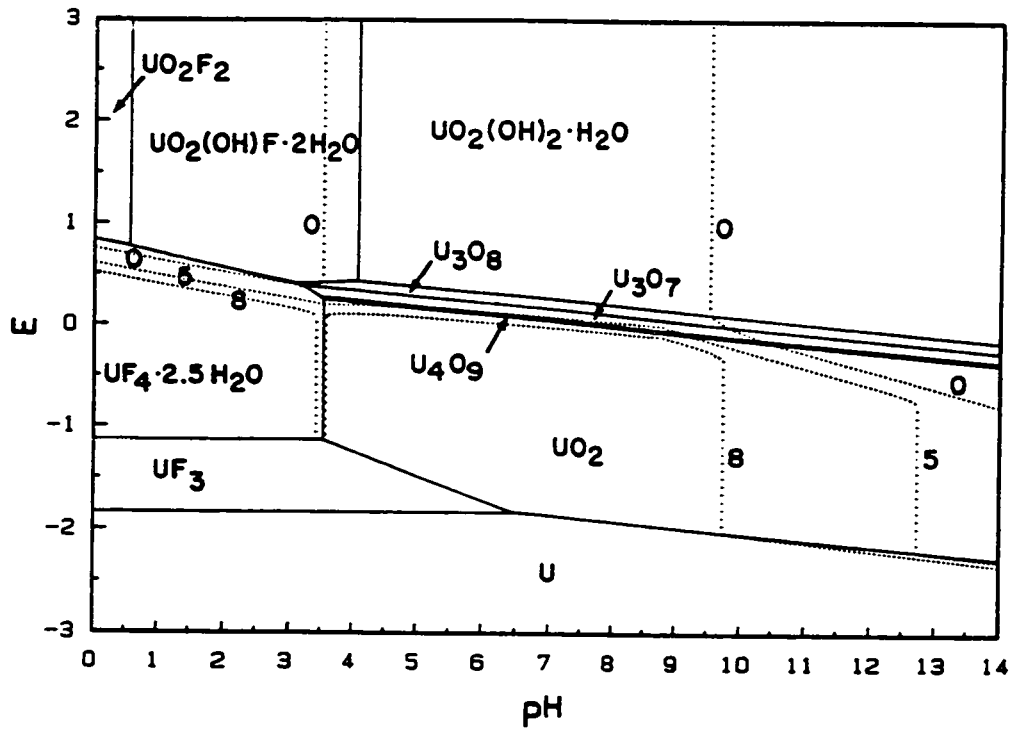

Figure 4–3 Pourbaix diagram for the aqueous U–F^-–CO_2(g) system at $a_{F^-} = 0.0001$ and $a_{CO_2(g)} = 0.00033$. Contours of constant a_U are shown for the following values of $-\log_{10} a_U$: 0, 5, 8. Carbonates were the only carbon–containing species used in the calculation of this diagram.

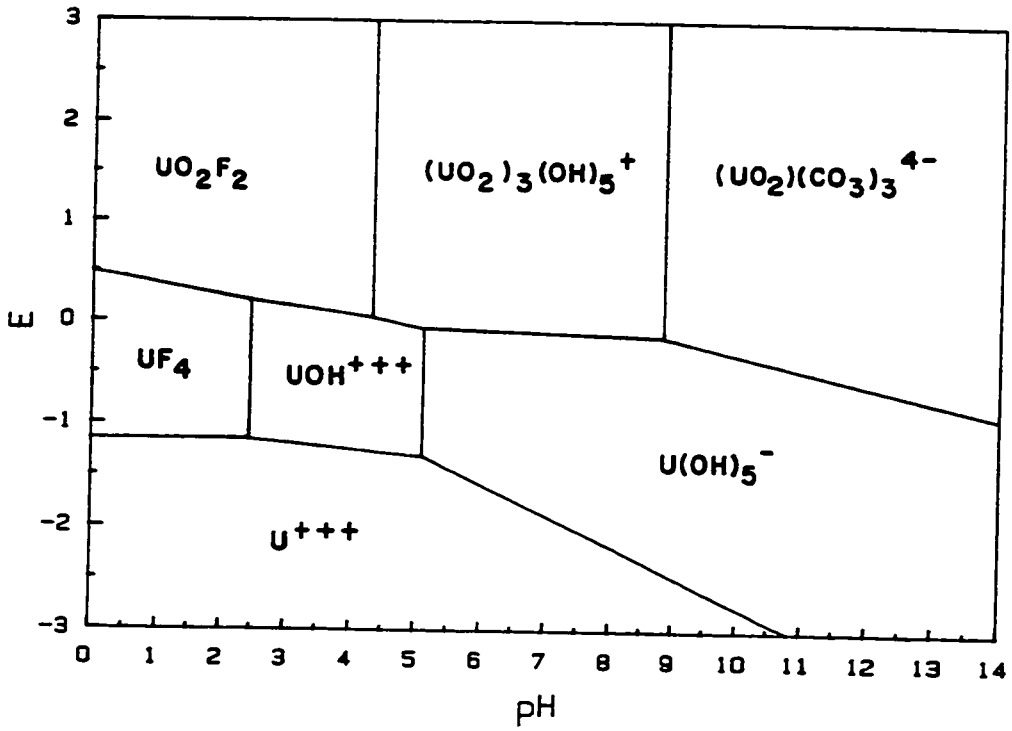

Figure 4–4 Predominance diagram for the aqueous U–F^-–CO_2(g) system at $a_{F^-} = 0.0001$ and $a_{CO_2(g)} = 0.00033$. Carbonates were the only carbon–containing species used in the calculation of this diagram.

Table 4–2

Aqueous $U–F^-–CO_2$ System: Species Included in Calculations

In addition to the species listed in Table 4–1, the following species were included in calculations for the aqueous $U–F^-–CO_2$ system:

Solid Species	Dissolved Species
UF_3	UF^{3+}
UF_4	UF_2^{2+}
$UF \cdot 2.5H_2O$	UF_3^+
UOF_2	UF_4
$UOF_2 \cdot H_2O$	UF_5^-
$UF_{4.25}$	UF_6^{2-}
$UF_{4.5}$	UO_2F^+
UF_5–alpha	UO_2F_2
UF_6	$UO_2F_3^-$
$UO_2(OH)F \cdot H_2O$	$UO_2F_4^{2-}$
$UO_2(OH)F \cdot 2H_2O$	UO_2CO_3
UO_2F_2	$UO_2(CO_3)_2^{2-}$
UO_2CO_3	$UO_2(CO_3)_3^{4-}$

4–2 and 4–4 shows that F^- and CO_2 form important complexes in solution.

4.3 Discussion

4.3.1 Limitations of Calculated Potential–pH Diagrams

Before using calculated potential–pH diagrams, it is important to recognize their inherent limitations. Potential–pH diagrams are equilibrium diagrams. Real systems, which are subject to kinetic limitations, may not behave as predicted by equilibrium thermodynamic calculations. Also, computed potential–pH diagrams are valid only for the species included in the data base. If important species in a system are not included in the thermodynamic calculations, then the resulting potential–pH diagram will not be correct. Potential–pH diagrams are only as good as the thermodynamic data from which they are calculated. Errors or uncertainties in the free energy data used lead to errors in the diagrams. Furthermore, most compilations of potential–pH diagrams assume ideal solution behavior and that the term $\ln a_w$ can be ignored.

4.3.2 Advantages of the New Method

The first advantage of the new method of calculating potential–pH diagrams is in the manner in which the problem is formulated. Once the component species have been chosen and the stoichiometric coefficients and free energy data for each species have been entered, no further balancing of equations is necessary. All reactions are written as formation reactions from components, whether or not they involve a redox transition. Species can be added to or deleted from the data set without changing the algebraic structure of the problem.

The new computational method is very efficient, making it suitable for

implementation on a microcomputer. For fixed activities of the component species, the activities of all other dissolved species can be determined sequentially, rather than simultaneously, with Equation 2.3–9. This is an enormous computational simplification.

Note that the activities of the S_k, i.e., the dissolved species containing the active redox element, can be determined without including a charge balance. In addition to the S_k, H^+, OH^-, X and Y, an aqueous redox system can contain "inert" counter ions that do not form species with the active redox element. For any net charge due to the S_k, H^+, OH^-, X and Y in the solution, the concentration of an inert counter ion necessary to maintain electroneutrality can be determined. However, when the ln a_{H_2O} term is neglected in Equation 2.3–9, the activities of the S_k do not depend on the activity of the inert counter ion. Thus, a charge balance is not necessary to calculate the activities of the S_k. (In very careful calculations, the activities of all dissolved species are related to a_{H_2O} by the Gibbs–Duhem equation.)

If ideal solution behavior is assumed (all $\gamma_k = 1$), then the concentrations of the S_k and the activities of the S_k are simply equated.

The determination of the concentrations when $\gamma_k \neq 1$ is a more complicated problem since activity coefficients generally depend on the total concentration of the solution, including inert counter ions. A simultaneous solution of the charge balance and the equilibrium equations for the S_k requires an iterative solution. However, even in this case, the new computational method provides a convenient computational framework for the problem.

The new computational method makes no assumptions about the activities of the dissolved species in calculating the contours of constant total dissolved

activity, a_M. In determining a_M, the activities of all dissolved species are taken into account, rather than assuming that only one species will be significant. In general, the total activity contours are curved lines; their representation as polygonal structures is an unnecessary artifact in computer generated Pourbaix diagrams.

In many instances, published potential–pH diagrams are "hybrids" of the Pourbaix and predominance diagrams described above. Such diagrams divide the potential–pH plane into polygonal areas of predominance, assigning solid species to some areas and and dissolved species of fixed activities to others. This is essentially an ad–hoc procedure. Pourbaix diagrams are most useful when the solubility contours on the solid stability fields are calculated using all dissolved species. Predominance diagrams are most useful when they show only dissolved species and when they are constructed so as to be independent of concentration (Angus and Angus, 1985). "Hybrid" diagrams, which show boundaries between a solid and a single dissolved species, can not show true activity contours because all dissolved species but one are neglected. Furthermore, the "hybrid" diagrams can have little or no relationship to experimentally determined diagrams.

Pourbaix wrote of determining the domains of predominance of solid species and the domains of predominance of the dissolved species and superimposing the two (1966). Therefore, the convention employed here of computing separate predominance and Pourbaix diagrams, which may be then be superimposed, not only gives a more accurate representation of the redox system, but is also more consistent with the original conception of Pourbaix.

4.3.3 Specification of Components and Their Activities

The new computational method here is extremely efficient when the chemical potentials of the "additional components" (i.e., those other than the active redox element M, H^+, e^-, and H_2O) are fixed. These chemical potentials are fixed by specification of activities, e.g., $a_{Cl^-} = 1$ or $a_{CO_2(g)} = 10^{-2}$.

In many cases, the total moles of related dissolved species, e.g., CO_3^{2-}, HCO_3^- and H_2CO_3, are constant. In some cases, these dissolved species may form complexes with the active redox element. For example, in the uranium system, total carbonate concentration, [C], is given by $[C] = [CO_3^{2-}] + [HCO_3^-] + [H_2CO_3] + [UO_2(CO_3)] + 2[UO_2(CO_3)_2^{2-}] + 3[UO_2(CO_3)_3^{4-}]$. In order to perform mole balances in a general case like this, an iterative calculation must be performed. The new method could be adapted to cases such as this.

Calculated diagrams must be interpreted carefully, in light of the components chosen and the activities specified. For example, the choice of CO_3^{2-} as a component and specification of $a_{CO_3^{2-}} = 1$ may be appropriate for analyzing the behavior of a system at high pH. However, these constraints imply enormous $CO_2(g)$ pressures at low pH, making that part of the diagram physically unrealistic. In all cases, it is important that the chemistry of the system is kept in mind during the calculation of potential–pH diagrams.

4.3.4 Specification of a Second Redox Element

The computational method presented in this chapter permits the use of other elements (as components) which may undergo redox transitions. Consider an aqueous system containing both Fe and S. Further assume that $SO_2(g)$ is chosen as one of the component species. The data set can contain species

containing different oxidation states of both Fe and S, for example, FeO, Fe_2O_3, FeS and SO_3. The new computational method will properly treat this situation. Note, however, that specification of the chemical potential of the component species $SO_2(g)$ by fixing its partial pressure restricts the chemical potential of sulfur to a single value at each pH. The chemical potential of iron, of course, is allowed to vary. A computational method that allows the chemical potentials of two redox elements to vary is certainly of interest; such a method is introduced in Chapter 7.

4.3.5 Gaseous Species Containing the Active Redox Element

Gaseous species containing the active redox element can be considered within the framework of the new method of calculation in two different ways.

The activities of gaseous redox species in equilibrium with the aqueous redox system can be computed directly with the equations for the activities of dissolved species, e.g., Equations 2.3–9, 2.3–24 and 2.3–28.

The gaseous redox species at fixed activities (fugacities or partial pressures) can also be considered. Gaseous redox species at fixed activities are computationally equivalent to additional solids in the equilibrium calculations. However, because the activity of a gaseous redox species S_g will not generally be fixed at one (as was the case with pure solids), Equation 2.3–21 must be used to compute the chemical potential of redox element M in S_g:

$$\left[\frac{(\mu_M - \mu_M^\circ)}{RT}\right]_g = -h_g(\ln 10)pH + w_g \ln a_{H_2O} + x_g \ln a_X + y_g \ln a_Y - z_g\left[\frac{F}{RT}\right](E - E_g^\circ) + \nu_{M,g} \ln a_g \qquad (2.3\text{–}21)$$

Equation 2.3–21 can be substituted into Equation 2.3–19 to give an expression for

the activity of a dissolved species S_d in equilibrium with S_g, a gaseous redox species at fixed activity, a_g.

$$a_d^{\nu_{M,k}} = (h_d - h_g)(\ln 10)pH - (w_d - w_g)\ln a_{H_2O} - (x_d - x_g)\ln a_X - (y_d - y_g)\ln a_Y + \frac{F}{RT}\left[z_d(E - E_d^\circ) - z_g(E - E_g^\circ)\right] + \nu_{M,g}\ln a_g \quad (4.3\text{–}1)$$

Notice that Equation 4.3–1 reduces to Equation 2.3–24 for $a_g = 1$. Equation 4.3–1 is a generalized version of Equation 2.3–24 that can be used to calculate the activity of a dissolved species in equilibrium with a gaseous or solid redox species at fixed activity.

Similarly, Equation 2.3–21 can be used to generalize Equations 2.3–26, 2.3–31, 2.3–32 and 2.3–33. With these generalized equations, Pourbaix diagrams can be constructed for aqueous systems containing gaseous redox species at fixed activities, as well as solid and dissolved species, using the algorithm in Chapter 4.2.4.

CHAPTER 5

ELECTRON NUMBER DIAGRAMS FOR AQUEOUS SYSTEMS CONTAINING ONE ACTIVE REDOX ELEMENT

5.1 Introduction

5.1.1 Problems with Potential–pH Diagrams

As documented in Chapter 3, potential–pH diagrams have proven to be very useful in a wide variety of applications. However, they have shortcomings which arise from the use of potential as an independent variable.

First, because potential is not a conserved quantity, one cannot locate a point on a potential–pH diagram from a knowledge of composition and pH. This is a serious difficulty in many practical situations where composition is the independent variable that is known and controlled rather than potential. As a corollary, one cannot follow simple process trajectories nor can one make graphical material balances on potential–pH diagrams.

Secondly, in the vicinity of stable compounds, very small changes in chemical composition can give rise to very large differences in potential. Conversely, when two solid phases are present, very large changes in composition can give rise to no change in potential. Therefore, large areas on a potential–pH diagram can correspond to small regions in composition space and vice versa. Consequently, the diagrams do not always lend themselves to easy, intuitive interpretation.

5.1.2 Basic Concept of Electron Number Diagrams

The three–dimensional equilibrium surface in a Pourbaix diagram defines the solubility limit of the active redox element M. The equilibrium surface divides the three–dimensional space defined by E, pH and $-\log a_M$ into an accessible region in which the undersaturated aqueous phase exists and an inaccessible region in which the solubility limit is exceeded. On the surface, the aqueous phase exists in equilibrium with a solid phase.

A new representation of the equilibrium surface is proposed which retains the remarkable information content of the Pourbaix diagram, but which gains the advantages of conventional metallurgical phase diagrams. To achieve this the electrochemical potential is replaced with the number of electrons per atom of active element. The chemical potential of electrons and the number of electrons are conjugate thermodynamic variables. The resulting diagrams are closely analogous to conventional metallurgical phase diagrams and have many of their useful features. These features arise because electrons are conserved in a chemical reaction just as atoms are conserved.

In this connection, note that the normal variables used in plotting phase diagrams are T and x (mole fraction). Diagrams of T vs. μ (chemical potential) have not found as widespread use. The new diagrams are analogous to T–x diagrams; Pourbaix diagrams are analogous to T–μ diagrams.

5.2 Electron Numbers

5.2.1 Choice of System

Consider a reaction mixture containing an arbitrary number of species which can undergo redox transitions with each other. The discussion here is

restricted to situations involving a single active redox element. The thermodynamic system is comprised of all species containing that active element.

For example, the reaction mixture could be a piece of solid CuO in contact with an aqueous solution. The active redox element is copper. The system is the solid CuO and all copper containing species in the solution.

The concept of electron number can be extended to aqueous systems containing more than one redox element. This will be described in Chapter 7.4.

5.2.2 Practical Measure of Electron Concentration

A simple, practical measure of the electron concentration in a system containing a single active redox element is required. The considerations for choice of this measure are similar to those encountered when defining elemental (atomic) composition. For example, the measure should be normalized by the scale of the system to permit consideration of systems of arbitrary size. The measure should be unambiguous and independent of thermal expansion or contraction. Finally, the numerical values of the measure should be on the order of unity and should be easy to compute and to remember.

The measure of electron concentration is chosen as the difference between the number of electrons per atom of active element in the system and in the pure elemental form.

For example, consider a system comprised of a single chemical species, S_i, which contains the active element, M. The electron number, z_i, of S_i is defined by:

$$z_i \equiv n_0 - n_i \tag{5.2–1}$$

where n_0 is the number of electrons per atom of element M in its elemental form

and n_i is the number of electrons per atom of active element M in the species S_i.

The above definition is convenient because the numerical value of z_i for a single species, S_i, is just equal to the electrochemical valence as conventionally defined. In other words, it is the number of electrons participating in the half cell reaction between the species S_i and one atom of the active element, M. Expressed in terms of Equations 2.1–5 and 2.1–8

$$M = \nu_{M,i}S_i + h_iH^+ + w_iH_2O + z_ie^- + x_kX + y_kY \qquad (5.2\text{–}2a)$$

For example, for $S_i = Cu_2O$ one has

$$Cu = 1/2Cu_2O + H^+ - 1/2H_2O + e^- \qquad (5.2\text{–}2b)$$

where $\nu_{Cu,i} = 1/2$, $h_i = 1$, $w_i = -1/2$ and $z_i = 1$.

Equation 5.2–2a may also be written as

$$0 = \nu_{M,i}S_i + h_iH^+ + w_iH_2O + z_ie^- + x_kX + y_kY - M \qquad (5.2\text{–}3a)$$

In Equation 5.2–3a, all species participating in the reaction are written on one side of the equation. When reactions are written in this common form, reactants are conventionally assigned negative stoichiometric coefficients and products are assigned positive stoichiometric coefficients. Notice that the term z_ie^- is assigned a positive coefficient in Equation 5.2–3a, which is an oxidation when $z_i > 0$ and a reduction when $z_i < 0$. In either case, the electron number and the valence of the active redox element in S_i are unambiguously given by the coefficient of the electrons in the formation reaction.

Equation 5.2–2b, rewritten in the form of Equation 5.2–3a, becomes:

$$0 = 1/2Cu_2O + H^+ - 1/2H_2O + e^- - Cu \qquad (5.2\text{–}3b)$$

Notice that the coefficient of the e^- term (+1), is equal to z_i and to the valence of copper in Cu_2O.

In most situations of practical interest, numerous species containing the

active element are present. Let $\alpha_{M,i}$ be the number of atoms of active element in one molecule of species S_i (for Cu_2O, $\alpha_{Cu,i} = 2$) and N_i the number of moles of species S_i. A measure of the total number of electrons in such a system is obtained by multiplying Equation 5.2–1 by $\alpha_{M,i}N_i$ and summing over all species:

$$\Sigma\, \alpha_{M,i} z_i N_i = \Sigma\, \alpha_{M,i}(n_o - n_i)N_i \tag{5.2–4}$$

$$\Sigma\, \alpha_{M,i} z_i N_i = N_{e,o} - N_{e,t} \tag{5.2–5}$$

where $N_{e,t} = \Sigma \alpha_{M,i} n_i N_i$ is the total number of moles of electrons associated with the active element in the system and $N_{e,o} = \Sigma \alpha_{M,i} n_o N_i$ is the total number of moles of electrons associated with the active element in the system if it were in the elemental state. The sums in Equations 5.2–4 and 5.2–5 are over all species containing the active element.

The total number of moles, $B_{M,t}$, of active element M in the system is just:

$$B_{M,t} = \Sigma\, \alpha_{M,i} N_i \tag{5.2–6}$$

where the sum is taken over all species in the system that contain active redox element M. The average electron number, $\bar{z}$, of the system is defined as the atom number average, i.e.,

$$\bar{z} \equiv \frac{N_{e,o} - N_{e,t}}{B_{M,t}} \tag{5.2–7}$$

Or alternately, using equations 5.2–5, 5.2–6 and 5.2–7

$$\bar{z} \equiv \frac{\Sigma\, \alpha_{M,i} z_i N_i}{\Sigma\, \alpha_{M,i} N_i} \tag{5.2–8}$$

Equation 5.2–8 is an atom average. For example, if the system contained three moles of Cu^{++} and three moles of Cu°,

$$\bar{z} = [(1)(2)(3) + (1)(0)(3)]/[(1)(3) + (1)(3)] = 1 \tag{5.2–9}$$

For a system comprised entirely of 0.1 mole of $Na_2Cr_2O_7$, the $\bar{z}$ for Cr is:

$$\bar{z} = (2)(6)(0.1)/(2)(0.1) = +6 \tag{5.2–10}$$

Numerically, $\bar{z}$ is a number average valence. However, thinking of $\bar{z}$ as a measure of the number of electrons emphasizes that it is a conserved quantity.

5.2.3 Elementary Calculations Using Electron Numbers

The above measure of electron concentration permits the derivation of very simple and useful relationships which describe electron conservation in complex systems containing solid phases and an aqueous phase with many active redox species. For example, consider the very common situation of a single solid phase, S_s, in equilibrium with an aqueous phase containing a number of dissolved species, S_k. Equation 5.2–8 can be rewritten:

$$\bar{z} = \frac{\alpha_{M,s} z_s N_s + \sum_{aq} \alpha_{M,k} z_k N_k}{\alpha_{M,s} N_s + \sum_{aq} \alpha_{M,k} N_k} \tag{5.2–11}$$

For the aqueous phase alone

$$\bar{z}_{aq} = \frac{\sum_{aq} \alpha_{M,k} z_k N_k}{\sum_{aq} \alpha_{M,k} N_k} \tag{5.2–12}$$

The summations in Equations 5.2–11 and 5.2–12 are taken over all dissolved species.

Equation 5.2–12 can be rewritten

$$\bar{z}_{aq} B_{M,aq} = \sum_{aq} \alpha_{M,k} z_k N_k \tag{5.2–13}$$

where $B_{M,aq}$ is the total number of moles of active element M in the aqueous phase given by

$$B_{M,aq} = \sum_{aq} \alpha_{M,k} N_k \tag{5.2–14}$$

where N_k is the number of moles of species S_k. The total number of moles of active element M in the solid phase is just

$$B_{M,s} = \alpha_{M,s} N_s \tag{5.2–15}$$

so using Equations 5.2–11 through 5.2–15, along with Equation 5.2–6, the following equation can be obtained:

$$\bar{z}B_{M,t} = z_s B_{M,s} + \bar{z}_{aq} B_{M,aq} \tag{5.2–16}$$

Equation 5.2–16 is the expression that must be obeyed to insure conservation of electrons in a redox system containing a solid phase and an aqueous phase. One also has the conservation of atoms of active element, M. This is simply

$$B_{M,t} = B_{M,s} + B_{M,aq} \tag{5.2–17}$$

The two conservation laws embodied in Equations 5.2–16 and 5.2–17 can be used to perform electron and atom balances on electron number diagrams; this will be demonstrated later.

In the analysis of aqueous redox systems, the relationship between electron number and the concentrations of the dissolved species containing the active redox element is quite useful. Dividing both sides of Equation 5.2–14 by the total mass of water in the system in kilograms, m_{H_2O}, gives an expression relating the total molal concentration of the active redox element, $[M]_{aq}$, to the molal concentrations of the dissolved species in the system:

$$[M]_{aq} = \sum_{aq} \alpha_{M,k}[S_k] \tag{5.2–18}$$

where $[M]_{aq} \equiv B_{M,aq}/m_{H_2O}$ and $[S_k] \equiv N_k/m_{H_2O}$. The average electron number in the aqueous phase is obtained by dividing the top and bottom of the right hand side of Equation 5.2–12 by m_{H_2O}.

$$\bar{z}_{aq} = \frac{\sum_{aq} \alpha_{M,k} z_k [S_k]}{\sum_{aq} \alpha_{M,k} [S_k]} \qquad (5.2\text{–}19)$$

5.3 Examples of Electron Number Diagrams

5.3.1 Computations

The redox equilibria were solved using the method of virtual species described in Chapter 4. Ideal solutions, pure solid phases, a pressure of 1 atmosphere and a temperature of 25°C were assumed. The thermochemical data used were chosen to facilitate comparison of the new diagrams with published Pourbaix diagrams (Pourbaix, 1966; Wagman, et al., 1982). The species considered in the calculations are listed in Table 5–1 unless otherwise indicated.

At any E and pH, the stable solid phase was determined by the phase stability criterion described in Chapter 4. The equilibrium concentrations, $[S_k]$, of all dissolved species, S_k, in equilibrium with the stable solid phases were computed using the methods of Chapter 4 (Angus and Angus, 1985; Angus, Lu and Zappia, 1987).

5.3.2 Plotting Electron Number Diagrams

Pourbaix diagrams can be visualized as three–dimensional surfaces in $E/pH/-\log_{10}a_M$ space, as described in Chapters 3 and 4. The transformed diagrams, which could be represented in $\bar{z}/pH/-\log_{10}a_M$ space, are actually represented in $\bar{z}/pH/-\log_{10}a^*_M$ space. The activity a^*_M was defined in Equation 2.3–37. For simplicity, the γ_i of all dissolved species i are generally assumed to be equal to unity. With this assumption, a^*_M becomes equal to the total dissolved

Table 5–1

Species Used to Calculate the Electron Number Diagrams in Figures 5–3 Through 5–13

Aqueous Cu System: Species Included in Calculations

Solid Species

Cu	Cu_2O	CuOH
$Cu(OH)_2$	CuO	Cu_2O_3
CuCl	$CuCl_2$	$CuCl_2 \cdot 2H_2O$
$CuCl_2 \cdot 3Cu(OH)_2$		

Dissolved Species

Cu^+	Cu^{2+}	CuO_2^{2-}
$HCuO_2^-$	Cu^{3+}	CuO_2^-
$CuCl_2^-$	$CuCl_3^{2-}$	$CuCl^+$
$CuCl_2$		

Table 5–1 (continued)

Aqueous S System: Species Included in Calculations

Solid Species

S

Dissolved Species

S^{2-}	HS^{-}	H_2S
$S_2O_3^{2-}$	$HS_2O_3^{-}$	$H_2S_2O_3$
SO_3^{2-}	HSO_3^{-}	H_2SO_3
S_2^{2-}	S_3^{2-}	S_4^{2-}
S_5^{2-}	SO_4^{2-}	HSO_4^{-}

Table 5–1 (continued)

Aqueous Cr System: Species Included in Calculations

Solid Species

Cr	$Cr(OH)_2$	$Cr(OH)_3$
Cr_2O_3	CrO_2	CrO_3

Dissolved Species

Cr^{2+}	Cr^{3+}	$CrOH^{2+}$
$Cr(OH)_2^{+}$	$Cr(OH)_3$	$Cr_2(OH)_2^{4+}$
$Cr_3(OH)_4^{5+}$	$Cr(OH)_4^{-}$	CrO_2^{-}
CrO_3^{3-}	CrO_4^{3-}	CrO_4^{2-}
$HCrO_4^{-}$	H_2CrO_4	$Cr_2O_7^{2-}$

concentration, $[M]_{aq}$, of active element M. The new diagrams are consequently represented in $\bar{z}$/pH/$-\log_{10}[M]_{aq}$ space.

The three–dimensional nature of Pourbaix diagrams for aqueous systems containing a single redox element was discussed in Chapter 3. Dimensionality is preserved in the transformation to electron number diagrams, which must also be three–dimensional. Three–dimensional electron number diagrams, constructed in $\bar{z}$/pH/$-\log_{10}[M]_{aq}$ space, are shown for the aqueous copper system in Figure 5–1 and for the aqueous sulfur system in Figure 5–2. These diagrams can be compared with the three–dimensional Pourbaix diagrams in Figures 3–2 and 3–3, which were calculated using the same species. Figures 5–1 and 5–2 actually show the surface representing the aqueous phase in equilibrium with the stable solid phases in a system. For example, each point on the equilibrium surface in Figure 5–2 is in equilibrium with solid S, for which $z = 0$.

The three principal axes (E, pH and $-\log_{10}a_m$) of Pourbaix diagrams are measures of chemical potentials, which must be equal in all phases at equilibrium. However, phases in equilibrium generally have different values of $\bar{z}$. Thus, projections of the three–dimensional electron number figure, onto the $\bar{z}$/pH plane for example, are not simple to produce or interpret. It is much more instructive to plot intersections of the three–dimensional figure with planes of constant pH, $\log_{10}[M]_{aq}$ or $\bar{z}$.

Examples of intersections with planes of constant pH for the copper, sulfur, chromium and uranium systems are shown in Figures 5–3 through 5–14. It should be emphasized that these diagrams are computed and presented for illustration and for comparison with existing Pourbaix diagrams. The intersections of the three–dimensional electron number figure for the aqueous sulfur system with

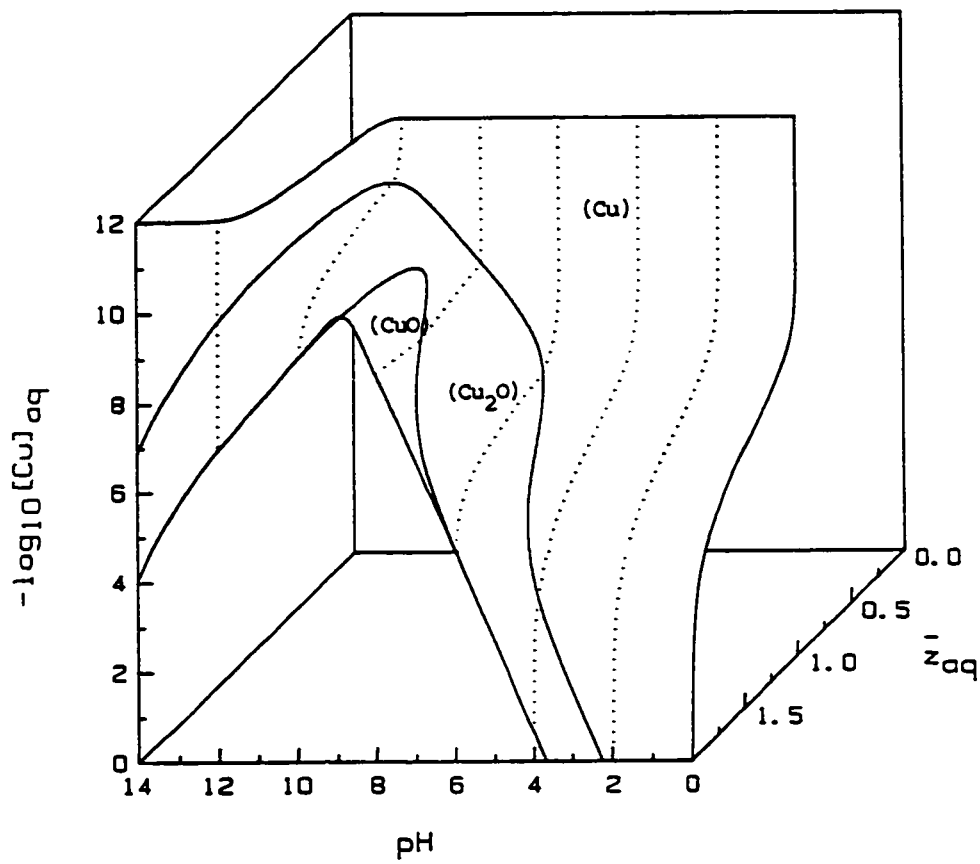

Figure 5–1 Three-dimensional electron number diagram for the aqueous copper system. The surface shows the electron number of the aqueous phase in equilibrium with stable copper–containing solids. The solids in parentheses are in equilibrium with the designated sections of the aqueous surface.

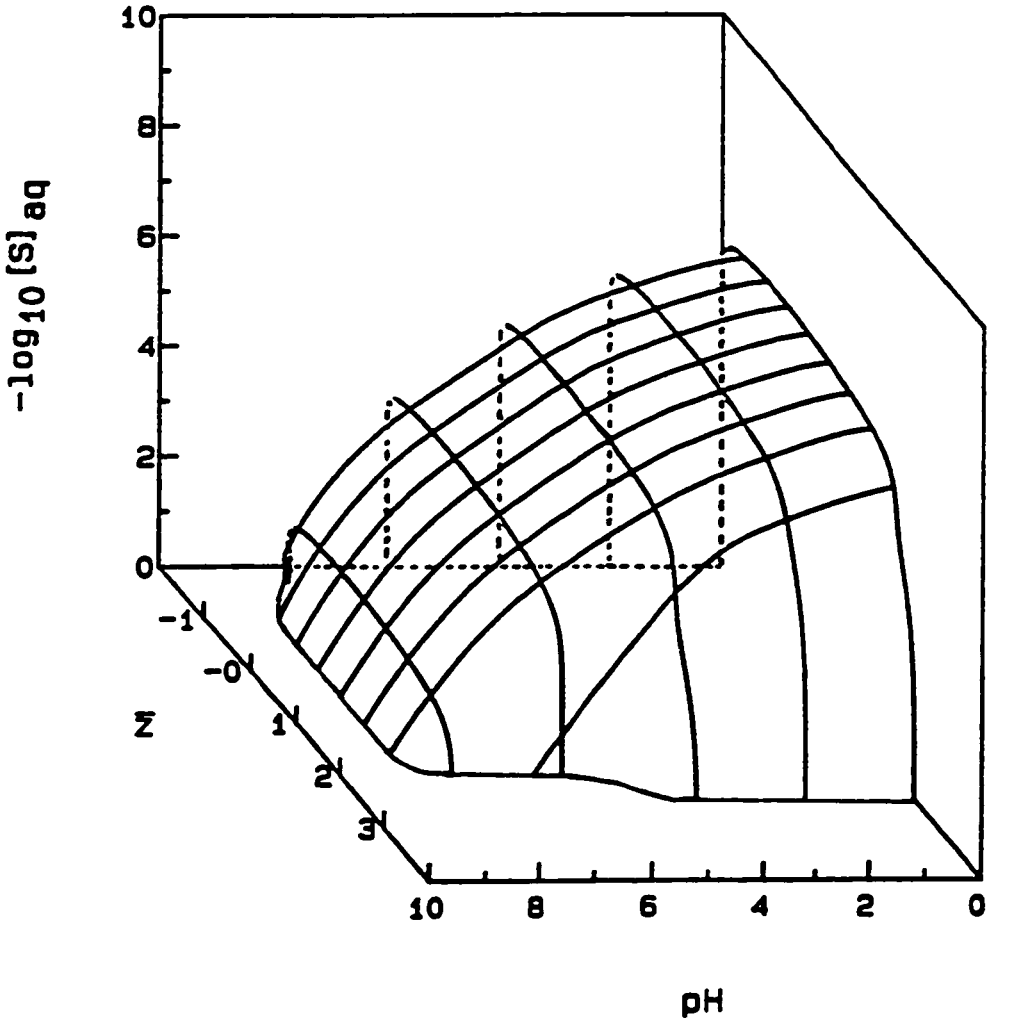

Figure 5–2 Three–dimensional electron number diagram for the aqueous sulfur system. The surface shows the electron number of the aqueous phase in equilibrium with solid S ($z = 0$).

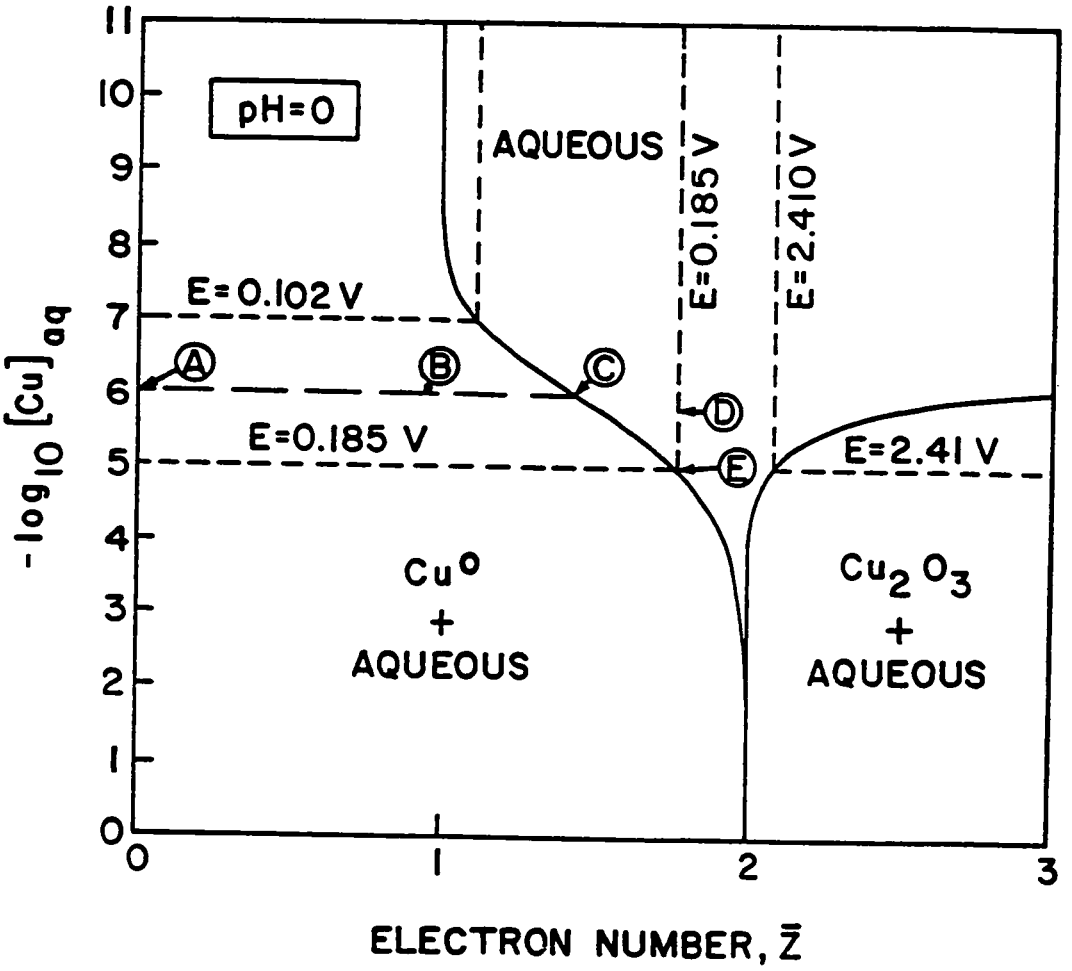

Figure 5–3 Electron number diagram for the aqueous copper system at pH = 0. Equilibrium line of a solution ($[Cu]_{aq} = 10^{-6}$ molal) with solid Cu is shown along line $\overline{ABC}$. Evaporation trajectory at constant $\bar{z} = 1.75$ is shown along the line $\overline{DE}$.

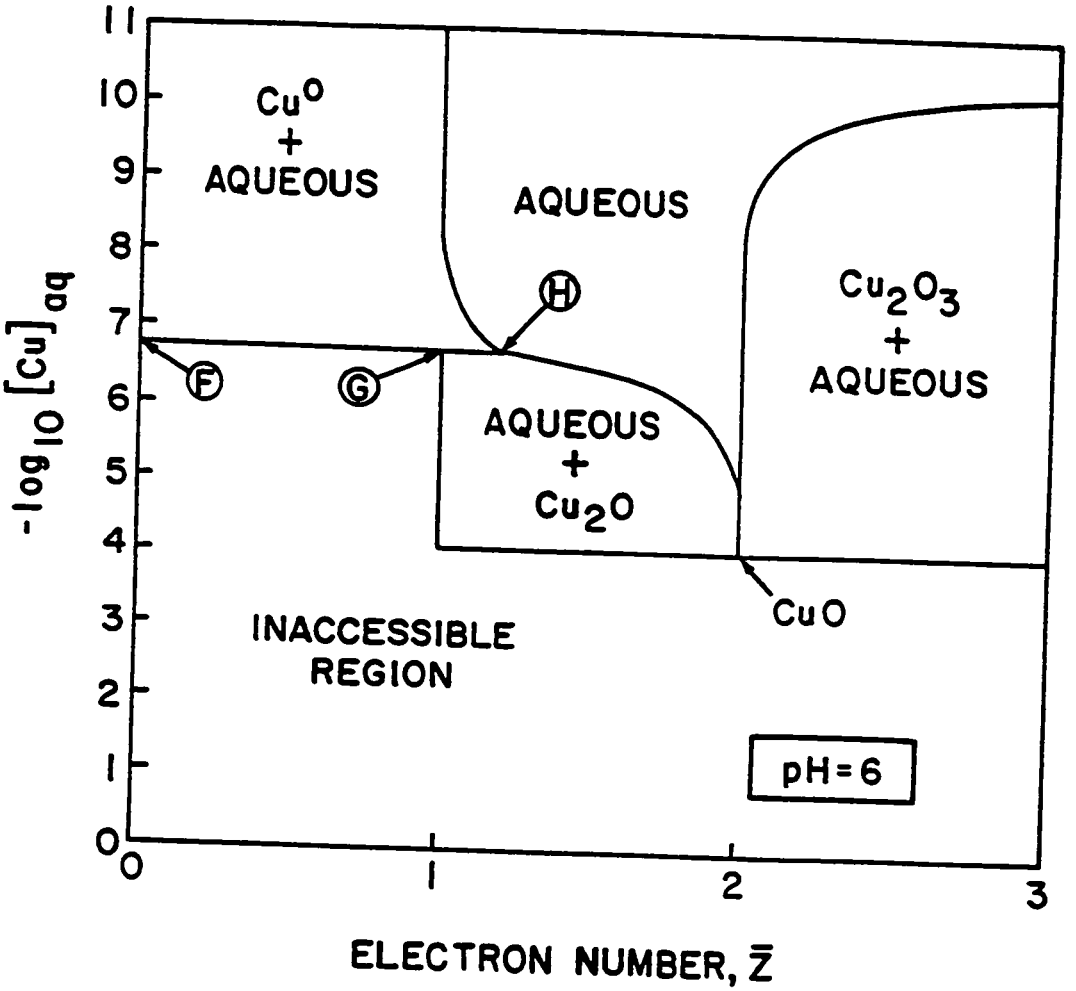

Figure 5–4 Electron number diagram for the aqueous copper system at pH = 6. Note the peritectic reaction between Cu, Cu_2O and the aqueous phase along the line $\overline{FGH}$.

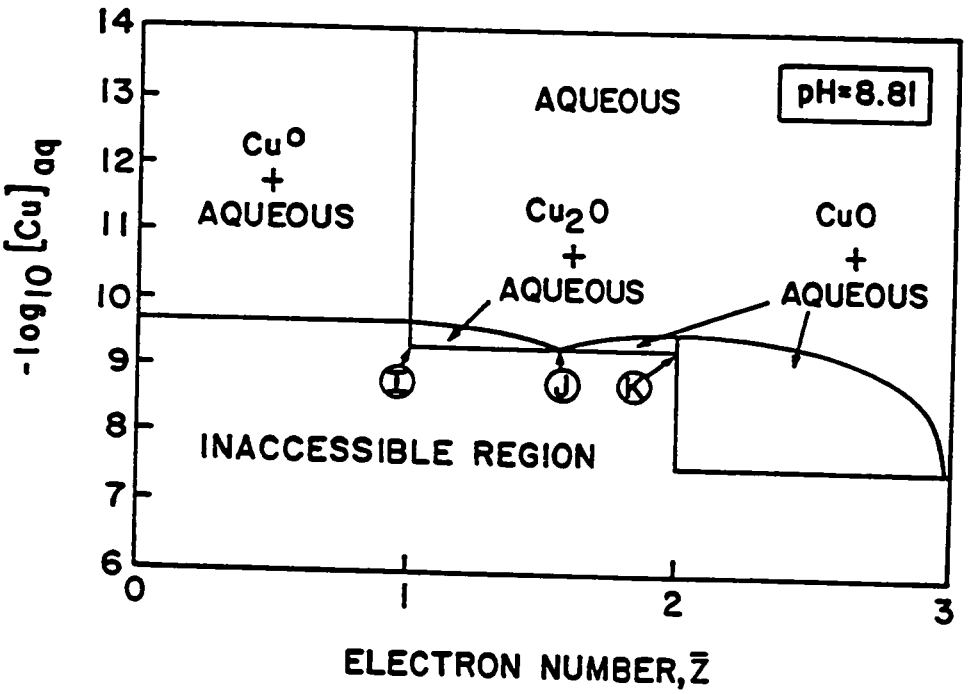

Figure 5–5 Electron number diagram for the aqueous copper system at pH = 8.81. Note the eutectic reaction between Cu_2O, the aqueous phase and CuO along the line $\overline{IJK}$.

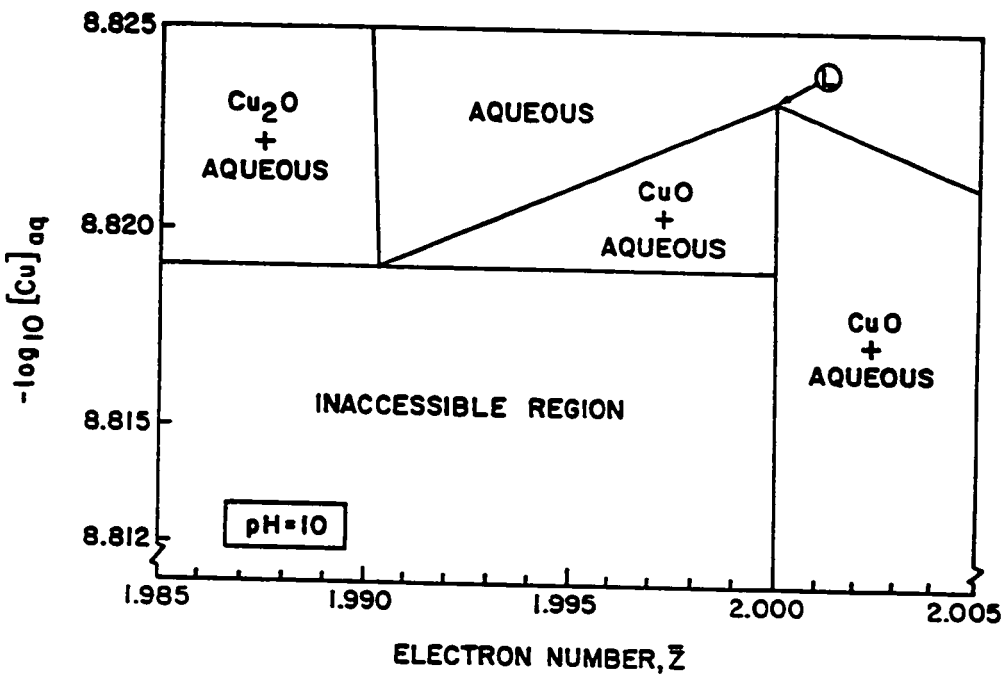

Figure 5–6 Electron number diagram for the aqueous copper system at pH = 10. Detail of electron number diagram near $\bar{z} = 2$. Note the congruent type dissolution of CuO at point L and the eutectic type reaction between Cu_2O, the aqueous phase and CuO.

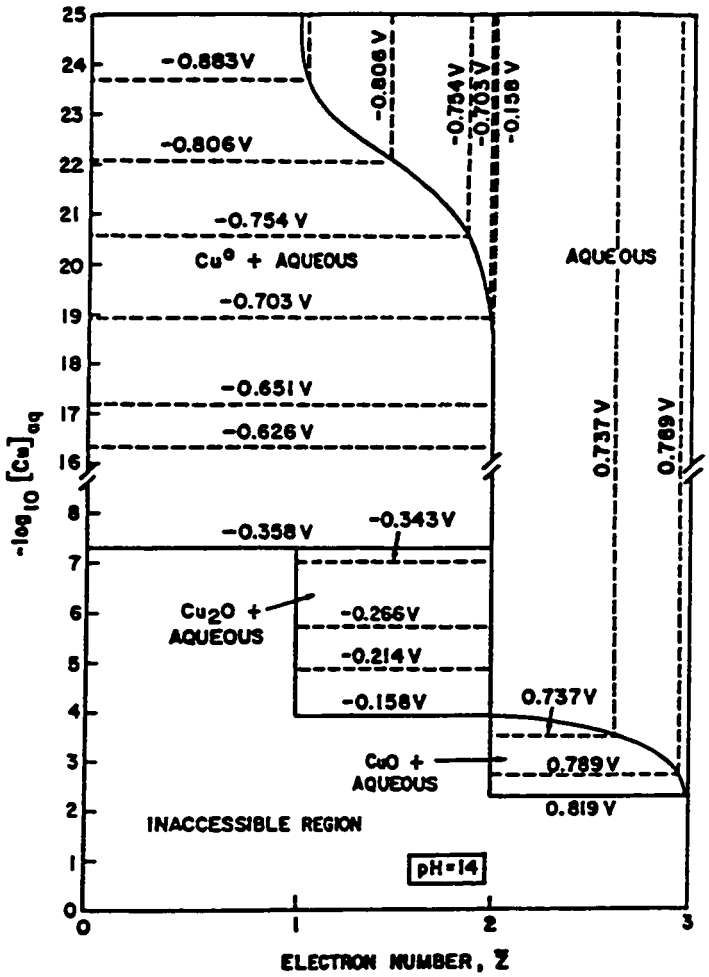

Figure 5–7 Electron number diagram for the aqueous copper system at pH = 14. Constant potential lines are shown.

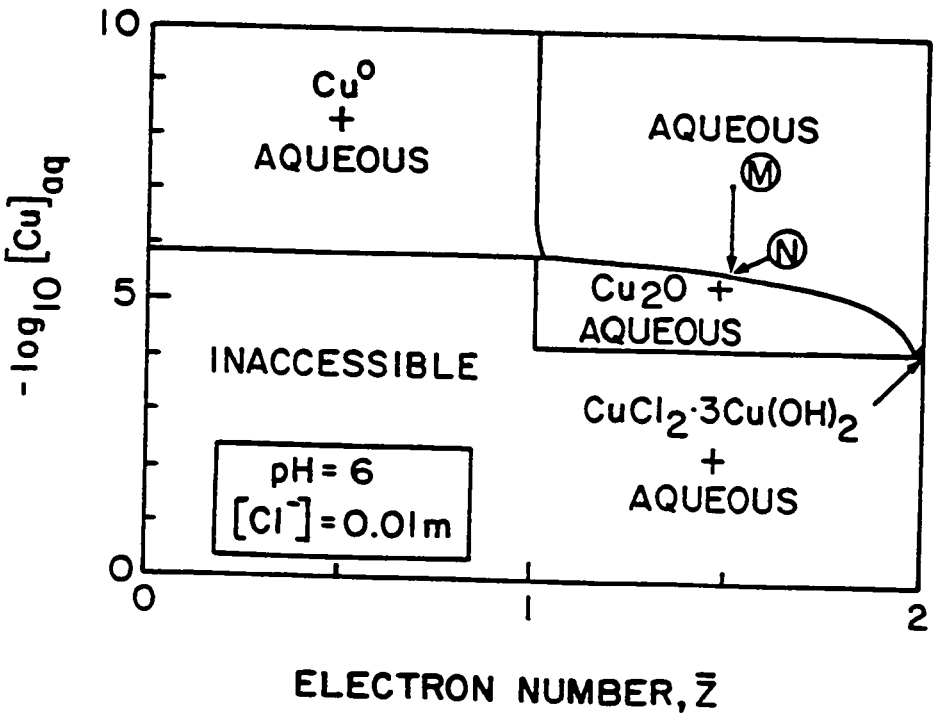

Figure 5–8 Electron number diagram for the aqueous Cu–Cl^- system at pH = 6 and $[Cl^-] = 0.01$m. Evaporation of a solution with $\bar{z} = 1.5$ at constant pH and $\bar{z}$ follows the line $\overline{MN}$. Solid Cu_2O precipitates out at point N.

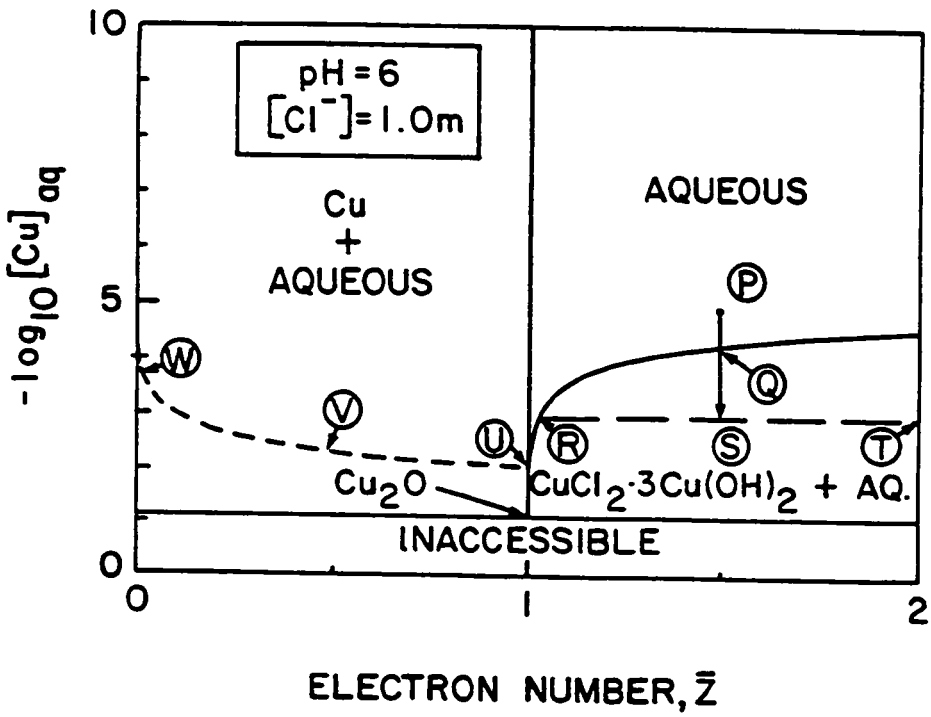

Figure 5–9 Electron number diagram for the aqueous Cu–Cl^- system at pH = 6 and $[Cl^-] = 1.0m$. The evaporation trajectory along a path of constant $\bar{z} = 1.5$ is shown along line $\overline{PQS}$. The final equilibrium state is along the line $\overline{RST}$. The trajectory followed during electroplating of a solution with original concentration of 0.01 molal dissolved copper is shown along the line $\overline{UVW}$.

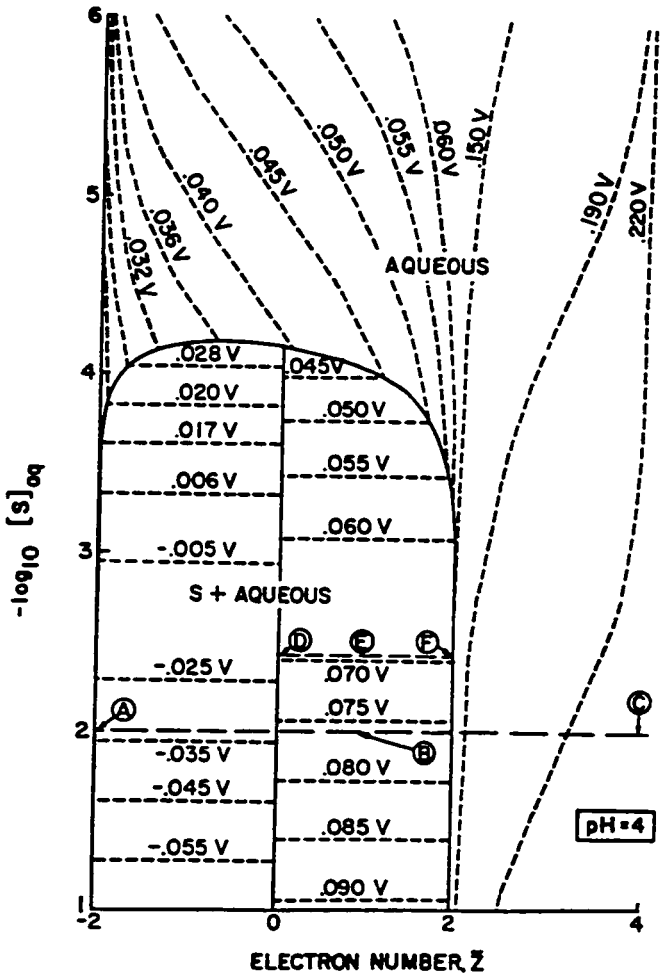

Figure 5–10 Electron number diagram for the aqueous sulfur system at pH = 4. The mixing of equal amounts of 0.01 molal solutions of S^{2-} (point A) and SO_3^{2-} (point C) to give a mixing point of B is illustrated. Because of precipitation of solid sulfur, the final system point moves to E. In the final equilibrium state, a two–phase system exists along line $\overline{DEF}$.

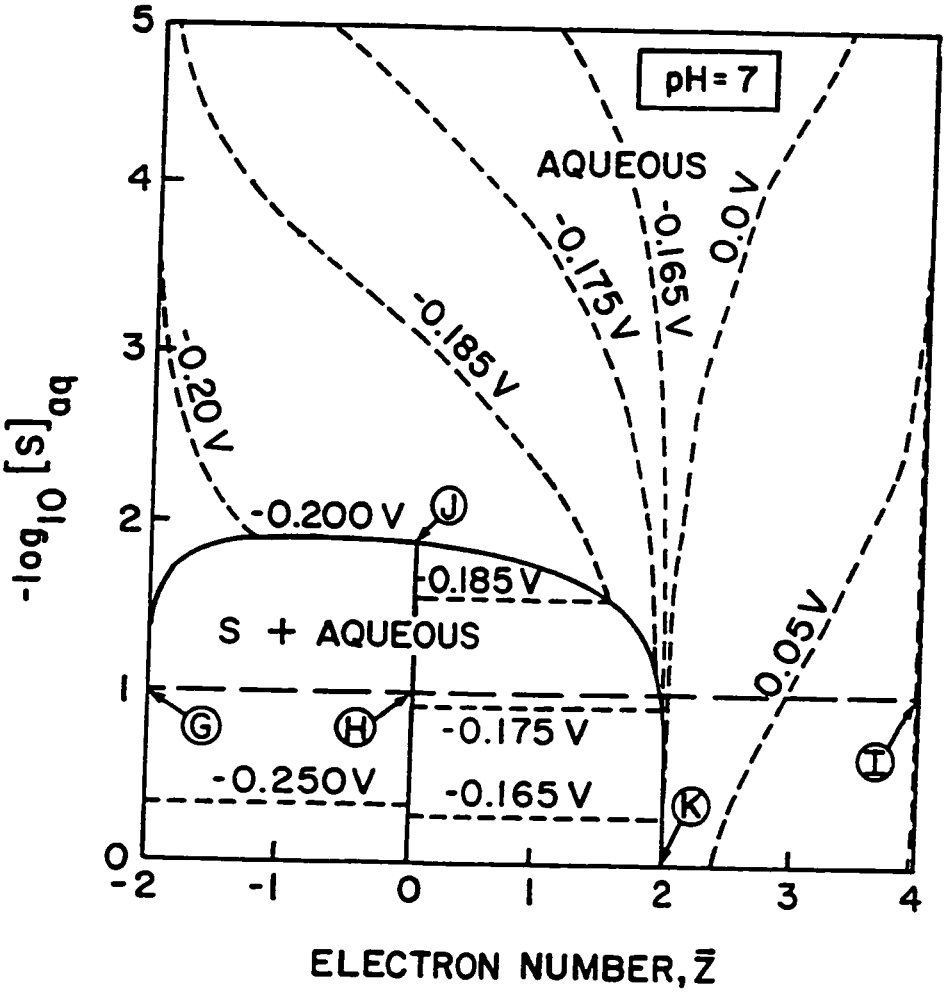

Figure 5–11 Electron number diagram for the aqueous sulfur system at pH = 7. (Bisulfate and sulfate ions are not included in the calculation.) The mixing of 0.1 molal solutions of S^{2-} (point G) and SO_3^{2-} (point I) in the ratio of 2/1 to give a mixing point at H with $\bar{z} = 0$ is shown. Because of the requirement that the solution have $\bar{z}_{aq} = 0$, the final state of the solution is at point J.

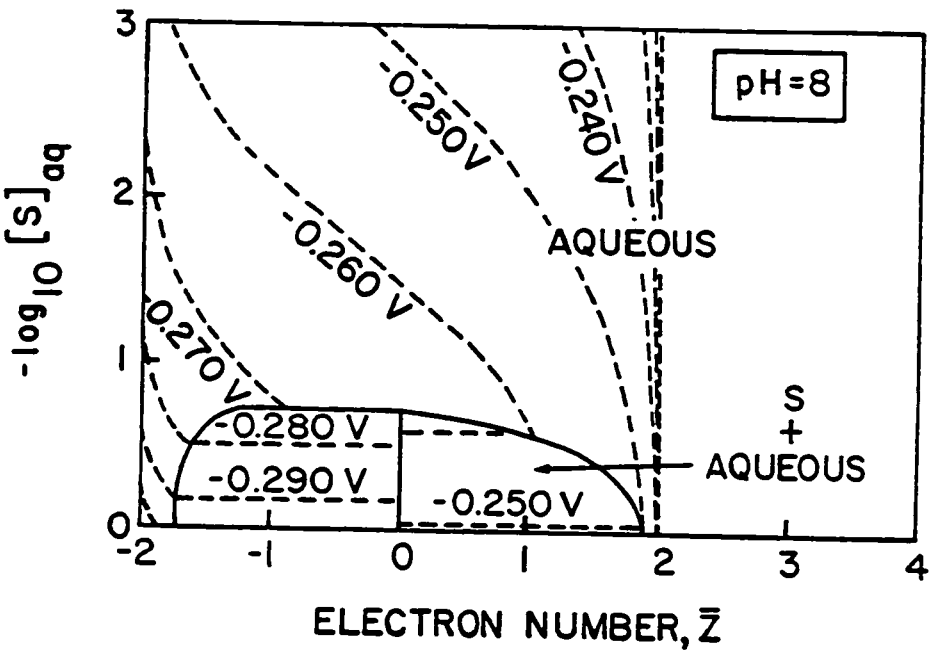

Figure 5–12a Electron number diagram for the aqueous sulfur system at pH = 8. (Bisulfate and sulfate ions are not included in the calculation.)

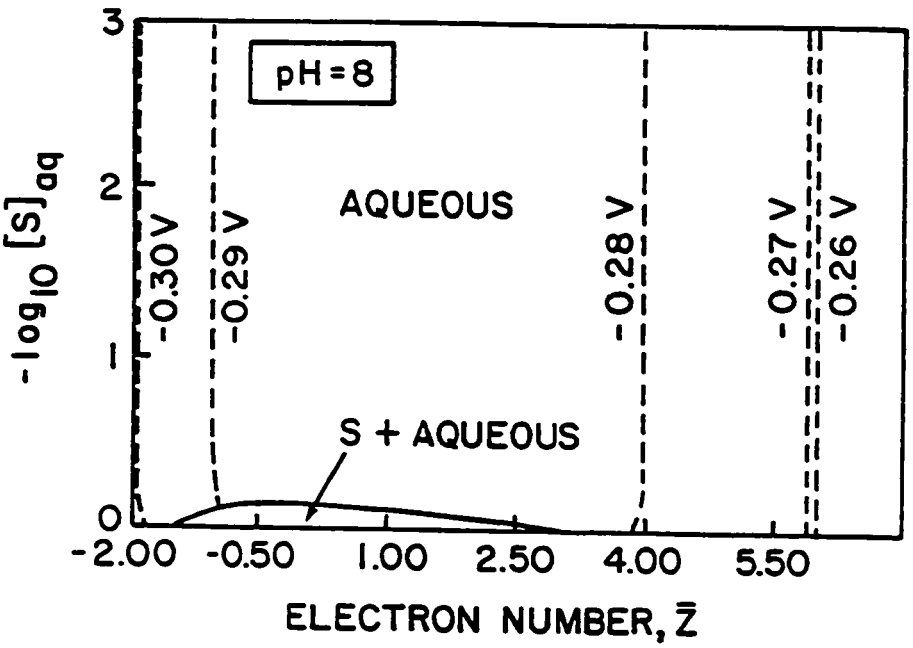

Figure 5–12b Electron number diagram for the aqueous sulfur system at pH = 8. (Bisulfate and sulfate ions are included in the calculation.) Note the greatly increased solubility of sulfur compared to that shown in Figure 5–12a.

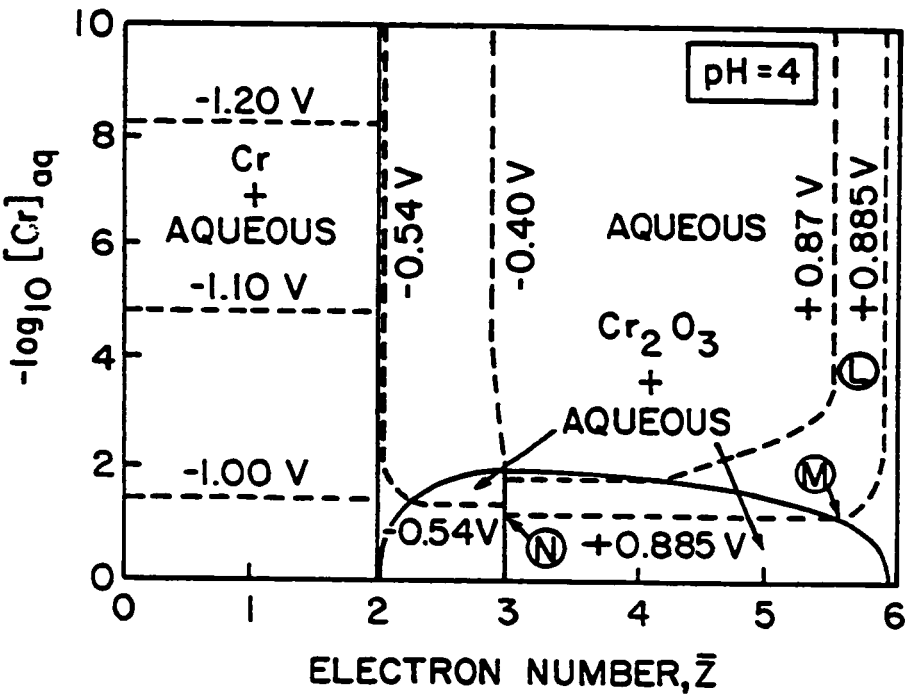

Figure 5–13 Electron number diagram for the aqueous chromium system at pH = 4. Evaporation trajectory of a solution held at 0.885V (≈.07ppm O_2 in N_2) is shown along the line $\overline{LMN}$.

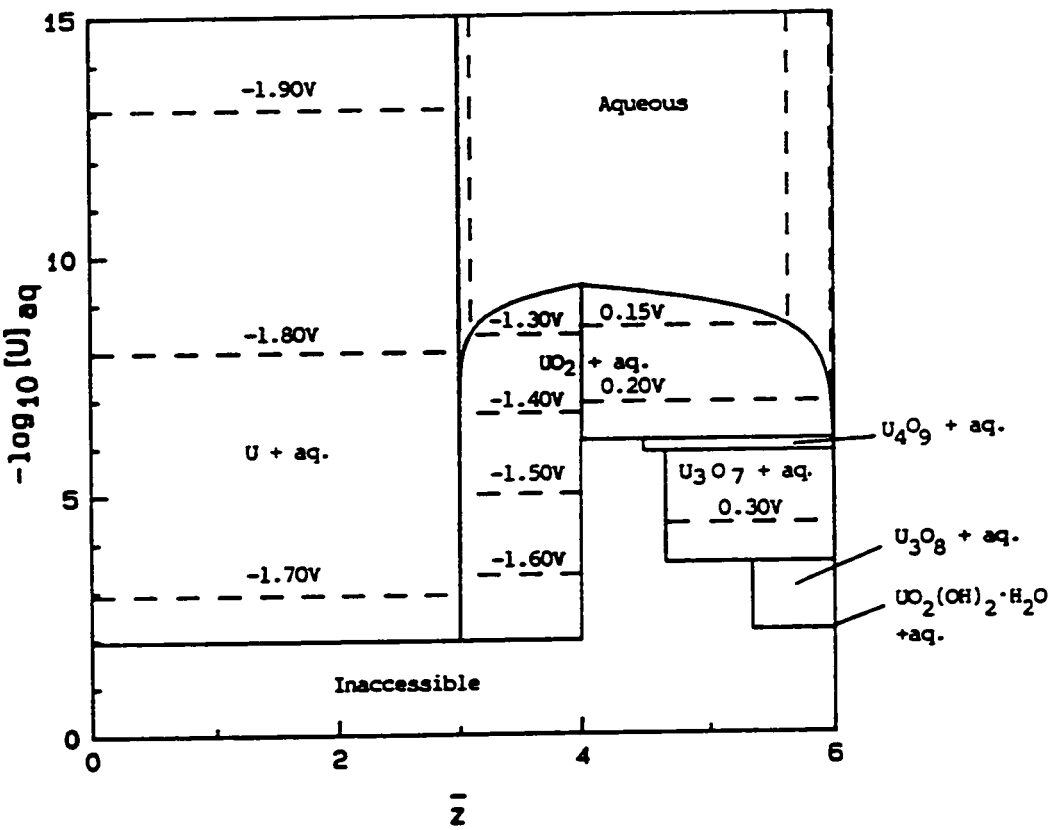

Figure 5–14 Electron number diagram for the aqueous uranium system at pH = 4.

planes of constant $\bar{z}$ are shown in Figures 5–15 and 5–16. Finally, intersections of the three–dimensional electron number figure for the aqueous copper system with planes of constant $-\log_{10}[Cu]_{aq}$ are shown in Figures 5–17 and 5–18.

Non–idealities in the solution and the presence of species not considered in the calculations will cause the diagrams, computed with the assumption of ideal solution behavior, to differ from experimentally determined diagrams. In Figures 5–3 through 5–7, the counter ions were assumed to form no insoluble salts or complexes with any of the active ions present. This assumption, commonly used in constructing Pourbaix diagrams, may be relaxed if desired. For example, in Figures 5–8 and 5–9, the reactive ion Cl^- is present and complexes, e.g., $CuCl^+$, and insoluble chloride compounds, e.g., $CuCl_2$, were considered in the calculations. The diagrams for sulfur shown in Figures 5–10, 5–11 and 5–12a were constructed without considering the presence of sulfates or bisulfates. However, the sulfur diagram shown in Figure 5–12b does include sulfate and bisulfate ions.

5.3.3 Examples of $-\log_{10}[M]_{aq}$ versus $\bar{z}$ Diagrams

Intersections of the three–dimensional figure with planes of constant pH give two–dimensional diagrams of $-\log_{10}[M]_{aq}$ versus $\bar{z}$. In interpreting the $-\log_{10}[M]_{aq}$ versus $\bar{z}$ diagrams, note that the total dissolved concentration of active redox element, $[M]_{aq}$, increases as one moves downward on the diagram. Furthermore, keep in mind that an aqueous phase is present at all accessible points on the diagram, including those points where vertical lines indicate the presence of one of the solid phases.

The three types of regions that can appear on $-\log_{10}[M]_{aq}$ versus $\bar{z}$ diagrams are shown in Figure 5–5, an electron number diagram for the aqueous

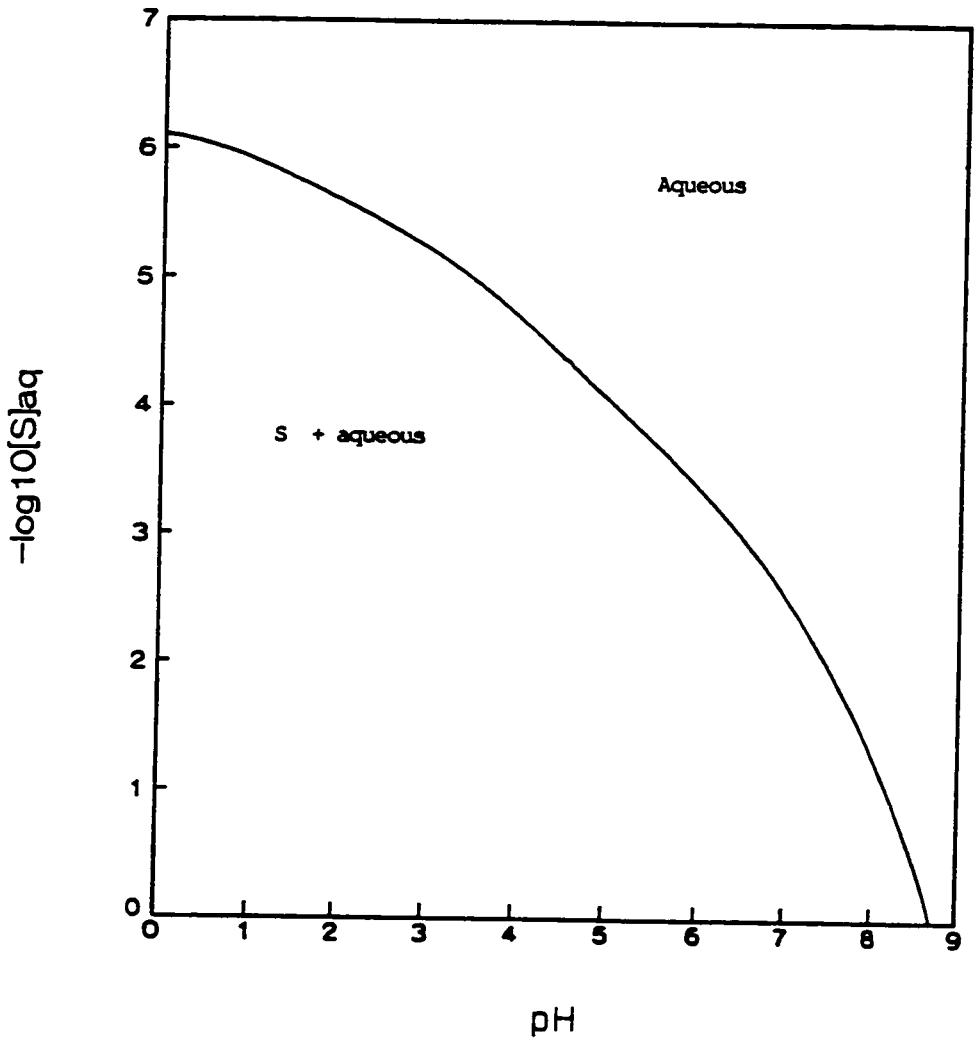

Figure 5–15 $-\log_{10}[S]_{aq}$ vs. pH diagram for the aqueous sulfur system at $\bar{z}_{aq} = -1$.

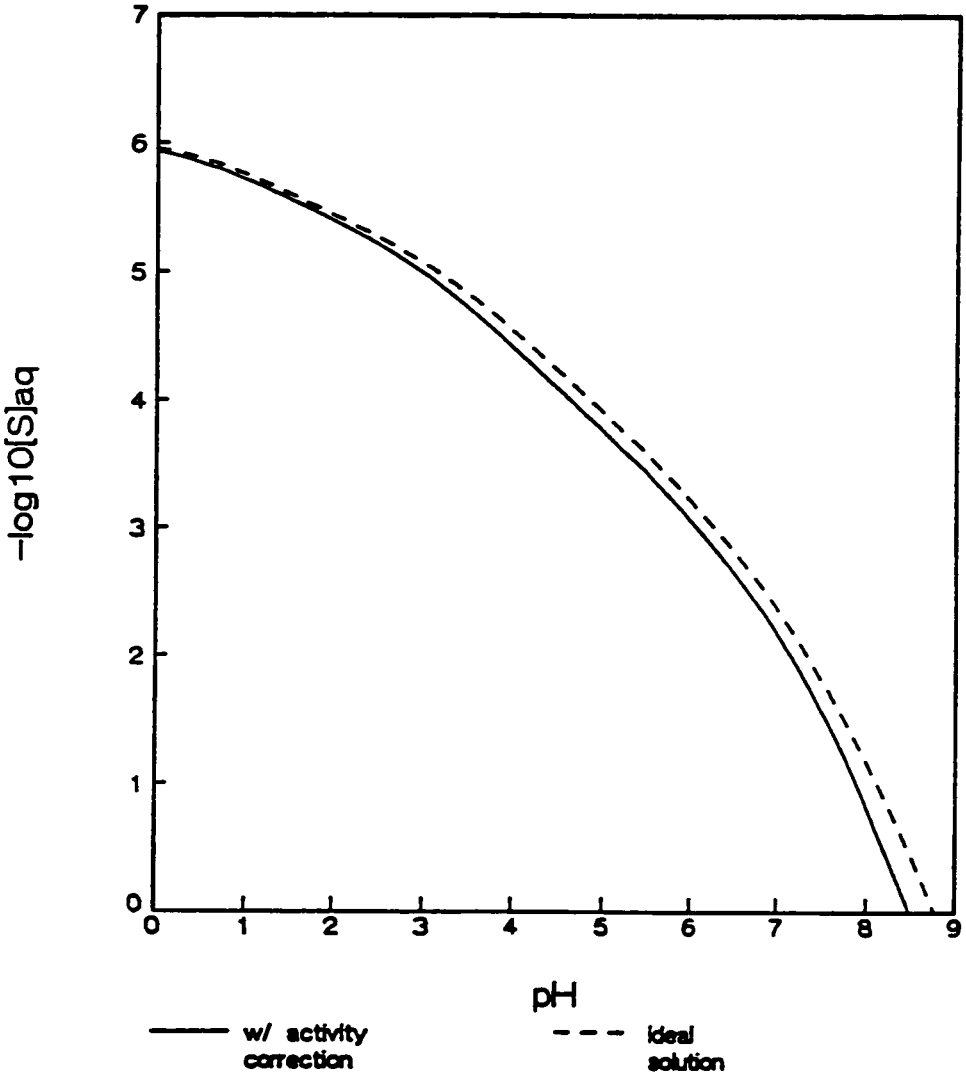

Figure 5–16 The effect of activity coefficients on calculated sulfur solubility as a function of pH. Both the ideal solution and activity coefficient curves are drawn for $\bar{z}_{aq} = 1$. The activity coefficents were calculated using the Davies Equation.

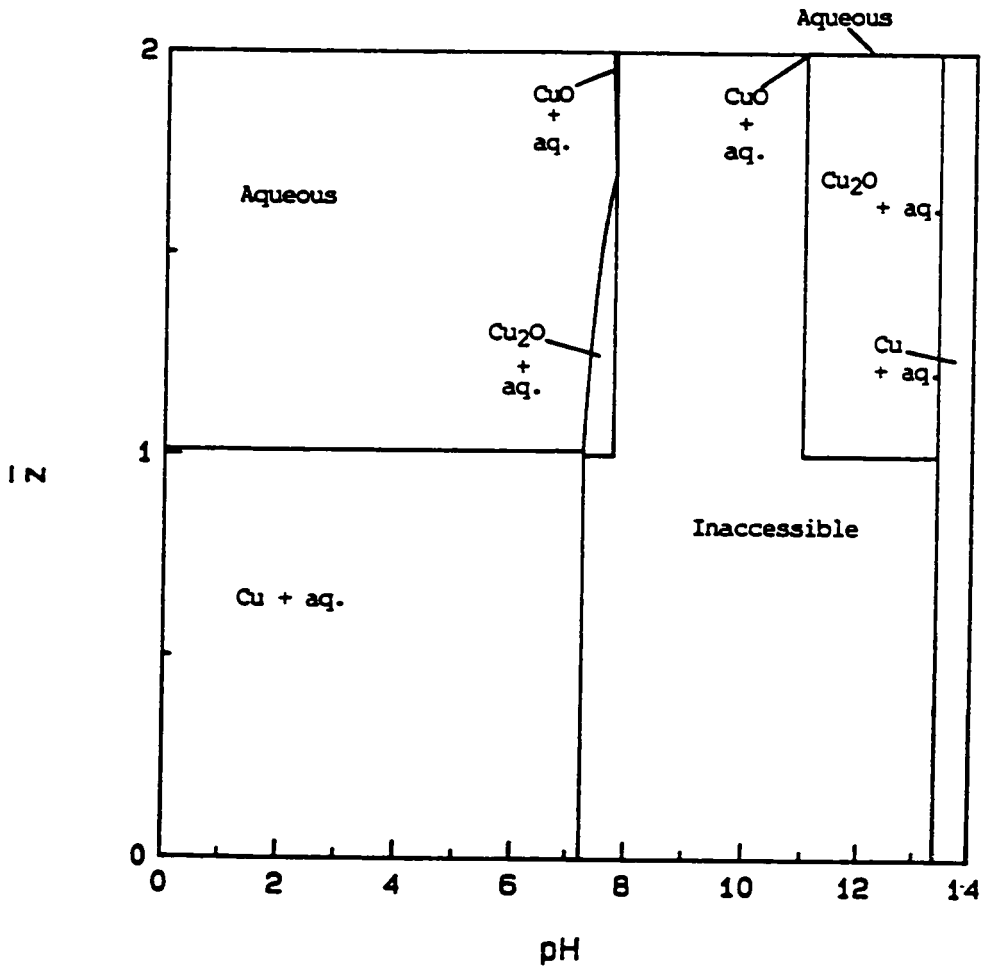

Figure 5–17 $\bar{z}$ vs. pH diagram for the aqueous copper system at $-\log_{10}[Cu]_{aq} = 8$. In the two–phase regions, note that the tie–lines, if drawn, would be vertical.

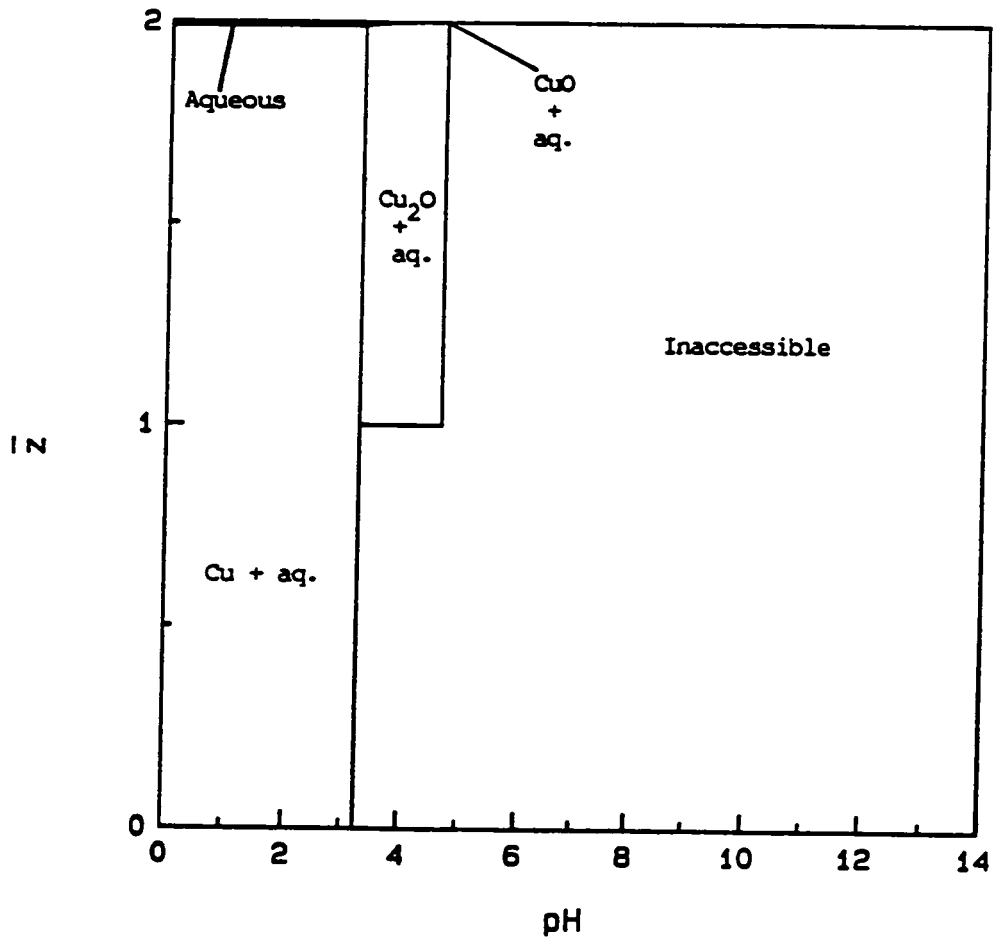

Figure 5–18 $\bar{z}$ vs. pH diagram for the aqueous copper system at $-\log_{10}[Cu]_{aq} = 2$. In the two–phase regions, note that the tie–lines, if drawn, would be vertical.

copper system at pH = 8.81. In the single–phase aqueous region, copper is present only in dissolved species. In a two–phase region, solid Cu_2O exists in equilibrium with an aqueous phase containing dissolved copper; two–phase regions also exist for the solids CuO and Cu. Along the lowest lying lines, three phases coexist in equilibrium. For example, along line $\overline{IJK}$, solids Cu_2O (point I, $z = 1$) and CuO (point K, $z = 2$) exist in equilibrium with an aqueous phase (point J, $\bar{z} \simeq 1.56$) at $-\log_{10}[Cu]_{aq} \simeq 9.3$. In the inaccessible region below the three–phase lines, solubility limits would be exceeded and the aqueous copper system can not exist in equilibrium.

The three–dimensional potential–pH diagram for the aqueous copper system (shown in Figure 3–2) consists of a two–phase surface which divides space into an aqueous region and an inaccessible region. An intersection of this figure with a plane of constant pH would give a diagram consisting of *two–phase lines* (associated with the various solids) separating the aqueous region from the inaccessible region. In diagrams of $-\log_{10}[M]_{aq}$ versus $\bar{z}$, *two–phase regions* (associated with the various solids) separate the aqueous region from the inaccessible region. This difference results from the fact that phases in equilibrium are at the same electrochemical potential, but the electron numbers of phases in equilibrium are not generally equal.

Consider an aqueous copper system at pH = 0, shown in Figure 5–3 on a diagram of $-\log_{10}[Cu]_{aq}$ versus $\bar{z}$. Line $\overline{ABC}$ shows the equilibrium between solid elemental copper and a solution with a total dissolved copper concentration of 10^{-6}m. The relative amounts of solid Cu (point A, $z = 0$) and copper in dissolved species (point C, $\bar{z} \simeq 1.44$) in the system determine the average electron number, $\bar{z}$, of the system and thus fix the system point on line $\overline{ABC}$.

The strong resemblance of the $-\log_{10}[M]_{aq}$ versus $\bar{z}$ diagrams to conventional metallurgical phase diagrams is most striking. The diagrams show features closely analogous to peritectic reactions, eutectics and congruently melting compounds. For example, Figure 5–4 shows a "peritectic" type reaction along the line $\overline{FGH}$ where Cu_2O disproportionates into elemental Cu° and a solution of slightly greater than 10^{-7} molal total dissolved copper. Figure 5–5 shows the presence of a "eutectic" type reaction along the line $\overline{IJK}$ where Cu_2O, CuO and the aqueous phase are in equilibrium. In Figure 5–6, which is a detail of the region near $\bar{z} = 2$ for pH = 10, CuO dissolves "congruently" at point L.

The influence of complexing ions, e.g., Cl^-, can easily be displayed. Compare, for example, Figures 5–4, 5–8 and 5–9. Each is for the copper system at pH = 6. However, Figure 5–8 is for a Cl^- concentration of 0.01 molal and Figure 5–9 for a Cl^- concentration of 1.0 molal. The greatly increased solubility and the greater stability range of the complex compound, $CuCl_2 \cdot 3Cu(OH)_2$, at the higher chloride ion concentrations are clearly shown.

Diagrams for the sulfur system are shown in Figures 5–10, 5–11 and 5–12. The large two–phase region where solid sulfur coexists with the aqueous phase is visible in each diagram. In Figure 5–10, a minimum solubility of slightly less than 10^{-4} molal of total dissolved sulfur is indicated. Note also that in the two–phase region the potential undergoes a discontinuous change at $\bar{z} = 0$. Figures 5–10, 5–11 and 5–12a were constructed without consideration of sulfate and bisulfate species. (In some circumstances it has been reported that the formation of these ions is so sluggish that the experimental solubilities are most accurately described without including them in the equilibrium calculations (Peters, 1976).) Inclusion of SO_4^{2-} and HSO_4^- ions greatly increases the solubility. (See Figure 5–12b in

which the sulfate and bisulfate ions were included.)

The close resemblance between the $-\log_{10}[M]_{aq}$ versus $\bar{z}$ plots and conventional metallurgical phase diagrams is not simply fortuitous. The basic geometric features of both are fixed by the requirements of the phase rule. Furthermore, the features in both types of diagrams arise from the various possible types of intersections of solubility curves.

In the following discussions, the term "electron number diagrams" will refer to diagrams of $-\log_{10}[M]_{aq}$ versus $\bar{z}$ at fixed pH, unless otherwise stated.

5.3.4 Constant Potential Lines

The main purpose of this description of electron number diagrams is to focus on the phase and solubility relationships. Consequently, to avoid cluttering the diagrams, constant potential lines were not cross plotted on all of the figures. In a comprehensive study of a particular system, it would be useful to include closely spaced constant potential lines. Representative constant potential lines relative to the standard hydrogen electrode are shown on Figures 5–3, 5–7, 5–10, 5–11, 5–12a, 5–12b and 5–13.

From the phase rule analysis in Chapter 2.2, the maximum number of degrees of freedom in an aqueous system containing one active redox element (at fixed activities of any additional components X and Y) is three. On an electron number diagram, at fixed pH, this maximum is reduced to two. Therefore, in a single–phase aqueous region on an electron number diagram, E and $-\log_{10}[M]_{aq}$ may be chosen independently, i.e., there are two remaining degrees of freedom. In a two–phase region (solid plus aqueous) one degree of freedom is lost and the lines of constant E and $-\log_{10}[M]_{aq}$ must be identically coincident. In other words, in

the two–phase regions, fixing E fixes $-\log_{10}[M]_{aq}$ and vice versa.

As shown in Chapter 2, the Nernst relationships between E and the activities of redox species are preserved at all points on electron number diagrams.

It can be shown that for an ideal solution at fixed pH and $\bar{z}$, E is independent of total concentration, $[M]_{aq}$, if $\alpha_{M,k} = 1$ for all species. Similarly, for ideal solutions at fixed $\bar{z}$ and $[M]_{aq}$, E is independent of pH if $h_k = 0$ for all species. If both $\alpha_{M,k} = 1$ and $h_k = 0$ for all species, the constant potential surfaces are sheets parallel to the constant $\bar{z}$ planes.

Examples of this behavior can be seen on the computed diagrams. For the copper system $\alpha_{Cu,k} = 1$ for all dissolved species. Therefore, on Figures 5–3 and 5–7 the constant potential lines are coincident with the constant $\bar{z}$ lines in the single–phase aqueous regions. (If the solutions were not assumed to be ideal, the lines would not be exactly coincident.) On the other hand, in the sulfur system the thiosulfate species, $S_2O_3^{2-}$, $HS_2O_3^-$ and $H_2S_2O_3$ with $\alpha_{S,k} = 2$, and polysulfides with $\alpha_{S,k} = 2$, 3, 4 and 5, are important and the constant potential lines are not parallel to the lines of constant $\bar{z}$, even though the calculations assume ideal solutions. (See Figures 5–10, 5–11, 5–12a and 5–12b.) Similarly, in the chromium system, species such as $Cr_2O_7^{2-}$ are important and the constant potential lines in the single–phase aqueous region are curved. (See Figure 5–13.)

As a solution becomes more dilute, species with $\alpha_{M,k} = 1$ become thermodynamically favored over species with $\alpha_{M,k} > 1$. Consequently, if the solution is diluted sufficiently, the species with $\alpha_{M,k} = 1$ become dominant and the constant potential lines become parallel to the lines of constant $\bar{z}$. This effect, which is exactly analogous to the dissociation of dimers in a gas phase as the pressure is lowered, is shown clearly in Figure 5–13.

5.3.5 Lines of Constant Gas Pressure

Lines of constant oxygen and hydrogen partial pressure could also have been cross plotted on electron number diagrams. For the formation of oxygen,

$$2\,H_2O = O_2(g) + 4\,H^+ + 4\,e^- \qquad (5.3\text{–}1)$$

the relationship between E, pH and p_{O_2} is given by

$$E\,(V) = 1.229 - 0.0592\,pH + 0.0149 \log p_{O_2(g)} \qquad (5.3\text{–}2)$$

For the formation of hydrogen,

$$2\,H^+ + 2\,e^- = H_2(g) \qquad (5.3\text{–}3)$$

the relationship between E, pH and p_{H_2} is given by

$$E\,(V) = -0.0592\,pH - 0.0296 \log p_{H_2(g)} \qquad (5.3\text{–}4)$$

On a $-\log_{10}[M]_{aq}$ versus $\bar{z}$ plot, pH is fixed, so constant p_{O_2} and p_{H_2} lines are coincident with the constant potential lines. For example, on Figure 5–3, which is drawn for pH = 0, the p_{H_2} = 1 atm line would be coincident with the E = 0 line. It should be noted, parenthetically, that some of the regions shown in the figures correspond to unrealistically large pressures of oxygen or hydrogen. For example, the equilibrium partial pressure of O_2 in equilibrium with Cu_2O_3 and H_2O is unrealistically large. These regions are included to facilitate comparison with published Pourbaix diagrams.

The gas pressures are those required to prevent the reduction or oxidation of water. Lines for p_{O_2} = 1 atm and p_{H_2} = 1 atm are often shown on conventional potential–pH diagrams as the "water stability lines."

5.3.6 Examples of $-\log_{10}[M]_{aq}$ versus pH Diagrams

Intersections of the three–dimensional electron number equilibrium figure with planes of constant average electron number, $\bar{z}$, also produce interesting

diagrams. Figure 5–15 shows the intersection of the sulfur equilibrium surface from Figure 5–2 with the $\bar{z} = -1$ plane. Along the two–phase line, solid sulfur ($z_S = 0$) coexists with an aqueous phase containing sulfur with an average electron number of negative one ($\bar{z}_{aq} = -1$). A single aqueous phase, containing dissolved sulfur species with $\bar{z}_{aq} = -1$, exists above the two–phase line, i.e., at lower dissolved sulfur concentrations. Below the two–phase line, solid sulfur is in equilibrium with an aqueous phase containing dissolved sulfur species for which $\bar{z}_{aq} < -1$. This can be seen in Figure 5–2. At each point in this two–phase region below the equilibrium line, fixed relative amounts of sulfur in the solid and aqueous phase are required to satisfy the constraint $\bar{z} = -1$. This ratio can be determined using Equation 5.2–16. Further examples of $-\log_{10}[M]_{aq}$ versus pH diagrams for the aqueous sulfur system apppear in Chapter 6.

Diagrams of $-\log_{10}[M]_{aq}$ versus pH must be calculated iteratively, even in the case of ideal solutions.

5.3.7 Examples of $\bar{z}$ versus pH Diagrams

Intersections of the three–dimensional electron number figure with planes of constant $-\log_{10}[M]_{aq}$ produce diagrams like those shown in Figures 5–17 and 5–18. Figure 5–17 shows a $\bar{z}$ versus pH diagram for the aqueous copper system from Figure 5–1 at $-\log_{10}[Cu] = 8$. Note the similarities to $-\log_{10}[M]_{aq}$ versus $\bar{z}$ diagrams. The $\bar{z}$ versus pH diagram consists of single–phase, two–phase and inaccessible regions. In the two–phase regions, tie–lines, if drawn, coincide with constant pH lines. Vertical three–phase lines appear on $\bar{z}$ versus pH diagrams. For example, at pH =7.75, Cu_2O ($z = 1$), CuO ($z = 2$) and an aqueous phase ($\bar{z} \simeq 1.70$) coexist in equilibrium.

Figure 5–18 shows a $\bar{z}$ versus pH diagram for the aqueous copper system from Figure 5–1 at $-\log_{10}[Cu] = 2$. At all accessible values of pH on $\bar{z}$ versus pH diagrams, a single–phase aqueous region exists. In Figure 5–18, the single–phase aqueous region exists over a very narrow range of electron number near $\bar{z} = 2$ for $0 \leq pH < 4.8$. A similar, narrow single–phase aqueous region exists in Figure 5–17 at high pH.

Diagrams of $\bar{z}$ versus pH must be calculated iteratively, even in the case of ideal solutions.

5.4 Use of Electron Number Diagrams

5.4.1 Material Balances on Electron Number Diagrams

Consider a two–phase system comprised of N_s gram moles of a solid phase and an aqueous phase containing N_k gram moles each of the several dissolved species M_k. From Equations 5.2–11, 5.2–13, 5.2–14 and 5.2–15, the total overall $\bar{z}$ of this two–phase system is:

$$\bar{z} = \frac{z_s B_{M,s} + \bar{z}_{aq} B_{M,aq}}{B_{M,s} + B_{M,aq}} \tag{5.4–1}$$

Multiply both sides of Equation 5.4–1 by $B_{M,s} + B_{M,aq}$ and then divide by $B_{M,aq}$ to obtain

$$\bar{z}\left[\frac{B_{M,s}}{B_{M,aq}} + 1\right] = \frac{B_{M,s} z_s}{B_{M,aq}} + \bar{z}_{aq} \tag{5.4–2}$$

Equation 5.4–2 can be immediately rearranged to give:

$$\frac{\bar{z} - \bar{z}_{aq}}{z_s - \bar{z}} = \frac{B_{M,s}}{B_{M,aq}} \tag{5.4–3}$$

Equation 5.4–3 is the algebraic statement of the so–called "inverse lever arm

rule." In other words, the right hand side of Equation 5.4–3 is just the ratio of the amount of active element in the system that resides in the solid phase to the amount of active element that is in the aqueous phase. Geometrically, on an electron number diagram, the left hand side of Equation 5.4–3 is the ratio of the horizontal distance between $\bar{z}$ and $\bar{z}_{aq}$ to the distance between z_s and $\bar{z}$. Equation 5.4–3 may be converted to another useful form by adding 1 to both sides, multiplying through and using Equation 5.2–17. One finds

$$\frac{z_s - \bar{z}_{aq}}{z_s - \bar{z}} = \frac{B_{M,t}}{B_{M,aq}} \tag{5.4–4}$$

where $B_{M,t}$ is the total number of gram atoms of active element M in the system.

Equation 5.4–4 may be further reduced to a form which is sometimes more convenient for use with the electron number diagrams by using the relationship:

$$B_{M,aq} = m_{H_2O}[M]_{aq} \tag{5.4–5}$$

Equation 5.4–4 becomes

$$\frac{z_s - \bar{z}_{aq}}{z_s - \bar{z}} = \frac{B_{M,t}}{m_{H_2O}[M]_{aq}} \tag{5.4–6}$$

An example of the use of the inverse lever arm rule on electron number diagrams is shown in Figure 5–3. The line segment $\overline{ABC}$ represents the equilibrium between solid elemental Cu^0 and dissolved copper. For the case shown, point B corresponds to the situation where there are twice as many moles of copper in the solution as in the solid phase, i.e., $\overline{AB}/\overline{BC} = 2$.

5.4.2 Electron Balances on Electron Number Diagrams

The trajectories followed when electrons are introduced into a system, e.g., in electro–reduction or electroplating operations, may be followed on electron

number diagrams. Consider the situation where electrons are added to the system of active redox species through an inert electrode. Only one active redox element, e.g., copper, is assumed to be present.

The overall electron number, $\bar{z}$, is very simply related to the number of electrons through Equation 5.2–7. If the total number of moles of active element is constant, the relationship between changes in $\bar{z}$ and $N_{e,t}$ is

$$\Delta\bar{z} = \frac{-\Delta N_{e,t}}{B_{M,t}} \tag{5.4–7}$$

If only an aqueous phase is present, the trajectory followed when electrons are added to the system is simply a horizontal line at constant $[M]_{aq}$. However, a more interesting situation occurs when a solid phase is electrodeposited. The trajectory in this case can be obtained by using Equation 5.4–6 in the form

$$[M]_{aq} = \left[\frac{z_s - \bar{z}}{z_s - \bar{z}_{aq}}\right]\left[\frac{B_{M,t}}{m_{H_2O}}\right] \tag{5.4–8}$$

where $B_{M,t}$ is the total number of moles of active element in both the aqueous and solid phases, and m_{H_2O} is the mass of the water in kilograms. During electrodeposition $B_{M,t}$ and m_{H_2O} remain constant. Equation 5.4–8 therefore is an algebraic equation relating $[M]_{aq}$, $\bar{z}$ and $\bar{z}_{aq}$ during electrodeposition. As electrons are added to the system, changes in $\bar{z}$ are given by Equation 5.4–7. The third relationship between the variables is given by the solubility curve ($[M]_{aq}$ versus $\bar{z}_{aq}$) on the electron number diagram. The trajectory, i.e., the path of $[M]_{aq}$ versus $\bar{z}$, on the electron number diagram may therefore be determined.

An example of the trajectory followed during the electroplating of a solution with an initial concentration of $[Cu]_{aq} = 0.01$ molal is shown in Figure 5–9 as curve UVW.

5.4.3 Concentration or Dilution Trajectories at Constant $\bar{z}$

Consider a system of chemically reacting species undergoing redox transitions. If no electrons are added or subtracted by means of an external system, then no matter what arbitrary redox transitions take place, the electrons lost by one species must be gained by other species in the system. A knowledge of initial composition fixes $\bar{z}$, which remains unchanged if no electrons are added or removed. In other words, any process not involving electron transfer to or from the system must lie in the constant $\bar{z}$ plane.

For example, consider a solution at pH = 0 comprised of 0.75×10^{-6} molal Cu^{++} and 0.25×10^{-6} molal Cu^{+}. The total concentration of dissolved copper, $[Cu]_{aq}$, is 10^{-6} molal. The average electron number of the copper is computed from Equation 5.2–19 and found to be 1.75. The initial conditions place the system at point D in Figure 5–3. This point lies on the 0.185V equipotential line. If no electrons are transferred to or from the system of the copper species, the electron number remains constant. For example, this means that no oxidation or reduction of the solvent (H_2O) by the copper species or no electrolysis involving the copper species takes place. Therefore, if H_2O is removed at constant pH, the operating point moves vertically downward on Figure 5–3. When the concentration reaches 10^{-5} molal, i.e., point E on the diagram, solid Cu° starts to precipitate out.

5.4.4 Concentration or Dilution Trajectories at Constant E

There are situations in which a system may be held at constant E rather than $\bar{z}$. For example, evaporation of a well buffered body of water in equilibrium with air will follow a trajectory of (approximately) constant pH and E. This

trajectory is easily followed by following the appropriate constant potential line on a $-\log_{10}[M]_{aq}$ versus $\bar{z}$ diagram. In general, the $\bar{z}$ will change during this process because the system is maintained in contact with a source/sink of electrons at constant potential. For example, consider the chromium system held at pH = 4 shown in Figure 5–13. Assume the solution is in equilibrium with an inert gas phase at atmospheric pressure containing approximately 0.07 ppm of O_2. At pH = 4, this corrosponds to a potential of 0.885V. The evaporation trajectory will follow the E = 0.885V line from L to M to N. At point M solid Cr_2O_3 starts to precipitate and further evaporation leads one horizontally along the constant potential line until point N is reached. Systems with an average electron number of less than 3 can not coexist with a gas phase of this composition.

5.4.5 Precipitation of Solid Phases

The diagrams clearly show under what conditions a solid phase may form directly by evaporation. For example, consider Figures 5–8 and 5–9 which are drawn for the copper system at a pH of 6 and chloride ion concentrations of 0.01 molal and 1.00 molal respectively. Consider a solution made up by mixing equimolar amounts of 10^{-6} molal cupric and cuprous solutions. From Equation 5.2–19, the value of $\bar{z}$ will be 1.5. The total copper concentration, $[Cu]_{aq}$, will be 10^{-6} molal. It is assumed that the concentration of chloride ion is 0.01 molal. The initial condition is therefore point M on Figure 5–8. When this solution is evaporated at constant pH and $\bar{z}$, the operating point follows a vertical line downward. When point N is reached, a solid phase, Cu_2O, starts to precipitate. However, when the same process is followed with a solution containing 1 molal chloride ion, a different solid phase, $CuCl_2 \cdot 3Cu(OH)_2$, precipitates. This is

shown as line $\overline{PQ}$ on Figure 5–9.

Furthermore, if the evaporation process shown on Figure 5–9 is continued, more solid $CuCl_2 \cdot 3Cu(OH)_2$ precipitates and the solution composition moves along the solubility curve. The relative amounts of copper in the solid and aqueous phases can be obtained by application of the lever arm rule embodied in Equation 5.4–3. For example, when the concentration reaches 10^{-3} molal, the equilibrium is described by line $\overline{RST}$ on Figure 5–9. The ratio of copper present in the solid $CuCl_2 \cdot 3Cu(OH)_2$ to the copper present in the solution is given by the ratio of the line segments $\overline{RS}/\overline{ST}$.

5.4.6 Mixing Processes

Consider Figure 5–10. The mixing of 0.01 molal solutions of Na_2SO_3 ($z_i = +4$, point C) and Na_2S ($z_i = -2$, point A) at a pH of 4 is illustrated. The amount of the solutions is chosen so that 0.02 mole of Na_2SO_3 and 0.02 mole of Na_2S are mixed. The mixing point in this case is exactly half way between A and C at point B, which is within the two–phase envelope. The average electron number, $\bar{z}$, is 1.0. i.e., the final point after mixing and precipitation of sulfur lies somewhere along the line $\bar{z} = 1$. The final concentration and relative amounts of sulfur present as solid sulfur and in the solution phase can be obtained by a mole balance on the sulfur. This is most easily done algebraically rather than graphically because of the non–linear concentration scale. The sulfur mole balance can be written:

$$B_{S,s} + B_{S,aq} = \left(N_{Na_2S} + N_{Na_2SO_3} \right)_{initial} \qquad (5.4\text{–}9a)$$

$$B_{S,s} + B_{S,aq} = 0.02 + 0.02 \qquad (5.4\text{–}9b)$$

$$B_{S,s} + m_{H_2O}[S]_{aq} = 0.04 \qquad (5.4\text{–}9c)$$

where $B_{S,s}$ is the number of moles of solid sulfur formed, $B_{S,aq}$ is the total number of moles of sulfur remaining in the aqueous phase and m_{H_2O} is the mass of water, in this case 4 kilograms. Another equation relating the variables is obtained from Equations 5.4–3 and 5.4–5.

$$\frac{B_{S,s}}{m_{H_2O}[S]_{aq}} = \frac{\bar{z} - \bar{z}_{aq}}{z_S - \bar{z}} \qquad (5.4\text{–}10)$$

Since, in this case, $\bar{z} = 1$ and $z_S = 0$, Equation 5.4–10 reduces to

$$\frac{B_{S,s}}{m_{H_2O}[S]_{aq}} = \bar{z}_{aq} - 1 \qquad (5.4\text{–}11)$$

Another relationship between $[S]_{aq}$ and $\bar{z}_{aq}$ is given by the solubility curve of Figure 5–10. A point on this solubility curve which satisfies both Equation 5.4–9c and Equation 5.4–11 may be found by trial and error. The values of the three variables $B_{S,s}$, $[S]_{aq}$ and $\bar{z}_{aq}$ may be determined in this manner. In the present situation it is easily shown that one half of the total sulfur precipitates as solid sulfur ($B_{S,s} = 0.02$ moles) and the solution concentration moves to point F on the diagram, $\bar{z}_{aq} = 2$. The final equilibrium state is shown by the line $\overline{DEF}$.

A special case occurs when the Na_2SO_3 and Na_2S solutions are mixed in a molar ratio of 1 to 2. From Equation 5.2–19, one finds that in this situation the overall $\bar{z}$ is zero. Therefore, since the $\bar{z}$ of the solid phase (elemental sulfur) is zero, it follows directly from Equation 5.2–16 that the $\bar{z}$ of the aqueous phase must also be 0. The process may be illustrated graphically on Figure 5–11. It is assumed the process is done at pH = 7 and the initial concentrations of Na_2SO_3 and Na_2S were 0.1 molal. The initial electron balance is shown by the line $\overline{GHI}$. Graphically the mixing point H is determined by the condition that $\overline{HI}/\overline{GH} = 2$.

From Figure 5–11 the final state of the solution must be at point J, i.e., the only point on the solubility curve where $\bar{z}_{aq} = 0$. The final concentration of sulfur in the aqueous phase is slightly greater than 10^{-2} molal and the potential is approximately –0.20V. About 90% of the sulfur has been precipitated. Physically this process is dominated by overall stoichiometric reactions of the Claus type, e.g.,

$$2HS^- + HSO_3^- + 3H^+ = 3S + 3H_2O \qquad (5.4\text{–}12)$$

The residual solubility arises not only from unreacted ions with $z_k = -2$ and $+4$, but also from the presence of thiosulfates and polysulfides. Because of the conditions imposed upon the system, the remaining ions must be present in such amounts that the $\bar{z}_{aq}$ is 0.

5.4.7 Precipitation of Solids at Constant $\bar{z}$ and Variable pH

Diagrams of $-\log_{10}[M]_{aq}$ versus pH at constant $\bar{z}$ are of use in predicting the formation of solids in cases where $\bar{z}$ is constant but pH is changing. The acidification or basification of a solution of known electron number and concentration appears as a horizontal line on a $-\log_{10}[M]_{aq}$ versus pH diagram. Such trajectories can be used to predict the onset of solid formation or the nature of the solids formed when the pH of a system in changed. For example, according to Figure 5–15, a basic 0.01 molal aqueous sulfur solution at $\bar{z}_{aq} = -1$ should, upon acidification, begin to form solid sulfur near pH = 7.5. Furthermore, these diagrams can be used to analyze evaporation processes at constant $\bar{z}$, if the pH–concentration relationship for the system of interest is known.

5.5 Discussion

5.5.1 Relationship Between E and $\bar{z}$

The relationship between E and $\bar{z}$ can be described in terms of conjugate thermodynamic variables. Examples of conjugate thermodynamic variables include pressure and volume, temperature and entropy, and chemical potential and mole number. The relationship between the Gibbs free energy of a system (G), the chemical potential of a species i (μ_i) and the mole number of species i (n_i) is given by

$$\mu_i \equiv \left[\frac{\partial G}{\partial n_i}\right]_{T,P,n_{j\neq i}} \tag{5.5–1}$$

where the partial derivative is evaluated at constant temperature, pressure and mole numbers of all species except i. The definition in Equation 5.5–1 is normally applied to chemical species.

The thermodynamic system of interest consists of all species containing a single active redox element M. Electrons may be added to, removed from or exchanged among species containing the active redox element. The other components of the system (H^+, H_2O, X and Y) are treated as purely chemical species which are forbidden to undergo redox transitions. By analogy to Equation 5.5–1, the chemical potential of electrons in the thermodynamic system of interest is given by:

$$\mu_{e^-} \equiv \left[\frac{\partial G}{\partial N_{e,t}}\right]_{T,P,n_{j\neq e^-}} \tag{5.5–2}$$

where $N_{e,t}$ is the total number of moles of electrons associated with the active redox element in the system and the partial derivative is evaluated at constant temperature, pressure and mole numbers of all system components except electrons. Thus, μ_{e^-} and $N_{e,t}$ are thermodynamic conjugate variables.

$N_{e,t}$ and μ_{e^-} can be related to more convenient variables. The chemical potential of electrons is related to the potential E by

$$\mu_{e^-} = -FE \tag{5.5-3}$$

The relationship between $N_{e,t}$ and $\bar{z}$ was given in Equation 5.2–7.

$$\bar{z} \equiv \frac{N_{e,o} - N_{e,t}}{B_{M,t}} \tag{5.2-7}$$

This is analogous to the replacement of the number of moles of a chemical species with a more convenient measure of composition, the mole fraction.

5.5.2 The Relationship Between Electron Number Diagrams and Prior Diagrams

Pourbaix diagrams are three–dimensional surfaces in $E/pH/-\log_{10}a_M$ space. An electron number diagram is a transformation of that surface obtained by replacing the potential, E, with the electron number, $\bar{z}$. The potential, E, is a measure of the chemical potential of the electrons and $\bar{z}$ is a measure of the number of electrons; μ_{e^-} and $N_{e,t}$ are conjugate thermodynamic variables just as pressure and volume are conjugate thermodynamic variables. Therefore, the transformation from $E/pH/-\log_{10}a_M$ space to $\bar{z}/pH/-\log_{10}a_M$ space has special properties. In particular, a single point that represents two (or three) phases in equilibrium in $E/pH/-\log_{10}a_M$ space is transformed into two (or three) separate points in $\bar{z}/pH/-\log_{10}a_M$ space. This is because the chemical potential of electrons is the same in phases in equilibrium, but the electron number $\bar{z}$ is generally different in the different phases. Similarly, large regions on a Pourbaix surface, which correspond to a single solid phase at different potentials, are transformed into a point. The transformation, in effect, turns a Pourbaix diagram "inside out".

For example, consider the aqueous uranium system shown in a Pourbaix diagram in Figure 4–1 and in an electron number diagram at pH = 4 in Figure 5–14. The equilibrium between U ($z = 0$), UO_2 ($z = 4$) and uranium in the aqueous phase ($\bar{z} = 3$) at pH = 4 appears as a line near $-\log_{10}[U]_{aq} = 2$ on the electron number diagram; this same equilibrium appears as a point on the Pourbaix diagram at pH = 4. Conversely, the equilibrium between $UO_2(OH)_2 \cdot H_2O$ and the aqueous phase at pH = 4 appears as a line on the Pourbaix diagram. However, the two–phase region associated with $UO_2(OH)_2 \cdot H_2O$ and the aqueous phase at pH = 4 on the electron number diagram is nearly reduced to a point.

Electron number diagrams are also related to the free energy–oxidation state diagrams proposed by Frost over thirty years ago (1951). Frost diagrams are a variant of the free energy–composition diagrams widely used in metallurgy. Frost diagrams, which have been further developed by Mueller (1969), are not widely known and have found little application although they have appeared in several text books as a pedagogical device (Phillips and Williams, 1965; Gray and Haight, 1967). They are related to the present work in the implicit use of average valence as a measure of electron concentration and in the stability criterion used.

5.5.3 Phase Behavior

The diagrams provide a very convenient means of displaying various types of phase behavior in multi–phase redox systems. For example, being able to determine whether a solid dissolves congruently or incongruently can be of value in synthetic procedures or in determining a possible sequence of events in the formation of evaporites in geological processes. (The importance of congruent and

incongruent melting behavior of solids is well known and well understood.)

The diagrams also illustrate other phase behavior that may be of importance in certain circumstances. For example, consider the sulfur diagrams shown in Figures 5–10, 5–11, 5–12a and 5–12b. If solid sulfur is partially dissolved in an aqueous medium, the composition of the aqueous phase and the potential will depend remarkably on whether the original aqueous solution was completely deoxygenated or not. For example, if the original aqueous solution contained significant quantities of dissolved oxygen, the final solution would lie along the oxidizing leg of the two–phase envelope, e.g., along line $\overline{JK}$ in Figure 5–11. On the other hand, if the original aqueous solution were reducing, the final solution would lie along the reducing leg, $\overline{JG}$. Relatively small differences in the state of the original solution can have result in striking differences in the final state of the system.

5.5.4 Solubility Curves

The value of $[M]_{aq}$ in equilibrium with a solid phase, M_s, is a measure of the solubility of the solid phase. The lines of $-\log_{10}[M]_{aq}$ versus $\bar{z}$ at constant pH show the solubility of the active element as a function of the overall oxidation state of the system. The slopes of these solubility curves must follow certain rules which can be obtained using results from Chapter 2.

First, consider the intersection of two solubility curves, for example, at point H on Figure 5–4. At the point of the intersection, the chemical potential, μ_M, of the active element in the aqueous phase and the two solid phases, u and v, must be equal.

$$\mu_{M,u} = \mu_{M,v} = \mu_{M,aq} \qquad (5.5–4)$$

Furthermore, at points just removed from the intersection, the stable solid phase will be the one with the lowest value of μ_M. Since the concentration of active element in equilibrium with solid phases increases with μ_M, the stable phase will have the lowest value of $[M]_{aq}$. On an electron number diagram, therefore, the solubility curve of the stable phase will lie above (lower $[M]_{aq}$) the extension of the solubility curve of the other solid phase. For example, in Figure 5–4 if the Cu_2O/aqueous solubility line were extended to the left of point H, it would lie below the Cu/aqueous solubility line. (The above arguments are strictly true for the total activity of the dissolved active element, a_M.)

The solubility curves must be considered as unrealistic for the lower concentrations shown, e.g., $[M]_{aq} < 10^{-8}$ molal. At these low concentrations the true equilibrium will be usually determined by other impurity ions. The solubility curves are extended into this range to show the general form and structure of the diagrams.

A detailed analysis of the slopes of the solubility curves for ideal solutions is given in the Appendix B. The results of the analysis can be of help in interpreting experimentally observed phase behavior and are also of value in checking computed diagrams.

5.5.5 Unusual Features on the Diagrams

Although the basic geometry of the diagrams is closely reminiscent of conventional metallurgical T–x diagrams, the relative scale of the features can be very different. This was already seen in Figure 5–6 in which the eutectic point appears very close to the solid compound CuO.

Another unusual feature is the existence of double "eutectics." See

Figure 5–4. There are two "eutectics," i.e., Cu_2O/CuO and CuO/Cu_2O_3, each in equilibrium with an aqueous phase with virtually the same total dissolved copper concentration. The two "eutectic" lines have very different potentials however. The explanation of this phenomenon is most easily understood by consideration of Equation 2.3–28, which gives the activity of any dissolved species, S_d, in equilibrium with two solids, S_u and S_v. Equations 2.3–28 and 2.3–41 can be combined for the special case of $z_d = z_u$ to give:

$$([S_d]\gamma_d)^{\nu_{M,d}} = \exp\{(\frac{F}{RT})z_d(E_u^o - E_d^o) + (\ln 10)(h_d - h_u)(pH) - (x_d - x_u)\ln a_X - (y_d - y_u)\ln a_Y\} \qquad (5.5\text{–}5)$$

Neither the potential E nor any properties of solid S_v appear in Equation 5.5–5. Therefore, the activity, $([S_d]\gamma_d)^{\nu_{M,d}}$, of any dissolved species for which $z_d = z_u$ is independent of E and the properties of solid S_v. (For ideal solutions the concentration $[S_d]$ will be independent of E.) If the dissolved species S_d is the dominant species in the solution, then the total activity of the active element will be essentially independent of E. In the double "eutectic" in Figure 5–4 the aqueous phase is dominated by ions with $z_d = +2$ and each eutectic contains CuO, with $z_u = +2$.

5.5.6 Experimental Diagrams

The figures shown here were all obtained by computation using the thermodynamic data from standard sources (Pourbaix, 1966; Wagman, et al., 1982). It should be emphasized, however, that the new representation may be of most value in displaying experimentally determined redox phase equilibria. The simple relationship between the diagrams and experimentally determined quantities makes this a particularly attractive procedure. For example, $\bar{z}$ can be

determined by initial weighing in of known compounds. Measured amounts of water can be added to the system and the potential monitored. Sharp breaks in the potential versus concentration curve will indicate the phase boundaries, somewhat analogous to the use of cooling curves to find phase boundaries in T–x diagrams.

5.5.7 Computed Diagrams

Computed diagrams may find considerable utility in exploring ranges of compositions not easily accessible to experiment. One example where these methods may be of value is in the study of systems where a number of possible oxide phases can exist and where the solubilities are extremely low and difficult to measure. Systems comprised of uranium oxides in contact with water are a case in point. An electron number diagram for the aqueous uranium system at pH = 4 is shown in Figure 5–14. Of course, to be of greatest value the calculations must incorporate the effect of non–idealities in the aqueous phase.

5.5.8 Systems with Two Active Elements

Systems with two or more active redox elements, e.g., Cu and Ag, are often of interest. These systems may be divided into two types: 1) systems that include no species containing both active elements and 2) systems that do include species containing both active elements. The former can be treated as two separate systems, each with only one active element. This procedure is implicit in the common practice of superimposing two single–element potential–pH diagrams to achieve a composite diagram. For systems of this type, separate electron number diagrams for each element can be drawn. Since the two systems interact through

the exchange of electrons, they must always have the same value of E. Also, for systems containing two elements, e.g., M and N, process trajectories are coupled by the conservation of electrons through the relation $B_{M,t}\,\Delta\bar{z}_M + B_{N,t}\,\Delta\bar{z}_N = 0$.

The second case, in which species involving two or more active redox elements are present, is of interest in many practical situations. For example, consider hydrometallurgical processes involving sulfide ores where such species as CuS are treated. Both the Cu and S can change oxidation states. Electron number diagrams for these systems are significantly more complex to compute and to represent graphically. A computational method for treating such systems has been discussed in Chapter 4. A general method of developing electron number diagrams for systems containing two active redox elements will be discussed in Chapter 7.

5.5.9 Activity Coefficients

Activity coefficient data and models can be used construct electron number diagrams that are not based on the assumption of ideal solutions. For the aqueous sulfur system containing the species listed in Table 3–2, activity coefficients were calculated using the Davies Equation, one of a number of empirical forms of the extended Debye–Huckel treatment of activity coefficients (Stumm and Morgan, 1981). This equation was chosen because it does not require specific parameters for the individual ionic species. Electron number diagrams calculated with activity coefficients showed slightly higher sulfur solubility than those based on ideal solution assumptions. The solubility differences between the two methods varied with pH as shown in Figure 5–16, a diagram of $-\log_{10}[S]_{aq}$ versus pH for $\bar{z} = 1$. The differences in sulfur solubility at $\bar{z} = 1$, based on the treatment of

activity coefficients, were typical of the differences across the the electron number range.

5.5.10 Comparison of Electron Number Diagrams and Potential–pH Diagrams

Because of the number of electrons and the chemical potential of electrons are conjugate thermodynamic variables, a special relationship exists between electron number diagrams and potential–pH diagrams. A set of electron number diagrams (with constant potential lines) at closely spaced values of pH and a complete potential–pH diagram (i.e., a Pourbaix diagram with closely spaced constant activity lines and a superimposed predominance diagram) contain much of the same information.

For example, consider the aqueous uranium system, shown in the Pourbaix diagram in Figure 4–1, the predominance diagram in Figure 4–2, and the electron number diagram in Figure 5–14. General information about the relative solubilities of the various solid phases and the solutions in equilibrium with those solid phases at pH = 4 can be obtained from either the electron number diagram or the superimposition of the Pourbaix and predominance diagrams. The electron number diagram, however, provides more detailed information about the overall solution composition ($\bar{z}_{aq}$) in equilibrium with the solids. Additionally, the electron number diagram displays the solubility information in a form similar to metallurgical T–x diagrams.

The fact that $\bar{z}$, unlike E, is a conserved variable results in significant differences between electron number diagrams and potential–pH diagrams. Graphical material and electron balances can be performed on electron number diagrams. From the composition of a system, a point can be located on an

electron number diagram. The trajectories of evaporation and dilution processes at constant $\bar{z}$ and mixing processes can be shown on electron number diagrams. Because E is not a conserved quantity and is not simply related to the composition of the system, potential–pH diagrams can not be used for these purposes.

In other cases, the use of potential–pH diagrams may be preferable. Examples of the many uses of potential–pH diagrams were given in Chapter 3.2. A single Pourbaix diagram provides an overview of equilibrium in a system over a range of pH values, while a single electron number diagram is constructed for a single value of pH. Additionally, a predominance diagram permits the identification of the dominant dissolved species at fixed values of E and pH. Although electron number diagrams provide information about overall solution composition, the identity of dominant dissolved species at fixed E and pH can not generally be determined from the diagrams because different dissolved species can have the same electron number.

Depending on the particular application, either electron number or potential–pH diagrams may be more convenient. However, since the two types of diagrams are complementary and are constructed from the same thermodynamic information, both types of diagrams should be constructed in the analysis of an aqueous redox system.

5.6 Conclusions

A new phase diagram, called an electron number diagram, is proposed for describing equilibrium in complex, multi–phase redox systems. The new diagrams may be regarded as transformed Pourbaix diagrams obtained by

replacing E, a measure of the chemical potential of electrons, with the electron number, $\bar{z}$, a measure of the number of electrons. Because the chemical potential of electrons and the number of electrons are conjugate thermodynamic variables, the resulting diagrams have special properties. Electron number diagrams are similar in form to conventional metallurgical phase diagrams. The phase chemistry is represented in a particularly simple and intuitively satisfying way. Because electrons are a conserved quantity, process trajectories and graphical material balances can be performed on the new diagrams. These advantages are not obtained at the expense of other information. A set of electron number diagrams (with constant potential lines) retains the information content of a conventional potential–pH diagram.

CHAPTER 6

EXPERIMENTAL ELECTRON NUMBER DIAGRAMS FOR THE AQUEOUS SULFUR SYSTEM

Two types of experiments have been used to construct experimental electron number diagrams for the aqueous sulfur system. In both types of experiments, the boundary between the single–phase aqueous region and the two–phase region where solid sulfur exists in equilibrium with dissolved sulfur was determined. In an *indirect* determination experiment, acidification of the starting solution caused the precipitation of solid sulfur. The distribution of sulfur between the solid and aqueous phases was then used together with mass and electron balances to determine a point on the phase boundary. The second type of experiment involved a *direct* visual determination of whether or not solid sulfur had formed. By determining points inside and outside the two–phase region, the phase boundary could be inferred.

6.1 Equipment and Procedure

The same experimental apparatus was used for both types of experiments. It consisted of a 250 ml glass jar with a Teflon–lined phenolic screw cap. Electrodes, burets and pipets were inserted through holes in the cap; O–rings on these inserts were clamped against the top of the cap to limit gas flow between the jar and the outside environment. The unused holes were tightly stoppered during the experimental runs. The apparatus is shown schematically in Figure 6–1.

Potential and pH measurements were made using an Orion EA940

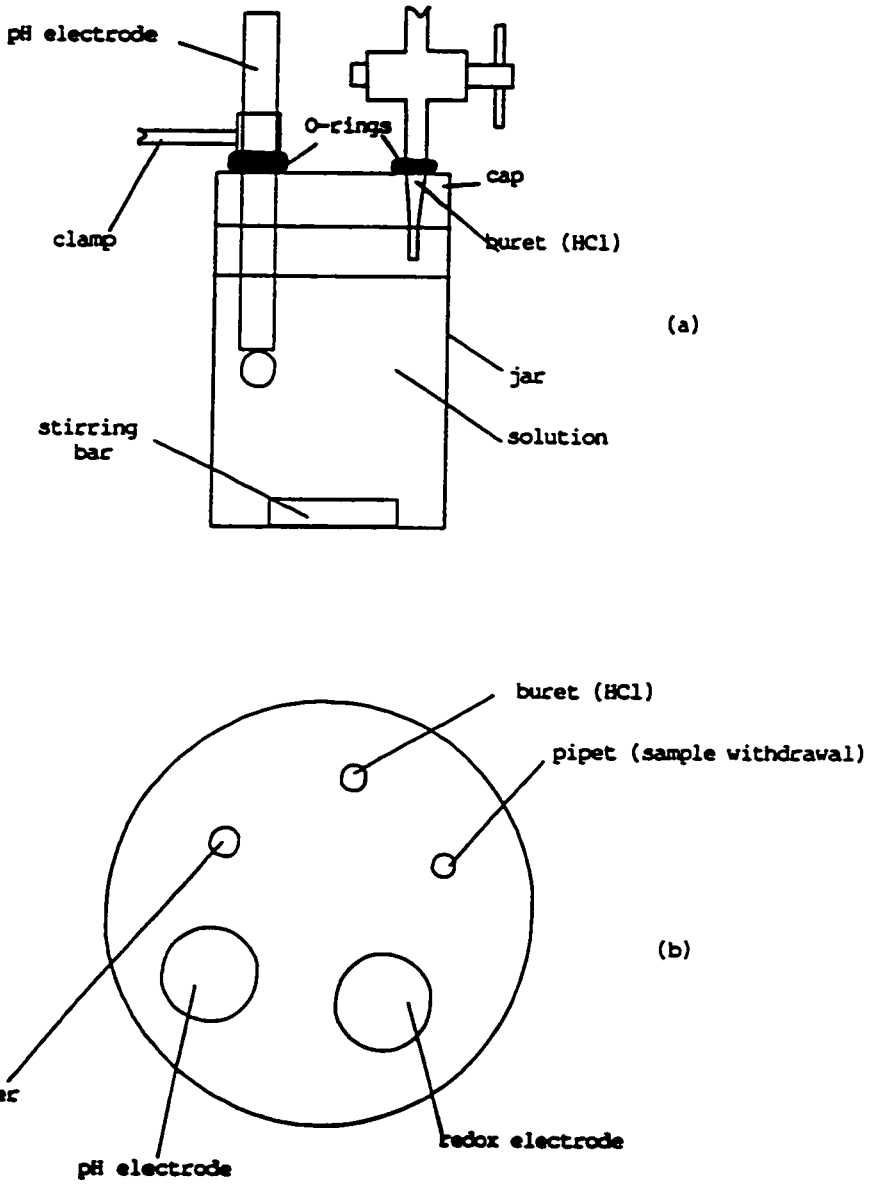

Figure 6–1 The experimental apparatus. (a) Schematic drawing of the experimental apparatus. (b) Top view of the cap. Holes are labelled with typical inserts.

IonAnalyzer. This meter was connected via a serial port to a microcomputer, allowing automated collection and storage of data. The combination pH electrodes used were Orion model 91–06 and Fisher AccupHast model 13–620–281. An Orion Platinum Redox Electrode (model 96–78) was also used in most of the indirect experiments.

Solutions were prepared using: deionized water, through which nitrogen had been bubbled to remove dissolved oxygen; Fisher Scientific Certified A.C.S. Na_2SO_3 (anhydrous), $Na_2S_2O_3 \cdot 5H_2O$ (crystal) and NaCl; and Fisher Scientific Reagent grade $Na_2S \cdot 9H_2O$ crystals. The starting solutions used in the experiments varied widely in total sulfur concentration, $[S]_{aq}$, and average electron number, $\bar{z}$. A range of average electron numbers was achieved by varying the relative quantities of sulfide ($z = -2$), thiosulfate ($z = 2$) and sulfite ($z = 4$) in the solutions. The vast majority of starting solutions were prepared by combining sulfide and sulfite; the few instances in which sulfide and thiosulfate were used will be noted. NaCl was also added to most of the starting solutions to raise ionic strength. Except where otherwise noted, the starting solutions were 0.2 M in NaCl for indirect experiments and 0.1 M in NaCl for direct experiments.

After the starting solution was transferred into the experimental apparatus by pipet, the electrodes and other inserts were clamped into place. Nitrogen was bubbled into the apparatus for approximately 10 minutes to reduce the amount of oxygen in the head space of the jar. After removal of the bubbler, the addition of HCl from a buret and the monitoring of pH were begun. Magnetic stirring was used to provide mixing. All experiments were conducted at room temperature ($25^\circ C \pm 2^\circ C$).

6.1.1 Indirect Determination Experiments

In the indirect determination experiments, the sulfur concentration and average electron number of the starting solution were chosen so that acidification to the pH of interest would cause the formation of solid sulfur. The starting solution was acidified with HCl until a predetermined pH was reached. In some cases, additional HCl was added if the pH continued to drift upward. Once the pH of the solution appeared to stabilize, the buret containing the acid was removed to prevent leakage of acid into the solution, and stirring was discontinued. The solution was then left undisturbed until the pH of the system stabilized and solid sulfur settled out of the solution; typically, the solution was left overnight. In cases in which the system pH drifted considerably, additional acid was sometimes added with stirring; the solution would then be allowed to settle for another day. The redox potential of the solution was also measured.

After the pH had stabilized and the solid sulfur had settled out of the solution, the contents of the experimental apparatus were divided into samples A and B. A volumetric pipet was used to draw a sample of clear supernatant liquid from the jar. This portion of clear liquid was designated sample A; sample B consisted of all remaining contents of the apparatus. Care was taken to minimize the amount of solid drawn in with sample A. Sample A was immediately basified with NaOH to reduce losses of gaseous sulfur species and then put aside for total sulfur analysis. Sample B was then basified with NaOH and solid sulfur adhering to the electrodes was rinsed into the sample. Sample B was then heated to near 100°C, with stirring, to convert the solid sulfur to dissolved species (Pryor, 1962). Samples A and B were then analyzed for total sulfur, as described in Appendix C. From these analyses, a point on the boundary between the single–phase and

two–phase regions was then calculated by the method described in Appendix D.2.

6.1.2 Direct Determination Experiments

In the direct visual determination experiments, pH was monitored as HCl was added. Once the pH of interest was reached, the HCl buret was removed from the apparatus and stirring was continued for approximately 30 minutes. The pH electrode was then removed from the jar, and screw cap of the apparatus was quickly replaced with a new cap without holes. If solid sulfur was detected in the solution within two days, then the point determined by the concentration and composition of the solution (see Appendix D.1) was in the two–phase region; otherwise, the point was located in the single–phase region. At the conclusion of the run, the pH of the solution was measured.

To aid in the detection of small quantities of solid in dilute solutions, a 5–mW helium–neon laser (Uniphase Model 1105P, $\lambda = 633$nm) was used. The beam was directed through the experimental solution in a darkened room and observed at a 90° angle to the direction of the incident beam. Colloidal sulfur particles caused scattering that was visible as line through the solution. The experimental solutions were compared to "background" solutions which contained comparable concentrations of sulfur species and NaCl, but which were kept at high pH where solid sulfur did not form.

6.2 Experimental Results

The results of indirect determination experiments for the aqueous sulfur system are listed in Table 6–1. The "negative" sulfur losses listed for several runs resulted from uncertainty in the total sulfur analysis. For all of the runs listed,

Table 6–1 Results of Indirect Determination Experiments for the Aqueous Sulfur System

Run Number	Initial $[S]_{aq}$ (M)	Initial $\bar{z}$	Final $\bar{z}_{aq}$	Final $-\log_{10}[S]_{aq}$	Final pH	Final E (V vs. NHE)	% S Lost
101	0.035	−1.14	−1.56	1.78	2.89		14.8
10	0.035	−1.14	−1.29	1.60	2.75	0.055	7.4
7	0.040	−0.50	−0.02	1.59	2.58	0.085	24.3
6	0.040	−0.50	0.32	1.68	2.85	0.079	33.9
22	0.102	0.40	1.35	1.25	3.01		22.3
33	0.110	0.73	1.35	1.29	2.74	0.151	−2.5
32	0.112	0.73	1.37	1.29	2.86	0.104	−1.7
9	0.040	1.00	1.52	1.58	4.95	−0.032	2.1
2	0.040	1.00	1.53	1.52	2.86	0.223	11.5
8	0.035	1.43	1.67	1.52	2.56		2.8
102	0.125	1.20	1.94	1.17	2.87		−1.0
27	0.109	1.27	1.94	1.21	2.88	0.170	−1.1
28	0.109	1.27	1.97	1.21	2.86	0.149	−2.7
25	0.080	1.75	1.97	1.19	3.08	0.226	−2.0
26	0.109	1.27	2.00	1.22	2.72	0.192	−1.7
16	0.081	1.75	2.07	1.20	2.50	0.184	0.8
18	0.100	0.40	2.07	1.48	2.92		19.8
34	0.404	1.75	2.07	0.63	2.70	0.178	−1.6
17	0.100	1.00	2.16	1.33	2.75	0.198	7.6
29	0.404	1.75	2.18	0.64	2.85	0.086	0.5

the starting solution contained a background NaCl concentration of 0.2 M. For all of the listed runs except Run 102, the starting solutions were made from sulfide and sulfite; the starting solution for Run 102 was made from sulfide and thiosulfate. The results of indirect determination experiments can be grouped by pH and plotted as in Figure 6–2, which shows experimental data for pH = 2.8 ± 0.3 on a field of $-\log_{10}[S]_{aq}$ vs. average electron number, $\bar{z}$. The theoretical curves, which show the boundary between the single–phase aqueous region and the two–phase region, in Figure 6–2 and all subsequent figures in this chapter were calculated using the species listed in Table 3–2.

Table 6–2 lists additional results of indirect determination experiments (Yung, 1989). These experiments were performed in an apparatus designed specifically to reduce losses of gaseous sulfur species. The background NaCl concentration used for these runs was 0.1 M.

Potential data from the two–phase region, where solid sulfur exists in equilibrium with sulfur in the aqueous phase, can be displayed on a field of $\bar{z}_{aq}$ vs. E. Such data from Tables 6–1 and 6–2 are shown in Figure 6–3 for pH = 2.8 ± 0.3 and in Figure 6–4 for pH = 5.3 ± 0.2.

Results of direct determination experiments for the aqueous sulfur system are listed in Table 6–3; the results are grouped by the average electron number, $\bar{z}$, of the solution. The starting solutions for all of these runs were prepared from sulfide and sulfite and contained a background NaCl concentration of 0.1 M.

Data from Table 6–3 are shown in the form of $-\log_{10}[S]_{aq}$ vs. $\bar{z}$ diagrams for pH = 2.80 in Figure 6–5 and for pH = 4.7 ± 0.5 in Figure 6–6.

The behavior of these experimental systems with time was also investigated. Figure 6–7 shows how the pH of Run 2, an indirect determination

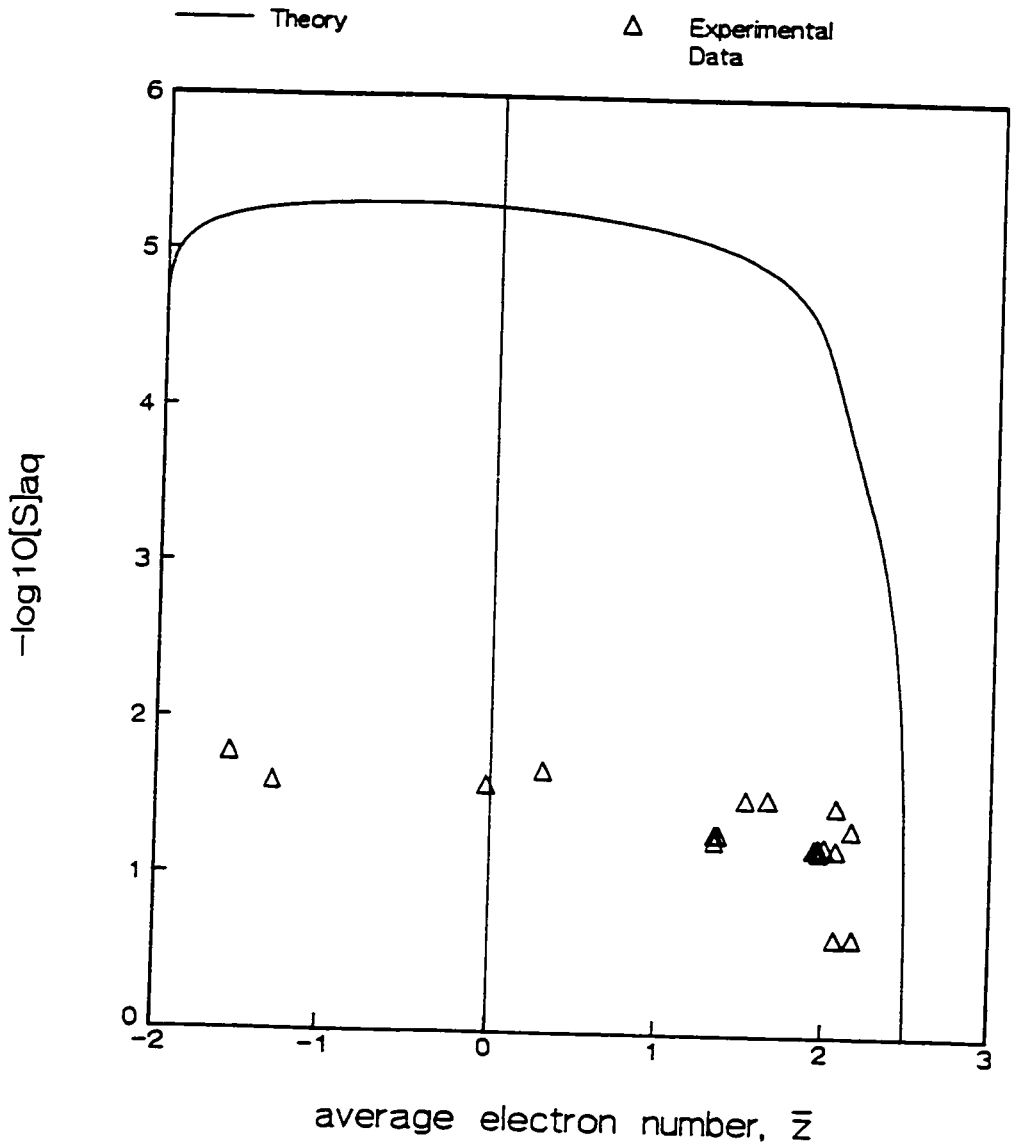

Figure 6–2 Results of indirect determination experiments for the aqueous sulfur system at pH = 2.8 ± 0.3. Experimental data are shown as triangles. The solid line is the theoretical curve.

Table 6–2 Results of Additional Indirect Determination Experiments for the Aqueous Sulfur System

Run Number	Initial $[S]_{aq}$ (M)	Initial $\bar{z}$	Final $\bar{z}_{aq}$	Final $-\log_{10}[S]_{aq}$	Final pH	Final E (V vs. NHE)
SEB12.2	0.080	1.50	1.69	1.19	5.43	–0.047
SEB13	0.083	1.00	1.14	1.18	5.32	–0.088
SEB14	0.100	0.00	0.00	1.13	5.14	–0.102
SEB15	0.100	–1.00	–1.21	1.16	3.79	–0.036
SEB16	0.080	–1.50	–1.73	1.22	3.07	0.010

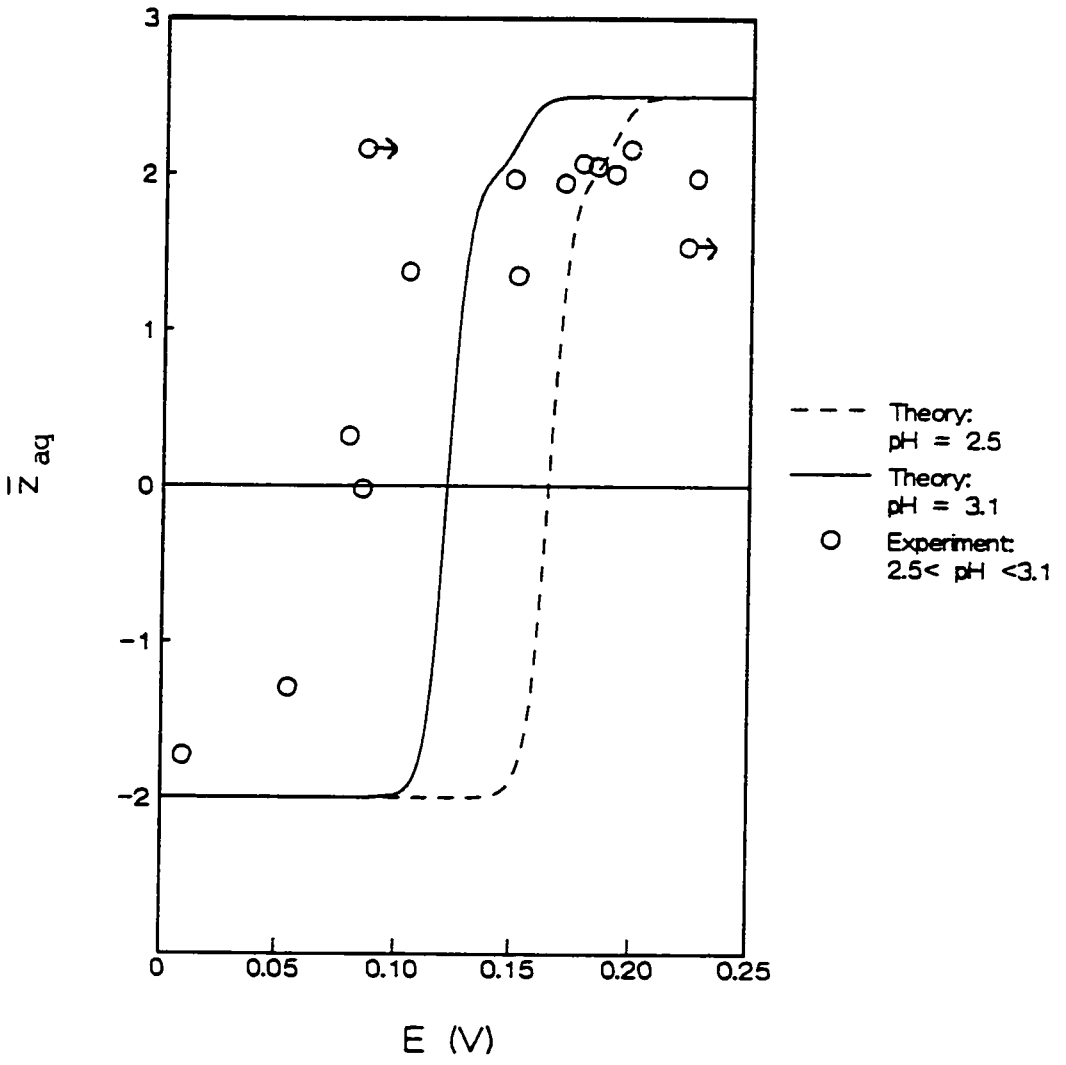

Figure 6–3 Potential measurements for the aqueous sulfur system at pH = 2.8 ± 0.3. The experimental data are shown as circles. Arrows indicate the direction of drift in cases where steady potential drift continued until to end of the run. $\bar{z}_{aq}$ is the average electron number of dissolved sulfur in equilibrium with solid sulfur. Theoretical curves are shown for the extremes of the pH range of the data.

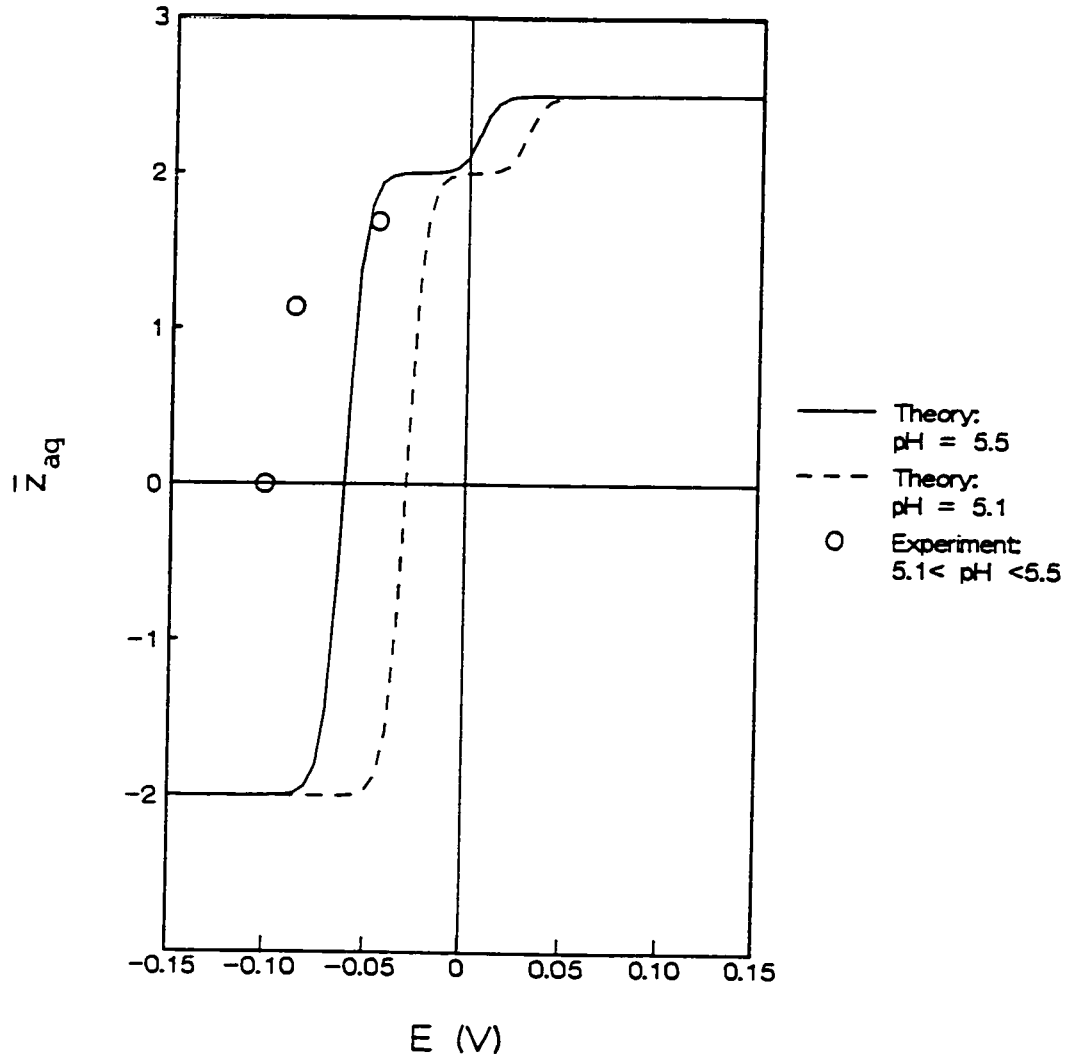

Figure 6–4 Potential measurements for the aqueous sulfur system at pH = 5.3 ± 0.2. The experimental data are shown as circles. $\bar{z}_{aq}$ is the average electron number of dissolved sulfur in equilibrium with solid sulfur. Theoretical curves are shown for the extremes of the pH range of the data.

Table 6–3
Results of Direct Determination Experiments
for the Aqueous Sulfur System

Run Number	Average Electron Number, $\bar{z}$	pH	$-\log_{10}[S]_{aq}$	Solid (1) No Solid (0)
9–2	–1.85	3.94	3.79	1
9–1	–1.85	3.97	4.09	0
9–3	–1.85	4.26	3.20	1
9–10	–1.85	5.50	2.69	1
9–9	–1.85	5.52	2.72	1
9–4	–1.85	5.56	2.93	0
9–11	–1.85	6.02	2.39	1
9–12	–1.85	6.10	2.69	0
9–13	–1.85	6.13	2.99	0
9–5	–1.85	6.69	2.69	1
9–6	–1.85	6.69	2.49	0
9–14	–1.85	6.92	1.41	1
9–8	–1.85	7.01	1.66	1
9–7	–1.85	7.16	1.81	0
133	–1.84	5.02	3.24	0
129	–1.84	5.08	3.07	1
122	–1.50	2.46	4.26	1
121	–1.50	2.80	4.24	1
128	–1.50	2.80	4.33	0
110	–1.50	2.80	4.03	1
112	–1.50	2.80	4.16	1
6–13	–1.50	3.97	3.72	1
6–2	–1.50	4.02	4.02	0
6–1	–1.50	4.03	4.22	0
6–4	–1.50	4.85	3.03	0
132	–1.50	4.89	3.17	1
126	–1.50	4.92	3.34	0
6–3	–1.50	5.20	3.33	0
6–9	–1.50	5.29	2.81	1
6–10	–1.50	5.75	2.49	1
6–5	–1.50	5.95	2.86	0
6–6	–1.50	6.05	2.65	0
6–12	–1.50	7.04	1.77	1
6–11	–1.50	7.06	1.98	0
6–7	–1.50	7.18	2.06	0
6–8	–1.50	7.35	1.84	0
2–3	–1.00	2.80	4.24	1
2–5	–1.00	2.80	4.33	0

Table 6–3 (continued)

Run Number	Average Electron Number, $\bar{z}$	pH	$-\log_{10}[S]_{aq}$	Solid (1) No Solid (0)
5–1	–1.00	4.04	4.24	0
5–2	–1.00	4.07	4.05	1
5–3	–1.00	4.57	3.53	0
5–4	–1.00	4.77	3.24	0
5–9	–1.00	4.83	3.53	0
5–10	–1.00	4.93	3.23	0
5–12	–1.00	4.94	3.53	0
5–13	–1.00	5.45	3.01	0
5–11	–1.00	5.58	2.70	1
5–14	–1.00	5.73	2.64	1
5–6	–1.00	5.78	2.75	0
5–5	–1.00	5.90	2.93	0
5–8	–1.00	7.02	1.93	0
5–7	–1.00	7.05	2.06	0
5–15	–1.00	7.10	1.84	1
52	–0.50	2.73	3.80	1
53	–0.50	2.80	3.92	1
51	–0.50	2.80	4.10	1
49	–0.50	2.83	3.70	1
50	–0.50	2.86	2.70	1
120	0.00	2.40	4.38	0
115B	0.00	2.80	4.24	1
119	0.00	2.80	4.36	0
4–19	0.00	4.01	3.92	0
4–23	0.00	4.65	3.37	0
4–17	0.00	4.65	3.30	1
4–20	0.00	4.69	3.15	1
135	0.00	4.70	3.33	1
4–24	0.00	4.71	3.14	1
124	0.00	4.73	3.23	1
4–14	0.00	4.77	2.95	1
4–18	0.00	4.78	3.07	1
125	0.00	4.79	3.53	0
4–27	0.00	4.94	3.13	0
4–29	0.00	4.99	2.84	1
123	0.00	5.01	2.84	1
4–31	0.00	5.18	2.84	1
4–21	0.00	5.40	2.96	0
4–22	0.00	5.55	2.74	0
4–30	0.00	6.06	2.84	0
4–25	0.00	6.47	2.93	0

Table 6–3 (continued)

Run Number	Average Electron Number, $\bar{z}$	pH	$-\log_{10}[S]_{aq}$	Solid (1) No Solid (0)
4–28	0.00	6.63	2.93	0
4–26	0.00	6.99	1.67	1
4–15	0.00	7.20	1.89	0
4–16	0.00	7.40	2.04	0
58	0.25	2.80	4.73	0
65	0.25	2.80	4.03	1
64	0.25	2.80	4.03	1
54	0.25	2.80	3.73	1
56	0.25	2.80	5.03	0
59	0.25	2.80	4.73	0
61	0.25	2.80	4.43	0
57	0.25	2.80	5.03	0
55	0.25	2.80	3.73	1
62	0.25	2.80	4.13	1
63	0.25	2.80	4.13	0
60	0.25	2.80	4.43	0
1–13	1.00	2.80	4.11	1
1–11	1.00	2.80	4.16	0
7–2	1.00	4.00	3.83	1
7–1	1.00	4.03	4.10	0
7–4	1.00	4.23	3.01	1
7–3	1.00	4.30	3.31	1
7–10	1.00	4.35	3.11	1
7–9	1.00	4.40	3.20	1
7–14	1.00	4.55	2.93	0
7–5	1.00	4.63	2.70	1
7–6	1.00	4.95	2.46	1
7–19	1.00	5.11	2.70	1
7–20	1.00	5.49	2.31	1
7–15	1.00	5.82	2.81	0
7–16	1.00	6.20	2.56	0
7–22	1.00	6.25	2.31	1
7–12	1.00	6.31	2.56	0
7–11	1.00	6.32	2.70	0
7–17	1.00	6.33	2.44	0
7–18	1.00	6.64	2.02	1
7–13	1.00	6.75	1.94	1
7–7	1.00	6.80	1.84	1
7–8	1.00	6.98	1.72	1
7–21	1.00	7.05	2.01	0

Table 6–3 (continued)

Run Number	Average Electron Number, $\bar{z}$	pH	$-\log_{10}[S]_{aq}$	Solid (1) No Solid (0)
116	1.50	1.35	4.68	0
114	1.50	1.65	4.83	0
107	1.50	2.80	4.13	1
105	1.50	2.80	3.73	1
106	1.50	2.80	3.95	1
111	1.50	2.80	4.23	0
8–2	1.50	3.90	3.75	0
8–1	1.50	3.95	3.97	0
8–3	1.50	4.01	3.15	1
8–14	1.50	4.03	3.33	1
8–15	1.50	4.11	2.64	1
8–10	1.50	4.15	2.94	1
127	1.50	4.30	3.33	0
8–4	1.50	4.47	2.94	1
8–22	1.50	4.50	2.93	1
8–21	1.50	4.51	2.93	1
8–24	1.50	4.58	2.93	1
8–20	1.50	4.60	2.64	1
8–5	1.50	4.68	2.53	1
8–18	1.50	4.73	2.75	1
8–6	1.50	4.74	2.38	1
8–12	1.50	5.02	2.33	0
8–23	1.50	5.28	2.64	1
8–9	1.50	5.39	3.15	0
8–16	1.50	5.89	2.15	0
8–11	1.50	6.34	2.55	0
8–13	1.50	6.35	1.55	1
8–19	1.50	6.40	1.85	1
8–17	1.50	6.83	1.53	1
8–8	1.50	7.05	1.65	0
8–7	1.50	7.06	1.76	0
130	1.80	4.59	2.89	1
136	1.80	4.68	3.27	0
10–10	1.86	3.90	3.76	0
10–2	1.86	3.97	3.38	1
10–9	1.86	3.97	3.98	0
10–1	1.86	3.98	3.56	1
10–18	1.86	4.14	2.87	1
10–11	1.86	4.21	3.16	1
10–21	1.86	4.30	2.87	1

Table 6–3 (continued)

Run Number	Average Electron Number, $\bar{z}$	pH	$-\log_{10}[S]_{aq}$	Solid (1) No Solid (0)
10–15	1.86	4.51	2.87	1
10–17	1.86	4.68	3.16	0
10–12	1.86	4.89	2.87	1
10–3	1.86	5.02	2.70	1
10–4	1.86	5.06	2.56	1
10–6	1.86	6.11	2.05	0
10–5	1.86	6.25	2.21	0
10–13	1.86	6.28	1.87	1
10–19	1.86	6.88	2.16	0
10–7	1.86	6.98	1.41	1
10–14	1.86	7.00	1.69	1
10–8	1.86	7.03	1.23	1
10–20	1.86	7.21	1.86	1
10–16	1.86	7.31	1.77	1
11–7	2.00	3.97	3.85	0
11–1	2.00	3.97	3.35	1
11–6	2.00	3.97	4.05	0
11–4	2.00	4.01	3.65	1
11–2	2.00	4.06	3.10	1
11–8	2.00	4.48	2.65	1
11–9	2.00	4.54	2.45	1
11–11	2.00	4.71	2.49	1
11–10	2.00	4.98	2.67	0
11–3	2.00	5.00	1.78	1
11–5	2.00	5.05	2.13	1
11–12	2.00	5.54	2.39	0
131	2.13	5.31	1.82	1
12–3	2.25	3.63	2.75	1
12–2	2.25	3.75	2.45	1
12–8	2.25	3.94	3.55	1
12–5	2.25	3.97	3.45	1
12–6	2.25	3.98	3.15	1
12–4	2.25	4.00	2.98	1
12–7	2.25	4.00	3.85	0
12–1	2.25	4.45	2.15	1
seb11–2	2.50	2.57	–0.22	0
seb11–1	2.50	7.30	–0.15	0

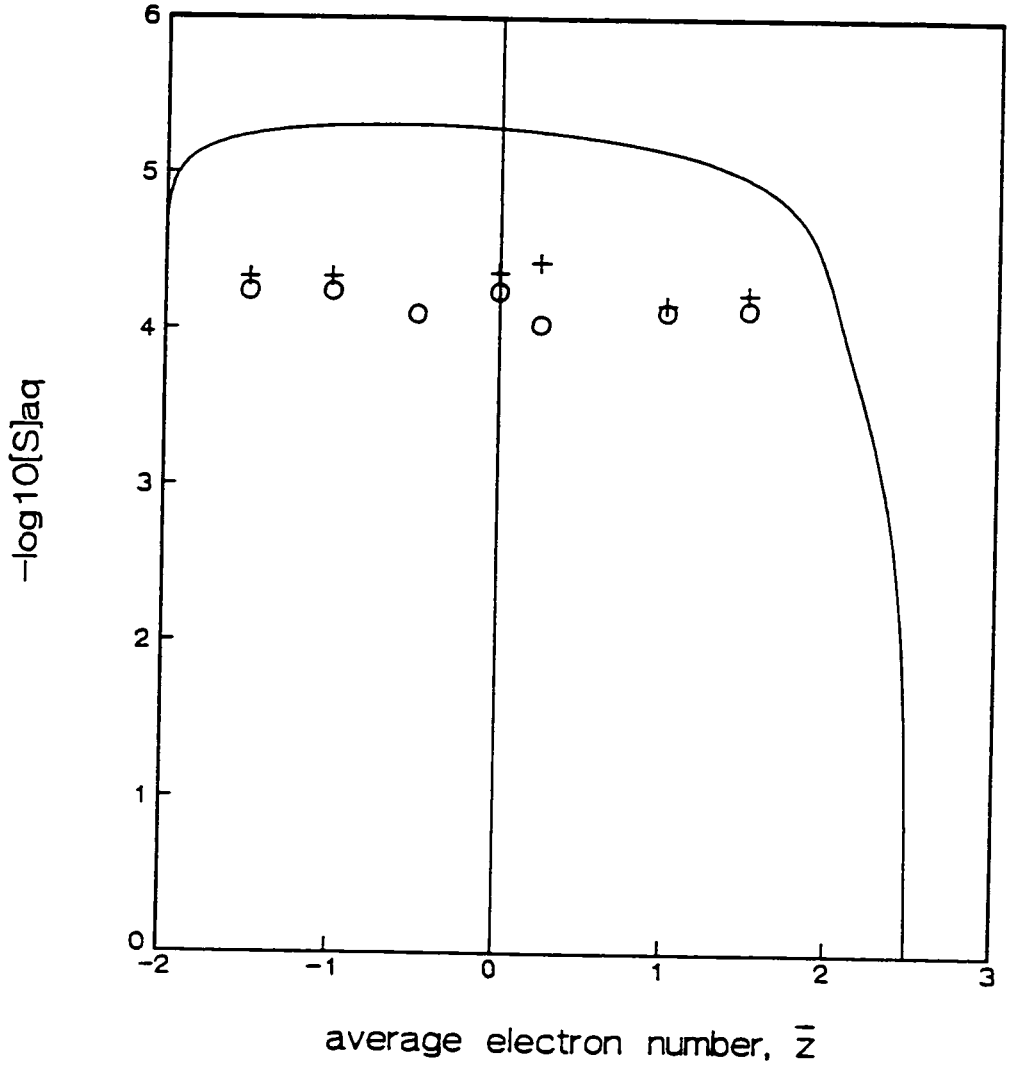

Figure 6–5 Results of direct determination experiments for the aqueous sulfur system at pH = 2.8. The solid line is the theoretical curve. Experimental data are indicated by symbols: "o"'s indicate points where solid formation was observed; at points indicated by "+"'s, no solid formation was observed.

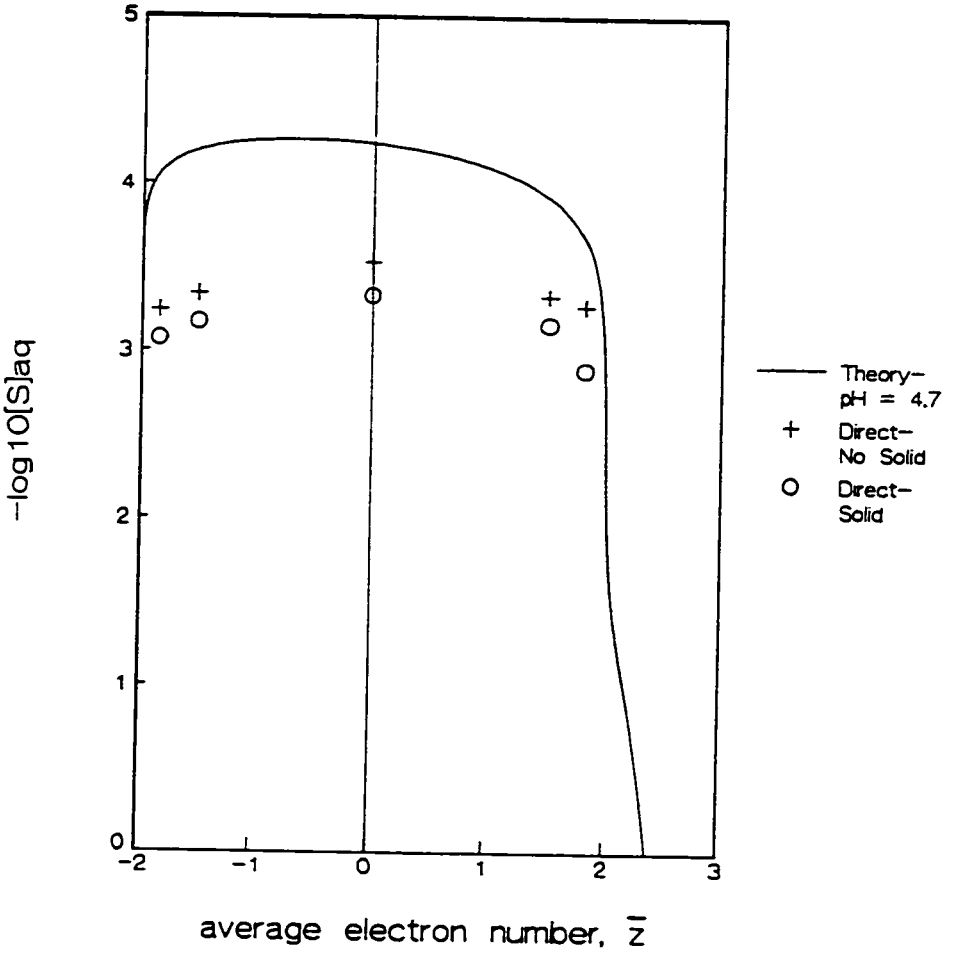

Figure 6–6 Results of direct determination experiments for the aqueous sulfur system at pH = 4.7 ± 0.5. The solid line is the theoretical curve. Experimental data are indicated by symbols: "o"'s indicate points where solid formation was observed; at points indicated by "+"'s, no solid formation was observed.

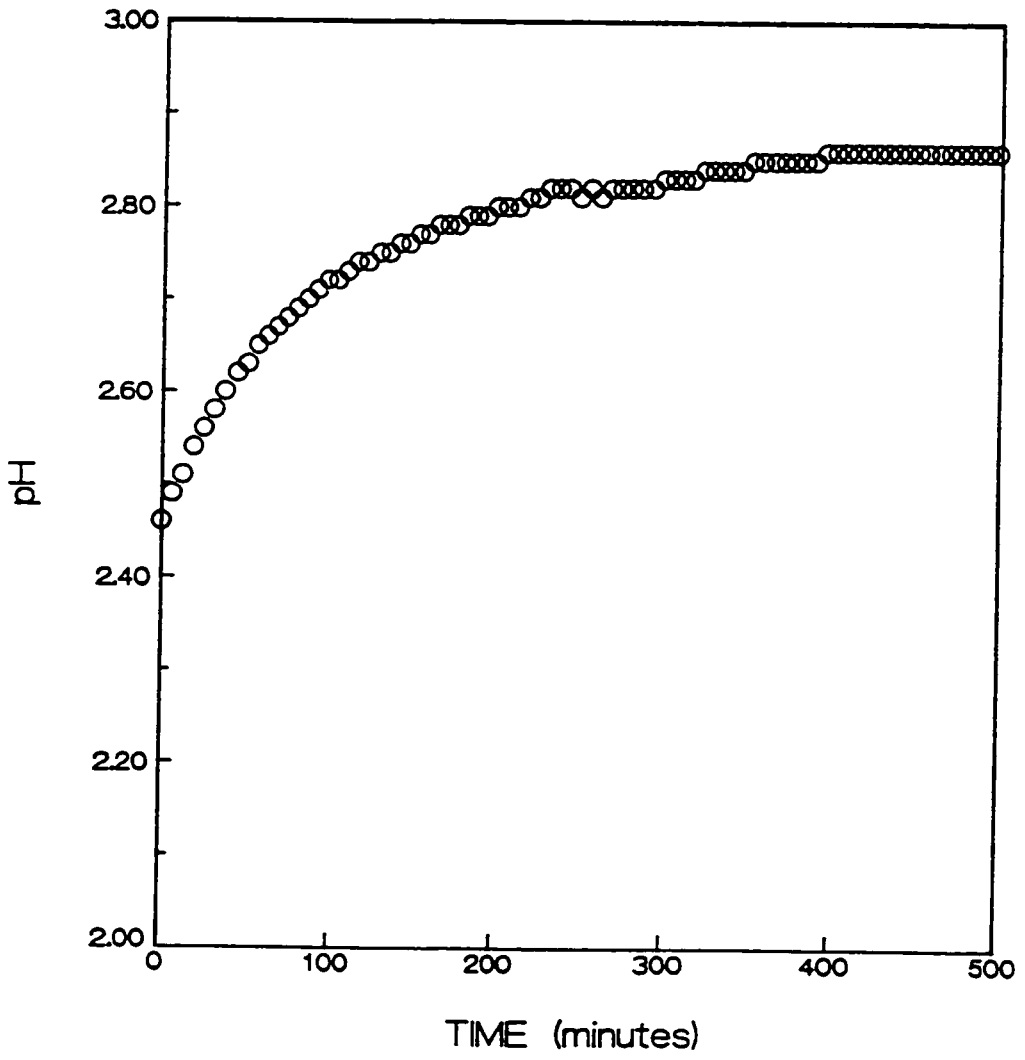

Figure 6–7 The change in pH versus time for Run 2, an indirect determination experiment.

experiment, changed with time. Table 6–4 summarizes three indirect determination experiments in which solution samples were withdrawn and analyzed after one day and after either one or five months. Figure 6–8 shows how the pH of Run 136, an indirect determination experiment, changed with time.

Direct determination experiments were also done using starting solutions made from sulfide and thiosulfate. Table 6–5 summarizes the comparison of these results with the results of similar experiments done with sulfide–sulfite starting solutions.

The data from Table 6–3 can also be grouped by $\bar{z}$ and shown on diagrams of $-\log_{10}[S]_{aq}$ versus pH. Figures 6–9 through 6–17 are diagrams of this type for values of $\bar{z}$ from –1.85 to 2.25.

A Princeton Gamma–Tech System 4 Energy Dispersion Spectroscopy unit was used to verify that the solid produced in these experiments was elemental sulfur.

6.3 Discussion

Despite its relatively simple electron number diagram, the aqueous sulfur system is quite complex. Acidification of systems containing sulfide and sulfite produces solutions similar to Wackenroder's liquid, a complex metastable mixture of sulfur species, including colloidal sulfur (Nickless, 1968; Karchmer, 1970). In these solutions, which contain numerous species including polythionates, many simultaneous redox, catenation and disproportionation reactions can occur (Greenwood and Earnshaw, 1984). Furthermore, over the ranges of concentration, electron number and pH investigated here, significant differences are expected in the chemistries of individual experimental runs.

Table 6–4
Summary of Long Term Indirect Experiments

Run MTH1

$\bar{z}_{in} = -1.29$ $([S]_{aq})_{in} = 0.170M$ pH = 2.48

After 1 day:
pH = 2.67 $[S]_{aq} = 0\ 0449M$

After 5 months:
pH = 3.24 $[S]_{aq} = 0\ 0145M$

Total sulfur lost: 74.6%

Run MTH2

$\bar{z}_{in} = -0.167$ $([S]_{aq})_{in} = 0.144M$ pH = 2.44

After 1 day:
$[S]_{aq} = 0\ 0213M$

After 5 months:
pH = 3.47 $[S]_{aq} = 0\ 0182M$

Total sulfur lost: 24.3%

Run 25

$\bar{z}_{in} = 1.75$ $([S]_{aq})_{in} = 0.080M$ pH = 2.80

After 1 day:
$[S]_{aq} = 0\ 0648M$

After 1 month:
pH = 3.08 $[S]_{aq} = 0\ 0650M$

Total sulfur lost: –2.0%

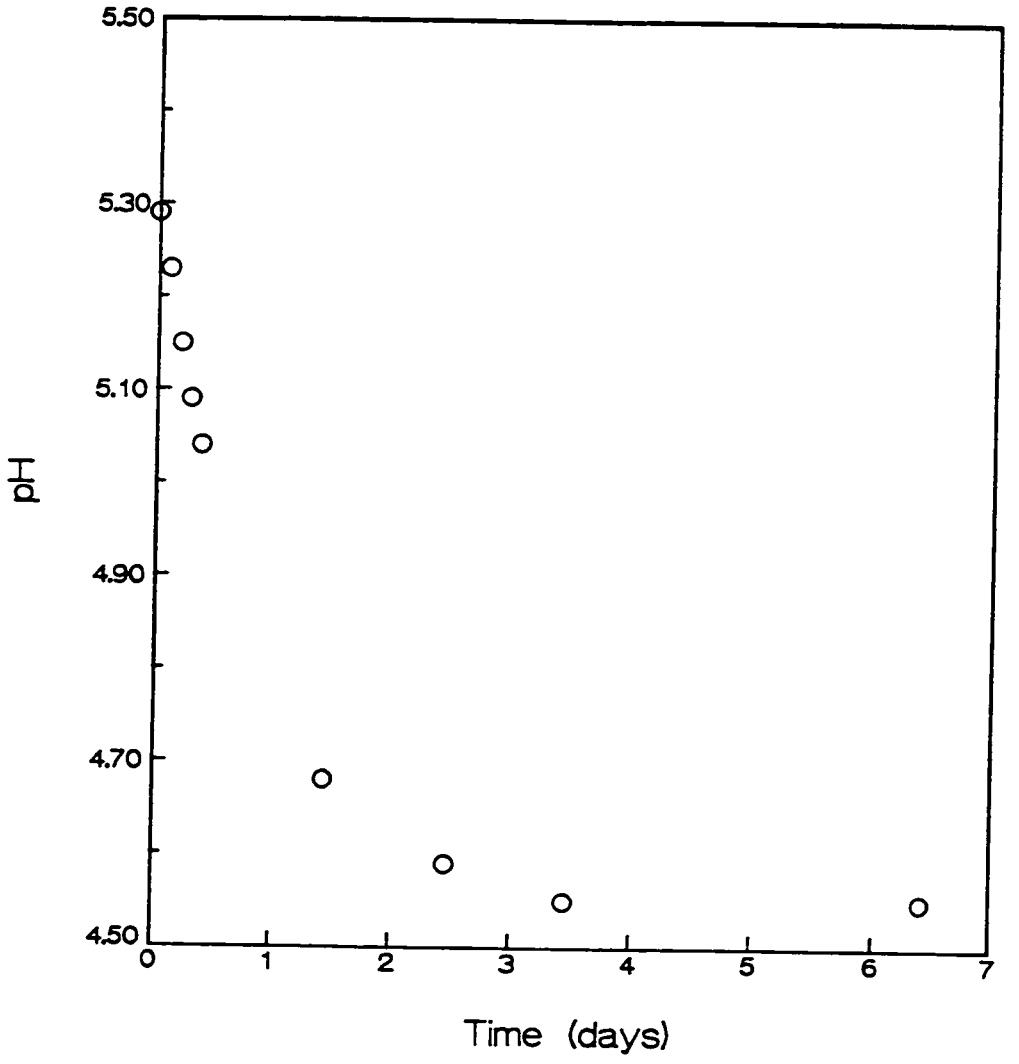

Figure 6–8 **The change in pH versus time for Run 136, a direct determination experiment.**

Table 6–5
Results of Direct Determination Experiments Using Sulfite and Thiosulfate Solutions at pH = 2.80 and z = 0.00

Run Number	$-\log_{10}[S]_{aq}$	Solid (1) No Solid (0)	Sulfite (S) Thiosulfate (T)
108	3.41	1	T
109	3.94	0	T
103	4.01	0	T
118	4.01	0	T
104	4.24	0	T
113	4.06	1	S
115B	4.24	1	S
119	4.36	0	S

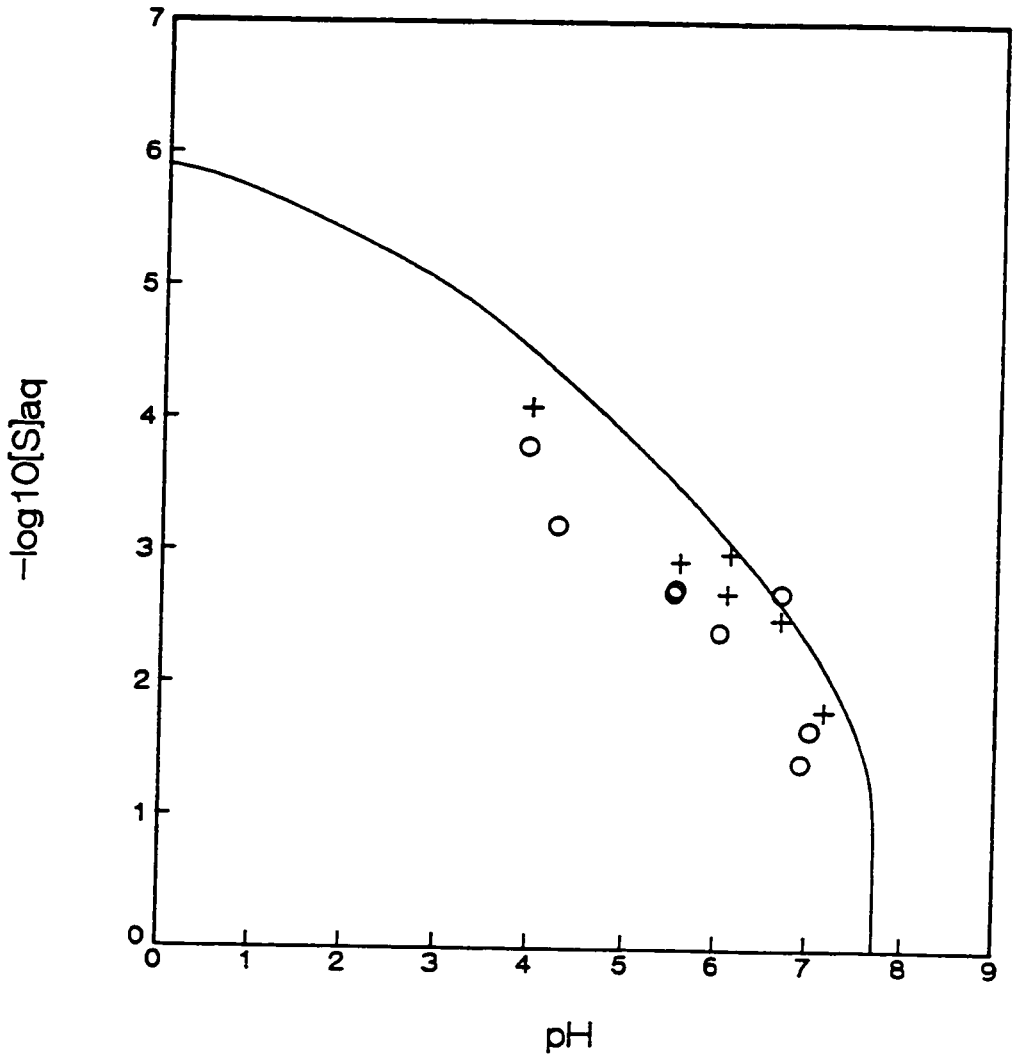

Figure 6–9 Results of direct determination experiments for the aqueous sulfur system at $\bar{z} = -1.85$. The solid line is the theoretical curve. Experimental data are indicated by symbols: "o"'s indicate points where solid formation was observed; at points indicated by "+"'s, no solid formation was observed.

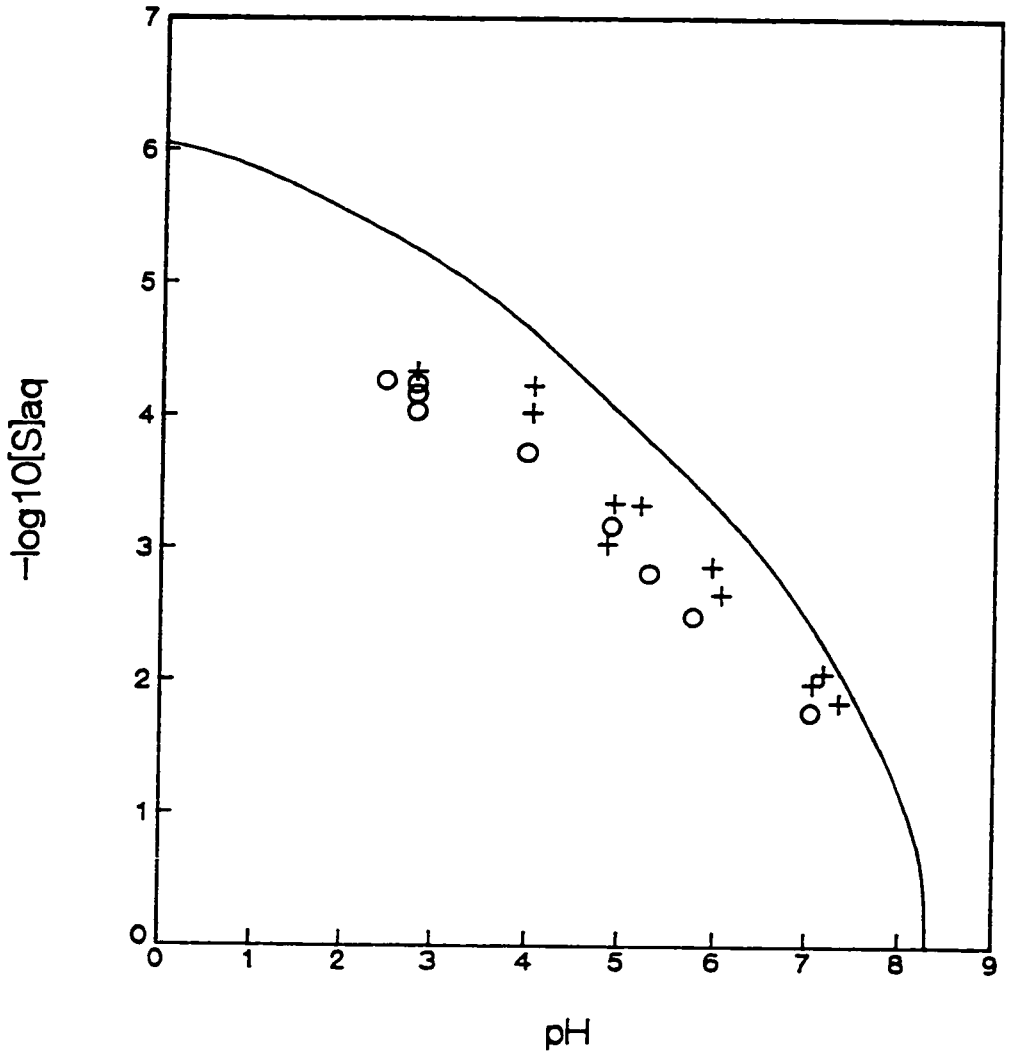

Figure 6–10 Results of direct determination experiments for the aqueous sulfur system at $\bar{z} = -1.5$. The solid line is the theoretical curve. Experimental data are indicated by symbols: "o"'s indicate points where solid formation was observed; at points indicated by "+"'s, no solid formation was observed.

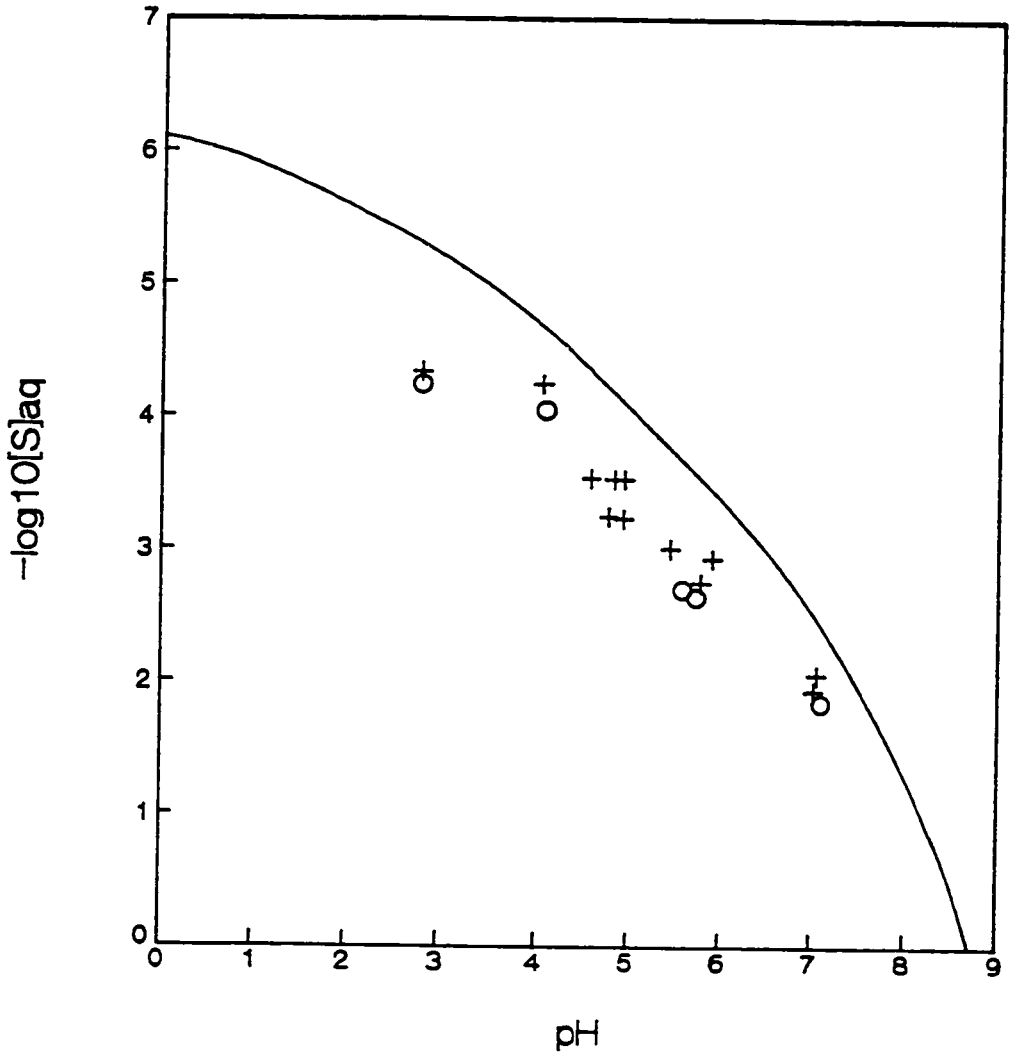

Figure 6–11 Results of direct determination experiments for the aqueous sulfur system at $\bar{z} = -1.0$. The solid line is the theoretical curve. Experimental data are indicated by symbols: "o"'s indicate points where solid formation was observed; at points indicated by "+"'s, no solid formation was observed.

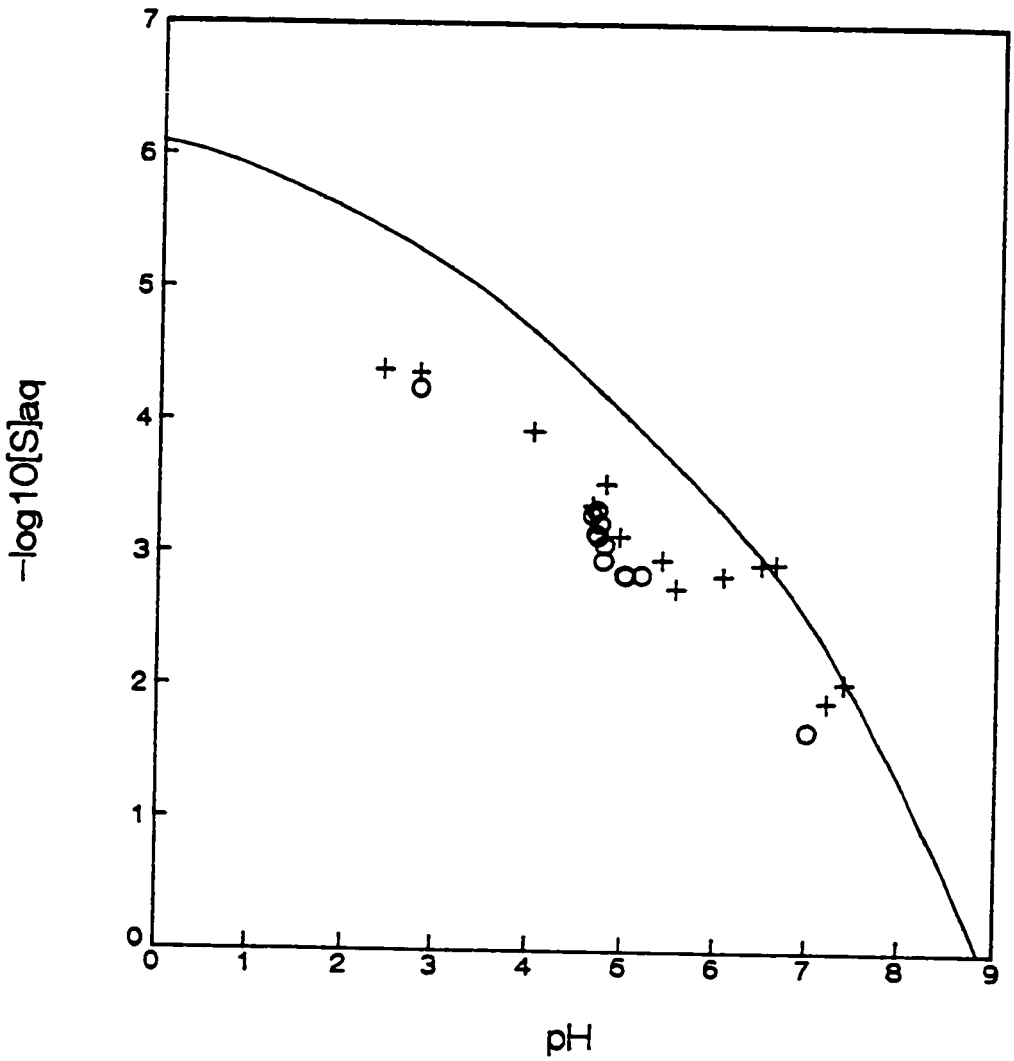

Figure 6–12 Results of direct determination experiments for the aqueous sulfur system at $\bar{z} = 0.0$. The solid line is the theoretical curve. Experimental data are indicated by symbols: "o"'s indicate points where solid formation was observed; at points indicated by "+"'s, no solid formation was observed.

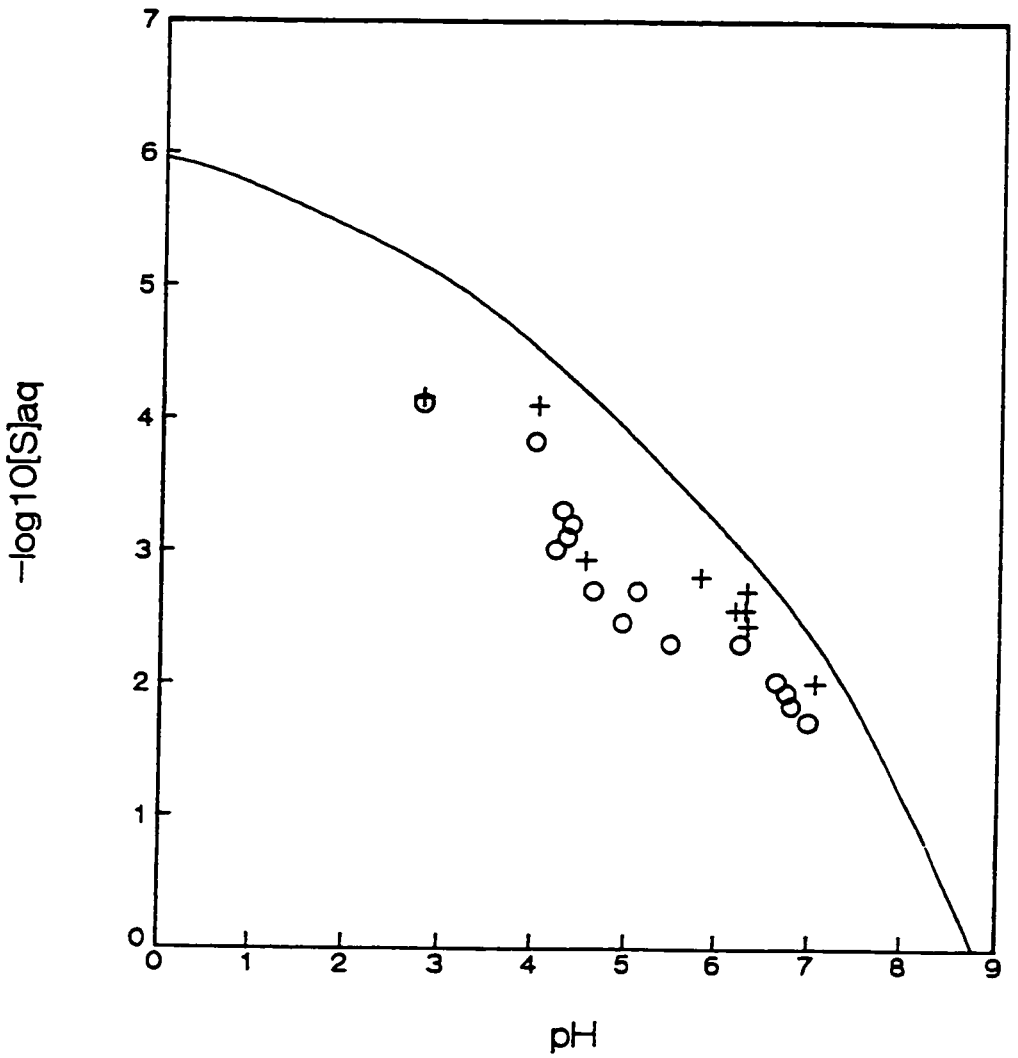

Figure 6–13 Results of direct determination experiments for the aqueous sulfur system at $\bar{z} = 1.0$. The solid line is the theoretical curve. Experimental data are indicated by symbols: "o"'s indicate points where solid formation was observed; at points indicated by "+"'s, no solid formation was observed.

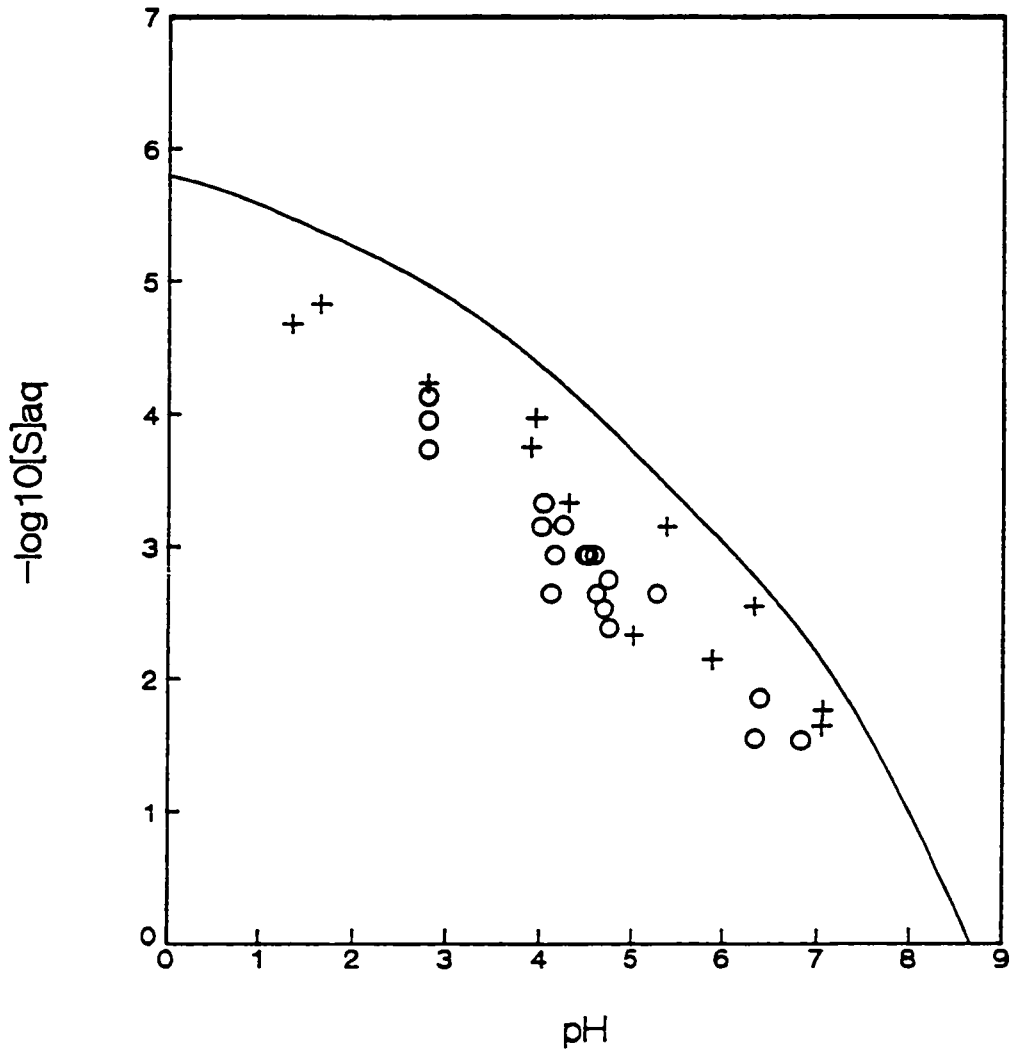

Figure 6–14 Results of direct determination experiments for the aqueous sulfur system at $\bar{z} = 1.5$. The solid line is the theoretical curve. Experimental data are indicated by symbols: "o"'s indicate points where solid formation was observed; at points indicated by "+"'s, no solid formation was observed.

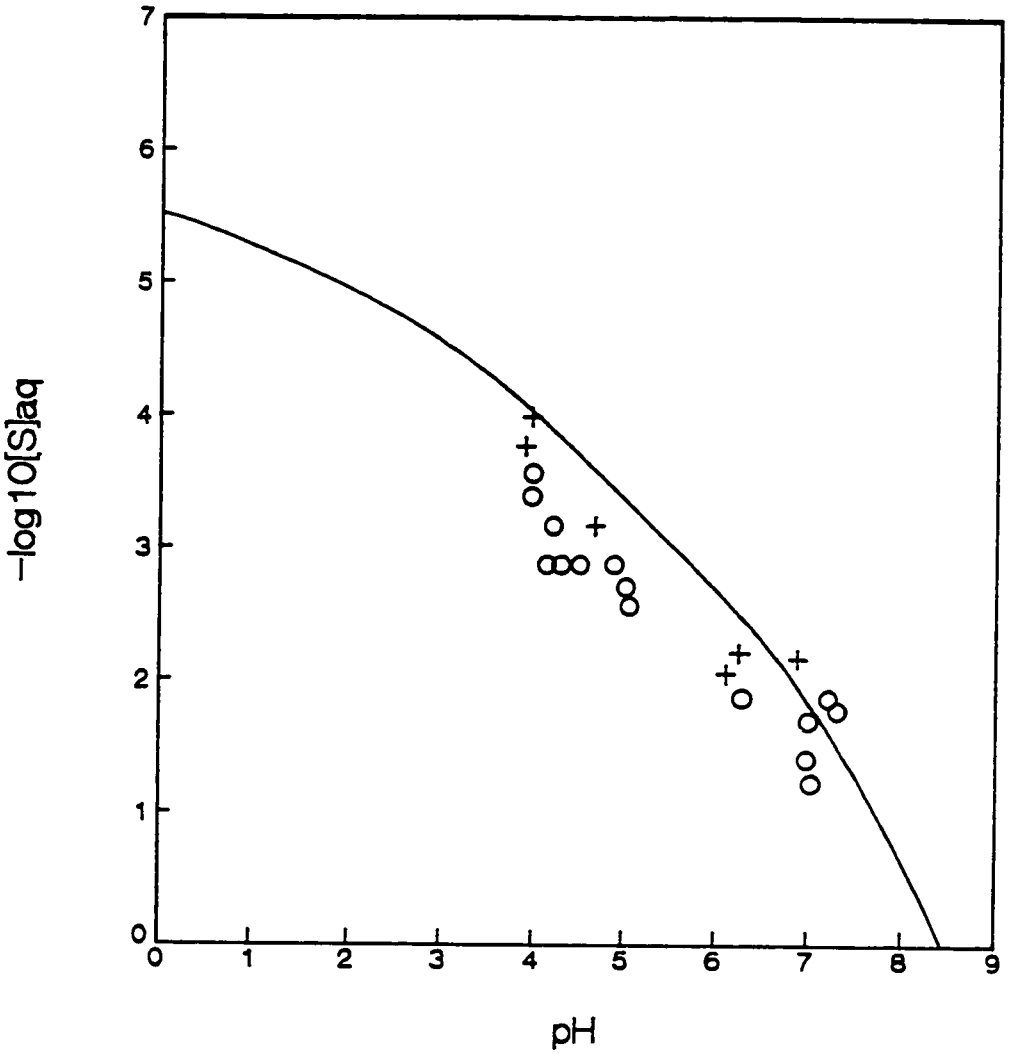

Figure 6–15 Results of direct determination experiments for the aqueous sulfur system at $\bar{z} = 1.86$. The solid line is the theoretical curve. Experimental data are indicated by symbols: "o"'s indicate points where solid formation was observed; at points indicated by "+"'s, no solid formation was observed.

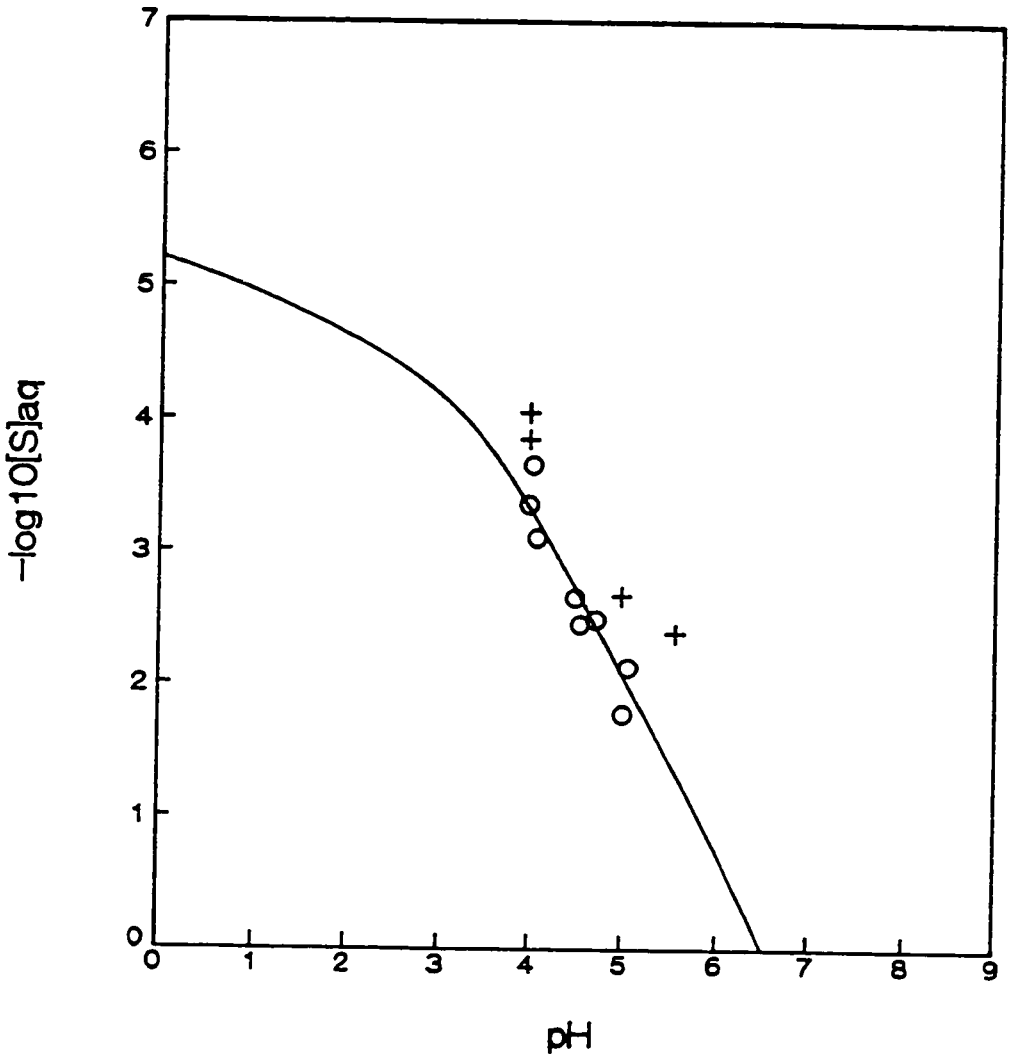

Figure 6–16 Results of direct determination experiments for the aqueous sulfur system at $\bar{z} = 2.0$. The solid line is the theoretical curve. Experimental data are indicated by symbols: "o"'s indicate points where solid formation was observed; at points indicated by "+"'s, no solid formation was observed.

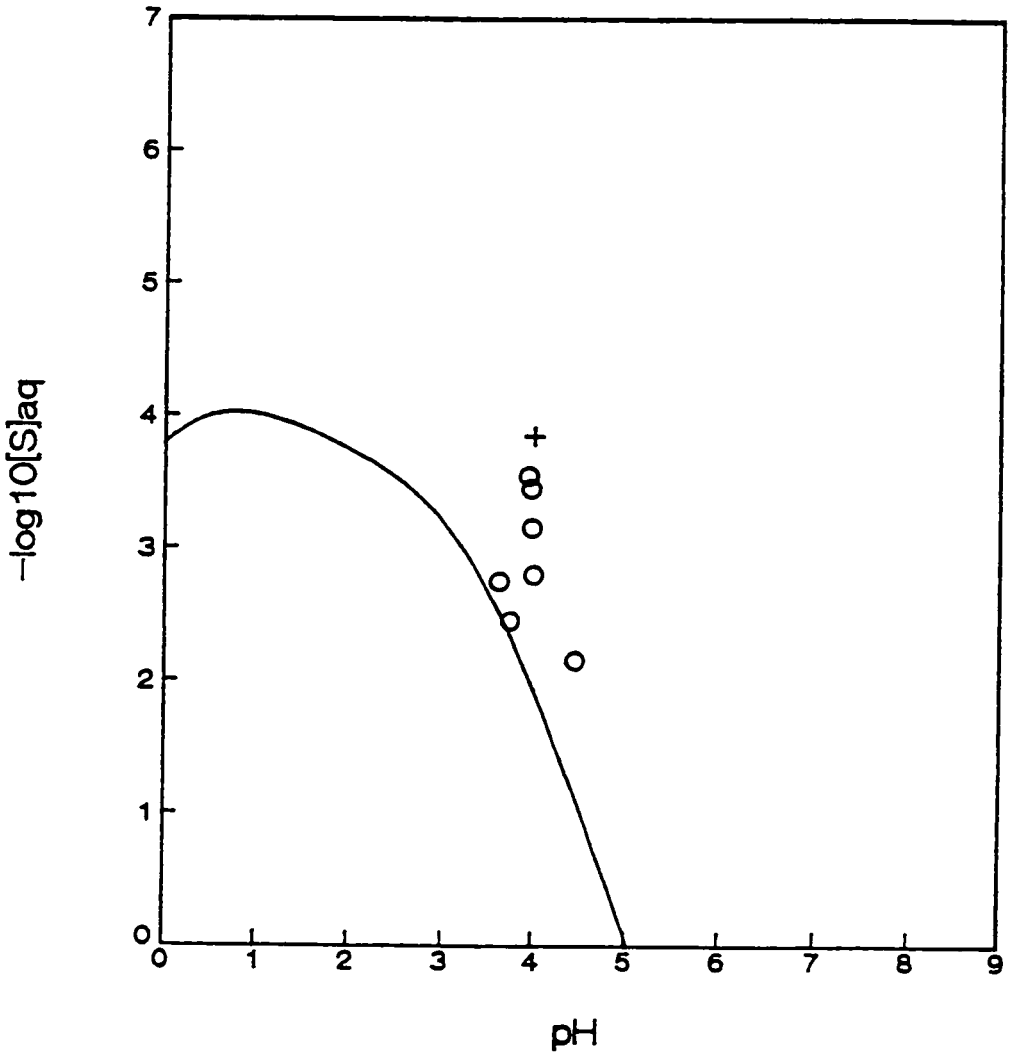

Figure 6–17 Results of direct determination experiments for the aqueous sulfur system at $\bar{z} = 2.25$. The solid line is the theoretical curve. Experimental data are indicated by symbols: "o"'s indicate points where solid formation was observed; at points indicated by "+"'s, no solid formation was observed.

6.3.1 Duration of Experimental Runs

Experiments were conducted on the aqueous sulfur system for comparison with theoretical equilibrium predictions. Thus, the duration of the experiments had to be sufficient to permit the establishment of equilibrium. Previous work suggested time scales ranging from an hour to days. In a study involving the acidification of solutions of KHS and K_2SO_3, equilibrium was established among sulfur species within one hour (Heunisch, 1977). In another study in which elemental sulfur was dissolved in Na_2S solutions, sulfur solubilities measued after three days were equal to those measured after three weeks and longer (Arntson, Dickson and Tunell, 1958).

In the indirect determination experiments, pH was used as a guide in deciding when equilibrium had been established. Constant pH and/or sulfur solubility do not insure true thermodynamic equilibrium; with slow reactions or the formation of metastable species, an "effective" equilibrium could be reached. Normally, pH stability occurred within 24 hours; often it occurred sooner, as shown in Figure 6–7, the pH vs. time curve for Run 2.

In an effort to understand the long term behavior of indirect determination experiments, a study was done using systems with low, moderate and high initial average electron number, $\bar{z}_{in}$. The results appear in Table 6–4. In each case, a run was begun, and once pH had stabilized (within 24 hours in each instance here), a liquid sample was withdrawn for total sulfur analysis. The experimental apparatus was then tightly recapped and left undisturbed for one to five months; another liquid sample was then withdrawn for analysis and the normal post–run sulfur analysis was then done. For the case of $\bar{z}_{in} = -1.29$, the sulfur concentration of the solution decreased by two–thirds over five months. The

recovery of only about 25% of the total sulfur the system indicated that losses as $H_2S(g)$, rather than solid formation, accounted for the decrease in solution concentration. For the case of $\bar{z}_{in} = -0.167$, the sulfur concentration of the solution decreased by 15% over five months and one–fourth the total sulfur in the system was lost. For the case of $\bar{z}_{in} = 1.75$, the sulfur concentration of the solution remained virtually unchanged after one month and no sulfur was lost from the system. It appeared that the solution at $\bar{z}_{in} = 1.75$, and probably the solution at $\bar{z}_{in} = -0.167$, reach equilibrium upon pH stabilization. For the solution at $\bar{z}_{in} = -1.29$, and to a lesser degree for the case at $\bar{z}_{in} = -0.167$, sulfur losses increased with time.

The indirect determination experiments were allowed to continue for up to two days, although the result (solid or no solid) did not generally change from day one to day two. In any case in which the total dissolved sulfur concentration of the starting solution was much less than $[H^+]$, the pH of the experimental solution stabilized immediately upon acidification. This was the case for the indirect experiments at pH = 2.80. However, in the range $4.5 < pH < 6.2$, the pH of the solutions tended to drift, apparently because of continuing reactions among the sulfur species. Figure 6–8 shows the pH vs. time data for Run 136. Notice that by day two, the pH of the system had very nearly reached its final value.

6.3.2 Effect of Thiosulfate Ion

Table 6–5 shows the comparison between direct determination experiments conducted using starting solutions made with sulfide and either sulfite or thiosulfate. The phase boundary is located at a significantly higher value of $-\log_{10}[S]_{aq}$ for the sulfite case (between 4.24 and 4.36) than in the thiosulfate case

(between 3.41 and 3.94). The runs using sulfite ion are closer to the equilibrium line than the runs using thiosulfate, indicating that reactions in the former case are proceeding more rapidly.

Among the indirect runs listed in Table 6–1, Run 102 (sulfide/thioslfate starting solution) can be compared to Runs 26, 27 and 28 (sulfide/sulfite starting solutions), which were conducted under similar conditions of average electron number and concentration. Note the similarity in the results.

If all of the reactions in the aqueous sulfur system were reversible, then the outcome of an experiment would depend only on the average electron number and concentration of sulfur in the system; whether sulfite or thiosulfate was originally present would not make any dfference. The results of these tests indicate that the sulfide/thiosulfate and sulfide/sulfite solutions may produce similar or different results depending on the particular experimental case.

6.3.3 Experimental Error

6.3.3.1 Indirect Determination Experiments

The loss of sulfur from solution in the form of gaseous species, especially H_2S, was significant in the indirect experiments. Because losses from solutions with high sulfide concentrations were high, while losses from solutions with high sulfite concentrations were negligible, all losses from the acidified sulfur solutions were attributed to the formation of $H_2S(g)$. This is also consistent with the thermodynamic data for H_2S and SO_2 in the gaseous and dissolved states. Furthermore, the odor of H_2S was noticeable during runs involving high sulfide concentrations. These H_2S losses could be accounted for and included in the sulfur balance as described in Appendix D.2. However, these losses increased the

uncertainty in the calculated value of $\bar{z}_{aq}$, the average electron number in equilibrium with the solid sulfur.

The indirect determination experiments were also subject to errors arising from the experimental procedure for the analysis of total sulfur (Appendix C). Incomplete conversion of sulfur species to sulfate would lead to an underestimation of total sulfur; the presence of insoluble impurities in the experimental solutions could lead to an overestimation of total sulfur. The latter appeared to be a more common problem, sometimes leading to errors of up to 3% in the determination of total sulfur in the system.

The total sulfur concentration of the clear, supernatant liquid was also subject to overestimation. Despite efforts to withdraw the clear solution with minimal disturbance of the solid sulfur, sulfur particles were sometimes drawn up with the solution sample. Also, in some cases, the solution did not clear completely and colloidal sulfur was drawn in with the sample.

The presence of dissolved oxygen in the experimental system was another potential source of error. Efforts were made to reduce the amount of dissolved O_2 in the starting solution and keep O_2 out of the apparatus.

Other possible sources of error included the uncertainties in the average electron number and concentration of the starting solution. Also, the final volume of the experimental solution after acid addition was based on the assumption of ideal mixing, as described in Appendix D.

Even these small uncertainties were significant in the calculation of $\bar{z}_{aq}$. Details of the estimation of experimental uncertainties are given in Appendix D.3. Figure 6–18 shows the indirect determination data for the aqueous sulfur system at pH = 2.8 ± 0.3 with error bars on the data points. Notice that the vertical scale

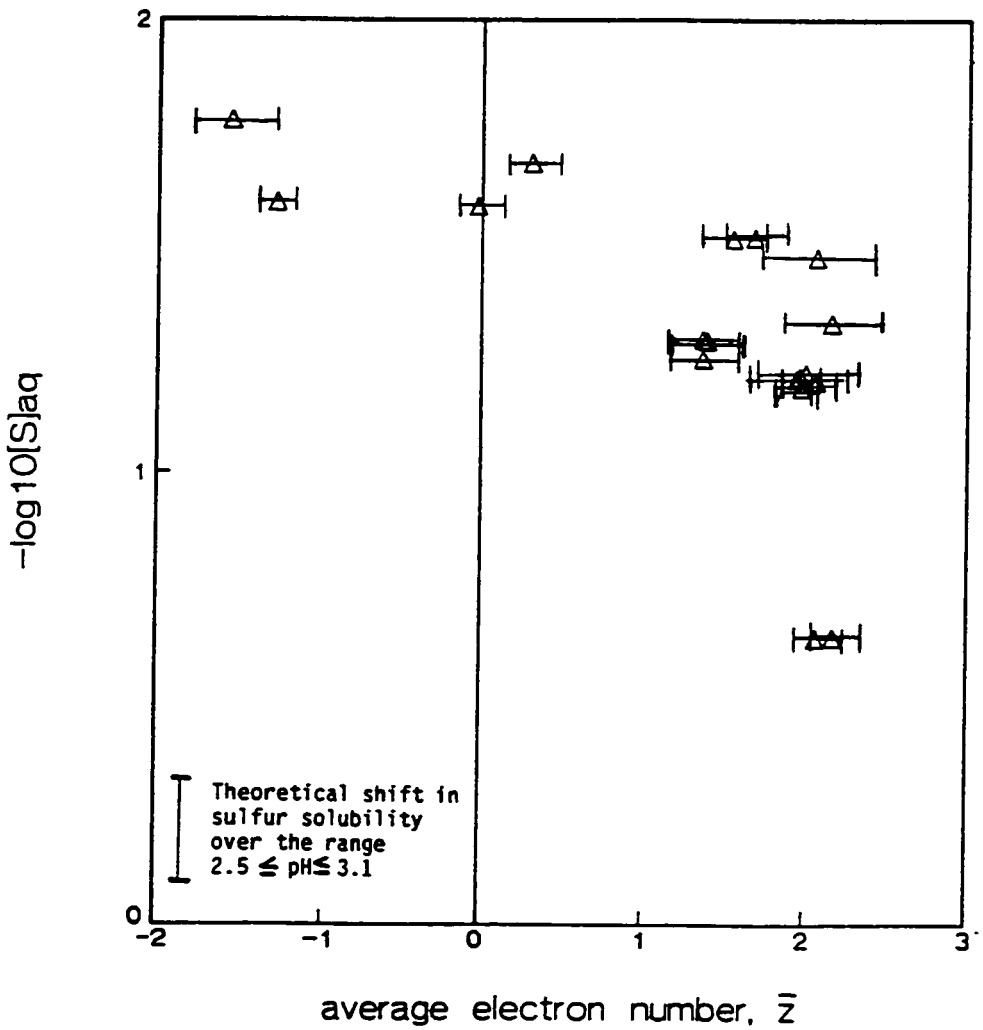

Figure 6–13 Results of indirect determination experiments for the aqueous sulfur system at pH = 2.8 ± 0.3, with estimated experimental uncertainties. Experimental data are shown as triangles; error bars are placed on the experimental points. The theoretical shift in sulfur solubility over the range of the experimental data is also indicated.

differs from that in Figure 6–2, but that the same horizontal scale is used. Because the concentrations in electron number diagrams are shown on a logarithmic scale, vertical uncertainties in the data points are very small. Because the data in Figure 6–18 do not represent a single value of pH, the theoretical shift in sulfur solubility over the pH range 2.5 to 3.1 is shown.

The potential measurements made during the indirect experiments were also subject to uncertainties. A variety of factors could have influenced these measurements including: the kinetics of reactions in the solution and on the electrode surface; the presence electroactive species other than the sulfur species, such as dissolved O_2; and film formation on the electrode surface. Estimation of uncertainties in these measurements was difficult. Also, in two cases the electrode potentials were still drifting upward steadily when the final measurements were made; arrows on Figure 6–3 show the direction of the drift on these points.

6.3.3.2 Direct Determination Experiments

The sensitivity of detection of solid sulfur was the chief source of uncertainty in the direct determination experiments. For values of $-\log_{10}[S]_{aq}$ up to 4.3, solid sulfur was detected. The lower limit of detection was fixed by the levels of insoluble impurities in the experimental solutions; very small quantitiies of solid sulfur were indistinguishable from the background impurity level of suspended solids. Over the average electron number range form –1.8 to 1.8 at pH = 2.8, the highest value of $-\log_{10}[S]_{aq}$ (i.e., the lowest sulfur concentration) at which solids were detected ranged from approximately 4.1 to 4.3. The maximum sensitivity of this method can therefore be conservatively estimated at $-\log_{10}[S]_{aq} = 4.1$.

Another factor to consider is that once individual elemental sulfur atoms had begun to form in solution, some supersaturation was necessary before the formation of colloidal particles began (Van de Hulst, 1957).

Losses of sulfur as $H_2S(g)$ were generally expected to be small because of the relatively low sulfur concentrations used in the direct determination experiments at low pH.

6.3.4 Comparison of Experimental Results with Theoretical Predictions

All theoretical curves used for comparison with experimental data in this chapter have been calculated with the sulfur species in Table 3–2. This data set includes thionates, which are expected to appear under the experimental conditions being investigated. The sulfate and bisulfate ions were not included in this data set because sulfur does not readily oxidize to sulfate despite oxidizing potentials (Peters, 1976).

The indirect determination experimental data for the aqueous sulfur system at pH = 2.8 ± 0.3, shown with error bars in Figure 6–18 and with the theoretical curve in Figure 6–2, follow the slope of the theoretical curve fairly well. However, the experimental solubility is more than three orders of magnitude greater than the theoretical prediction. The most likely explanation of this extreme difference is that species not included in the theoretical data set are metastable under the conditons of these experiments. In particular, the protonated polysulfides, HS_n^- and H_2S_n (n = 2, 3, 4,...), may exist in significant quantities in these systems. The high concentration of dissolved sulfur and the presence of large amounts of elemental sulfur in this acidic experimental system, along with the known tendency of sulfur to form long chains, would be conducive to the formation of

HS_n^- or other similar species. However, free energy data for these species could not be found so they could not be included in the theoretical calculation.

The direct determination data for the aqueous sulfur system at pH = 2.80, shown in Figure 6–5, are much closer to the theoretical curve than the indirect data were. Once again, the experimental data appears to match the shape of the theoretical curve. However, above approximately $-\log_{10}[S]_{aq} = 4.1$, distinguishing colloidal sulfur from background impurities became difficult. Thus, the actual experimental boundary may lie at even lower dissolved sulfur concentrations, i.e., at higher values of $-\log_{10}[S]_{aq}$. Furthermore, the use of activity coefficients would move the theoretical curve even closer to the experimental data, as indicated by Figure 5–16.

Under the conditions of the direct experiments, i.e., dilute solutions and little or no solid sulfur, the formation of polysulfides or other possible metastable intermediates was not as likely as in the indirect runs. Therefore, it is not surprising that the two types of experiments gave very different results for the sulfur system at pH = 2.80.

Experimental electron number data were also plotted on diagrams of $-\log_{10}[S]_{aq}$ versus pH at constant values of average electron number, $\bar{z}$. The experimental data in Figures 6–9 through 6–15 for the electron number range $-1.85 \leq \bar{z} \leq 1.86$ show somewhat higher solubility than the predicted values, but match the slopes of the theoretical curves reasonably well.

The experimental data actually indicate lower solubility than the theoretical predictions at $\bar{z} = 2.00$ and $\bar{z} = 2.25$, as shown in Figures 6–16 and 6–17 respectively. However, in the direct determination experimental runs at $\bar{z} =$ 2.50, no solid sulfur was detected upon acidification, even at total sulfur

concentrations exceeding 1M. This indicates that sulfate and bisulfate, for which $\bar{z} = 6$, were not present in the experimental system in significant amounts. Furthermore, the location of the phase boundary between $\bar{z} = 2$ and $\bar{z} = 2.5$ suggests that thionates were present in these experimental systems.

Figure 6–6 shows direct determination experimental data for the aqueous sulfur system at pH = 4.7 ± 0.5. Over the range of a full pH unit, sulfur solubility, a function of both pH and $\bar{z}$, varies considerably. However, examination of Figures 6–9 to 6–15 shows that the slopes of the theoretical curves over the range $4.2 \leq pH \leq 5.2$ are reasonable approximations of the slopes of the phase boundaries suggested by the experimental data. This observation can be used to make a correction for pH.

Choose Run 127 from Table 6–3 as an example of how experimental data can be corrected to pH = 4.70. At $\bar{z} = 1.50$, an experimental data point is located at pH = 4.30 and $-\log_{10}[S]_{aq} = 3.33$. On the theoretical curve at $\bar{z} = 1.5$, shown in Figure 6–14:

$$(-\log_{10}[S]_{aq})^{theory}_{4.70} - (-\log_{10}[S]_{aq})^{theory}_{4.30} = -0.26 \qquad (6.3\text{–}1)$$

If the assumption is made that the slopes of the experimental and theoretical boundaries are the same over the range of interest then:

$$(-\log_{10}[S]_{aq})^{corrected}_{4.70} - (-\log_{10}[S]_{aq})^{expt.}_{4.30}$$
$$= (-\log_{10}[S]_{aq})^{theory}_{4.70} - (-\log_{10}[S]_{aq})^{theory}_{4.30} \qquad (6.3\text{–}2)$$

Substitution of Equation 6.3–1 and the experimental sulfur solubility at pH = 4.30 into Equation 6.3–2, followed by rearrangement gives:

$$(-\log_{10}[S]_{aq})^{corrected}_{4.70} = 3.33 - 0.26 = 3.07 \qquad (6.3\text{–}3)$$

Figure 6–6 is replotted, with data corrected to pH = 4.70, in Figure 6–19. Table 6–6 lists the corrections for all data points in Figure 6–19.

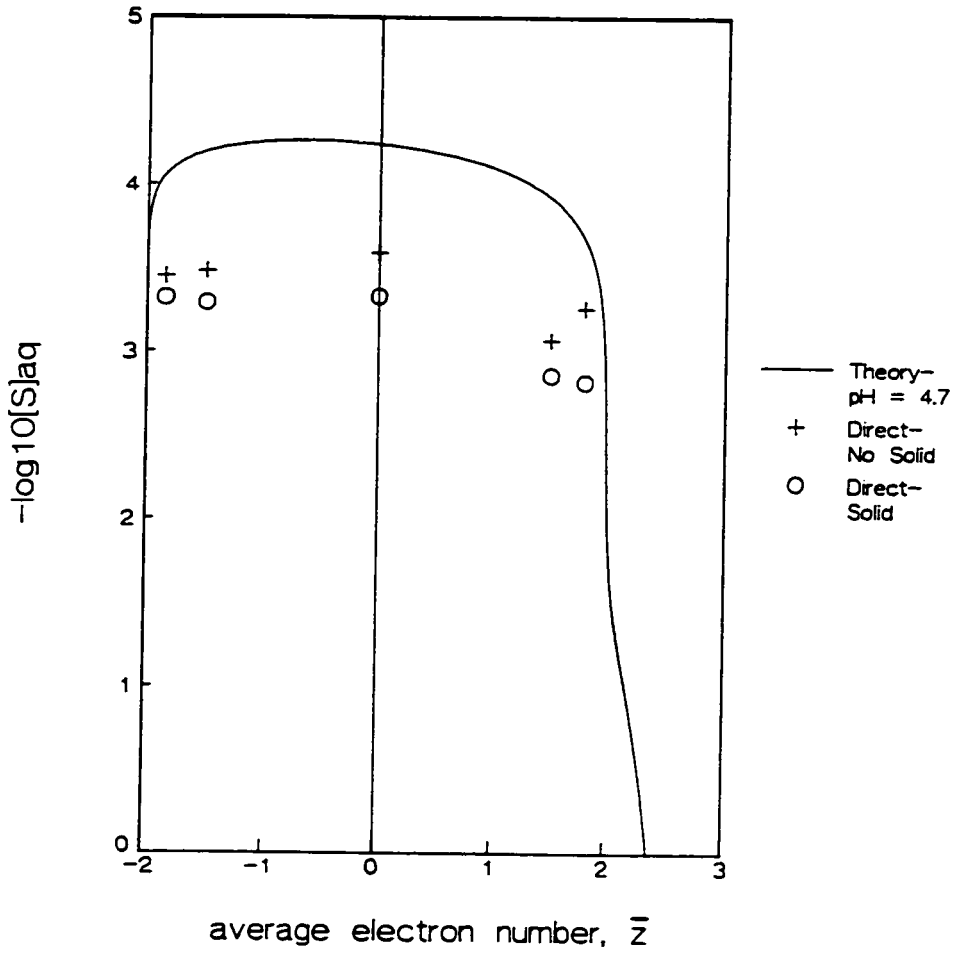

Figure 6–19 **Direct determination experimental data for the aqueous sulfur system at pH = 4.7 ± 0.5, corrected for pH (See Table 6–6). The solid line is the theoretical curve. Experimental data are indicated by symbols: "o"'s indicate points where solid formation was observed; at points indicated by "+"'s, no solid formation was observed.**

Table 6–6 Correction of Direct Experimental Data to pH = 4.7

Run Number	Average Electron Number, $\bar{z}$	pH	Experimental $-\log_{10}[S]_{aq}$	Correction for pH	Corrected $-\log_{10}[S]_{aq}$	Solid (1) No Solid (0)
129	−1.84	5.08	3.07	0.25	3.32	1
134	−1.84	5.02	3.24	0.21	3.45	0
126	−1.50	4.92	3.34	0.14	3.48	0
132	−1.50	4.89	3.17	0.12	3.29	1
125	0.00	4.79	3.53	0.06	3.59	0
135	0.00	4.70	3.33	0.00	3.33	1
127	1.50	4.30	3.33	−0.26	3.07	0
133	1.50	4.24	3.16	−0.30	2.86	1
130	1.80	4.59	2.89	−0.07	2.82	1
136	1.80	4.68	3.27	−0.01	3.26	0

The experimental potential measurements shown in Figure 6–4 for pH = 5.3 ± 0.2 and in Figure 6–3 for pH = 2.8 ± 0.3 show the same trends as the experimental curves. On each diagram, theoretical curves are shown for the extremes of the pH range of the data to demonstrate the sensitivity of potential to variations in pH in this system. The data generally follow the theoretical curves; potential rises quickly as $\bar{z}_{aq}$ increases from negative values and then flattens out at higher values of $\bar{z}_{aq}$.

6.4 Utility of Experimental Electron Number Diagrams

Electron number diagrams have served as a convenient form for the display of experimental sulfur solubility data as a function of composition and pH. In addition, they provided insight into the chemical nature of the experimental systems. For example, comparison of the plots of indirect and direct experimental data for the aqueous sulfur system at pH = 2.8 dramatically illustrated a significant difference between the chemical processes occurring in these two types of experiments. Furthermore, the location of the phase boundary in the range from $\bar{z} = 2.00$ and $\bar{z} = 2.50$ indicated that sulfates ($z = 6$) are not important components of either experimental system.

CHAPTER 7

ELECTROCHEMICAL PHASE DIAGRAMS FOR AQUEOUS SYSTEMS CONTAINING TWO REDOX ELEMENTS

7.1 Importance of Diagrams Containing Two Redox Elements

Electrochemical phase diagrams for aqueous systems containing one active redox element have been widely used. However, in many systems of interest, two or more active redox elements play significant roles. It is not always possible to understand the thermodynamics of a system containing two active redox elements from examination of the electrochemical phase diagrams for the independent single–element systems, especially when species are present that contain both of the redox elements.

Electrochemical phase diagrams for aqueous systems containing two redox elements are of interest in a variety of applications. Species such as FeS and FeS_2 are very important in the Fe–S–H_2O system, which has been widely studied in corrosion research (Macdonald and Syrett, 1979; Pound, Wright and Sharp, 1985). In studies of the electrodeposition of II–VI and III–V semiconductors, the species containing the two redox elements are those of great interest. The thermodynamics of metal sulfides are important in the design and analysis of hydrometallurgical processes.

7.2 Previous Computational Methods

Potential–pH diagrams for systems containing two redox elements have been constructed using approximate methods based on the techniques used to

generate diagrams for systems containing one redox element. Most of the diagrams for systems containing two redox elements involve combinations of the diagrams for the separate single–element systems; some link between the two systems must be provided to allow consideration of species containing both redox elements. The following approximate method is generally used to provide this link (Garrels and Christ, 1966). Take the aqueous Fe–S system as an example. (In the following discussion, the term "predominance area diagrams" refers to those diagrams in which areas of stability may contain either solids or dissolved species.) First, a predominance area diagram, containing both solid and dissolved sulfur species, is constructed for some predetermined dissolved sulfur activity (typically, 10^{-6}). The activity of the predominant sulfur species in each area is fixed (at unity for solid species and at 10^{-6}, for example, for dissolved species); within each area, the predominant species is considered to be the only stable sulfur species. For each such area on the sulfur diagram, a separate predominance area diagram is then constructed for the remaining species (containing Fe and both Fe and S); each of these diagrams is constructed for a fixed activity of dissolved Fe. These small predominance area diagrams, each computed for the area of predominance of a single sulfur species, are the pieces, which taken together, give an approximation to the potential–pH diagram for the system containing Fe and S. The sulfur predominance area diagram is sometimes superimposed on the final diagram.

Although the above procedure was developed for manual calculation of potential–pH diagrams for systems containing two redox elements, it is still used in computer algorithms for generation of potential–pH diagrams (Cubicciotti, 1988a, b). Another algorithm for computer–aided construction of potential–pH

diagrams for systems containing two redox elements also used the above rationale in a somewhat more efficient form (Imai, Osato and Nakauchi, 1987). Other algorithms, based on the convex polygon method, have used similar methods to construct diagrams for systems containing two redox elements (Froning, Shanley and Verink, 1976; Chen and Aral, 1982).

Potential–pH diagrams for aqueous systems containing two redox elements can also be generated using the so–called point–by–point methods. By calculating the predominant species at very small intervals of pH and E, stability fields were determined for various species in Mo–S–H_2O, Pb–S–H_2O and Zn–S–H_2O systems over a range of temperatures (El–Raghy and El–Dermerdash, 1988).

Previous potential–pH diagrams for aqueous systems containing two redox elements have generally been constructed for fixed activities of both redox elements. These constraints, along with the superimposition of stability fields, are often physically unrealistic and confuse geometric interpretation and phase rule analysis of these diagrams. Also, as in the case of potential–pH diagrams for a single redox element, these diagrams do not include all dissolved species in the calculation of solid stability fields.

7.3 Method of Calculation

A new computational method which avoids the problems of the earlier methods has been developed. Consider an aqueous system containing two redox elements, M and N, and two additional components, X and Y. The general formation equation for a species S_k in this system is given by Equation 2.1–1.

$$\left[\frac{\alpha_{M,k}}{\alpha_{M,k} + \alpha_{N,k}}\right] M + \left[\frac{\alpha_{N,k}}{\alpha_{M,k} + \alpha_{N,k}}\right] N$$

$$= \left[\frac{1}{\alpha_{M,k} + \alpha_{N,k}}\right] S_k + h_k H^+ + w_k H_2O + x_k X + y_k Y + z_k e^- \qquad (2.1\text{–}1)$$

In Equation 2.1–1, seven components are needed to specify the system. Therefore, by Equation 2.2–9, the dimensionality of this system is six. To reduce the dimensionality to three, the chemical potentials of three components must be fixed. The chemical potentials of M, N and electrons have been chosen as the independent variables; the activity of H_2O has been treated in the manner described in Chapter 4 for systems containing one redox element. Therefore, activities of H^+, X and Y will be fixed.

The algorithm for solution of the equilibrium equations begins with the determination of all points where four phases (three solids and the aqueous phase) coexist in equilibrium. Equation 2.3–5 can be written for each solid species S_s in the system.

$$\left[\frac{\alpha_{M,s}}{\alpha_{M,s} + \alpha_{N,s}}\right]\frac{(\mu_M - \mu_M^\circ)}{RT} + \left[\frac{\alpha_{N,s}}{\alpha_{M,s} + \alpha_{N,s}}\right]\frac{(\mu_N - \mu_N^\circ)}{RT} - z_s\frac{(\mu_{e^-})}{RT}$$

$$= -h_s(\ln 10)pH + w_s \ln a_{H_2O} + x_s \ln a_X + y_s \ln a_Y + \frac{\Delta G_s^\circ}{RT}$$

$$+ \left[\frac{1}{\alpha_{M,s} + \alpha_{N,s}}\right] \ln a_s \qquad (2.3\text{–}5)$$

Every set of three solids (S_t, S_u, S_v) in the system is considered, and Equation 2.3–5 is written for each of the three solids in a set. Pure solid phases are assumed ($a_s = 1$). The resulting equations may be written in the following form:

$$\begin{bmatrix} A_t & B_t & C_t \\ A_u & B_u & C_u \\ A_v & B_v & C_v \end{bmatrix} \begin{bmatrix} (\mu_M - \mu_M^\circ)/RT \\ (\mu_N - \mu_N^\circ)/RT \\ \mu_{e^-}/RT \end{bmatrix} = \begin{bmatrix} K_t \\ K_u \\ K_v \end{bmatrix}. \qquad (7.3\text{–}1a)$$

Equation 7.3–1a can also be written in a more compact form:

$$A\vec{\mu}/RT = \vec{K} \tag{7.3-1b}$$

where A is the coefficient matrix, $\vec{\mu}$ is the vector of chemical potentials and $\vec{K}$ is the vector of constants. The elements of the coefficient matrix in Equation 7.3–1a are given by:

$$A_s = \left[\frac{\alpha_{M,s}}{\alpha_{M,s} + \alpha_{N,s}}\right] \tag{7.3-2}$$

$$B_s = \left[\frac{\alpha_{N,s}}{\alpha_{M,s} + \alpha_{N,s}}\right] \tag{7.3-3}$$

$$C_s = -z_s \tag{7.3-4}$$

where $\alpha_{M,s}$ is the number of atoms of element M per molecule of species S_s, $\alpha_{N,s}$ is the number of atoms of element N per molecule of species S_s, and z_s is the electron number of species S_s. The μ_i are the chemical potentials of the two active redox elements, M and N, and of electrons; the superscripts $^\circ$ indicate standard state values. Notice that division of the μ_i by RT gives dimensionless chemical potentials. The constants K_s are defined by

$$K_s \equiv -h_s(\ln 10)pH + w_s \ln a_{H_2O} + x_s \ln a_X + y_s \ln a_Y + \frac{\Delta G_s^\circ}{RT} + \left[\frac{1}{\alpha_{M,s} + \alpha_{N,s}}\right] \ln a_s \tag{7.3-5}$$

When the determinant of the coefficient matrix, A, is nonzero, a solution may be obtained for Equation 7.3–1. The solution is the vector of dimensionless chemical potentials for the two redox elements, M and N, and the electrons. Stability criteria are then invoked to determine whether the solution of Equation 7.3–1 represents a stable four–phase point. This is done using Equation 2.3–7; the relative stabilities of solids S_t, S_u and S_v are tested against all other solid species in the system as described in Chapter 2.4.2.

Following the determination of any stable four–phase points, points on the boundaries of the system must be considered. The equilibrium problem is solved over previously chosen ranges of μ_M, μ_N and E ($= \mu_{e^-}/F$); the upper and lower limits on these variables form a prism in chemical potential space, as shown in Figure 7–1. On each of the six faces of this bounding prism, all possible pairs of solid species, S_t and S_u, are considered as possible stable three–phase points, i.e., points where two solids and the aqueous phase are in equilibrium. Equation 2.3–5 can be written for each solid. Since one of the three chemical potentials is fixed, two equations in two unknowns are generated for each pair of solids. Solution of these equations to obtain the two remaining chemical potentials is followed by stability testing with Equation 2.3–7.

After determination of stable four–phase and three–phase points, an analogous procedure is used to determine stable two–phase points (one solid plus the aqueous phase). These two–phase points lie along the twelve edges of the bounding prism, where two of the three chemical potentials are fixed.

Once all of the stable four–phase, three–phase and two–phase points have been determined, straight lines are drawn to connect points with two solids in common, or with both one solid and one face of the bounding prism in chemical potential space in common.

The equilibrium problem has now been solved, and the equilibrium surface can now be constructed in the chemical potential space defined by $(\mu_M - \mu_M^\circ)/RT$, $(\mu_N - \mu_N^\circ)/RT$ and E. Figure 7–2 shows the equilibrium surface for the aqueous U–C system at pH = 4. Table 7–1 lists the species, in addition to those listed in Table 4–1, considered in the construction of Figure 7–2; only the solid species were necessary for the construction of this figure.

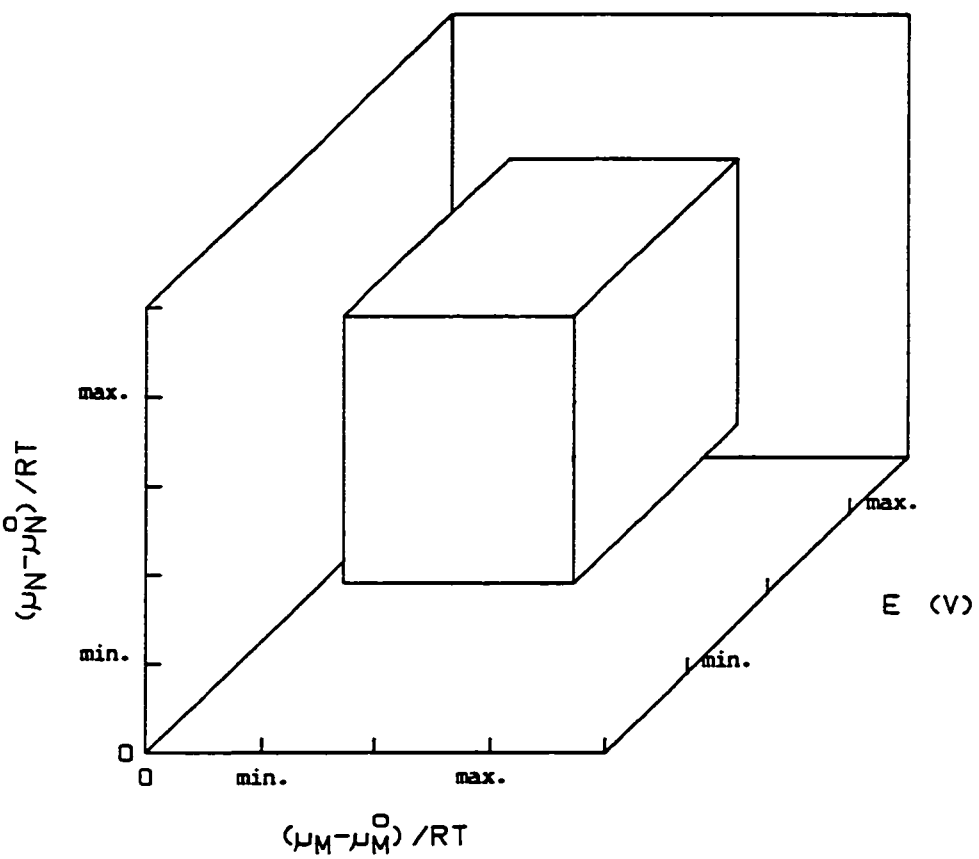

Figure 7–1 Prism in chemical potential space, formed by the minimum and maximum values of $(\mu_M - \mu_M^\circ)/RT$, $(\mu_N - \mu_N^\circ)/RT$ and E.

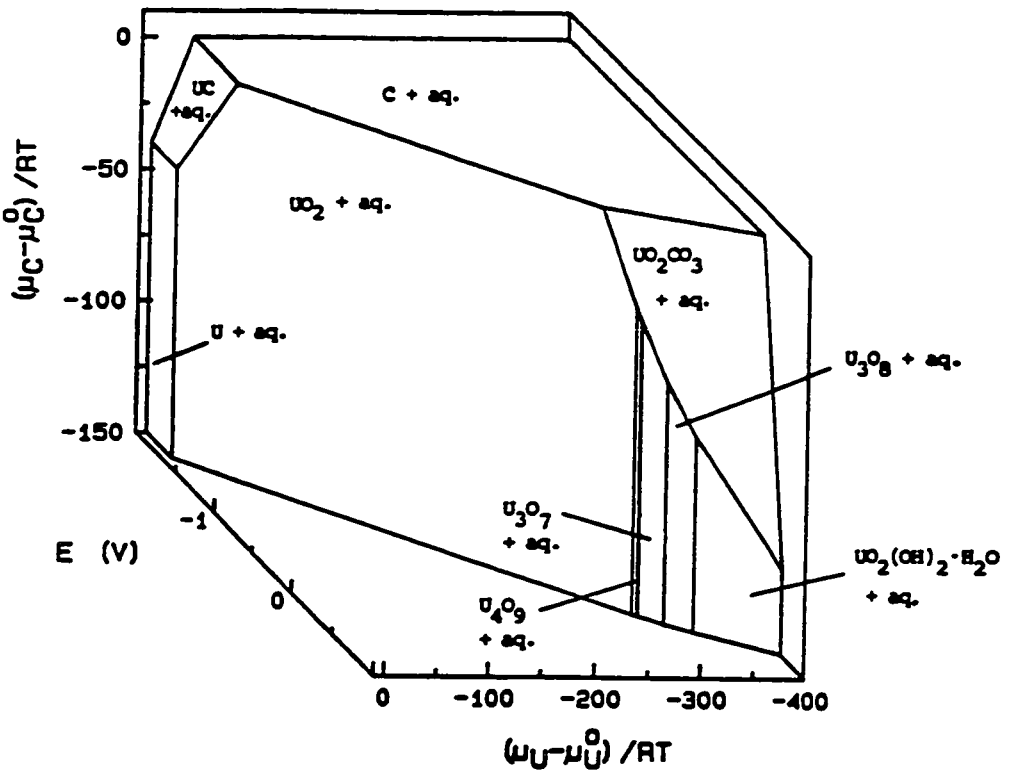

Figure 7–2 Equilibrium diagram for the aqueous U–C system at pH = 4 in chemical potential space.

Table 7–1

Aqueous U–C System: Species Included in Calculations

In addition to the species listed in Table 4–1, the following species were included in calculations for the aqueous U–C system:

Solid Species

UO_2CO_3	UC	$UC_{1.94}$
U_2C_3		

Dissolved Species

$UO_2(CO_3)_2^{2-}$	$UO_2(CO_3)_3^{4-}$	UO_2CO_3

The equilibrium surface in Figure 7–2 has been formed from intersecting planes, each representing the solubility of a different solid species. On the surface, the aqueous phase exists in equilibrium with a solid. Outside and above the surface , i.e., at higher values of μ_M and μ_N, the system cannot exist in equilibrium. Physically, it would be supersaturated. Inside the surface, i.e., at lower values of μ_M and μ_N, no solid phases are stable and a single aqueous phase exists. The planar nature of the solid surfaces is the result of the assumption of pure solid phases, and thus the assumption of unit activity for all solids. In general, alloys and phases of variable composition would be appear as curved surfaces in this chemical potential space.

At any point in chemical potential space where the system can exist in equilibrium, the activities of all dissolved species containing the active redox elements can be computed with Equation 2.3–3. The activity of species S_k is given by:

$$a_k = \exp\left[(\alpha_{M,k} + \alpha_{N,k})\left[\left[\frac{\alpha_{M,k}}{\alpha_{M,k} + \alpha_{N,k}}\right]\frac{(\mu_M - \mu_M^\circ)}{RT} + \left[\frac{\alpha_{N,k}}{\alpha_{M,k} + \alpha_{N,k}}\right]\frac{(\mu_N - \mu_N^\circ)}{RT} + h_k(\ln 10)pH - w_k \ln a_{H_2O} - x_k \ln a_X - y_k \ln a_Y + z_k\left[\frac{F}{RT}\right]E - \frac{\Delta G_k^\circ}{RT}\right]\right] \qquad (2.3\text{–}3)$$

The equilibrium surface in chemical potential space provides useful information about phase stability, e.g., which phases can coexist in equilibrium. These chemical potential diagrams are similar to those used previously in the study of paragenesis of minerals (Korzhinskii, 1959).

The equilibrium surface from chemical potential space can also be

reconstructed in other three–dimensional spaces of interest, such as $-\log_{10}[M]_{aq}/-\log_{10}[N]_{aq}/$ E space or $-\log_{10}[M]_{aq}/-\log_{10}[N]_{aq}/\bar{z}$ space. These alternative representations are constructed from the same thermodynamic information present in the chemical potential diagram, but they can provide further insight into the structure of the aqueous redox system. Examples of these alternative representations, as well as additional three–dimensional chemical potential diagrams, will be given in the next section.

In order to construct diagrams in which $-\log_{10}[M]_{aq}$ and $-\log_{10}[N]_{aq}$ are used as axes, a method for following constant concentration contours on the equilibrium surface is necessary. Calculation of these contours is an iterative process. The method used here is described in Appendix E.

Computer programs, written in Pascal, have been developed to calculate electrochemical phase diagrams for aqueous systems containing two redox elements on microcomputers; provisions have also been made to plot the resulting diagrams. These programs can be used to generate diagrams in the following coordinate systems: the chemical potential space defined by $(\mu_M-\mu_M^\circ)/RT$, $(\mu_N-\mu_N^\circ)/RT$ and E; $-\log_{10}[M]_{aq}/-\log_{10}[N]_{aq}/E$ space; and $-\log_{10}[M]_{aq}/-\log_{10}[N]_{aq}/\bar{z}$ space.

The programs actually calculate diagrams in $-\log_{10}a_M^*/-\log_{10}a_N^*/E$ space. (The activity a_M^* was defined in Equation 2.3–37.) If the activity coefficients, γ_i, of all dissolved species are set to unity, then a_M^* and a_N^* reduce to $[M]_{aq}$ and $[N]_{aq}$ respectively. Here, ideal solutions have been assumed. This assumption is not necessary for the new computational method to work, although it does simplify the calculations.

As in an aqueous system containing a single active redox element, gaseous

species containing the active redox elements can be considered in two ways. The activities of gaseous redox species can be computed directly with Equation 2.3–3. Alternatively, gaseous redox species at fixed activity can be treated as additional solids in the algorithm described above.

7.4 Examples of Diagrams for Systems Containing Two Redox Elements

Many aqueous systems of current interest contain two active redox elements. For example, the stability of phases in aqueous U–C system has implications in nuclear waste storage. The stability diagram for the aqueous U–C system at pH = 4, shown in Figure 7–2, can be replotted in $-\log_{10}[U]_{aq}/-\log_{10}[C]_{aq}/E$ space, as shown in Figure 7–3. Extreme "concentration" ranges have been shown to illustrate the form and structure of the diagrams and to show the relative stabilities of phases. Obviously, realistic physical conditions exist in only a small portion of Figure 7–3.

Diagrams in chemical potential space and in $-\log_{10}[U]_{aq}/-\log_{10}[C]_{aq}/E$ space are shown for the aqueous U–C–F^- system at pH = 4 and $a_{F^-} = 0.1$ in Figures 7–4 and 7–5, respectively. Similar diagrams for the same system at pH = 4 and $a_{F^-} = 1$ are shown in Figures 7–6 and 7–7. Figures 7–4 through 7–7 were calculated using the species listed in Tables 4–1, 4–2 and 7–1. Note the changes in the stable phases as F^- is added to the system and its concentration is increased.

In the study of the electrodepostion of III–V semiconductors, the aqueous Ga–As system is of interest (Perrault, 1989; Chandra and Khare, 1987a,b). An equilibrium diagram, in chemical potential space, for the aqueous Ga–As system at pH = 13 is shown in Figure 7–8; the equilibrium surface is replotted in

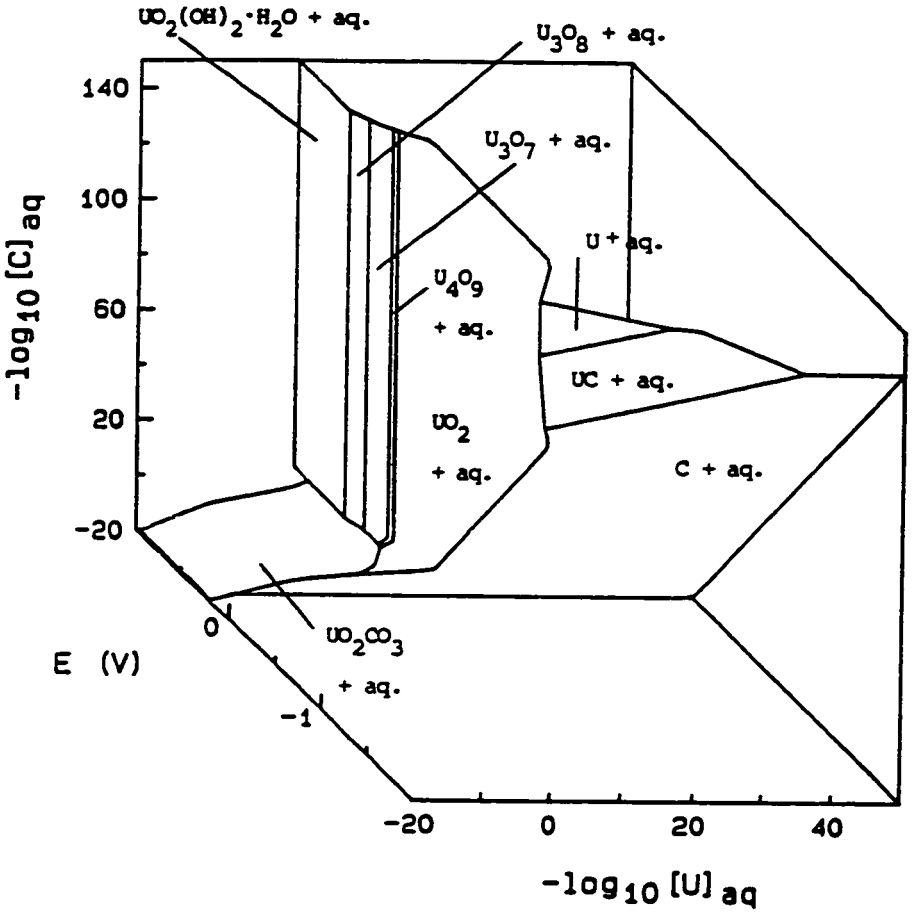

Figure 7–3 Equilibrium diagram for the aqueous U–C system at pH = 4 in $-\log_{10}[U]_{aq}/-\log_{10}[C]_{aq}/E$ space.

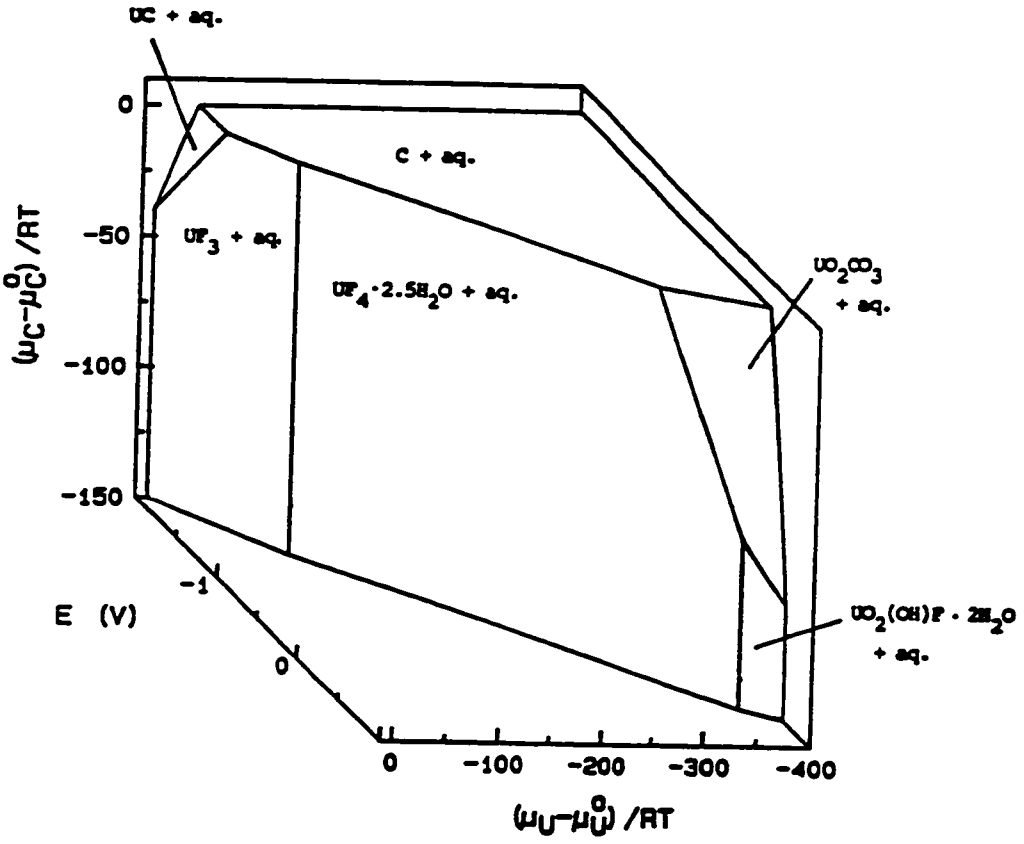

Figure 7–4 Equilibrium diagram for the aqueous U–C–F^- system at pH = 4 and $a_{F^-} = 0.1$ in chemical potential space.

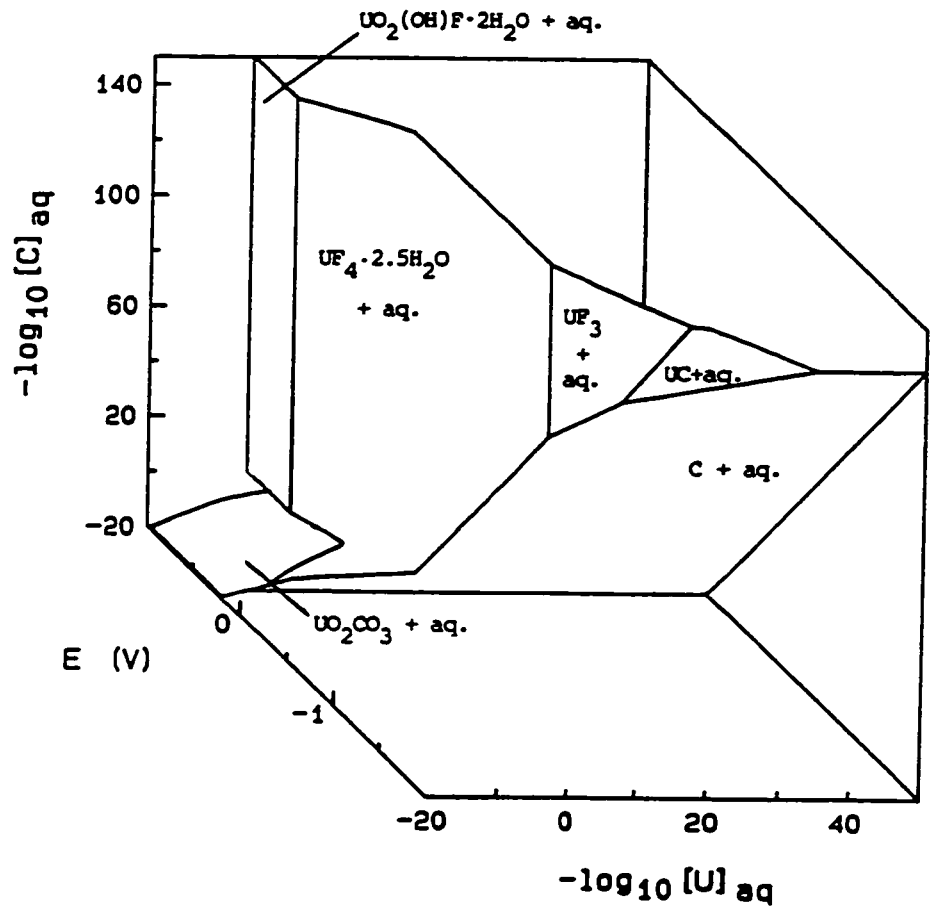

Figure 7–5 Equilibrium diagram for the aqueous U–C–F^- system at pH = 4 and $a_{F^-} = 0.1$ in $-\log_{10}[U]_{aq}/-\log_{10}[C]_{aq}/E$ space.

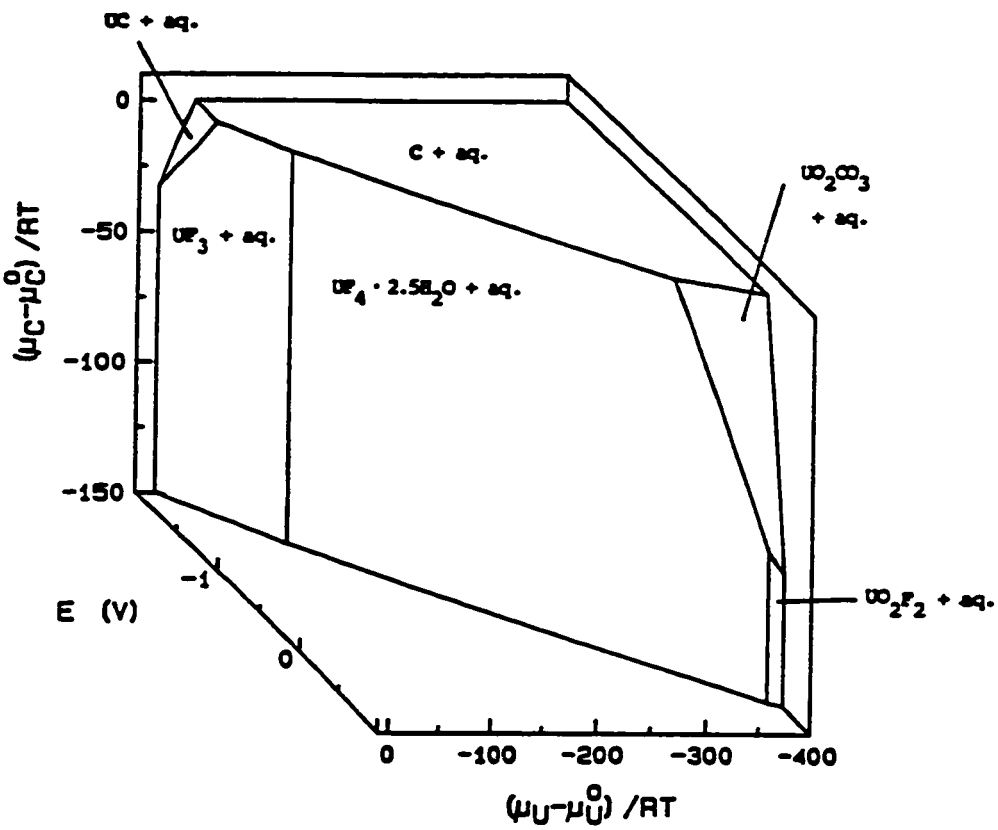

Figure 7–6 Equilibrium diagram for the aqueous U–C–F^- system at pH = 4 and $a_{F^-} = 1$ in chemical potential space.

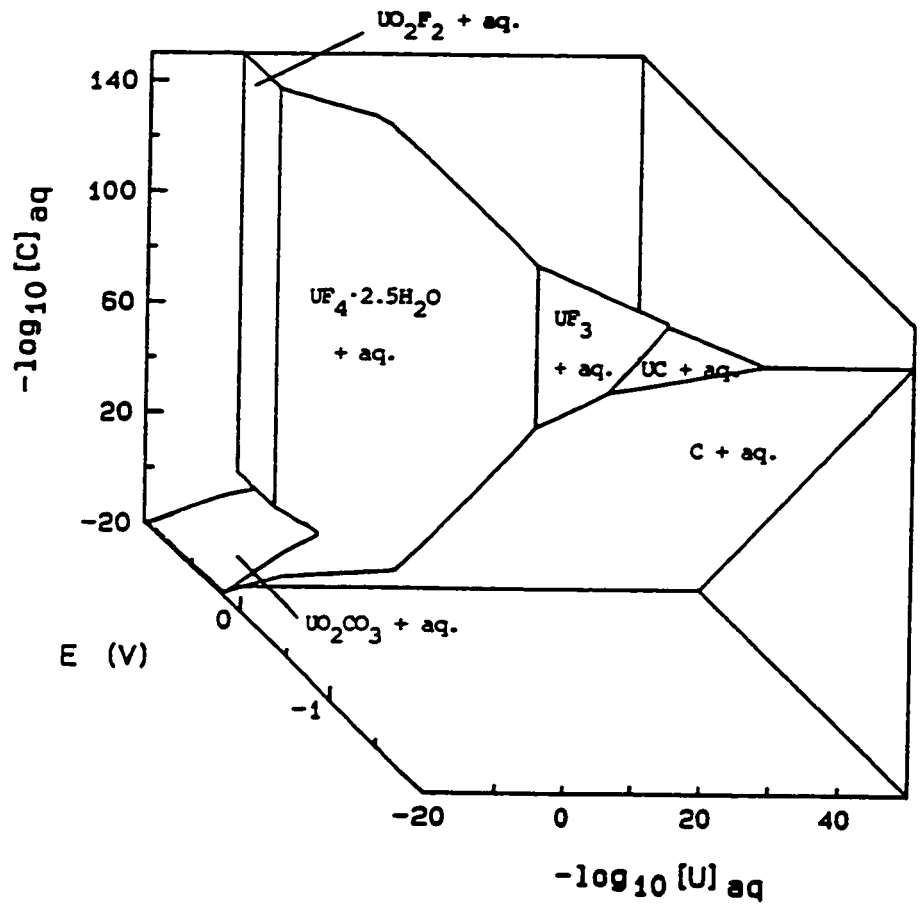

Figure 7–7 Equilibrium diagram for the aqueous U–C–F^- system at pH = 4 and $a_{F^-} = 1$ in $-\log_{10}[U]_{aq}/-\log_{10}[C]_{aq}/E$ space.

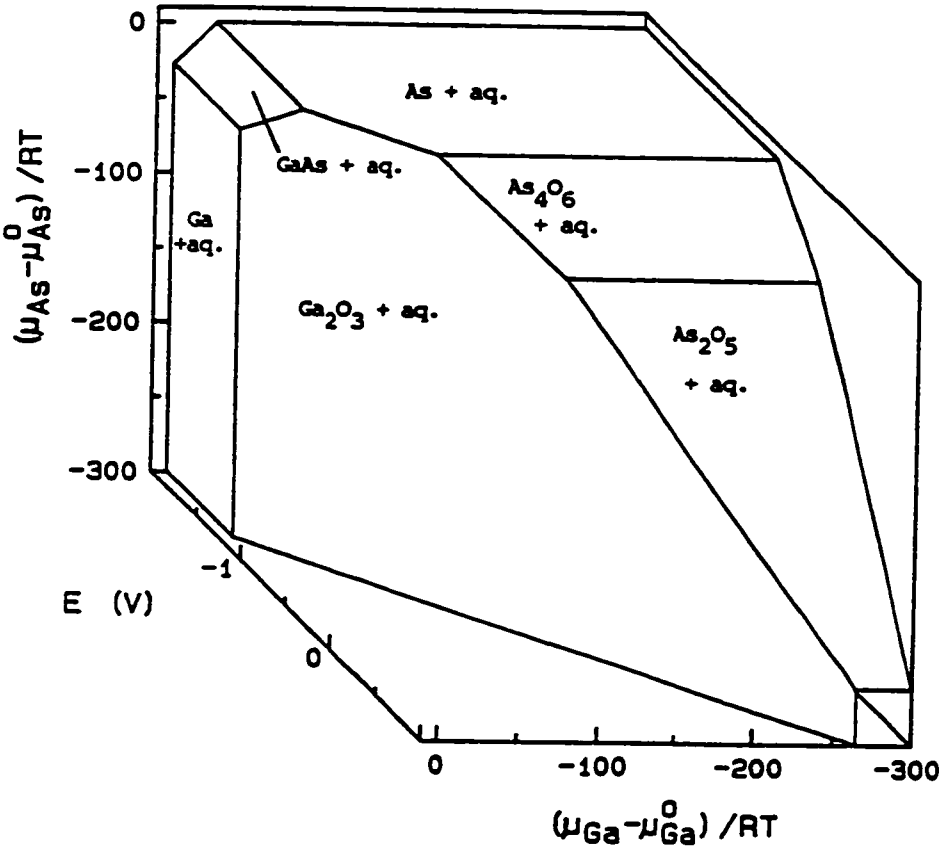

Figure 7–8 Equilibrium diagram for the aqueous Ga–As system at pH = 13 in chemical potential space.

$-\log_{10}[Ga]_{aq}/-\log_{10}[As]_{aq}/E$ space in Figure 7–9. The species included in the calculations are listed in Table 7–2.

Attempts to electrodeposit II–VI semiconductors, such as CdTe, have also been reported (Ogden and Tench, 1981; Llabres and Delmas, 1986). Equilibrium diagrams for the aqueous Cd–Te system at pH = 2.5 and at pH =10 have been constructed in both chemical potential space (Figures 7–10 and 7–12) and $-\log_{10}[Cd]_{aq}/-\log_{10}[Te]_{aq}/E$ space (Figures 7–11 and 7–13). These diagrams were calculated using the species listed in Table 7–3.

Electron number can be defined in a system containing two active redox elements. The electron number of a species, S_k, containing two active redox elements, M and N, is simply defined as the coefficient z_k in the general formation reaction in Equation 2.1–1. The average electron number, $\bar{z}_k$, is still defined as an atom average, now taken over all atoms of elements M and N.

The equilibrium figure for the aqueous Cd–Te system at pH = 10 can also be constructed in $-\log_{10}[Cd]_{aq}/-\log_{10}[Te]_{aq}/\bar{z}$ space. In this space, Figure 7–14 shows the three–dimensional electron number diagram for the aqueous phase in equilibrium with solid CdTe. Because $z_{CdTe} = 0$, each point on the surface in Figure 7–14 would be connected by a horizontal tie–line to a point on the $\bar{z} = 0$ plane at the same values of $-\log_{10}[Cd]_{aq}$ and $-\log_{10}[Te]_{aq}$. For purposes of clarity, this plane, as well as the surfaces associated with the other solid phases, are not shown here.

7.5 Extension to Systems of Arbitrary Complexity

From the phase rule analysis in Chapter 2.2, it is clear that addition of another component X (i.e., a complexing species) to the system increases the

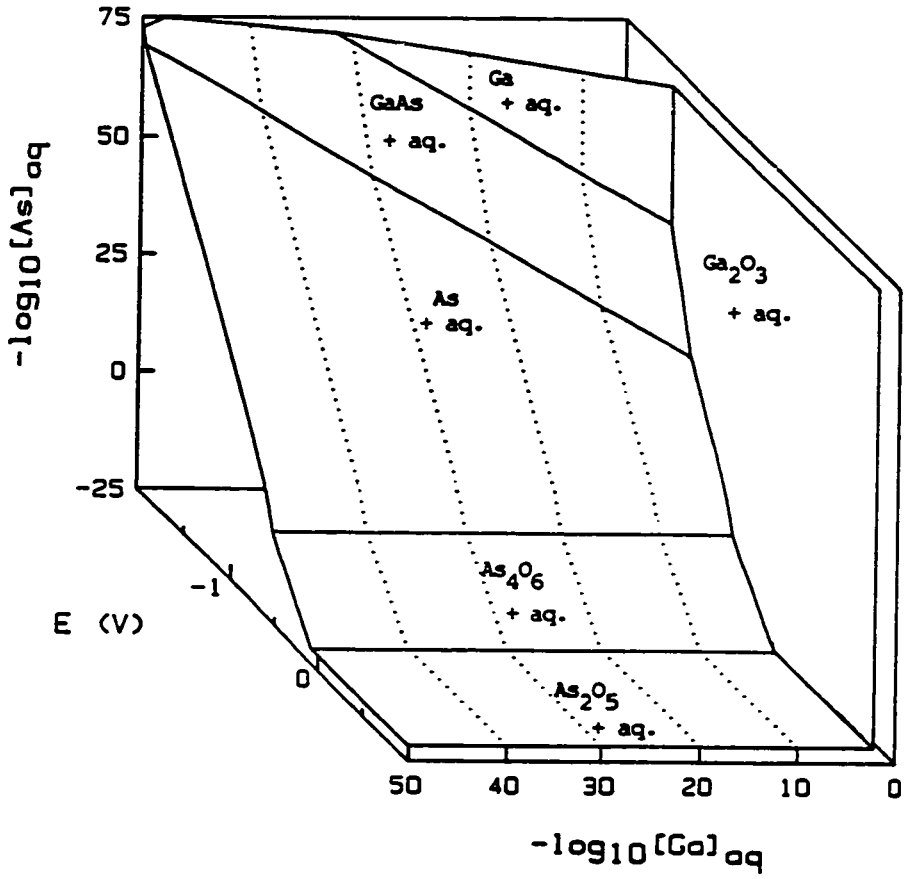

Figure 7–9 Equilibrium diagram for the aqueous Ga–As system at pH = 13 in $-\log_{10}[Ga]_{aq}/-\log_{10}[As]_{aq}/E$ space.

Table 7–2

Aqueous Ga–As System: Species Included in Calculations

Solid Species

Ga	$Ga_2O_3(\beta)$	$Ga(OH)_3$
$As(\alpha)$	As_2O_5	As_4O_6(octahedral)
As_4O_6(monoclinic)	GaAs	

Dissolved Species

Ga^{2+}	Ga^{3+}	GaO_3^{3-}
$GaOH^{2+}$	$HGaO_3^{2-}$	$Ga(OH)_2^{+}$
$H_2GaO_3^{-}$	AsO^{+}	AsO_2^{-}
AsO_4^{3-}	$HAsO_2$	$HAsO_4^{2-}$
$H_2AsO_4^{-}$	H_3AsO_4	

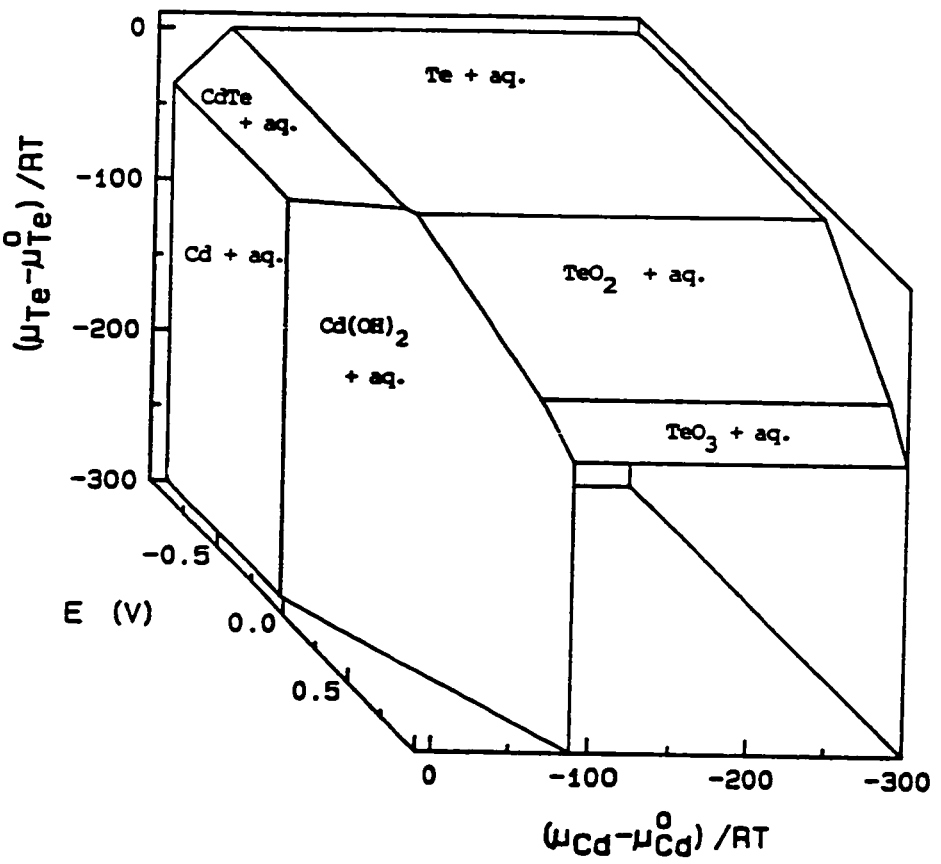

Figure 7–10 Equilibrium diagram for the aqueous Cd–Te system at pH = 2.5 in chemical potential space.

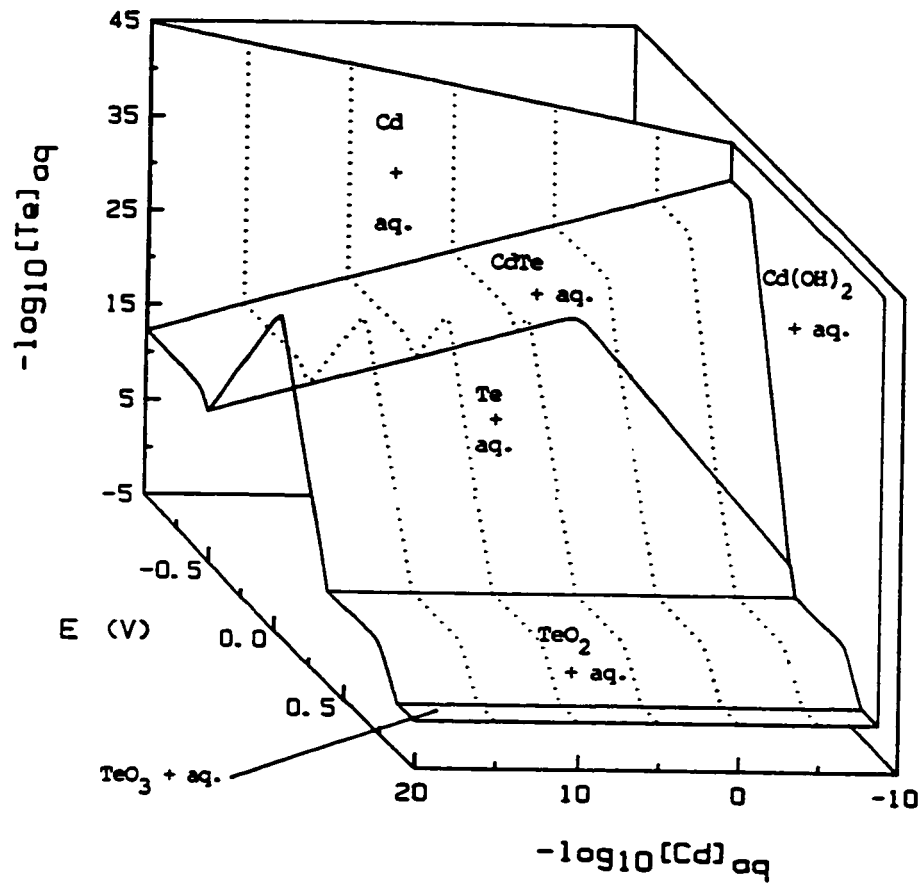

Figure 7–11 Equilibrium diagram for the aqueous Cd–Te system at pH = 2.5 in $-\log_{10}[Cd]_{aq}/-\log_{10}[Te]_{aq}/E$ space.

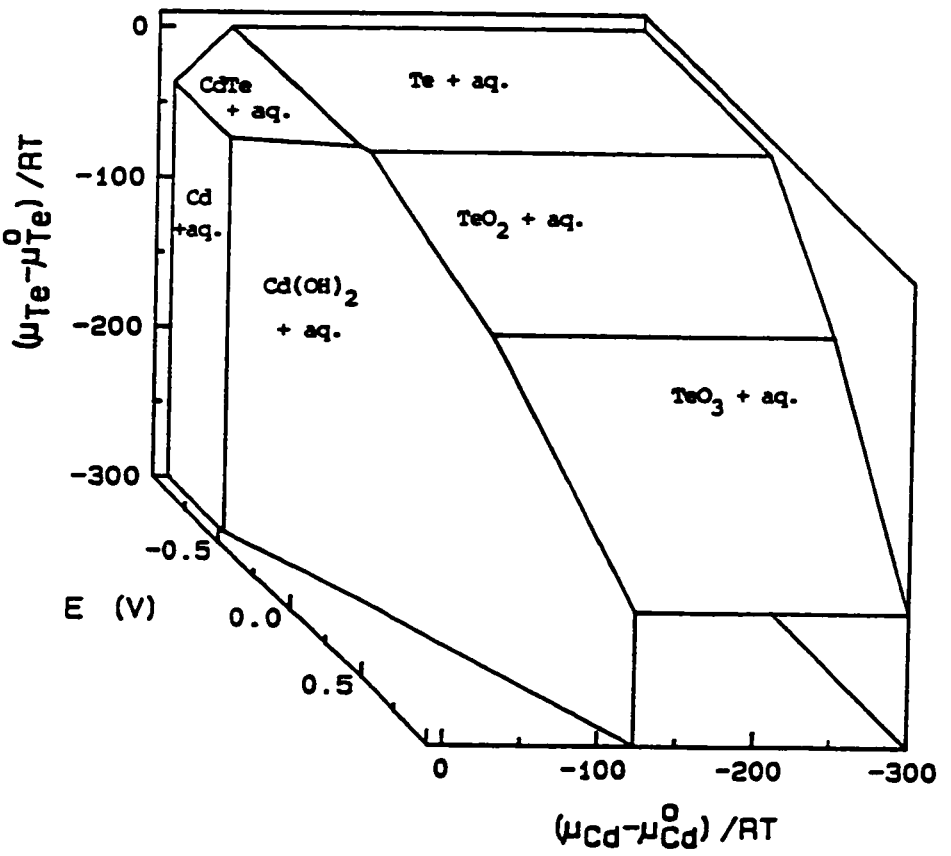

Figure 7–12 Equilibrium diagram for the aqueous Cd–Te system at pH = 10 in chemical potential space.

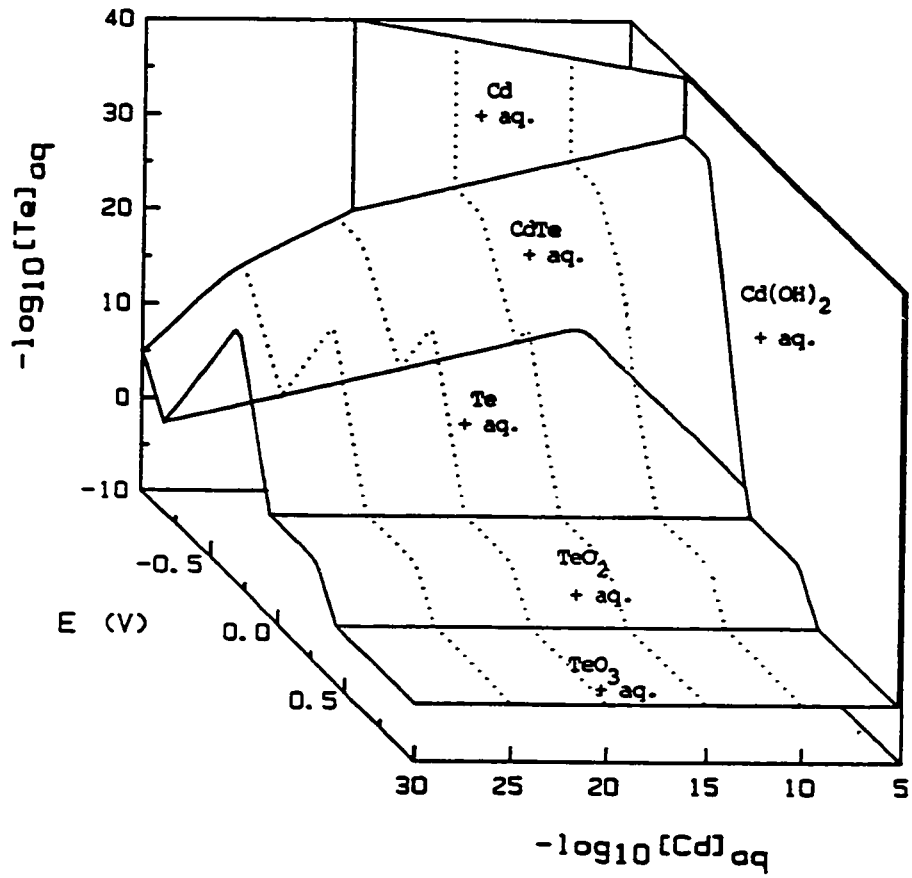

Figure 7–13 Equilibrium diagram for the aqueous Cd–Te system at pH = 10 in $-\log_{10}[Cd]_{aq}/-\log_{10}[Te]_{aq}/E$ space.

Table 7–3

Aqueous Cd–Te System: Species Included in Calculations

Solid Species

Cd	CdO	$Cd(OH)_2$
Te	TeO_2	H_2TeO_3
TeO_3(hydr.)	CdTe	

Dissolved Species

Cd^{2+}	CdO_2^{2-}	$Cd(OH)_2$
$HCdO_2^-$	$CdOH^+$	H_2Te
HTe^-	Te^{2-}	Te_2^{2-}
Te^{4+}	$HTeO_2^+$	$HTeO_3^-$
TeO_3^{2-}	H_2TeO_4	$HTeO_4^-$
TeO_4^{2-}		

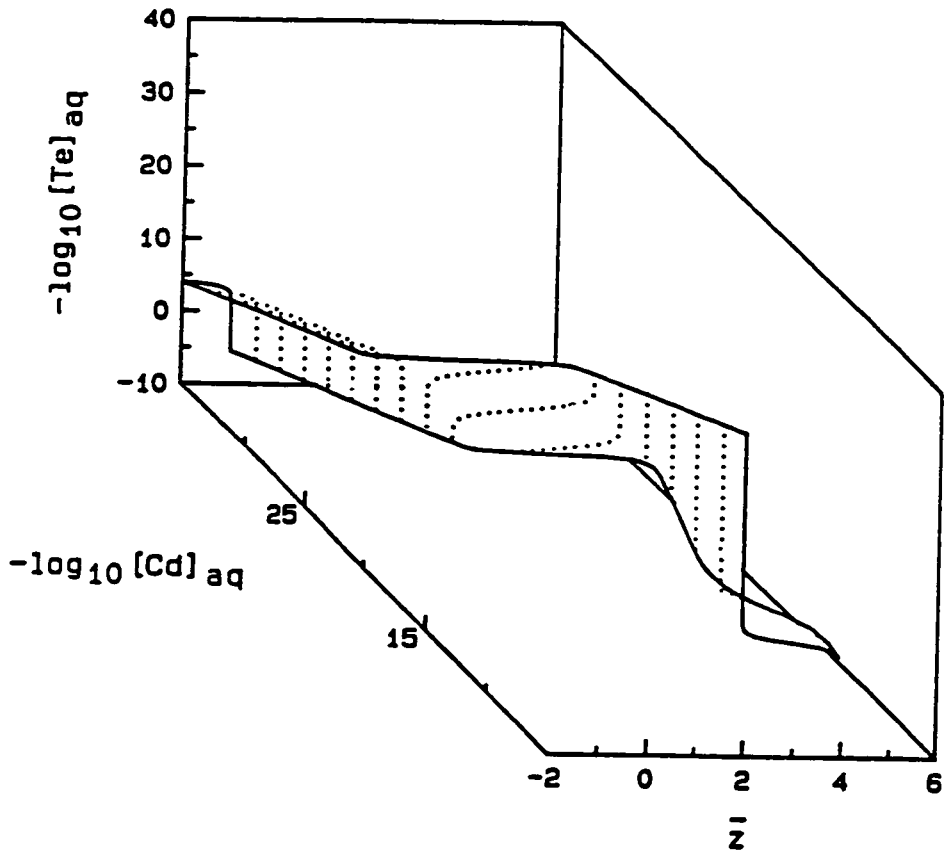

Figure 7–14 Equilibrium diagram for the aqueous Cd–Te system at pH = 10 in $-\log_{10}[Cd]_{aq}/-\log_{10}[Te]_{aq}/\bar{z}$ space. The surface is the three–dimensional electron number diagram for the Cd and Te–containing species in the aqueous phase in equilibrium with solid CdTe.

number of degrees of freedom in the system by one. However, as long as the activity of the additional component is specified, thereby fixing the chemical potential of X, the mathematical complexity of the problem remains unchanged. In fact, an arbitrary number of additional components X can be added in this manner.

The addition of an another active redox element to the system also increases the number of degrees of freedom by one. Thus, either one additional chemical potential must be fixed or the dimensionality of the system will increase by one. Normally, the chemical potential of a redox element is not fixed. (The exception occurs if a system is constrained such that one particular redox element is always present in elemental form; in effect, this fixes the chemical potential of that element at zero.) Therefore, the addition of a redox element to the system will normally increase the dimensionality of the system by one.

The extension of the method described in Chapter 7.3 to systems containing more than two redox elements is straightforward. The formation reaction would be generalized to include m redox elements. The coefficient matrix A in Equation 7.3–1b would thus be (m+1) by (m+1), if the chemical potentials of electrons and the m redox elements were used as the independent variables. The simultaneous solution of the m+1 linear equations in Equation 7.3–1b and subsequent stability tests would give points where m+2 phases were stable. The "boundary" points could be determined by solving Equation 7.3–1b as more chemical potentials are specified. After specifying the connections among the stable points, calculation of the equilibrium surface in chemical potential space would be complete. To this point, only linear equations have had to be solved.

As the dimensionality of the system increases, producing a meaningful

graphical representation of the equilibrium figure becomes much more difficult. To reduce dimensionality, the total activities of some redox elements could be fixed. However, the iterative calculations required to implement this procedure would likely make calculation of the diagram on a microcomputer impractical for a total number of redox elements in excess of three.

CHAPTER 8

CONCLUSIONS AND RECOMMENDATIONS

8.1 Conclusions

The conclusions drawn from this study may be summarized as follows:

1. An entirely new type of electrochemical phase diagram, the electron number diagram, has been discovered. The theoretical foundation for the electron number diagram and its relationship to conventional potential–pH diagrams have been developed. The areas in which electron number diagrams provide information complementary to and in addition to that from conventional potential–pH diagrams have been identified.

2. Experimental electron number diagrams have been constructed for one redox system, the aqueous sulfur system. Two–dimensional sections of the three–dimensional electron number diagram at both constant pH and constant electron number were determined and compared with the sections computed from theory. Agreement between the computed and measured diagrams was found.

3. A rigorous thermodynamic theory for complex aqueous redox systems was developed and used for interpretation of the various types of electrochemical phase diagrams. The dimensionality of potential–pH and electron number diagrams was related to the Gibbs phase rule analysis of aqueous redox systems. The theoretical analysis permits a classification of potential–pH diagrams into two basic types: 1) Pourbaix diagrams, in which the stability field of solid phases and contours of constant activity of the redox element are displayed and 2) predominance diagrams, in which the regions of dominance of dissolved species

are shown. Electron number diagrams are obtained by a thermodynamic transformation in which potential is replaced by a measure of the number of electrons. The chemical potential of electrons and the number of electrons are conjugate thermodynamic variables.

4. An efficient computational method, based on the theoretical analysis of complex aqueous redox systems, was developed. The equations describing the equilibrium composition were obtained from a minimum set of formation reactions. The formation reactions used a set of reactants (components) whose chemical potentials are chosen to be the independent variables in the computation. This procedure permits the sequential rather than simultaneous solution of the equation set in the case of ideal solutions. Efficient stability criteria, obtained from theory, were used to determine the stability of solid phases. The algorithm was implemented on IBM PCs and compatible computers.

5. Electron number, potential–pH and chemical potential diagrams were computed for a variety of complex aqueous systems, including the following systems containing two active redox elements: the aqueous Cd–Te system; the aqueous Ga–As system; and the aqueous U–C system.

8.2 Recommendations

Further development of the work described in this thesis is recommended. The following specific items are particularly important.

1. Develop methods for computation and display of electron number diagrams for solid–aqueous redox systems containing three or more active redox elements. These will be necessary for the most interesting corrosion, geological and mineral processing applications.

2. Develop algorithms for computation and display of generalized chemical potential/temperature/pressure diagrams. These "intensive property" diagrams will contain conventional Pourbaix and Ellingham diagrams as a subset.

3. Improve the data–base supporting the computations by providing an interface to the most recent compilations of thermodynamic data, e.g., that of the National Institute for Standards and Technology (Wang and Neumann, 1989). The algorithms should also be extended by building in methods for computing activity coefficients and for extrapolating data to elevated temperatures.

4. Additional experimental electron number diagrams should be constructed. The aqueous system containing copper and chlorine should exhibit many interesting phase phenomena in a region that is easily accessible experimentally. Work on the aqueous sulfur system should be expanded and should include: 1) development of a more complete data base to support the computed diagrams and 2) more accurate potential measurements.

5. Additional applications for electron number diagrams should be sought and developed. These might be drawn from the following fields: corrosion, nuclear waste containment, wet sulfur removal processes and electroplating of III–V semiconductor compounds.

6. Extension of the concept of electron number diagrams to non–aqueous systems, e.g., molten salts and organic solvents, should be explored.

LIST OF SYMBOLS

a_i	activity of species S_i
a_{M^*}	activity of active element in solution, defined by Equation 2.3–39
a_M	activity of active element in solution, defined by Equation 2.3–37
A	defined by Equation 2.3–33
A	coefficient matrix in Equation 7.3–1; the elements of this matrix are defined by Equations 7.3–2, 7.3–3 and 7.3–4
B_M	number of moles of active element M
D	dimensionality of diagram
E	electrochemical potential
E_i^o	standard electrochemical potential for formation reaction for species S_i
f	degrees of freedom
F	Faraday's constant
G	Gibbs free energy of a system
ΔG_k^o	standard free energy change for the formation of species S_k by the reaction in Equation 2.1–1; given by Equation A–13
$\Delta_f G_k^o$	standard free energy of formation of species k from the elements
h_i	stoichiometric coefficient for H^+ in formation reaction for S_i
log X	base 10 logarithm of X
ln X	natural logarithm of X
$\vec{K}$	vector of constants in Equation 7.3–1; defined by Equation 7.3–5
m	number of active redox elements in a system
m_{H_2O}	mass of H_2O in kilograms
M	symbol for the active redox element

$[M]_{aq}$	concentration of active element in the solution, $[M]_{aq} \equiv B_{M,aq}/m_{H_2O}$
n	the number of species in a system
n_o	number of electrons per atom of active element M in elemental form
n_i	number of electrons per atom of active element M in species S_i
n_3	number of possible sets of three solids
n_i	number of moles of species i
N	symbol for the second active redox element
$N_{e,t}$	total number of moles of electrons contained in active element as it exists in the system
$N_{e,o}$	number of moles of electrons contained in active element if all of the active element were present in the elemental form
N_i	number of moles of species S_i
p_{H_2}	partial pressure of hydrogen
p_{O_2}	partial pressure of oxygen
P	number of phases
r	number of independent reactions
R	gas constant
s	number of species
S_i	symbol for ith species containing redox element (M and/or N)
$[S_k]$	molal concentration of dissolved species S_k, $[S_k] \equiv N_k/m_{H_2O}$ (Note: in Chapter 6 only, molar concentrations are used exclusively)
t	total number of component species necessary to describe the stoichiometry of a reacting system
T	temperature
w_i	stoichiometric coefficient for H_2O in formation reaction for S_i

x	mole fraction
x_i	stoichiometric coefficient for X in formation reaction for S_i
X	component species in formation reaction for S_i
y_i	stoichiometric coefficient for Y in formation reaction for S_i
Y	component species in formation reaction for S_i
$\bar{z}$	average electron number, defined by Equation 5.2–7
$\bar{z}_{aq}$	average electron number of aqueous phase, defined by Equation 5.2–12
z_i	electron number of species S_i; the coefficient of e^- in the formation reaction in Equation 2.1–1; also defined by Equation 5.2–1 for a species S_i containing a single redox element M
$\alpha_{M,i}$	number of atoms of active element M in one molecule of species S_i. $(\alpha_{M,i} = 1/\nu_{M,i})$
γ_i	activity coefficient of species S_i
μ_M	chemical potential of active element M
$\mu_{M,i}$	chemical potential of active element M in species S_i
$\vec{\mu}$	vector of chemical potentials in Equation 7.3–1
$\nu_{M,i}$	stoichiometric coefficient for species S_i in formation reaction $(\nu_{M,i} = \alpha_{M,i}^{-1})$

Subscripts

aq	refers to the aqueous phase
g	refers to a general species S_g, gaseous or solid
i	refers to a general species S_i, solid or dissolved
k	refers to a general species, S_k, solid or dissolved
s	refers to a solid phase
t	refers to the total amount including aqueous plus solid phases

Superscripts

o	standard state
r	reference electrode

REFERENCES

Angus, J.C., Angus, C.T. *J. Electrochem. Soc.* **1985**, 132, 1014.

Angus, J.C., Lu, B., Zappia, M.J. *J. Applied Electrochem* **1987**, 17,1.

Angus, J.C., Zappia, M.J. *J. Electrochem. Soc.* **1987**, 134, 1374.

Angus, J.C., Zappia, M.J., Lu, B. "PPE Computer Software Package," to be published by Wiley (U.K.), 1990.

Arntson, R.H., Dickson, F.W., Tunnell, G. *Science* **1958**, 128, 716.

Bard, A.J., Faulkner, L.R. "Electrochemical Methods: Fundamentals and Applications," John Wiley & Sons: New York, 1980.

Barner, H.E., Scheuermann, R.V. "Handbook of Thermochemical Data for Compounds and Aqueous Species," Wiley–Interscience: New York, 1978.

Barry, T.I., in "Thermodynamics of Aqueous Systems with Industrial Applications," ACS Symposium Series 133 (ed. by S.A. Newman), ACS: Washington, 1980, 681.

Barry, T.I., Dinsdale, A.T. *Materials Science and Technology* **1987**, 3, 501.

Chandra, S., Neeraj, K. *Semiconductor Science and Technology* **1987**, 2, 214.

Chandra, S., Neeraj, K. *Semiconductor Science and Technology* **1987**, 2, 220.

Chen, C.M., Aral, K. *Corrosion*, **1982**, 38, 184.

Cubicciotti, D. *J. Electrochem. Soc.* **1985**, 132, 987.

Cubicciotti, D. *Corrosion* **1988**, 44, 875.

Cubicciotti, D. *J. Nuclear Materials* **1988**, 152, 259.

Davis, G.D., Moshier, W.C., Ahearn, J.S., Hough, H.F., Cote, G.O. *J. Vac. Sci. Technol.* **1987**, A5(4), 1152.

Downing, J.H., in "Diagrams of Chemical and Electrochemical Equilibria: Their Setting–Up and Applications," Pourbaix, M., Pourbaix, A., eds., Proceedings of a NATO Advanced Research Workshop, Brussels, 2–5 September, 1981, CEBELCOR's Reports Techniques 142, RT 263, CEBELCOR, Brussels, 1982, 193.

El–Raghy, S.M., El–Dermerdash, M.F., in "Proceedings of the International Symposium on Electrochemistry in Mineral and Metal Processing II," Richardson, P.E., Woods, R., eds., Proceedings Volume 88–21, The Electrochemical Society, Pennington, NJ, 1988, 372.

Froning, M.H., Shanley, M.E., Verink, E.D. *Corros. Sci.* **1976**, 16, 371.

Frost, A.A. *J. Am. Chem. Soc.* **1951**, 73, 2680.

Garrels, R.M., Christ, C.L. "Solutions, Minerals and Equilibria," Harper & Row: New York, 1966.

Garrels, R.M. in "Diagrams of Chemical and Electrochemical Equilibria: Their Setting–up and Applications," Pourbaix, M., Pourbaix, A., eds., Proceedings of a NATO Advanced Research Workshop, Brussels, 2–5 September, 1981, CEBELCOR's Reports Techniques 142, RT 236, CEBELCOR, Brussels, 1982, 247.

Gray, H.B.; Haight, G.P. "Basic Principles of Chemistry," W.A. Benjamin Inc.: New York, 1967.

Greenwood, N.N., Earnshaw, A. "Chemistry of the Elements," Pergamon Press: Oxford, 1984, 757–881.

Heunisch, G.W. *Inorg. Chem.* **1977**, 16, 1411.

Imai, Y., Osato, K., Nakauchi, H. *Boshoku Gijutsu* **1987**, 36, 195.

Jantzen, C.M. in "Scientific Basis for Nuclear Waste Management XI," Apted, M.J., Westerman, R. E., eds., Materials Research Society Symposium Proceedings, Volume 112, 1988, 519.

Jingyi, Z., Pourbaix, M., Chunchun, X., Youping, L. *Corros. Sci.* **1989**, 29, 557.

Karchmer, J.H. "The Analytical Chemistry of Sulfur and its Compounds, Part 1," Wiley–Interscience: New York, 1970.

Kruger, J. in "Diagrams of Chemical and Electrochemical Equilibria: Their Setting–up and Applications," Pourbaix, M. Pourbaix, A., eds., Proceedings of a NATO Advanced Research Workshop, Brussels, 2–5 September, 1981, CEBELCOR's Reports Techniques 142, RT 236, CEBELCOR, Brussels, 1982, 215.

Langmuir, D. *Geochim. Cosmochim. Acta* **1978**, 42 547.

Lee, J.B. *Corrosion* **1981**, 37, 467.

Lennon, S.J., Robinson, F.P.A. *Corros. Sci.* **1986**, 26, 995.

Llabres, J., Delmas, V. *J. Electrochem. Soc.* **1986**, 133, 2580.

Macdonald, D.D., Syrett, B.C., Wing, S.S. *Corrosion* **1979**, 35, 1.

Macdonald, D.D., Syrett, B.C. *Corrosion* **1979**, 10, 471.

McCafferty, E. *Corros. Sci.* **1989**, 29, 391.

Mueller, M. "Free Energy, Oxidation States and Equilibrium," Privately Published, 1969.

Nickless, G. "Inorganic Sulfur Chemistry," Elsevier: Amsterdam, 1968.

Ogden, C., Tench, D. "Electrodeposition of Device–Quality Semiconductor Materials," U.S. DOE Contract No. XS–0–9010–7, 1981.

Osseo–Asare, K., Fuerstenau, D.W., in "Fundamental Aspects of Hydrometallurgical Processes," Chapman, T.W., Tavlarides, L.L., Hubred, G.L., Wellek, R.M., eds., AIChE Symposium Series 74 (173), AIChE: New York, 1.

Pelton, A.D., Bale, C.W., Thompson, W.I., NBS SP–496, "Applications of Phase Diagrams in Metallurgy and Ceramics," Proceedings of Workshop held at Gaithersburg, MD, 10–12 January, 1977, 1077.

Peters, E. *Metall. Trans. B* **1976**, 7B, 505.

Perrault, G.G. *J. Electrochem Soc.* **1989**, 136, 2845.

Phillips, C.S.G., Williams, R.J.P. "Inorganic Chemistry, I, Principles and Non–Metals," Oxford University Press: Oxford, 1965.

Pound, B.G., Wright, G.A., Sharp, R.M. *Aust. J. Chem.* **1985**, 38, 643.

Pourbaix, M. "Thermodynamics of Dilute Aqueous Solutions: Graphical Representation of the Role of pH and Potential," Thesis, Delft, 1945, CEBELCOR Publication F. 227 (reprinted 1963 in French).

Pourbaix, M. "Atlas of Electrochemical Equilibria in Aqueous Solutions," Pergamon: New York, 1966.

Pourbaix, M., Yang, X., Zhang, H.M., Zhang, C.Z. *Corros. Sci.* **1986**, 26, 873.

Pryor, W.A. "Mechanisms of Sulfur Reactions," McGraw–Hill Book Company: New York, 1962.

Radhakrishnamurty, P., Adaikkalam, P. *Corros. Sci.* **1982**, 22, 753.

Ramsey, J.B. *J. Electrochem. Soc.* **1957**, 104, 255.

Rapp, R.A. *Corrosion* **1986**, 42, 568.

Rapp, R.A. *Materials Science and Engineering* **1987**, 87, 319.

Rosof, B.H., NBS SP–496 "Applications of Phase Diagrams in Metallurgy and Ceramics," Proceedings of Workshop held at Gaithersburg, MD, 10–12 January, 1977, 1090.

Silverman, D.C. *Corrosion* **1982**, 38, 541.

Stumm, W., Morgan, J.J. "Aquatic Chemistry: An Introduction Emphasizing Equilibria in Natural Waters," John Wiley & Sons: New York, 1970, 1981.

Van de Hulst, H.C. "Light Scattering by Small Particles," John Wiley & Sons: New York, 1957.

Wagman, D.D., Evans, W.H., Parker, V.P., Schumm, R.H., Halow, I., Bailey, S.M., Churney, K.L., Nuttal, R.L. *J. Phys. Chem. Ref. Data.* Vol II, Suppl. no. 2, 1982.

Wang, P., Neumann, D.B. *J. Chem. Inf. Comput. Sci.* **1989**, 29, 31.

White, W.B. *J. Chem. Phys.* **1967**, 46, 4171.

Woods, T.L., Garrels, R.M. *Appl. Geochem.* **1986**, 1, 181.

Yung, R., M.S. Thesis, Case Western Reserve University, 1990.

APPENDIX A

DERIVATION OF THE GENERAL EQUATION FOR ACTIVITY IN AQUEOUS SYSTEMS CONTAINING TWO REDOX ELEMENTS

Consider an aqueous redox system containing two active redox elements, M and N, as well as two additional components, X and Y. A formation equation of the following form can be written for each species S_k.

$$\left[\frac{\alpha_{M,k}}{\alpha_{M,k} + \alpha_{N,k}}\right] M + \left[\frac{\alpha_{N,k}}{\alpha_{M,k} + \alpha_{N,k}}\right] N = \left[\frac{1}{\alpha_{M,k} + \alpha_{N,k}}\right] S_k + h_k H^+ + w_k H_2O + x_k X + y_k Y + z_k e^- \quad (A-1)$$

where $\alpha_{M,k}$ is the number of atoms of element M per molecule of species S_k and $\alpha_{N,k}$ is the number of atoms of element N per molecule of species S_k.

The free energy change for Equation A–1 is given by:

$$\Delta G_k = \left[\frac{1}{\alpha_{M,k} + \alpha_{N,k}}\right] \mu_k + h_k \mu_{H^+} + w_k \mu_{H_2O} + x_k \mu_X + y_k \mu_Y + z_k \mu_{e^-} - \left[\frac{\alpha_{M,k}}{\alpha_{M,k} + \alpha_{N,k}}\right] \mu_M - \left[\frac{\alpha_{N,k}}{\alpha_{M,k} + \alpha_{N,k}}\right] \mu_N \quad (A-2)$$

At equilibrium, $\Delta G_k = 0$, so Equation A–2 becomes:

$$0 = \left[\frac{1}{\alpha_{M,k} + \alpha_{N,k}}\right] \mu_k + h_k \mu_{H^+} + w_k \mu_{H_2O} + x_k \mu_X + y_k \mu_Y + z_k \mu_{e^-} - \left[\frac{\alpha_{M,k}}{\alpha_{M,k} + \alpha_{N,k}}\right] \mu_M - \left[\frac{\alpha_{N,k}}{\alpha_{M,k} + \alpha_{N,k}}\right] \mu_N \quad (A-3)$$

In most listings of standard free energy of formation data, including the main source used here (Wagman, et al., 1982), the free energies of formation of ions in solution are based on the convention

$$\Delta_f G^\circ_{H^+} = 0 \ (= \mu^\circ_{H^+}) \tag{A-4}$$

Furthermore, the formation processes of ions in the standard state in solution are defined in terms of redox reactions versus a reference electrode, here chosen to be the standard hydrogen electrode. For the standard hydrogen electrode reaction

$$e^- = \tfrac{1}{2} H_2(g) - H^+ \tag{A-5a}$$

the associated equilibrium equation is given by

$$\mu^r_{e^-} = \tfrac{1}{2} \mu^\circ_{H_2(g)} - \mu^\circ_{H^+} \tag{A-5b}$$

where the superscript ^{r} indicates the chemical potential of the electrons in equilibrium with the standard hydrogen reference electrode. Thus, in defining the standard free energy of formation of a dissolved species M^{n+} from element M, Equation A–5a would be used to replace electrons. In other words, the reaction

$$M = M^{n+} + n\, e^- \tag{A-6a}$$

is replaced with

$$M + n\, H^+ = M^{n+} + (n/2)\, H_2(g) \tag{A-6b}$$

The standard free energy of the formation reaction of species S_k (for the reaction in Equation A–1) can be computed from the standard free energies of the component species and the free energy of formation of species S_k.

$$\Delta G^\circ_k = \left[\frac{1}{\alpha_{M,k} + \alpha_{N,k}}\right] \mu^\circ_k + h_k \mu^\circ_{H^+} + w_k \mu^\circ_{H_2O} + x_k \mu^\circ_X + y_k \mu^\circ_Y$$
$$- \left[\frac{\alpha_{M,k}}{\alpha_{M,k} + \alpha_{N,k}}\right] \mu^\circ_M - \left[\frac{\alpha_{N,k}}{\alpha_{M,k} + \alpha_{N,k}}\right] \mu^\circ_N + z_k \left[\frac{1}{2} \mu^\circ_{H_2(g)} - \mu^\circ_{H^+}\right] \tag{A-7}$$

Equation A–7 gives the free energy change for reaction A–1 if all species are in their standard states and if the standard free energies of formation of all ionic species in Equation A–1 are referred to the standard hydrogen electrode. The standard state, by convention, is denoted by the superscript $^\circ$.

Subtraction of Equation A–7 from Equation A–3 gives:

$$\left[\frac{1}{\alpha_{M,k} + \alpha_{N,k}}\right](\mu_k - \mu_k^\circ) + h_k(\mu_{H^+} - \mu_{H^+}^\circ) + w_k(\mu_{H_2O} - \mu_{H_2O}^\circ) + x_k(\mu_X - \mu_X^\circ)$$
$$+ y_k(\mu_Y - \mu_Y^\circ) - \left[\frac{\alpha_{M,k}}{\alpha_{M,k} + \alpha_{N,k}}\right](\mu_M - \mu_M^\circ) - \left[\frac{\alpha_{N,k}}{\alpha_{M,k} + \alpha_{N,k}}\right](\mu_N - \mu_N^\circ)$$
$$+ z_k\left[\mu_{e^-} - \frac{1}{2}\mu_{H_2(g)}^\circ + \mu_{H^+}^\circ\right] = -\Delta G_k^\circ \qquad \text{(A–8)}$$

The following convention, which agrees in magnitude with that of Ramsey (1957), can be used to relate the chemical potential of electrons to electrode potential

$$\mu_{e^-} = -FE \qquad \text{(A–9a)}$$

Combining Equations A–5b and A–9a gives

$$E^r = -\frac{1}{F}\left[\frac{1}{2}\mu_{H_2(g)}^\circ - \mu_{H^+}^\circ\right] \qquad \text{(A–9b)}$$

where E^r is the potential of the standard hydrogen electrode.

The following conventions, which relate chemical potential differences to practical variables, are used to simplify Equation A–8:

$$\mu_i = \mu_i^\circ + RT \ln a_i \qquad \text{(A–10a)}$$

$$\mu_{H^+} - \mu_{H^+}^\circ = RT \ln a_{H^+} = -RT(\ln 10)pH \qquad \text{(A–10b)}$$

The activity, a_k, of species S_k can be obtained using Equations A–8, A–9 and A–10:

$$a_k = \exp\left[(\alpha_{M,k} + \alpha_{N,k})\left[\left[\frac{\alpha_{M,k}}{\alpha_{M,k} + \alpha_{N,k}}\right]\frac{(\mu_M - \mu_M^\circ)}{RT}\right.\right.$$
$$+ \left[\frac{\alpha_{N,k}}{\alpha_{M,k} + \alpha_{N,k}}\right]\frac{(\mu_N - \mu_N^\circ)}{RT} + h_k(\ln 10)pH - w_k \ln a_{H_2O}$$
$$\left.\left. - x_k \ln a_X - y_k \ln a_Y + z_k\left[\frac{F}{RT}\right](E - E^r) - \frac{\Delta G_k^\circ}{RT}\right]\right] \qquad \text{(A–11)}$$

However, $\mu^{\circ}_{H_2(g)} = 0$, and by the convention in Equation A–4, $\mu^{\circ}_{H+} = 0$. Therefore, according to Equation A–9b,

$$E^r = 0 \tag{A–12}$$

Thus, convention of setting the potential of the standard hydrogen electrode to zero is equivalent to the convention of setting $\mu^{\circ}_{H^+} = 0$.

Equation A–7 can be simplified using Equations A–9b and A–12 to give

$$\Delta G^{\circ}_k = \left[\frac{1}{\alpha_{M,k} + \alpha_{N,k}}\right]\mu^{\circ}_k + h_k\mu^{\circ}_{H^+} + w_k\mu^{\circ}_{H_2O} + x_k\mu^{\circ}_X + y_k\mu^{\circ}_Y - \left[\frac{\alpha_{M,k}}{\alpha_{M,k} + \alpha_{N,k}}\right]\mu^{\circ}_M - \left[\frac{\alpha_{N,k}}{\alpha_{M,k} + \alpha_{N,k}}\right]\mu^{\circ}_N \tag{A–13a}$$

Using the relationship $\mu^{\circ}_i = \Delta_f G^{\circ}_i$, Equation A–13a becomes

$$\Delta G^{\circ}_k = \left[\frac{1}{\alpha_{M,k} + \alpha_{N,k}}\right]\Delta_f G^{\circ}_k + h_k\,\Delta_f G^{\circ}_{H+} + w_k\,\Delta_f G^{\circ}_{H_2O} + x_k\,\Delta_f G^{\circ}_X + y_k\,\Delta_f G^{\circ}_Y - \left[\frac{\alpha_{M,k}}{\alpha_{M,k} + \alpha_{N,k}}\right]\Delta_f G^{\circ}_M - \left[\frac{\alpha_{N,k}}{\alpha_{M,k} + \alpha_{N,k}}\right]\Delta_f G^{\circ}_N \tag{A–13b}$$

where $\Delta_f G^{\circ}_i$ is the standard free energy of formation of i from the elements. Notice that ΔG°_k is simply the standard free energy for the formation of species S_k from the system components (Equation A–1) as conventionally defined, i.e., considering only chemical species.

Using Equation A–12, Equation A–11 can be simplified to give

$$a_k = \exp\left[(\alpha_{M,k} + \alpha_{N,k})\left[\left[\frac{\alpha_{M,k}}{\alpha_{M,k} + \alpha_{N,k}}\right]\frac{(\mu_M - \mu^{\circ}_M)}{RT} + \left[\frac{\alpha_{N,k}}{\alpha_{M,k} + \alpha_{N,k}}\right]\frac{(\mu_N - \mu^{\circ}_N)}{RT} + h_k(\ln 10)pH - w_k \ln a_{H_2O} - x_k \ln a_X - y_k \ln a_Y + z_k\left[\frac{FE}{RT}\right] - \frac{\Delta G^{\circ}_k}{RT}\right]\right] \tag{A–14}$$

Equation A–14 can be used in this general form to calculate activities involving both redox and chemical equilibria. In the case where $z_k = 0$, a_k is independent of E. In the case where $z_k \neq 0$, it is possible, though not necessary, to express Equation A–14 in a slightly different form.

$$a_k = \exp\left[(\alpha_{M,k} + \alpha_{N,k})\left[\left[\frac{\alpha_{M,k}}{\alpha_{M,k} + \alpha_{N,k}}\right]\frac{(\mu_M - \mu_M^\circ)}{RT} + \left[\frac{\alpha_{N,k}}{\alpha_{M,k} + \alpha_{N,k}}\right]\frac{(\mu_N - \mu_N^\circ)}{RT} + h_k(\ln 10)pH - w_k \ln a_{H_2O} - x_k \ln a_X - y_k \ln a_Y + z_k\left[\frac{F}{RT}\right](E - E_k^\circ)\right]\right] \quad \text{(A–15)}$$

where E_k°, the standard electrode potential for the formation of S_k, is defined by

$$E_k^\circ \equiv \frac{\Delta G_k^\circ}{z_k F} \qquad \text{for } z_k \neq 0 \quad \text{(A–16)}$$

Consider the special case of a species S_k which contains only one redox element M. When $\alpha_{N,k}$ is set to zero, Equation A–15 simplifies to give

$$a_k = \exp\left[(\alpha_{M,k})\left[\frac{(\mu_M - \mu_M^\circ)}{RT} + h_k(\ln 10)pH - w_k \ln a_{H_2O} - x_k \ln a_X - y_k \ln a_Y + z_k\left[\frac{F}{RT}\right](E - E_k^\circ)\right]\right] \quad \text{(A–17)}$$

Notice that the definition of E° in Equation A–16 agrees with that of Pourbaix (1966).

For a pure solid phase of species S_k, which may contain one or both of the active redox elements,

$$a_k = 1 \quad \text{(A–18)}$$

Equation A–18 can be combined with Equation A–14, the general activity

expression, to give the following equation for solid species S_k:

$$\left[\frac{\alpha_{M,k}}{\alpha_{M,k} + \alpha_{N,k}}\right]\frac{(\mu_M - \mu_M^\circ)}{RT} + \left[\frac{\alpha_{N,k}}{\alpha_{M,k} + \alpha_{N,k}}\right]\frac{(\mu_N - \mu_N^\circ)}{RT} + z_k\left[\frac{F}{RT}\right]E$$

$$= -h_k(\ln 10)pH + w_k \ln a_{H_2O} + x_k \ln a_X + y_k \ln a_Y + \frac{\Delta G_k^\circ}{RT} \qquad \text{(A–19)}$$

Alternatively, Equations A–19 and A–9a can be combined and rearranged to give

$$\left[\frac{\alpha_{M,k}}{\alpha_{M,k} + \alpha_{N,k}}\right]\frac{(\mu_M - \mu_M^\circ)}{RT} + \left[\frac{\alpha_{N,k}}{\alpha_{M,k} + \alpha_{N,k}}\right]\frac{(\mu_N - \mu_N^\circ)}{RT} - z_k\frac{(\mu_{e^-})}{RT}$$

$$= -h_k(\ln 10)pH + w_k \ln a_{H_2O} + x_k \ln a_X + y_k \ln a_Y + \frac{\Delta G_k^\circ}{RT} \qquad \text{(A–20)}$$

Equations A–19 and A–20 apply at equilibrium conditions for the formation reaction of Equation A–1. Another expression, analogous to Equation A–19, can be derived for ΔG_k, the free energy change associated with the formation of solid species S_k from the redox elements M and N as shown in Equation A–1.

$$\frac{\Delta G_k}{RT} = -h_k(\ln 10)pH + w_k \ln a_{H_2O} + x_k \ln a_X + y_k \ln a_Y + \frac{\Delta G_k^\circ}{RT}$$

$$-\left[\frac{\alpha_{M,k}}{\alpha_{M,k} + \alpha_{N,k}}\right]\frac{(\mu_M - \mu_M^\circ)}{RT} - \left[\frac{\alpha_{N,k}}{\alpha_{M,k} + \alpha_{N,k}}\right]\frac{(\mu_N - \mu_N^\circ)}{RT}$$

$$-z_k\left[\frac{F}{RT}\right]E \qquad \text{(A–21)}$$

Finally, for a system containing one redox element, M, and a pure solid phase containing M, Equations A–17 and A–18 can be combined and rearranged to give the following expression for the chemical potential of the active redox element M in equilibrium with solid species S_k:

$$\frac{(\mu_M - \mu_M^\circ)}{RT} = -h_k(\ln 10)pH + w_k \ln a_{H_2O} + x_k \ln a_X + y_k \ln a_Y$$

$$-z_k\left[\frac{F}{RT}\right](E - E_k^\circ) \qquad \text{(A–22)}$$

APPENDIX B

LIMITING SLOPES OF SOLUBILITY CURVES ON ELECTRON NUMBER DIAGRAMS IN SYSTEMS CONTAINING ONE ACTIVE REDOX ELEMENT

The theoretical limiting slope of the $-\log_{10}[M]_{aq}$ versus $\bar{z}$ curve along a solubility line is of interest. The theoretical slope of the solubility curves can be obtained for the special case of ideal solutions. To within the constant $-(2.30259)^{-1}$, this derivative is:

$$\left[\frac{\partial \ln[M]_{aq}}{\partial \bar{z}_{aq}}\right]_{pH}$$

Using the chain rule

$$\left[\frac{\partial \ln[M]_{aq}}{\partial \bar{z}_{aq}}\right]_{pH} = \left[\frac{\partial \ln[M]_{aq}}{\partial E}\right]_{pH} \left[\frac{\partial E}{\partial \bar{z}_{aq}}\right]_{pH} \tag{B-1}$$

and the identity

$$\left[\frac{\partial \bar{z}_{aq}}{\partial E}\right]_{pH} = \left[\frac{\partial E}{\partial \bar{z}_{aq}}\right]_{pH}^{-1} \tag{B-2}$$

gives

$$\left[\frac{\partial \ln[M]_{aq}}{\partial \bar{z}_{aq}}\right]_{pH} = \left[\frac{\partial \ln[M]_{aq}}{\partial E}\right]_{pH} \left[\frac{\partial \bar{z}_{aq}}{\partial E}\right]_{pH}^{-1} \tag{B-3}$$

Each derivative on the right hand side of Equation B–3 is evaluated separately as described below.

For an aqueous system containing a single active redox element, M, it has been shown (Angus and Angus, 1985; Angus, Lu and Zappia, 1987) that the concentration of any dissolved species, S_k, in equilibrium with a solid phase, S_s, can be written in the form

$$[S_k] = \frac{1}{\gamma_k} \exp\left[C_k + \frac{F}{RT}(\alpha_{M,k})(z_k - z_s)E\right] \qquad \text{(B–4)}$$

where C_k is a term that does not depend on E. For example, for simple systems containing only the elements M, H and O, C_k is given by

$$C_k = 2.30259\,(\alpha_{M,k})(h_k - h_s)(pH) + \frac{F}{RT}(\alpha_{M,k})(z_s E_s^o - z_k E_k^o) \qquad \text{(B–5)}$$

The special case of ideal solutions ($\gamma_k = 1$) is considered and Equation B–4 is substituted into Equation 5.2–18 yielding

$$[M]_{aq} = \sum_{aq} (\alpha_{M,k}) \exp\left[C_k + \frac{F}{RT}(\alpha_{M,k})(z_k - z_s)E\right] \qquad \text{(B–6)}$$

The aq below the summation indicates that the sum is taken over all dissolved species. Equation B–6 can be differentiated with respect to E.

$$\left[\frac{\partial [M]_{aq}}{\partial E}\right]_{pH} = \left[\frac{F}{RT}\right] \sum_{aq} (\alpha_{M,k})^2 (z_k - z_s) \exp\left[C_k + \frac{F}{RT}(\alpha_{M,k})(z_k - z_s)E\right] \qquad \text{(B–7)}$$

$$\left[\frac{\partial [M]_{aq}}{\partial E}\right]_{pH} = \frac{F}{RT} \sum_{aq} (\alpha_{M,k})^2 (z_k - z_s)[S_k] \qquad \text{(B–8)}$$

Dividing Equation B–8 by $[M]_{aq} = \sum_{aq} (\alpha_{M,k})[S_k]$ gives

$$\left[\frac{\partial \ln [M]_{aq}}{\partial E}\right]_{pH} = \left[\frac{F}{RT}\right] \frac{\sum_{aq} (\alpha_{M,k})^2 (z_k - z_s)[S_k]}{\sum_{aq} (\alpha_{M,k})[S_k]} \qquad \text{(B–9)}$$

The definition of an atom average quantity is now introduced.

$$\bar{u} \equiv \frac{\sum_{aq} u_k (\alpha_{M,k})[S_k]}{\sum_{aq} (\alpha_{M,k})[S_k]} \qquad \text{(B–10)}$$

Therefore, Equation B–9 can be rewritten as

$$\left[\frac{\partial \ln[M]_{aq}}{\partial E}\right]_{pH} = \left[\frac{F}{RT}\right] \overline{\alpha_M(z - z_s)} \qquad \text{(B–11)}$$

where, by the definition in Equation B–10, $\overline{\alpha_M(z - z_s)}$ is the atom average of the quantity $\alpha_{M,k}(z_k - z_s)$.

Next obtain the derivative $(\partial \bar{z}_{aq}/\partial E)_{pH}$. Equation B–4 with $\gamma_i = 1$ is substituted into Equation 5.2–19 giving

$$\bar{z}_{aq} = \frac{\sum_{aq} \alpha_{M,k} \; z_k \exp\left[C_k + \frac{F}{RT}(\alpha_{M,k})(z_k - z_s)E\right]}{\sum_{aq} \alpha_{M,k} \exp\left[C_k + \frac{F}{RT}(\alpha_{M,k})(z_k - z_s)E\right]} \qquad \text{(B–12)}$$

Differentiation of Equation B–12 and application of Equation B–10 gives

$$\left[\frac{\partial \bar{z}_{aq}}{\partial E}\right]_{pH} = \frac{F}{RT}\left[\overline{\alpha_M z(z - z_s)} - \bar{z}\,\overline{\alpha_M(z - z_s)}\right] \qquad \text{(B–13)}$$

Combining Equations B–11 and B–13 gives the desired result.

$$\left[\frac{\partial \ln[M]_{aq}}{\partial \bar{z}}\right]_{pH} = \frac{\overline{\alpha_M(z - z_s)}}{\overline{\alpha_M z(z - z_s)} - \bar{z}\,\overline{\alpha_M(z - z_s)}} \qquad \text{(B–14)}$$

The denominator of Equation B–14 is always greater than or equal to zero. The sign of the slope is therefore determined by the sign of $\overline{\alpha_M(z-z_s)}$.

$$\text{Sign}\left[\frac{\partial \ln[M]_{aq}}{\partial \bar{z}}\right]_{pH} = \text{Sign}\left[\overline{\alpha_M(z-z_s)}\right] \qquad \text{(B–15)}$$

Inspection of the curves shown in Figures 5–3 through 5–7 show that Equation B–15 is indeed obeyed. (For the aqueous copper system, the $\alpha_{Cu,i}$ for all the dissolved species were equal to one so $\overline{\alpha_{Cu}(z-z_s)} = \overline{(z-z_s)}$.)

Furthermore, when only one species is present in the solution

$$\overline{\alpha_M z(z-z_s)} = \bar{z}\,\overline{\alpha_M(z-z_s)} \qquad \text{(B–16)}$$

Therefore when the solution contains essentially only one species the slope given by Equation B–14 approaches infinity. This conclusion is also confirmed by the

computations, i.e., where the aqueous phase is dominated by one species, the slopes approach infinity.

Equation B–14 also shows that the slope is zero when $\overline{\alpha_{M^{(z-z_s)}}}$ is zero. For systems in which $\alpha_{M,k} = 1$ for all dissolved species, e.g., copper, this reduces to $\overline{z-z_s} = \bar{z} - z_s = 0$. In other words, in that special case, the maximum of the $-\log_{10}[M]_{aq}$ versus $\bar{z}$ curve (minimum solubility) occurs at the point where the electron numbers of the aqueous and solid phases are equal. For situations in which there is an appreciable concentration of ions with $\alpha_{M,k} \neq 1$, this is not true. The sulfur system, in which $S_2O_3^{2-}$, $HS_2O_3^-$, $H_2S_2O_3$ and polysulfides are important, is a case in point. The maximum of the solubility curve for solid sulfur shown in Figure 5–10 does not occur at $\bar{z} = 0$. Detailed calculations show that the maximum does occur at $\overline{\alpha_{M^{(z-z_s)}}} = 0$ as predicted by Equation B–14.

APPENDIX C

QUANTITATIVE ANALYSIS OF TOTAL SULFUR

The object of this analysis is the determination of total sulfur, in all species, in solution. The method chosen is conversion of all sulfur species to sulfate, which can then be determined gravimetrically as barium sulfate (Yung, 1990).

C.1 Conversion of All Sulfur to Sulfate

The first step in this procedure is conversion of all of the different dissolved sulfur species to sulfate ions.

1) Estimate a maximum concentration for the samples to be analyzed. A sample volume of 10.00 ml should be used if the sample concentration is greater than 0.1 M. Otherwise, a sample volume of 100.00 ml should be used. For extremely dilute samples, a larger volume may be desirable to increase the precision of later precipitate weighings.

As the entire procedure is rather time consuming, it is often advisable to run more than one sample concurrently. Two or three samples can be analyzed in the time required for one.

2) With a volumetric pipet, measure a sample volume into a 250 ml beaker and add a stirring bar. In the case of a typical 100 ml unknown, 50 ml test samples are desirable since a second analysis can then be performed in the event of an error in the procedure.

3) While wearing protective gloves and safety glasses, add enough 30% hydrogen peroxide (H_2O_2) to each sample to oxidize all the sulfur species present to sulfate. Excess H_2O_2 is added to insure that all sulfide will oxidize and to allow for any possible decomposition of the peroxide prior to use. A graduated cylinder is of sufficient accuracy for the peroxide measurement.

4) The samples are then heated to near boiling (80 to 90°C) for one hour to decompose the hydrogen peroxide by the reaction:

$$H_2O_2 \rightarrow \frac{1}{2} O_2(g) + H_2O \qquad \text{(C.1–1)}$$

If the peroxide is not removed here, it may later oxidize the chloride ions to perchlorate. The perchlorate ions may occlude in the barium sulfate crystal lattice as it grows, thus giving a higher weight.

During heating it may be advisable to add a small amount of double distilled water to maintain a constant volume.

C.2 Precipitation of Barium Sulfate

Be certain that adequate time is available for this section of the process. The goal here is the formation and filtration of a barium sulfate precipitate. The procedure should not be interrupted until the precipitate has been filtered because of the possibility of the formation of impure crystals.

1) Acidify the samples with 1.0 M HCl, and check with pH paper to insure that the solution is at a pH of 3 or lower. For best crystal growth, a low pH is required to force the H_2SO_4 equilibria to the right to give a low sulfate ion concentration, a condition desirable for slow growth of pure crystals.

$$SO_4^{2-} + 2H^+ \leftrightharpoons HSO_4^- + H^+ \leftrightharpoons H_2SO_4 \qquad \text{(C.2–1)}$$

2) Heat the sample and a 60 ml portion of 0.1 M barium chloride ($BaCl_2$) solution to near boiling (80 to 90°C). When the temperatures of both the sample and the $BaCl_2$ solution are in the correct range, add the $BaCl_2$ solution to the sample rapidly with stirring. Hold the solution at this temperature while any other samples are treated to avoid the side reactions that occur at low temperatures.

3) The precipitate must now be digested. Both phases (precipitate and mother liquid) should remain in contact with one another for a period of 1.5 to 2 hours at a temperature of 80 to 90°C. This will allow the phases to re–equilibrate and will increase both particle size and the purity of the crystals.

4) After digestion, the precipitate must be suction filtered while hot (80 to 90°C). Preweighed medium porosity sintered–glass crucibles are used for the process. After filtration, the filtrate should be clear. If it is turbid, then it still contains precipitate; in this case, the solution should be reheated and refiltered until the filtrate is clear. The clear filtrate can be discarded.

5) The precipitate and filter crucible should then be thoroughly rinsed to remove impurities that may adhere to surfaces. Distilled water should be heated to near–boiling and several small portions (25 to 30 ml) should be sequentially added to each sample and suction filtered to wash the precipitate.

6) The silver chloride test is used to insure that rinsing is complete. A few drops of silver nitrate ($AgNO_3$) are added to a small portion of the washings in a test tube. A cloudiness or the formation of a precipitate in the test tube is indicative of incomplete washing, i.e., chloride ions are still present. In that case, the precipitate should be rinsed several more times and retested. Gravimetric washing should be considered complete when a portion of the filtrate gives only a faint opalescence with $AgNO_3$ solution.

7) When the samples have been washed, the crucibles should be placed in a beaker and stored in an oven at a temperature of about 120°C. After 2 to 3 days of drying, the crucibles are ready for weighing.

C.3 Determination of the Weight of Barium Sulfate

1) Constant weight has been attained when the successive weight measurements are within ± 0.0005 g. Crucibles are placed in the oven for a minimum initial heating period of 2 to 3 days. The oven temperature must be maintained at a minimum of 100°C. The crucibles are removed from the oven for the initial weighing and cooled in a desiccator for 30 minutes to eliminate buoyancy effects. After weighing, the crucibles are then placed in the oven for at least 30 minutes of heating. The procedure is then repeated until successive measurements are within 0.0005 g. The constant weight of the crucible is then taken as the average of two successive constant weights.

2) The difference between the constant weight of the crucible plus precipitate and the intial weight of the crucible (from preweighing) is the amount of $BaSO_4$ produced. Division by the molecular weight (233.40 g/mol) yields the number of moles of $BaSO_4$. The number of moles of $BaSO_4$ produced is equal to the number of moles of sulfur in the solution. Division by the original sample volume gives the total sample concentration of sulfur species present.

APPENDIX D

CALCULATION OF POINTS ON EXPERIMENTAL ELECTRON NUMBER DIAGRAMS FROM EXPERIMENTAL DATA

In the description of the calculation of points on experimental electron number diagrams, the following definitions are made:

$c_A \equiv m_A/v_A$; total sulfur concentration of Sample A in indirect determination experiments (moles/liter)

$c_B \equiv m_B/v_B$; total sulfur concentration of Sample B in indirect determination experiments (moles/liter)

$c_f \equiv (m_S + m_{aq})/v_f$; the final sulfur (solid + dissolved) to volume ratio of the system in direct determination experiments (moles/liter)

$c_{ss} \equiv m_{ss}/v_{ss}$; sulfur concentration of the starting solution (moles/liter)

$m_A \equiv$ moles of sulfur in Sample A

$m_{aq} \equiv$ moles of dissolved sulfur in the aqueous phase

$m_B \equiv$ moles of sulfur (solid + dissolved) in Sample B

$m_{H_2S(g)} \equiv$ moles of sulfur in the gas phase as H_2S

$m_S \equiv$ moles of solid elemental sulfur

$m_{ss} \equiv$ moles of sulfur in starting solution

$[S]_{aq} \equiv m_{aq}/v_f$; total dissolved sulfur concentration of the aqueous phase

$v_A \equiv$ volume of Sample A in indirect determination experiments (liters)

$v_B \equiv$ volume of Sample B (the system immediately after removal of Sample A) in indirect determination experiments

$v_f \equiv$ final volume of solution (liters)

v_{HCl} ≡ volume of HCl used to acidify the system (liters)

v_{ss} ≡ volume of starting solution (liters)

$\bar{z}_{aq}$ ≡ average electron number of sulfur in the aqueous phase

$\bar{z}_f$ ≡ final overall average electron number of sulfur (including both solid and dissolved) in direct determination experiments

$z_{H_2S(g)}$ ≡ electron number of sulfur in gaseous H_2S ($z_{H_2S(g)} = -2$)

z_S ≡ electron number of solid sulfur ($z_S = 0$)

$\bar{z}_{ss}$ ≡ average electron number of sulfur in the starting solution

σ_i ≡ standard deviation of random variable i

D.1 Direct Determination Data

The object of the direct determination experiments was to determine the phase boundary between the single–phase region (dissolved sulfur only) and the two–phase region (solid sulfur and dissolved sulfur). This was done by locating points on both sides of the boundary, as shown in Figures 6–5, 6–6 and 6–9 through 6–17.

In each direct determination experiment, a known volume (v_{ss}) of a starting solution of known concentration (c_{ss}) and average electron number ($\bar{z}_{ss}$) was acidified with a known volume of hydrochloric acid (v_{HCl}). After allowing time for equilibration, the system was tested for solid sulfur. Based on this test, a point was then located in either the single–phase or the two–phase region.

If the loss of sulfur as gaseous species can be neglected relative to the total mass of dissolved and solid sulfur, then the following mass balance can be written:

$$m_{ss} = m_{aq} + m_S \qquad \text{(D.1–1)}$$

The assumption of negligible gas phase losses is expected to be reasonable in the

majority of direct determination experiments; the assumption begins to break down at low pH, especially at high dissolved sulfur concentrations.

The electron balance accompanying the mass balance in Equation D.1–1 is given by

$$m_{ss}\bar{z}_{ss} = (m_{aq} + m_S)\bar{z}_f \qquad \text{(D.1–2)}$$

Equations D.1–1 and D.1–2 can be combined to give

$$\bar{z}_{ss} = \bar{z}_f \qquad \text{(D.1–3)}$$

Thus, in the direct determination experiments, the final overall electron number of the system is equal to the electron number of the starting solution.

From the definition of c_{ss}, the following relationship can be obtained:

$$m_{ss} = c_{ss}v_{ss} \qquad \text{(D.1–4)}$$

Substitution of Equation D.1–4 into Equation D.1–1 and division of both sides by v_f yields

$$c_{ss}\frac{v_{ss}}{v_f} = \frac{m_S + m_{aq}}{v_f} \qquad \text{(D.1–5)}$$

Notice that the right side of Equation D.1–5 is, by definition, equal to c_f, the ratio of total moles of sulfur (dissolved + solid) to total volume of solution:

$$c_f \equiv \frac{m_S + m_{aq}}{v_f} \qquad \text{(D.1–6)}$$

Combining Equations D.1–5 and D.1–6 gives

$$c_{ss}\frac{v_{ss}}{v_f} = c_f \qquad \text{(D.1–7)}$$

Equation D.1–6 can be rewritten in the following form, which incorporates the definition of $[S]_{aq}$:

$$c_f = \frac{m_S}{v_f} + [S]_{aq} \qquad \text{(D.1–8)}$$

Since v_f is always positive and m_S is never negative, the following inequality

holds:

$$c_f \geq [S]_{aq} \qquad \text{(D.1–9)}$$

In the two–phase region, c_f is always greater than $[S]_{aq}$. Thus, c_f provides a conservative estimate of $[S]_{aq}$ in the two–phase region. As the amount of solid sulfur present decreases relative to the amount of dissolved sulfur, c_S approaches $[S]_{aq}$. Examination of Equation D.1–8 shows that in the single–phase aqueous region (where $m_S = 0$), c_f equals $[S]_{aq}$. Therefore, at fixed pH and $\bar{z}$, values of c_f in the single–phase and the two–phase regions bracket the value of $[S]_{aq}$ at the boundary between the regions.

The experiments to determine electron number diagrams for the aqueous sulfur system involved the combination of starting solutions and dilute HCl. If the volume changes associated with mixing and the subsequent reactions are neglected, then the final solution volume, v_f, is given by

$$v_f = v_{ss} + v_{HCl} \qquad \text{(D.1–10)}$$

This is expected to be a reasonable assumption. Substitution of Equation D.1–10 into Equation D.1–7 gives

$$c_f = \frac{v_{ss}}{v_{ss} + v_{HCl}} c_{ss} \qquad \text{(D.1–11)}$$

All terms on the right side of Equation D.1–11 can be determined conveniently. Equation D.1–11 can be used with Equation D.1–3 and a pH measurement to locate a point ($\bar{z}_f$, $-\log_{10} c_f$, pH). After establishment of whether or not solid sulfur is present in the experimental system, the experimental point can be shown on a field of $-\log_{10}[S]_{aq}$ versus $\bar{z}_f$ at constant pH (e.g., Figure 6–5) or on a field of $-\log_{10}[S]_{aq}$ versus pH at constant $\bar{z}_f$ (e.g., Figure 6–9).

D.2 Indirect Determination Data

In each indirect determination experiment, a known volume (v_{ss}) of a starting solution of known concentration (c_{ss}) and average electron number ($\bar{z}_{ss}$) was acidified with a known volume of hydrochloric acid (v_{HCl}), producing solid sulfur. After allowing time for equilibration between the solid and solution phases, the system was divided into two samples. A known volume (v_A) of clear liquid was removed from the system and designated Sample A. Sample B consisted of the remaining volume of solution (v_B) and the solid sulfur. Both samples were then analyzed for total sulfur, as described in Appendix C. From these analyses, a point ($\bar{z}_{aq}$, $-\log_{10}[S]_{aq}$) on the boundary between the single–phase and two–phase regions could be determined.

In the indirect determination experiments, H_2S was the only gaseous species that formed in significant quantities. Consequently, a mass balance for sulfur in these experiments can be written as:

$$m_{ss} = m_{aq} + m_S + m_{H_2S(g)} \qquad \text{(D.2–1)}$$

The corresponding electron balance is given by

$$m_{ss}\bar{z}_{ss} = m_{aq}\bar{z}_{aq} + m_S z_S + m_{H_2S(g)} z_{H_2S(g)} \qquad \text{(D.2–2)}$$

As in the direct determination experiments, starting solutions and dilute HCl were combined. If the volume changes associated with mixing and the subsequent reactions are neglected, then the final solution volume, v_f, is given by

$$v_f = v_{ss} + v_{HCl} \qquad \text{(D.2–3)}$$

Because the total sulfur analysis of Samples A and B accounts for all of the solid and dissolved sulfur in the system, the following relationship can be written:

$$m_A + m_B = m_{aq} + m_S \qquad \text{(D.2–4)}$$

Using the definitions of c_A, c_B and $[S]_{aq}$, Equation D.2–4 can also be written as

$$c_A v_A + c_B v_B = [S]_{aq} v_f + m_S \qquad \text{(D.2–5)}$$

Other relationships among the variables can be written:

$$v_A + v_B = v_f \qquad \text{(D.2–6)}$$

$$c_A = [S]_{aq} \qquad \text{(D.2–7)}$$

$$c_A(v_A + v_B) = m_{aq} \qquad \text{(D.2–8)}$$

Equations D.2–6 and D.2–8 can be combined to give

$$m_{aq} = c_A v_f \qquad \text{(D.2–9)}$$

From Equations D.2–5, D.2–6 and D.2–7, an expression for m_S in terms of c_A, c_B, v_f and v_A can be obtained:

$$m_S = (c_B - c_A)(v_f - v_A) \qquad \text{(D.2–10)}$$

The following expression for the moles of $H_2S(g)$ formed can be obtained from Equation D.2–1 and the definition of c_{ss}:

$$m_{H_2S(g)} = c_{ss} v_{ss} - m_{aq} - m_S \qquad \text{(D.2–11)}$$

Substitution of Equations D.2–9 and D.2–10 into Equation D.2–11 yields

$$m_{H_2S(g)} = c_{ss} v_{ss} - c_A v_f - (c_B - c_A)(v_f - v_A) \qquad \text{(D.2–12)}$$

which can be simplified to

$$m_{H_2S(g)} = c_{ss} v_{ss} - c_A v_A - c_B(v_f - v_A) \qquad \text{(D.2–13)}$$

Using the definition of c_{ss}, Equation D.2–9 and Equation D.2–2, an expression for for $\bar{z}_{aq}$ can be obtained:

$$\bar{z}_{aq} = \frac{1}{c_A v_f}[c_{ss} v_{ss} \bar{z}_{ss} - m_S z_S - m_{H_2S(g)} z_{H_2S(g)}] \qquad \text{(D.2–14)}$$

Substitution of the electron numbers of solid S and H_2S into Equation D.2–14 gives

$$\bar{z}_{aq} = \frac{1}{c_A v_f}[c_{ss} v_{ss} \bar{z}_{ss} + 2m_{H_2S(g)}] \qquad \text{(D.2–15)}$$

Equation D.2–13 can be used in Equation D.2–15 to obtain

$$\bar{z}_{aq} = \frac{1}{c_A v_f}\{c_{ss} v_{ss} \bar{z}_{ss} + 2[c_{ss} v_{ss} - c_A v_A - c_B(v_f - v_A)]\} \qquad \text{(D.2–16)}$$

Equations D.2–7 and D.2–16 can be used to determine $[S]_{aq}$ and $\bar{z}_{aq}$ for each indirect determination experiment and thereby to locate a point on the boundary between the single–phase and two–phase regions.

The number of moles of $H_2S(g)$ formed, which is calculated using Equation D.2–13, can also be interpreted as sulfur lost from the solid–aqueous system. Thus, the percentage of sulfur lost from the solid–aqueous system is given by

$$\% \text{ S lost} = 100\,\frac{c_{ss} v_{ss} - c_A v_A - c_B(v_f - v_A)}{c_{s\,s}\, v_{ss}} \qquad \text{(D.2–17)}$$

Notice that if the amount of $H_2S(g)$ formed is negligible relative to the total amount of sulfur in the system, Equation D.2–15 reduces to

$$\bar{z}_{aq} = \frac{1}{c_A v_f}[c_{ss} v_{ss} \bar{z}_{ss}] \qquad \text{(D.2–18)}$$

The advantage of Equation D.2–18 for the calculation of $\bar{z}_{aq}$ is its simplicity; it contains fewer terms than Equation D.2–16 and is subject to less uncertainty. When the the percentage of sulfur lost from the solid–aqueous system (calculated using Equation D.2–17) was less than one percent, Equation D.2–18 was used to calculate $\bar{z}_{aq}$.

Equation D.2–18 was also used to calculate $\bar{z}_{aq}$ when Equation D.2–13 yielded a negative value of $m_{H_2S(g)}$ (and Equation D.2–17 thus gave a negative value for the percentage of sulfur lost). This physically unrealistic situation occasionally resulted from small errors in the determination of c_A and c_B in cases in which little or no H_2S was formed.

D.3 Error Analysis of Indirect Determination Experiments

The calculation of $\bar{z}_{aq}$ with Equation D.2–16 was subject to uncertainties in

the following quantities: c_A, c_B, $\bar{z}_{ss}$, c_{ss}, v_f, v_A and v_{ss}. (This analysis could also have been performed using m_A and m_B instead of c_A and c_B.) These uncertainties were due chiefly to lack of precision. The accuracy of the analytical method for the determination of total sulfur concentration was confirmed by testing solutions of known composition. The precision of the method was determined by repeated analysis of identical samples.

The following equation was used to estimate the uncertainty in $\bar{z}_{aq}$:

$$\sigma^2_{\bar{z}_{aq}} = \left[\frac{\partial \bar{z}_{aq}}{\partial c_A}\right]^2 \sigma^2_{c_A} + \left[\frac{\partial \bar{z}_{aq}}{\partial c_B}\right]^2 \sigma^2_{c_B} + \left[\frac{\partial \bar{z}_{aq}}{\partial \bar{z}_{ss}}\right]^2 \sigma^2_{\bar{z}_{ss}} + \left[\frac{\partial \bar{z}_{aq}}{\partial c_{ss}}\right]^2 \sigma^2_{c_{ss}} + \left[\frac{\partial \bar{z}_{aq}}{\partial v_f}\right]^2 \sigma^2_{v_f} + \left[\frac{\partial \bar{z}_{aq}}{\partial v_A}\right]^2 \sigma^2_{v_A} + \left[\frac{\partial \bar{z}_{aq}}{\partial v_{ss}}\right]^2 \sigma^2_{v_{ss}} \qquad \text{(D.3-1)}$$

Each partial derivative in Equation D.3–1 was taken with all other variables held constant. Using Equation D.2–16, the appropriate partial derivatives of $\bar{z}_{aq}$ were taken, and they are shown in Equations D.3–2 through D.3–8. The terms in boldface print drop out when Equation D.2–18 is used to compute $\bar{z}_{aq}$, thereby reducing the uncertainty in $\bar{z}_{aq}$.

$$\left[\frac{\partial \bar{z}_{aq}}{\partial c_A}\right] = -\frac{\bar{z}_{aq}}{c_A} - \frac{2v_A}{c_A v_f} \qquad \text{(D.3-2)}$$

$$\left[\frac{\partial \bar{z}_{aq}}{\partial c_B}\right] = -\frac{2(v_f - v_A)}{c_A v_f} \qquad \text{(D.3-3)}$$

$$\left[\frac{\partial \bar{z}_{aq}}{\partial \bar{z}_{ss}}\right] = \frac{c_{ss} v_{ss}}{c_A v_f} \qquad \text{(D.3-4)}$$

$$\left[\frac{\partial \bar{z}_{aq}}{\partial c_{ss}}\right] = \frac{v_{ss}\bar{z}_{ss}}{c_A v_f} + \frac{2v_{ss}}{c_A v_f} \tag{D.3-5}$$

$$\left[\frac{\partial \bar{z}_{aq}}{\partial v_f}\right] = -\frac{\bar{z}_{aq}}{v_f} - \frac{2c_B}{c_A v_f} \tag{D.3-6}$$

$$\left[\frac{\partial \bar{z}_{aq}}{\partial v_A}\right] = \frac{2(c_B - c_A)}{c_A v_f} \tag{D.3-7}$$

$$\left[\frac{\partial \bar{z}_{aq}}{\partial v_{ss}}\right] = \frac{c_{ss}\bar{z}_{ss}}{c_A v_f} + \frac{2c_{ss}}{c_A v_f} \tag{D.3-8}$$

In the indirect determination experiments, the solution did not always completely clarify upon standing. When Sample A was clear, the following estimate, used in the calculation of uncertainty in $\bar{z}_{aq}$, reflected the precision of the analytical method, as determined by repeated analysis of identical samples:

$$\sigma_{c_A} = 0.02c_A \tag{D.3-9}$$

In cases in which the solution was not clear, Sample A contained small amounts of colloidal sulfur. The precision of the analytical method was still reflected by Equation D.3-9. However, since solid sulfur could be included in the dissolved sulfur concentration, the accuracy of the analytical value of c_A was reduced. To estimate the increased uncertainty, the results of similar runs (i.e., runs which used starting solutions of similar concentration and $\bar{z}$) were analyzed. The values of c_A from similar runs that resulted in different types of solutions (clear or opaque) were compared. As a result of these comparisons, the uncertainty in $\bar{z}_{aq}$, in cases in which Sample A was not clear, was calculated using the following estimate:

$$\sigma_{c_A} = 0.075c_A \tag{D.3-10}$$

The following additional estimates were used in the calculation of

uncertainty in $\bar{z}_{aq}$. The precision of equipment used, tests on selected samples, repeated measurements of identical samples and judgments based on experience with the experiments were taken into account in the formulation of these estimates.

$$\sigma_{c_B} = 0.02c_B \tag{D.3–11}$$

$$\sigma_{\bar{z}_{ss}} = 0.020 \tag{D.3–12}$$

$$\sigma_{c_{ss}} = 0.015c_{ss} \tag{D.3–13}$$

$$\sigma_{v_f} = 0.015v_f \tag{D.3–14}$$

$$\sigma_{v_A} = 0.002v_A \tag{D.3–15}$$

$$\sigma_{v_{ss}} = 0.002v_{ss} \tag{D.3–16}$$

For each calculated value of $\bar{z}_{aq}$, the error bars in Figure 6–18 are drawn at $\bar{z}_{aq} \pm 2\sigma_{\bar{z}_{aq}}$.

APPENDIX E

CALCULATION OF CONTOURS OF CONSTANT CONCENTRATION ON THE SOLID–AQUEOUS EQUILIBRIUM SURFACE IN SYSTEMS CONTAINING TWO ACTIVE REDOX ELEMENTS

Within this appendix, the following definitions are made to simplify the equations.

$$A_k \equiv \frac{\alpha_{M,k}}{\alpha_{M,k} + \alpha_{N,k}}$$

$$B_k \equiv \frac{\alpha_{N,k}}{\alpha_{M,k} + \alpha_{N,k}}$$

$$C_k \equiv z_k$$

$$D_k \equiv h_k(\ln 10)pH - w_k \ln a_{H_2O} - x_k \ln a_X - y_k \ln a_Y - \frac{\Delta G_k^\circ}{RT}$$

$([M]_{aq})_f \equiv$ a fixed value of concentration for which a contour on the solid–aqueous surface is calculated

$$\mu_M^* \equiv \frac{(\mu_M - \mu_M^\circ)}{RT}$$

$$\mu_N^* \equiv \frac{(\mu_N - \mu_N^\circ)}{RT}$$

$$E^* \equiv \frac{EF}{RT}$$

Notice that μ_M^*, μ_N^* and E^* are dimensionless measures of the chemical potentials of the active redox elements M and N and the electrons.

The following procedure was used to calculate contours of constant $[M]_{aq}$ in equilibrium with a solid, S_s, in aqueous systems containing two active redox elements. Upon solution of the equilibrium problem in chemical potential space,

as described in Chapter 7.3, three–phase lines and intersections of the equilibrium surface with the system boundaries were searched for points at a chosen value of concentration, $([M]_{aq})_f$. Pairs of points in chemical potential space with a solid in common were treated as the endpoints of constant concentration contours on the equilibrium surface associated with S_s.

Combining Equations 2.3–5 and 5.5–3 for a pure solid S_s and using the definitions listed above gives:

$$A_s\mu_M^* + B_s\mu_N^* + C_sE^* + D_s = 0 \qquad \text{(E–1)}$$

Equation 2.3–43, written in terms of the definitions above for an ideal solution (all $\gamma_j = 1$) of total concentration $([M]_{aq})_f$, is

$$([M]_{aq})_f = \sum_j \alpha_{M,j}\exp\{(\alpha_{M,j} + \alpha_{N,j})(A_j\mu_M^* + B_j\mu_N^* + C_jE^* + D_j)\} \qquad \text{(E–2)}$$

where the sum is taken over all dissolved redox species, S_j.

To calculate constant concentration contours, points (μ_M^*, μ_N^*, E^*), which simultaneously satisfy Equations E–1 and E–2, must be determined. Equations E–1 and E–2 can be combined to give one equation in two variables. Equation E–1 can be solved for any of the three dimensionless chemical potentials:

$$\mu_M^* = -\frac{B_s}{A_s}\mu_N^* - \frac{C_s}{A_s}E^* - \frac{D_s}{A_s} \qquad (A_s \neq 0) \qquad \text{(E–3a)}$$

$$\mu_N^* = -\frac{A_s}{B_s}\mu_M^* - \frac{C_s}{B_s}E^* - \frac{D_s}{B_s} \qquad (B_s \neq 0) \qquad \text{(E–3b)}$$

$$E^* = -\frac{A_s}{C_s}\mu_M^* - \frac{B_s}{C_s}\mu_N^* - \frac{D_s}{C_s} \qquad (C_s \neq 0) \qquad \text{(E–3c)}$$

Since solid S_s contains active redox element, at least one of A_s and B_s must be non–zero. Therefore, at least one of the Equations E–3 can be written for S_s.

Each of Equations E–3 can be combined with Equation E–1 to eliminate one

of the three dimensionless chemical potentials. For example, substitution of Equation E–3a into Equation E–2 gives

$$\sum_j \alpha_{M,j} \exp\{(\alpha_{M,j} + \alpha_{N,j})\left[(A_j - \frac{A_s}{C_s} C_j)\mu_M^* + (B_j - \frac{B_s}{C_s} C_j)\mu_N^* + (D_j - \frac{D_s}{C_s} C_j)\right]\}$$

$$= ([M]_{aq})_f \qquad \text{(E–4a)}$$

Similarly, combining Equations E–2 and E–3b gives

$$\sum_j \alpha_{M,j} \exp\{(\alpha_{M,j} + \alpha_{N,j})\left[(A_j - \frac{A_s}{B_s} B_j)\mu_M^* + (C_j - \frac{C_s}{B_s} B_j)E^* + (D_j - \frac{D_s}{B_s} B_j)\right]\}$$

$$= ([M]_{aq})_f \qquad \text{(E–4b)}$$

and combining Equations E–2 and E–3c gives

$$\sum_j \alpha_{M,j} \exp\{(\alpha_{M,j} + \alpha_{N,j})\left[(B_j - \frac{B_s}{A_s} A_j)\mu_N^* + (C_j - \frac{C_s}{A_s} A_j)E^* + (D_j - \frac{D_s}{A_s} A_j)\right]\}$$

$$= ([M]_{aq})_f \qquad \text{(E–4c)}$$

Consider Equation E–4b. For a specified value of μ_M^*, E^* can be determined iteratively with Equation E–4b. The contour can be calculated by specifying successive values of μ_M^* and iteratively calculating the corresponding values of E^*. Conversely, μ_M^* can be determined for specified values of E^*.

A damped Newton–Raphson method was used to determine the iterative solutions along the contour at $([M]_{aq})_f$ on the equilibrium surface. The necessary partial derivatives were be calculated from Equations E–4. From Equation E–4a,

$$\left[\frac{\partial [M]_{aq}}{\partial \mu_M^*}\right]_{\mu_N^*} = \sum_j \alpha_{M,j}(\alpha_{M,j} + \alpha_{N,j})(A_j - \frac{A_s}{C_s} C_j)[S_j] \qquad \text{(E–5a)}$$

and

$$\left[\frac{\partial [M]_{aq}}{\partial \mu_N^*}\right]_{\mu_M^*} = \sum_j \alpha_{M,j}(\alpha_{M,j} + \alpha_{N,j})(B_j - \frac{B_s}{C_s} C_j)[S_j] \qquad \text{(E–5b)}$$

where $[S_j]$ is the concentration of species S_k.

From Equation E–4b,

$$\left[\frac{\partial\ [M]_{aq}}{\partial\ \overset{*}{\mu}_M}\right]_{\overset{*}{E}} = \sum_j \alpha_{M,j}(\alpha_{M,j} + \alpha_{N,j})(A_j - \frac{A_s}{B_s} B_j)[S_j] \qquad \text{(E–6a)}$$

and

$$\left[\frac{\partial\ [M]_{aq}}{\partial\ \overset{*}{E}}\right]_{\overset{*}{\mu}_M} = \sum_j \alpha_{M,j}(\alpha_{M,j} + \alpha_{N,j})(C_j - \frac{C_s}{B_s} B_j)[S_j] \qquad \text{(E–6b)}$$

From Equation E–4c,

$$\left[\frac{\partial\ [M]_{aq}}{\partial\ \overset{*}{\mu}_N}\right]_{\overset{*}{E}} = \sum_j \alpha_{M,j}(\alpha_{M,j} + \alpha_{N,j})(B_j - \frac{B_s}{A_s} A_j)[S_j] \qquad \text{(E–7a)}$$

and

$$\left[\frac{\partial\ [M]_{aq}}{\partial\ \overset{*}{E}}\right]_{\overset{*}{\mu}_N} = \sum_j \alpha_{M,j}(\alpha_{M,j} + \alpha_{N,j})(C_j - \frac{C_s}{A_s} A_j)[S_j] \qquad \text{(E–7b)}$$

The rate of convergence of the iterative scheme was quite sensitive to the initial guess used for the iterative variable. The cyclic relationship among partial derivatives can be used with Equations E–5, E–6 and E–7 to obtain additional relationships among the dimensionless chemical potentials. The partial derivatives at constant $[M]_{aq}$ are especially useful for improving initial guesses for the iterative variable. For example, the identity

$$\left[\frac{\partial\ [M]_{aq}}{\partial\ \overset{*}{\mu}_M}\right]_{\overset{*}{\mu}_N} \left[\frac{\partial\ \overset{*}{\mu}_M}{\partial\ \overset{*}{\mu}_N}\right]_{[M]_{aq}} \left[\frac{\partial\ \overset{*}{\mu}_N}{\partial\ [M]_{aq}}\right]_{\overset{*}{\mu}_M} = -1 \qquad \text{(E–8)}$$

can be rearranged to give

$$\left[\frac{\partial\ \overset{*}{\mu}_M}{\partial\ \overset{*}{\mu}_N}\right]_{[M]_{aq}} = -\left[\frac{\partial\ [M]_{aq}}{\partial\ \overset{*}{\mu}_M}\right]^{-1}_{\overset{*}{\mu}_N} \left[\frac{\partial\ [M]_{aq}}{\partial\ \overset{*}{\mu}_N}\right]_{\overset{*}{\mu}_M} \qquad \text{(E–9)}$$

Equations E–5a and E–5b can be substituted into Equation E–9 to give

$$\left[\frac{\partial \mu_M^*}{\partial \mu_N^*}\right]_{[M]_{aq}} = \frac{-\sum_j \alpha_{M,j}(\alpha_{M,j} + \alpha_{N,j})(B_j - \frac{B_s}{C_s} C_j)[S_j]}{\sum_j \alpha_{M,j}(\alpha_{M,j} + \alpha_{N,j})(A_j - \frac{A_s}{C_s} C_j)[S_j]} \quad \text{(E–10)}$$

Equation E–10 is useful when Equation E–4a is used to to determine constant concentration contours.

For example, consider a case in which μ_M^* is being determined iteratively at successive specified values of μ_N^*. Equation E–10, calculated at the previous point on the contour at $([M]_{aq})_f$, can be used to determine an initial guess for μ_M^* at a new value of μ_N^*.

The method discussed here for the calculation of constant concentration contours on the solid–aqueous equilibrium surface in systems containing two active redox elements can also be applied to systems containing one active redox element. For an aqueous system containing active redox element M, contours of constant $[M]_{aq}$ on the solid–aqueous equilibrium surface in the chemical potential space defined by μ_M, μ_{H^+} and μ_{e^-} can be determmined with the method described above. Note that protons would replace active redox element N in the analysis; equations analogous to those above could be derived. Contours of a_M (defined by Equation 2.3–39) can also be calculated. The use of a_M, rather than $[M]_{aq}$, simplifies the iterative process.